Author:
Gerardo-Aviles, Jose

Title:
Dysregulation of microRNAs in dementia

Dysregulation of microRNAs in Dementia

Jose Gabino Gerardo-Aviles

A dissertation submitted to the University of Bristol in accordance with the requirements for award of the degree of PhD in Translational Health Sciences in the Bristol Medical School.

Bristol Medical School, September 2019

42,220 words

Abstract

Dementia is a progressive neurological syndrome characterised by cognitive impairment, in particular with alterations in learning and memory. Alzheimer's disease and vascular dementia are the two most common forms of this syndrome. Although the pathophysiology of dementia is unknown, changes in several proteins are believed important in its development. These changes could be, to some extent, explained by microRNAs. MicroRNAs are posttranscriptional regulators of gene expression that repress protein synthesis. This thesis attempts to investigate the role of microRNAs in dementia from a more rigorous and biologically relevant perspective. I propose a hypothesis-driven approach considering some factors that have not been taken into account previously. I hypothesise that the levels of certain microRNAs with converging functions would be expressed differently in post-mortem brain tissue of patients diagnosed with Alzheimer's disease, vascular dementia and non-demented elderly, investigated using novel reference genes and two new formulas proposed to improve microRNA quantification.

A first panel of microRNAs was selected based on their proposed effects on proteins that have been implicated in Alzheimer´s disease. The levels of these microRNAs were significantly different in the Alzheimer's disease group. A second panel was selected for potential roles on proteins related to hypoxia, vascular dysfunction and the renin angiotensin system. Unexpectedly, no change was observed in the vascular dementia group whilst a statistically significant difference was observed in the Alzheimer´s disease group. Finally, the presence of selected microRNAs was explored in cell culture as potential modelling construct. My results provide new candidates and more rigorous approaches to the study of microRNAs in dementia research. This work will inform future research in the emerging field of microRNAs in dementia whilst also challenging the validity of findings to date.

Dedication and acknowledgements

This project would not have been possible without those patients and their families who were willing to donate their brains in times of struggle fighting the dementia process. I am also grateful to my supervisors Professor Patrick Kehoe and Dr. Shelley Allen for their guidance, support, patience and trust over this long journey of four years. Thanks to the Mexican Council of Science and Technology (CONACYT CVU 600220), the Alumni Foundation University of Bristol, Alzheimer Research UK and Mr. Graeme Coulthard for funding this project.

I would also like to thank the Dementia Research Group and the Clinical Neuroscience Department for their help and support. I am indebted to my friends Adrian, Alejandra, Danira, Jacobo, Lily, Perla, Victor and Yasmin for their support and companionship, always there hearing long monologues and keeping my mental health.

This thesis is a reflection of twenty four years of education and I am profoundly grateful to those that helped me in continuing my studies; to my parents for their support in my first years of education, to Erika Chargoy for her help and counselling throughout high school, to Erika Garza for her coaching during med school and to Dr. Zuner Bortolotto for his guidance and motivation in my master degree. Finally, I would like to dedicate this thesis to my grandmother Maria, who took care of me, raised me to be what I am and who suffered Alzheimer's disease over the last 8 years of her life.

Author's declaration

I declare that the work in this dissertation was carried out in accordance with the requirements of the University's Regulations and Code of Practice for Research Degree Programmes and that it has not been submitted for any other academic award. Except where indicated by specific reference in the text, the work is the candidate's own work. Work done in collaboration with, or with the assistance of, others, is indicated as such. Any views expressed in the dissertation are those of the author.

Author Jose Gabino Gerardo-Aviles Date September 2019

Some of the work have risen to the following publications and conference proceedings:

Gerardo-Aviles JG, Allen S & Kehoe P (2018) Variability in the small-nucleolar RNAs commonly used for microRNA normalisation in postmortem brain tissue of Alzheimer's and vascular dementia. Alzheimer's and Dementia; 14(7): 749 DOI: 10.1016/j.jalz.2018.06.899

Gerardo-Aviles JG, Allen S & Kehoe P (2017) Early dysregulation of microRNAs in the posterior cingulate gyrus of Alzheimer and vascular dementia. Neurodegener Dis; 17: (suppl 1): 788 DOI: 10.1159/000464378

Gerardo-Aviles JG, Allen S & Kehoe P (2017) Renin-Angiotensin System MicroRNAs, Special Focus on the Brain, Renin-Angiotensin System - Past, Present and Future, Anna Tolekova (Ed.), InTech, DOI: 10.5772/67080

Table of contents

Abstract 1

Dedication and acknowledgements 3

Author's declaration 5

Table of contents 7

List of Tables 14

List of Figures 16

Chapter 1.- Introduction 19

1.1. The clinical problem of dementia 19

1.2. The neuropathology of Alzheimer's disease 19

1.2.1. Neurofibrillary tangles 20

1.2.2. Amyloid plaques and cerebral amyloid angiopathy 22

1.2.3. Astrogliosis and reactive microglia 24

1.2.4. Vascular changes 26

1.3. Clinical presentation of dementia 26

1.4. Epidemiology of dementia 27

1.5. Genetics of dementia 28

1.6. Hypotheses of Alzheimer's disease 29

1.7. An introduction to microRNAs 30

1.7.1 miRNA biogenesis and function 32

1.8. miRNAs in dementia 34

1.8.1 Technical complexities related to research of miRNAs 35

Chapter 2.- Materials and methods 39

2.1 Study cohort 39

2.2 Brain tissue dissection and homogenisation 40

2.3 RNA isolation, quantification and standardisation 40

2.4 Homogenates and protein quantification 44

2.5 Simulation of postmortem delay 44

2.6 Quantitative real time polymerase chain reaction 45

2.7 Analysis of qPCR using the $2^{(-\Delta\Delta CT)}$ method 49

2.8 miRNA repositories (miRbase, mirgeneDB and miRbase tracker) 52

2.9 Genomic mapping (RNA central) 54
2.10 miRNA-target predicting software 54
2.11 GWAS Catalog NHGRI-EBI 54
2.12 R software 55
2.13 Software for analysis of target proteins (DAVID and PANTHER) 55
2.14 Western blotting 56
2.15 Cell culture 59
2.16 Statistical package Graph Pad Prism 60
Chapter 3.- miRNAs related to classical histopathological hallmarks of Alzheimer's disease 61
3.1. Introduction 61
3.1. Alzheimer's disease-related proteins and their associated miRNAs 61
3.1.1. Amyloid and its production 61
3.1.2. ApoE, ApoE receptors and lipidation of Aβ 62
3.1.3. Proteolytic degradation of amyloid 66
3.1.4. Tau phosphorylation 67
3.2. Hypothesis 69
3.3. Methods 69
3.3.1. Choice of miRNAs 69
3.3.2. Study cohort 71
3.3.3. Brain tissue dissection and homogenization 71
3.3.4. RNA isolation, quantification and standardization 72
3.3.5. Software for analysis of target proteins (DAVID and PANTHER) 72
3.3.6. Data collection and analysis 72
3.4. Results 72
3.4.1. miR-16 72
3.4.2. miR-29a/b 73
3.4.3. miR-34a 75
3.4.4. miR-125b 76
3.4.5. miR-132/212 77
3.4.6. Analysis of miRNAs with comparable patterns 79
3.5. Discussion and conclusions 82
Chapter 4.- Advancing the reliability of miRNA measurement 87

4.1. A critical appraisal of techniques for miRNA measurement 87
4.1.1. Challenges in the measurement of miRNAs 87
4.1.2. Newer approaches for measurement of miRNAs 88
4.2. A closer look at quantitative reverse transcription polymerase chain reaction 89
4.3. Hypothesis 95
4.4. Methods 95
4.4.1 Study cohort 96
4.4.2. Brain tissue dissection and homogenization 96
4.4.3. RNA isolation, quantification and standardization 96
4.4.5. Simulation of postmortem delay. 96
4.4.6 Data collection and analysis. 97
4.5. Results 97
4.5.1. Investigation of snRNA expression across the whole sample cohort 97
4.5.1.1. RNU43 97
4.5.1.2. RNU44 98
4.5.1.3. RNU48 99
4.5.1.4. RNU6B 99
4.5.1.5. miR-9-5p 100
4.5.1.6. miR-9-3p 101
4.5.1.7 Rank-ordering of the calibrator genes related to CT value differences from the geometric mean 101
4.5.2 Simulation of post-mortem delay 102
4.5.2.1. RNU43 102
4.5.2.2. RNU44 103
4.5.2.3. RNU48 103
4.5.2.4. RNU6B 104
4.5.2.5. miR-9-5p 105
4.5.2.6. miR-9-3p 106
4.5.2.7 Comparison and rank-ordering of observed transcript stabilities for investigated calibrators 106
4.5.3. Evaluation of calibrator genes according to disease pathology 107
4.5.3.1. RNU43 107
4.5.3.2. RNU44 109
4.5.3.3. RNU48 110

4.5.3.4. RNU6B 112
4.5.3.5. miR-9-5p 113
4.5.3.6. miR-9-3p 115
4.5.3.7. Ranking of calibrators according to expression in relation to neurodegenerative pathology and disease group 116
4.5.4. Overall ranking of small RNAs as calibrator gene 116
4.6. Discussion and conclusions 117
4.6.1 Summary of findings 117
4.6.2. Next steps 118
Chapter 5.- Evidence-based re-evaluation of examining miRNAs related to classical histopathological hallmarks of Alzheimer's disease 120
5.1 Introduction 120
5.2 Hypothesis 123
5.3 Methods 123
5.3.1. Study cohort 123
5.3.2. Brain tissue dissection and homogenization 123
5.3.3. RNA isolation, quantification and standardization 124
5.3.4. Software for analysis of target proteins (DAVID and PANTHER) 124
5.3.5. Data collection and analysis 124
5.4 Results 124
5.4.1. miR-16 family 125
5.4.1.1. miR-15a 125
5.4.1.2. miR-15b 126
5.4.1.3. miR-16 127
5.4.1.4. miR-195 128
5.4.1.4. miR-424 129
5.4.1.5. miR-497 130
5.4.1.5. Summary of miR-16 family results 131
5.4.1.6. Analysis of miR-16 family predicted target proteins 131
5.4.2. miR-29 family 134
5.4.2.1. miR-29a 134
5.4.2.2. miR-29b 135
5.4.2.3. miR-29c 136
5.4.2.4. Summary of miR-29 family results 137

5.4.2.5. Analysis of miR-29 family predicted target proteins 137
5.4.3. miR-34 family 140
5.4.3.1. miR-34a 140
5.4.3.2. miR-34b 141
5.4.3.3. miR-34c 141
5.4.3.4. miR-449 142
5.4.3.5. Summary of miR-34 family results 143
5.4.3.6. Analysis of miR-34 family predicted target proteins 144
5.4.4. miR-125 family 146
5.4.4.1. miR-125a 146
5.4.4.2. miR-125b 147
5.4.4.3. Summary of miR-125 family results 147
5.4.4.4. Analysis of miR-125 family predicted target proteins 148
5.4.5. miR-132/212 family 150
5.4.5.1. miR-132 150
5.4.5.2. miR-212 151
5.4.5.3. Summary of miR-132 family results 152
5.4.5.4. Analysis of miR-132 family predicted target proteins 152
5.5 Discussion and conclusions 154
Chapter 6.- miRNAs related to vascular factors and the renin angiotensin system 158
6.1. Introduction 158
6.1.1. A brief introduction to multi-functional miRNAs in RAS 163
6.1.2. miRNAs and single nucleotide polymorphisms 166
6.2. Hypotheses 168
6.3. Methods 168
6.3.1. Study cohort 168
6.3.2. Brain tissue dissection and homogenization 169
6.3.3. RNA isolation, quantification and standardization 169
6.3.4. Software for analysis of target proteins (DAVID and PANTHER) 169
6.3.5. GWAS Catalog NHGRI-EBI 169
6.3.6. Data collection and analysis 169
6.4. Results 170
6.4.1. miR-17 family 170

6.4.1.1. miR-17 170
6.4.1.2. miR-20a 171
6.4.1.3. miR-20b 172
6.4.1.4. miR-93 173
6.4.1.5. miR-106a 174
6.4.1.6. miR-106b 175
6.4.1.7. Summary of miR-17 family results 176
6.4.1.8. Analysis of miR-17 family predicted target proteins 176
6.4.2. miR-143 178
6.4.2.1. Analysis of miR-143 predicted target proteins 179
6.4.3. miR-320e 181
6.4.3.1. Analysis of miR-320e predicted target proteins 181
6.5 Discussion and conclusions 183
Chapter 7.- Evaluation of cell culture as an experimental model for the study of miRNAs in dementia 187
7.1 Introduction 187
7.2 Hypothesis 193
7.3 Methods 194
7.3.1. RNA isolation, quantification and standardization 194
7.3.2. Cell culture 194
7.3.3. Data collection and analysis. 195
7.4. Results 196
7.4.1. Selection of calibrator gene 196
7.4.2. miR-16 family 199
7.4.3. miR-29 family 201
7.4.4. miR-34 family 202
7.4.5. miR-125 family 203
7.4.6. miR-132/212 family 204
7.4.7. miR-17 family 205
7.5 Discussion and conclusions 207
Chapter 8.- General discussion and conclusions 212
8.1 Recapitulation of chapters 212
8.2 Strengths of this study 216

8.3 Weaknesses of this study....217
8.4 Recommendations for future research....218
Appendix 1....220
Appendix 2....221
Appendix 3....222
Appendix 4....228
References....234

List of Tables

Chapter 2

Table 2.1 Demographic information of the cohort. 40

Table 2.2 Constituents of the reverse transcription reaction assay. 45

Table 2. 3 Components of the quantitative polymerase chain reaction. 46

Table 2. 4 PCR program used. 47

Table 2. 5 Pre-designed primer sequences and assay IDs of requisition. 48

Table 2. 6 Antibodies, requisition ID's, concentration and dilutions used. 58

Chapter 3

Table 3. 1 Transcripts related to classical hallmarks of AD.....70

Table 3. 2 Preselected miRNA families. 71

Table 3. 3 Demographic information of the cohort used in Chapter 3.....71

Chapter 4

Table 4. 1 Commercially available snRNAs. 91

Table 4. 2 Demographic information of the cohort used in Chapter 4.....96

Chapter 5

Table 5. 1 Transcripts and miRNAs related to classical hallmarks of AD. 122

Table 5. 2 Demographic information of the cohort used in Chapter 5.....123

Table 5. 3 miRNA families studied in Chapter 5. 125

Table 5. 4 Analysis of predicted targets for miR-16 family by DAVID software. 132

Table 5. 5 Analysis of predicted targets for miR-16 family by PANTHER software. ...133

Table 5. 6 Analysis of predicted targets for miR-29 family by DAVID software. 138

Table 5. 7 Analysis of predicted targets for miR-29 family by PANTHER software. ...139

Table 5. 8 Analysis of predicted targets for miR-34 family by DAVID software. 144

Table 5. 9 Analysis of predicted targets for miR-34 family by PANTHER software. ...145

Table 5. 10 Analysis of predicted targets for miR-125 by DAVID software.....148

Table 5. 11 Analysis of predicted targets for miR-125 by PANTHER software.....150

Table 5. 12 Analysis of predicted targets for miR-132 family by DAVID software. 153

Table 5. 13 Analysis of predicted targets for miR-132 family by PANTHER software.153

Chapter 6

Table 6. 1 RAS elements with their total amount of miRNAs. 162
Table 6. 2 Combinations of RAS components and miRNAs in common. 164
Table 6. 3 Assessment of Mas receptor miRNAs.....166
Table 6. 4 Demographic information of the cohort used in Chapter 6.....168
Table 6. 5 Analysis of predicted targets for miR-17 family by DAVID software. 177
Table 6. 6 Analysis of predicted targets for miR-17 family by PANTHER software. ...178
Table 6. 7 Analysis of predicted targets for miR-143 by DAVID software.....180
Table 6. 8 Analysis of predicted targets for miR-143 by PANTHER software.....180
Table 6. 9 Analysis of predicted targets for miR-320e by DAVID software.....182
Table 6. 10 Analysis of predicted targets for miR-320e by PANTHER software.....183

Chapter 7

Table 7. 1 In-situ location of previously measured miRNAs in the human brain.....189
Table 7. 2 Spearman correlation test for members of the miR-16 family.....200
Table 7. 3 Spearman correlation test for members of the miR-29 family.....202
Table 7. 4 Spearman correlation test for members of the miR-34 family.....203
Table 7. 5 Spearman correlation test for members of the miR-17 family.....206

List of Figures

Chapter 1

Figure 1.1 miRNA biogenesis and function. 31

Chapter 2

Figure 2. 1 Example layout of qRT-PCR plates.....46

Figure 2. 2 Plot of 2-ΔΔCT values against ΔΔCT values and corresponding fold values of 2 points.....50

Figure 2. 3 Resulting values using the new formula termed Δ.....51

Chapter 3

Figure 3. 1 Percentage of difference for miR-16.....73

Figure 3. 2 Percentage of difference for miR-29a.....74

Figure 3. 3 Percentage of difference for miR-29b.....75

Figure 3. 4 Percentage of difference for miR-34a.....76

Figure 3. 5 Percentage of difference for miR-125b.....77

Figure 3. 6 Percentage of difference for miR-132.....78

Figure 3. 7 Percentage of difference for miR-212.....79

Figure 3. 8 Expression pattern of miRNAs according to Braak stage and VaD.....80

Figure 3. 9 Overlapping targets of miRNA families. 81

Chapter 4

Figure 4. 1 Plot of CT differences for RNU43 in individual samples of the cohort. 98

Figure 4. 2 Plot of CT differences for RNU44 in individual samples of the cohort. 98

Figure 4. 3 Plot of CT differences for RNU43 in individual samples of the cohort. 99

Figure 4. 4 Plot of CT differences for RNU6B in individual samples of the cohort. 100

Figure 4. 5 Plot of CT differences for miR-9-5p in individual samples of the cohort....100

Figure 4. 6 Plot of CT differences for miR-9-3p in individual samples of the cohort....101

Figure 4. 7 CT difference of individual samples to the 0 hours sample for RNU43.....102

Figure 4. 8 CT difference of individual samples to the 0 hours sample for RNU44.....103

Figure 4. 9 CT difference of individual samples to the 0 hours sample for RNU48.....104

Figure 4. 10 CT difference of individual samples to the 0 hours sample for RNU6B. ..105

Figure 4. 11 CT difference of individual samples to the 0 hours sample for miR-9-5p.105
Figure 4. 12 CT difference of individual samples to the 0 hours sample for miR-9-3p.106
Figure 4. 13 Percentage of difference for RNU43 by Braak stages. 108
Figure 4. 14 Percentage of difference for RNU43 by diagnostic groups. 108
Figure 4. 15 Percentage of difference for RNU44 by Braak stages. 109
Figure 4. 16 Percentage of difference for RNU44 by diagnostic groups. 110
Figure 4. 17 Percentage of difference for RNU48 by Braak stages. 111
Figure 4. 18 Percentage of difference for RNU48 by diagnostic groups. 111
Figure 4. 19 Percentage of difference for RNU6B by Braak stages. 112
Figure 4. 20 Percentage of difference for RNU6B by diagnostic groups. 113
Figure 4. 21 Percentage of difference for miR-9-5p by Braak stages. 114
Figure 4. 22 Percentage of difference for miR-9-5p by diagnostic groups.....114
Figure 4. 23 Percentage of difference for miR-9-3p by Braak stages. 115
Figure 4. 24 Percentage of difference for miR-9-3p by diagnostic groups.....116
Chapter 5
Figure 5. 1 Percentage of difference for miR-15a.....126
Figure 5. 2 Percentage of difference for miR-15b.....127
Figure 5. 3 Percentage of difference for miR-16.....128
Figure 5. 4 Percentage of difference for miR-195.....129
Figure 5. 5 Percentage of difference for miR-424.....130
Figure 5. 6 Percentage of difference for miR-497.....131
Figure 5. 7 Percentage of difference for miR-29a.....135
Figure 5. 8 Percentage of difference for miR-29b.....136
Figure 5. 9 Percentage of difference for miR-29c. 137
Figure 5. 10 Percentage of difference for miR-34a.....140
Figure 5. 11 Percentage of difference for miR-34b.....141
Figure 5. 12 Percentage of difference for miR-34c. 142
Figure 5. 13 Percentage of difference for miR-449.....143
Figure 5. 14 Percentage of difference for miR-125a.....146
Figure 5. 15 Percentage of difference for miR-125b.....147
Figure 5. 16 Percentage of difference for miR-132.....151

Figure 5. 17 Percentage of difference for miR-212.....152
Chapter 6
Figure 6. 1 The renin angiotensin system and its components.....161
Figure 6. 2 Percentage of difference for miR-17.....171
Figure 6. 3 Percentage of difference for miR-20a.....172
Figure 6. 4 Percentage of difference for miR-20b.....173
Figure 6. 5 Percentage of difference for miR-93.....174
Figure 6. 6 Percentage of difference for miR-106a.....175
Figure 6. 7 Percentage of difference for miR-106b.....176
Figure 6. 8 Percentage of difference for miR-143.....179
Figure 6. 9 Percentage of difference for miR-320e.....181
Chapter 7
Figure 7. 1 Percentage of difference for miR-15a in SH-SY5Y cells.....196
Figure 7. 2 Percentage of difference for miR-16 in SH-SY5Y cells.....197
Figure 7. 3 Percentage of difference for miR-497 in SH-SY5Y cells.....197
Figure 7. 4 Percentage of difference for miR-34a in SH-SY5Y cells.....198
Figure 7. 5 Percentage of difference for miR-125a in SH-SY5Y cells.....198
Figure 7. 6 Percentage of difference for miR-125b in SH-SY5Y cells.....199
Figure 7. 7 Percentage of difference for miR-16 family in SH-SY5Y cells.....200
Figure 7. 8 Percentage of difference for miR-29 family in SH-SY5Y cells.....201
Figure 7. 9 Percentage of difference for miR-34 family in SH-SY5Y cells.....202
Figure 7. 10 Percentage of difference for miR-125 family in SH-SY5Y cells.....204
Figure 7. 11 Percentage of difference for miR-132 family in SH-SY5Y cells.....205
Figure 7. 12 Percentage of difference for miR-17 family in SH-SY5Y cells.....206

Chapter 1.- Introduction

1.1. The clinical problem of dementia

Dementia is a chronic and progressive neurological syndrome characterized by impairment in cognitive capacities such as, reasoning, learning, memory, orientation, language, and emotional stability (1,2). In 2012, the World Health Organization declared this syndrome as a priority condition for public heath due to its high incidence of nearly 7.7 million per year and derived elevated costs for health systems (1). Around 70% of all dementia cases are caused by Alzheimer's disease (AD), which can be described to exist in two forms according to its onset. First is the rare early-onset (<65 years) familial AD type, which an autosomal dominantly inherited form of AD caused by mutations in APP, PSEN1 and PSEN2. Second is the most common sporadic late-onset (>65 years) form of AD, which represents 95% of all AD cases (1,3,4).

The second most common form of dementia (and how it will be referred to in this thesis) is vascular dementia (VaD), which accounts for about 15% of dementia cases. A further 10% of dementia cases are due to Lewy bodies' dementia and around 5% is associated to other conditions and comorbidities. Importantly, these categories are arguably artificially distinct and more commonly many people with dementia have one or more forms of pathology, giving rise to a mixed phenotype, often called mixed dementia (1,3,4). Post-mortem histopathological analysis remains the gold standard for accurate diagnosis of dementia and it usually as a result of this form of diagnosis that the true extent of comorbidities is identified.

1.2. The neuropathology of Alzheimer's disease

The histopathology of AD is characterised by intracellular neurofibrillary tangles, extracellular amyloid plaques, astrogliosis and reactive microglia. It also involves

vascular changes such as cortical microinfarcts, lacunar infarcts in the basal ganglia and cortical petechial microbleeds, as is also often observed in VaD. Moreover, some of these features are also linked to cerebral amyloid angiopathy, a risk factor for haemorrhage, caused by the deposition of a 40 amino acid variant of the amyloid beta peptide within the blood vessels of the brain, particularly in the posterior parietal and occipital areas of the brain (5).

1.2.1. Neurofibrillary tangles

Neurofibrillary tangles are composed of hyperphosphorylated forms of microtubule associated tau protein (5,6). Tau protein is coded by the *MAPT* gene, which is conserved across vertebrates with 182 orthologues, indicating that the gene has been preserved by natural selection (7). Tau is highly expressed in the brain and it is mainly an axonal protein in mature neurons (6,8). Most of tau is bound to microtubules and allows their stabilisation and assembly. Microtubules stabilisation in turn, permits arrangement of the neuronal cytoskeleton and allows axonal transport after neuronal maturation (8,9).

Although neurofibrillary tau tangles are a pathological hallmark of AD, they are not exclusive of AD. Indeed there are several tauopathies, the collective term used to describe disorders caused by tau phosphorylation, abnormal splicing and levels of tau or mutations in *MAPT*. These include AD, corticobasal degeneration, Down's syndrome, frontotemporal dementia, Pick's disease, postencephalic parkinsonism and progressive supranuclear palsy, and even include dementia resulting from repeated head injury in the form of chronic traumatic encephalopathy (CTE) (9).

Mutations in the *MAPT* gene impair the binding of tau to microtubules, similarly phosphorylation of tau at serine/threonine residues regulates its binding to microtubules and its hyperphosphorylation is associated with aberrant aggregation in disease (6,8). Tau phosphorylation alter the conformation and neutralizes the positive charge of the microtubule-binding domain of tau, detaching tau from microtubules and

destabilising them (6,8,9). Phosphorylated and detached tau accumulates in neuronal neurites, axons and cell bodies forming insoluble filaments and, eventually, neurofibrillary tangles in three main stages (5,8).

First, precursors of tangles are recognised by diffuse tau staining in the cytoplasm of neurons without recognised pathology, with conserved dendrites and a centred nucleus. Second, mature intracellular neurofibrillary tangles are composed of tau aggregates that destabilise the cytoskeleton and move the nucleus to the periphery. Tau aggregates also extend to distorted neurites and to the proximal segment of the axon affecting neuronal morphology and neurotransmitter trafficking. Third, extraneuronal tangles are released after the death of neurons containing tau tangles, identified by the absence of nucleus and cytoplasm (5).

In addition, tau phosphorylation and tangle deposition follows a spatiotemporal pattern across the cerebral cortex that correlates with the progression of disease and symptoms. Braak and Braak described this evolution of tau pathology as six stages. The neurofibrillary tangles first appear in the transentorhinal and entorhinal cortex (stage I), followed by the cornus ammonis region 1 (stage II) and then in the subiculum in the hippocampus (stage III). Next, tangles appear in the amygdala, thalamus and claustrum (stage IV), continuing to isocortical areas, first associative areas (stage V) and then to primary sensory, motor and visual areas (stage VI) (5).

As mentioned, *MAPT* gene conservation across species suggests a function preserved by natural selection. Tau phosphorylation is observed in other mammals when they hibernate and in other situations such as hypothermia and induced-anaesthesia (10–13). This is likely to have a neuroprotective effect reducing metabolic demands in the brain. For instance, therapeutic hypothermia is used in human medicine for brain injuries to reduce the metabolic demand, decreasing excitotoxicity, free radical formation and inflammation (14). During hypothermia, synaptic contacts between mossy fibres and hippocampal neurons present regressive or retractable changes that are reversible once euthermia is restablished (15).

Arendt *et al* have shown that highly phosphorylated tau in paired helical filaments is present in torpor during hibernation. The distribution of phosphorylated tau also followed a consistent pattern similar to Braak stage, being most intense in the entorhinal cortex, hippocampus, and isocortical areas. Phosphorylated tau in neurons of the cornus ammonis region 3 was paralleled by the regression of synaptic contacts of the mossy fiber system terminating on cornus ammonis region 3 apical dendrites. Mossy fiber afferentation was restored in arousal along with a reduction of phosphorylated tau in the cornus ammonis region 3 neurons (16).

A neuroprotective role for tau phosphorylation is reinforced by the fact that cellular antioxidant induction and tau expression oppose each other. Similarly, embryonic neurons that survive after treatment with oxidants have more phosphorylated tau in comparison to those that didn't survive (12). These findings together suggest that phosphorylation of tau might be a neuroprotective and physiological mechanism by which neurons reduce the metabolic demand in order to cope with adverse conditions or brain insults. However, the reversibility of phosphorylated tau in mentioned above studies still remains controversial to what is observed in AD brain.

Arendt *et al* suggested that brain hypometabolism triggers tau phosphorylation and that periods of recovery are necessary for the reversibility of tau. If hypometabolism continues and hyperphosphorylation of tau persists, the physiological protective mechanism becomes a chronic and aberrant dysfunction that impedes the recovery of tau, allows its propagation in a prion-like manner and leads to neurodegeneration (17). Thus, tau phosphorylation might initiate as a physiological protective mechanism triggered by a cerebral insult that after chronicity turns into an irreversible state that propagates across the cortex giving the flourished clinical manifestation of dementia.

1.2.2. Amyloid plaques and cerebral amyloid angiopathy

Amyloid plaques and cerebral amyloid angiopathy (CAA) are caused by deposits of two isoforms of amyloid beta (Aβ). The former is caused by insoluble Aβ that is

generally 42 (Aβ-42), and to a lesser extent 43 (Aβ-43) amino acids in length, whilst the latter is caused by soluble Aβ of 40 amino acids in length (Aβ-40), which is the most predominant form of Aβ. Aβ is derived from processing of the amyloid precursor peptide (APP) once it is transported to the cellular membrane and processed by β- and ɣ-secretases(18). Similar to *MAPT*, *APP* that encodes for APP is conserved across vertebrates, with 182 orthologues, indicating preservation by natural selection (7).

Aβ levels and metabolism are regulated by neuronal activity and the most prominent site of Aβ secretion are distal axons and synapses (18,19). Aβ is secreted from synapses as a consequence of neuronal activity and it serves as a feedback loop or physiological mechanism to restrict synaptic transmission and maintain physiological levels of neuronal activity (20). Patients with temporal lobe epilepsy, where neuronal activity is exacerbated without control, develop Aβ plaques (19).

Soluble oligomers of Aβ, both Aβ-40 and Aβ-42, derived from AD patients have been shown to increase long-term depression (LTD), whilst inhibiting long-term potentiation (LTP). LTD and LTP are mechanisms of synaptic plasticity necessary for learning and memory. These oligomers also decreased dendritic spine density *in vitro*, whilst *in vivo*, intracerebroventricular injection of Aβ oligomers impaired memory tasks in normal rats (21). Although Aβ-40 is less prone to aggregation and is the most common Aβ species; apart from its effect in synaptic plasticity, it could have further implications by affecting vascular permeability, cause damage to the blood brain barrier and even raise blood pressure (22).

CAA is a small vessel disease characterised by deposits of Aβ-40 in the tunica media of leptomeningeal and cortical capillaries, small arterioles and medium-size arteries, particularly in posterior parietal and occipital lobes of the brain. CAA disrupts the vessel wall and can cause haemorrhages and CAA is linked to the cortical petechial microbleeds observed in AD brain (5). Moreover, microbleeds observed using magnetic resonance imaging (MRI) in patients, have been associated with microinfarcts observed at post-mortem (also observed in AD brain), with an odds ratio of 8 (23).

It could be possible that amyloid production starts as a compensatory mechanism to reduce neuronal activity and in doing so, Aβ ends up deposited in the tunica media of vessels causing cerebral amyloid angiopathy. Imbalance between amyloid production, clearance and degradation are thought to be key factors in the development of Aβ - related pathology in AD and CAA.

Clearance of Aβ is believed to occur by perivascular drainage, suggested by the Aβ deposition that is seen in cerebral vessels and which follow the intramural perivascular drainage pathways. Age-related changes to glycoproteins and proteoglycans in vascular basement membranes, are believed to reduce their efficiency to clear Aβ and other solutes (24). The possession of ε4 variant *ApoE*, the greatest non-causative genetic risk factor for AD and VaD, also affects the flexibility of vascular membranes. Along with age, the greatest non-modifiable risk factor for AD, these structural changes and the properties of the resulting ApoE ε4 protein are thought to contribute to the failure of perivascular drainage of Aβ (24). Other processes believed to contribute to clearance of Aβ include phagocytosis and further degradation of Aβ occurs by perivascular macrophages, astrocytes and microglia (24,25).

1.2.3. Astrogliosis and reactive microglia

Microglia are macrophages or phagocytes in the brain, predominantly responsible for clearance of Aβ either by phagocytosis or local release of Aβ degrading enzymes. Reactive microglia, immunoglobulins and components of the complement cascade are found accompanying Aβ deposits in AD brain and mouse models of AD (26). After activated by neuronal debris or protein aggregates, microglia first extend their processes to the site of injury, and then migrate to the site and initiate an innate immune response (27).

After receptor ligation, microglia engulfs fibrillary Aβ by phagocytosis, and Aβ enters the endosomal/lysosomal pathway. Soluble Aβ can be directly degraded by a extracellular proteases released by microglia, most importantly neprilysin and insulin

degrading enzyme (27). Binding of Aβ to different receptors results in activation of microglia and production of proinflammatory cytokines and chemokines(27). Chronic activation of microglia can have a deleterious effect rather than beneficial for Aβ clearance. A phenotype of microglia found in conditions of chronic stress (dark microglia) exhibited a highly activated phenotype with strong expression of receptors such as CD11b and TREM2 and extensive encircling of synaptic clefts when the microglia were associated with amyloid deposits (26).

Reactive astrocytes are found surrounding Aβ plaques in a pattern similar to glial scarring (25) in both human AD brain and animal models (27). Similar to microglia, astrocytes can also engulf Aβ by phagocytosis. Phagocytosis of Aβ by astrocytes requires ApoE and astrocyte-dependent lipidation of ApoE increases the capability of microglia to clear Aβ. After exposure to Aβ, astrocytes release Aβ-degrading proteases, such as neprilysin, insulin degrading enzyme, endothelin-converting enzyme and angiotensin-converting enzyme. Furthermore, astrocytes also release cytokines, interleukins, nitric oxide, and other cytotoxic molecules that exacerbate the neuroinflammatory response(27).

In addition to the role of astrocytes in Aβ phagocytosis, astrocytes might also react to early vascular damage. Perivascular drainage occurs in the space located between endothelial cells and astrocytic endfeet, expressing the water channel aquaporin-4 (28). Indeed, astrocytes might become reactive earlier due to a response to vascular damage. Analysis of astrogliosis alongside Aβ deposition by PET scan of presymptomatic autosomal dominant AD carriers showed that fibrillar Aβ deposition was observed 17 years before the expected symptoms onset; at about the same time, astrocytosis was significantly elevated and then steadily declined, whilst Aβ plaque deposition increased with disease progression (29). Similarly, in APPswe transgenic mice, astrocytosis preceded Aβ plaque deposition (30).

1.2.4. Vascular changes

Both AD and VaD demonstrate vascular changes such as cortical microinfarcts, lacunar infarcts in the basal ganglia and cortical petechial microbleeds. Some of these features are also linked to CAA caused by the deposition of a 40 amino acid variant of the Aβ peptide within the blood vessels of the brain, particularly in the posterior parietal and occipital areas of the brain (5).

Cerebral microinfarcts are microscopic lesions of tissue damage caused by occlusion of cerebral blood flow. In contrast, microbleeds are derived from extravasation of cerebral blood flow into the brain parenchyma. Interestingly, post-mortem microinfarcts have been associated with previous microbleeds, as seen in patients' records of antemortem magnetic resonance imaging; this reached an odds ratio (OR) of 8.6. This 8-fold association is thought to be due to the vascular damage and BBB disruption caused by CAA pathology (23).

Both microinfarcts and microbleeds are common findings at post-mortem and are also both associated with cognitive decline regardless of the presence or not of dementia (31,32). Aβ accumulation in the form of CAA can cause vessel fragility and vascular haemorrhagic leakage, but also thickening of the microvasculature and occlusion of the vessel (23). Microinfarcts are caused by CAA, arteriolosclerosis, microemboli and hypoperfusion (31). Cortical microinfarcts but not subcortical microinfarcts are associated with cognitive impairment, in particular amongst individuals with risk factors for dementia (32).

1.3. Clinical presentation of dementia

Dementia due to AD is typically characterised as an insidious decline in cognitive functioning. Initial memory impairment is restricted to learning and short-term memory (i.e. anterograde amnesia). While these changes might be considered initially as benign forgetfulness, which is common in normal aging, memory decline derived

from AD pathology is progressive and irreversible. Early symptoms of AD are associated with selective damage to particular neuroanatomical networks with clinical deficits consistent with the anatomical locus of impact (33,34).

Evolution of the disease is gradual; progression also affects areas of cognition, such as, language, visuospatial, and executive abilities (34). Whilst AD progression is slow and gradual, cognitive deterioration in VaD is often fluctuating or stepwise. The clinical and neuropathological presentation of VaD is diverse and can include multi-infarct dementia, dementia due to infarction of specific brain areas, and subcortical ischemic vascular dementia (33).

1.4. Epidemiology of dementia

Globally, it has been estimated that dementia has a prevalence of 50 million (1,4). AD and other dementias are more common in women than in men; however this has been attributed to the greater longevity of women as there is no significant difference in the incidence between genders. Racial and ethnic differences in the prevalence and incidence of dementia might also exist, yet there is some evidence that indicates that differences based on race and ethnicity do not persist in rigorous analyses (35).

The prevalence of AD rises at exponential rates directly with age as it is the greatest risk factor for developing AD. At age 65 years, 10% of people have AD and it increases to 32% at age 85 years or older (35). In the United States, of people who have AD, 4% are 65 years old or younger, 16% are between 65 and 74 years old, 44% between 75 and 84 years old and 36% 85 years old or older (35). Other risk factors are cerebrovascular disease, diabetes, hypertension, smoking, obesity and dyslipidaemia (4).

In contrast, there are protective factors that reduce the risk of AD. Higher education and occupational accomplishment are proposed to reduce the risk of developing AD. Similarly, a diet rich in omega-3 fatty acids, vegetables, fruits, cereals, legumes and fish

is protective. Along with a Mediterranean-style diet, regular aerobic exercise is associated with a reduced risk for AD (4).

A recent study investigated the relation between a healthy lifestyle and a lower risk for dementia considering the genetic risk in 196 383 individuals. Although the changes in percentages observed in the study are quite low, it should be noted that the study represents an eight year follow up in individuals with an average age of 64 years (36). Nonetheless, this study considers the debate of nature versus nurture. The authors found that an unfavourable lifestyle and a high genetic risk were significantly associated with a higher risk for dementia. Conversely, a favourable lifestyle was associated with a lower risk in individuals with high genetic risk.

1.5. Genetics of dementia

Some studies suggest that AD has a strong genetic component with heritability up to 80% of AD cases (37,38). The rare early-onset (<65 years) familial AD type represents 5% of all AD cases. This autosomal dominantly inherited form of AD is caused by more than 200 mutations in the genes *APP*, *PSEN1* and *PSEN2* (38). The amyloid precursor peptide (APP) is encoded by the *APP* gene. Processing of the amyloid precursor peptide (APP) through the amyloidogenic pathway by β- and ɣ-secretases derives into the production of Aβ, which fibrillises and deposits in the parenchyma as amyloid plaques or in the blood vessels as cerebral amyloid angiopathy (18).

Presenilin (*PSEN1* or *PSEN2*) are part of the ɣ-secretase, which is a complex composed by four different proteins, presenilin, nicastrin, APH-1 (anterior pharynx-defective phenotype) and PEN-2 (presenilin enhancer) (39). Most of the mutations in *APP*, *PSEN1* and *PSEN2* result in an increase in the ratio of Aβ42:Aβ40. This promotes aggregation of Aβ into fibrils and ultimately amyloid plaques. The mutations related to the early onset AD are sufficient but not necessary to cause AD (38).

In contrast, the genetic risk factors for the sporadic form of AD (95% of all cases) are neither sufficient nor necessary to cause AD. Mutations that contribute for the late-onset of AD are thought to work as a complex genetic pattern in conjunction with life exposure events and environmental factors (38). By far, the greatest genetic risk factor for AD and VaD is the presence of the *APOE* ε4 allele, which is also associated with increased risk of CAA and CAA-related haemorrhages, normal aging-related cognitive decline, hyperlipidaemia, hypercholesterolemia, atherosclerosis, cardiovascular and cerebrovascular disorders (40).

In addition to *APOE*, some other genes associated with the sporadic form of AD are *SORL1* (Sortilin Related Receptor 1), *ACE* (Angiotensin converting enzyme), *PICALM* (Phosphatidylinositol Binding Clathrin Assembly Protein), *BIN1* (Bridging Integrator-1), *ABCA7* (ATP-binding cassette sub-family A member 7), *MS4A4* (Membrane-Spanning 4-Domains, Subfamily A, Member 4A), *EPHA1* (Ephrin Receptor A1), *CD33* (Siglec-3), *CLU* (Clusterin), *CD2AP* (CD2-associated protein) and *CR1* (Complement receptor type 1) (37,38,41). Genome wide association studies have also integrated the data from multiple genes that increase the risk for AD. These genes together are involved in cholesterol metabolism and immune response (42).

Similarly, the risk for developing dementia can be also attributed to the simultaneous presence of a number of genes that together potentiate the risk. Using the Polygenic Linkage disequilibrium- Adjusted Risk Score (POLARIS) method, Baker et al confirmed previously known risk genes for developing dementia and found three novel genes. The three genes discovered early this year 2019 were *RORA* (RAR Related Orphan Receptor A), *PPARGC1A* (PPARG Coactivator 1 Alpha), and *ZNF423* (Zinc Finger Protein 423) (119).

1.6. Hypotheses of Alzheimer's disease

The pathogenesis of AD has previously been explained predominantly by two hypotheses: the cholinergic hypothesis and the Aβ cascade hypothesis. The cholinergic

hypothesis describes that the early loss of cholinergic function is a major contributor to the progressive cognitive decline in AD. The cholinergic basal forebrain, which is affected at early stages in AD, is responsible for the main cholinergic input to the hippocampus and its appropriate function is necessary to avoid cognitive impairment. The loss of cholinergic function is caused by reduced synthesis of the neurotransmitter acetylcholine, altered transport or death of cholinergic neurons that lead to impairment of its input to the cortex, thus causing deficits in memory and attention (44).

The Aβ cascade hypothesis states that Aβ accumulates due to an imbalance between its production, degradation or clearance from the brain (43). Aβ deposition in the brain can be in the form of amyloid plaques and most commonly as cerebral amyloid angiopathy. Aβ oligomers can cause synaptic and mitochondrial failure, cellular membrane destabilization, inflammation, hyperphosphorylation of tau and tangle formation (4,43).

Other hypotheses that have been proposed are the vascular hypothesis, where vascular changes are thought to affect clearance of Aβ; the inflammatory hypothesis, where inflammation responds to Aβ accumulation; the mitochondrial cascade hypothesis, where inheritance of genes related to mitochondrial function affects energy utilization; and the oxidative stress hypothesis, where changes in the antioxidant system and higher levels of oxidative damage contribute to the progression of AD (45). Nonetheless, none of these hypotheses is able to fully explain the changes observed in AD pathology.

1.7. An introduction to microRNAs

MicroRNAs (miRNAs) are non-coding RNA sequences with a median length of 22–23 nucleotides. These miRNAs are present under physiological and pathological circumstances (46,47). Deletion of proteins that participate in the biogenesis of miRNAs produce detrimental and non-viable phenotypes, suggesting the essential participation of miRNAs in cellular development and differentiation (48,49).

MiRNAs suppress protein production through the complementary base pairing of the RNA sequences to the target protein mRNA. This is mediated through a seed-pairing region of 6-8 nucleotides at the 5′ end of the miRNA (Figure 1.E). MiRNAs mediate proteome remodeling and also interact with other non-coding RNAs that represent 98% of the genome. Non-coding RNAs include transfer and ribosomal RNA, small nuclear (snRNA) and nucleolar RNA (snoRNA), small interference RNA (siRNA), piwi-interacting RNA (piRNA), and long non-coding RNAs (lncRNA)(49,50).

Figure 1.1 miRNA biogenesis and function.

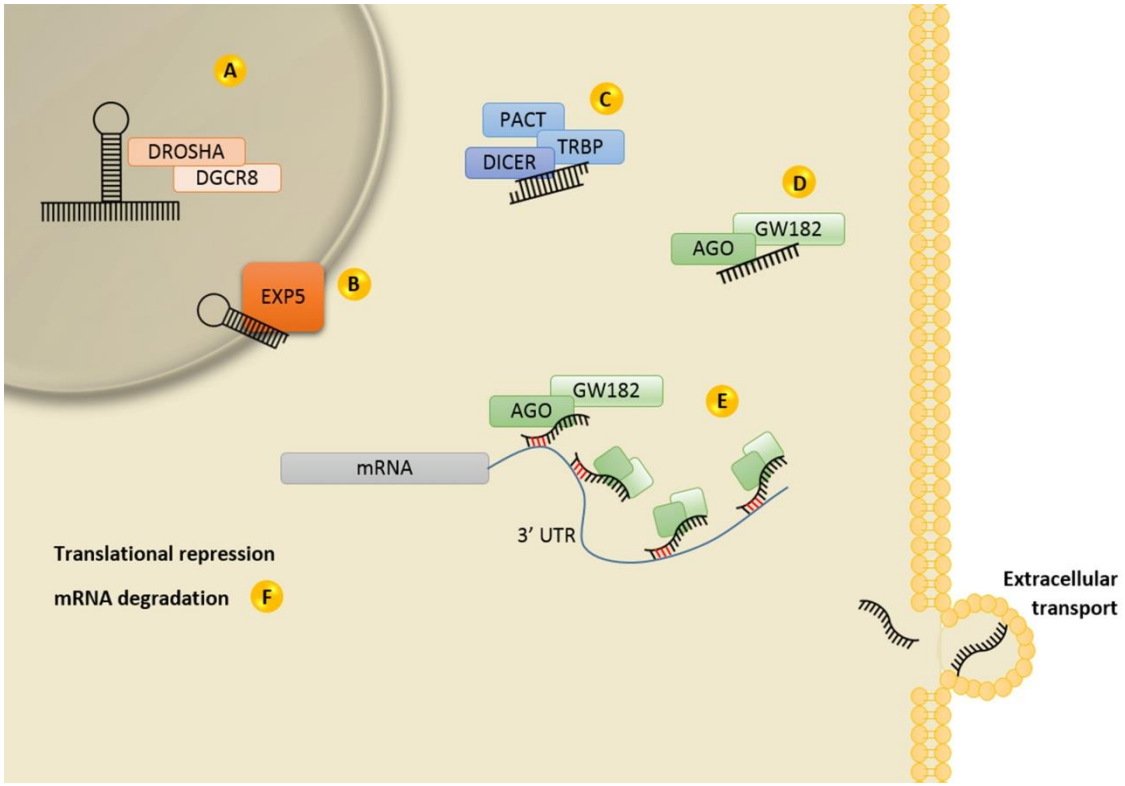

miRNA biogenesis and function (A) Primary miRNAs are cleaved in the nucleus by DROSHA and DGCR8. (B) Once the primary miRNA is cleaved, the nuclear transport receptor exportin 5 binds the pre-miRNA to export it to the cytoplasm. (C) Dicer, TRBP and PACT convert the pre-miRNA into the mature miRNA. (D) The guide strand is

loaded into the RNA-induced silencing complex (RISC). (E) Complementary pairing with the seed region to mRNAs determines target binding and guides argonaute proteins to stop translation. (F) Deadenylase complexes cause destabilization of the transcript and further degradation by RNase activity.

1.7.1 miRNA biogenesis and function

Canonical miRNA biogenesis starts with transcription of the primary miRNA by RNA polymerase II and III (Figure 1.A) (49). The sequences for 52% of human miRNAs are located in intergenic regions, 40% in intronic regions and 8% are in exons (51). Intergenic miRNAs are individually expressed through promoter elements. MiRNAs of the same family, that share the seed region and have the same targets, can be situated in different chromosomes and expressed in diverse conditions.

Intronic and exonic miRNAs that are clustered within 50 kilobases from each other usually have similar expression patterns whilst those spaced further apart tend not to (52). Nonetheless, some exemptions exist to this phenomenon and some miRNAs that are separated by more than 50 kilobases have been found to be highly correlated, which is likely to be a consequence of co-expression (53). The differential localisation and expression of miRNAs is likely to be an evolutionary response to environmental insults and the required response of specific cell functions. In accordance, the higher complexity of the organism, the higher number of miRNAs that are expressed (54–56).

The primary miRNA (Figure 1.A) is cleaved by a nuclear microprocessor complex comprised by the RNase III endoribonuclease DROSHA and its double-stranded RNA-binding protein DGCR8 –DiGeorge Critical Region 8 (57). Cleavage of the primary miRNA by DROSHA/DGCR8 (Figure 1.A) results in a 60 nucleotide stem-loop structure with a 3'-overhang, the pre-miRNA (46,57). In addition, another layer of complexity exists as the primary miRNA can be subject to RNA editing by ADARs (adenosine deaminases acting on RNA) that modify adenosine to inosine producing miRNA isoforms called isomirs (58).

After the primary miRNA is produced, the nuclear transport receptor exportin 5 specifically recognizes the 3'-overhang end and stem-loop of the pre-miRNA and exports it (Figure 1.B) from the nucleus to the cytoplasm (58). In the cytoplasm, the RNase III enzyme Dicer and binding partners, TRBP (trans-activation response RNA binding protein) and PACT (protein activator of RNA-activated protein kinase), recognize the 3′ overhang and cleave the pre-miRNA into the mature miRNA, liberating a nucleotide duplex (approximately 22 nucleotides) with 2 nucleotides protruding at the 3′ end (47,49).

Although TRBP and PACT are not essential to this process, they facilitate Dicer-mediated cleavage by stabilizing it. Unwinding of the duplex leads to the generation of 2 strands, the guide (3′) and passenger (5′) strands. Most of the effects that are attributed to miRNAs are mediated by the 3′ form. In contrast, the 5′ form comprises less than 10% of all miRNA reads in humans (58). The guide strand is loaded into the RNA-induced silencing complex (RISC) and the passenger strand is degraded by RNases. Modifications to the miRNA can also be produced at this step by trimming and capping of the mature miRNA and are called isomirs.

In contrast, non-canonical miRNA biogenesis is independent of DROSHA/DGCR8 processing in the nucleus. If an intron, lacking the sequence of the stem region of a primary miRNA and with the appropriate size to generate a pre-miRNA, it can be exported to the cytoplasm and further processed as a pre-miRNA and generate a mirtron. Alongside mirtrons, other RNA sequences derived from transfer RNA and small nucleolar RNA have been found to be loaded into the RISC complex and act as miRNAs, for example miRNA-451 (48,49,52).

Either as a result of canonical or non-canonical biogenesis, the miRNA guide strand and argonaute proteins (Figure 1.D) form the RISC, a ribonucleoprotein complex that mediates mRNA degradation, destabilization or translational inhibition. Complementary base pairing of the miRNA seed region (2nd to 8th position on the 5′ end) to the mRNA determine target binding and guide argonaute proteins (Figure 1.E)

(51). In humans, only argonaute 2 cleaves target mRNAs (52). MiRNA levels are dependent on argonautes, and as such down or upregulation of argonaute results in diminished or augmented miRNA levels respectively (59).

After the complementary coupling of the miRNA seed region, mRNA can be destabilized by deadenylation, degraded by argonaute 2 RNase activity and protein translation repressed. Argonaute 2, also called eukaryotic translation initiation factor 2C, blocks the action of other translation initiator factors and ribosomal subunits. Accumulation of untranslated mRNA in the cytoplasm permits argonaute 2 to recruit members of the GW182 protein family, enriched in cytoplasmic areas called processing bodies, p-bodies (60).

GW182 binding to argonaute 2 at the 3′ untranslated region (UTR) of the targeted mRNA permits de-adenylase complexes to have access to the poly(A) tail of the mRNA. This leads to de-adenylation, destabilization of the transcript and further degradation by RNase activity (61). The final effect on protein or mRNA levels is determined by where the miRNA binds to the mRNA sequence as 5 diverse types of miRNA binding have been described (47,62). The majority of miRNA effects are produced by binding at the 3′ UTR of the mRNA and further processing as described previously, non-canonical binding sites represent less than 1% (63).

1.8. miRNAs in dementia

More than 100 miRNAs have been reported to be dysregulated in AD (64). Nonetheless that has been considerable inconsistent between studies, likely related to the different methods used to measure miRNAs, as well as biomaterials studied given that miRNA expression is tissue and cell specific. Other contributing factors to some of the consistencies relate to the composition (e.g. diagnoses) and sizes of sample cohorts investigated, particularly since miRNAs may contribute to or be subject to the presence of comorbidities, which would undermine the statistical power and specificity of studies (64,65). Increasing the number of individuals and increasing the specificity of

studies might enable better discrimination between the effects of dysregulated miRNAs, wherein one may be able to more readily differentiate changes in miRNAs between different forms of dementia and in comparison to other neurodegenerative disorders.

1.8.1 Technical complexities related to research of miRNAs

MiRNA detection and measurement with high sensitivity and specificity is challenging. The target sequence is present in the primary transcript, the precursor and the mature miRNA. Furthermore, some miRNAs within the same family differ by just a single nucleotide (66,67). MiRNA measurement can be achieved by different methods that will be examined in detail in Chapter 4. Notably, despite there is yet no specific consensus paper, qRT-PCR has been extensively used and cited as the 'gold standard' measurement tool in miRNA research. This method is argued to provide reliable quantification and specificity using stem-loop primers and is recommended for validation of miRNAs found by next generation sequencing (NGS) (66,68). Furthermore, qRT-PCR which is relatively economical, can be used in conjunction with miRNA binding predicting software (of which a number exist with different scope) when unbiased methods are unavailable.

As alluded to, different miRNA binding predicting software programmes exist, but with different assumptions and parameters and this can yield different findings. By way of example, Zhao et al suggested that TREM2 expression was regulated by miR-34a using independent bioinformatics algorithms (69). However, when analysed by TargetScan and MiRanda miRNA binding predicting software, which examines only the 3' UTR, no binding sites are found. The existence of a site in the rarely used coding region of the transcript could not be excluded. Thus, such software, while helpful in providing supportive data should not be exclusively used and relied upon in isolation.

Another significant challenge is that miRNAs can target numerous proteins and similarly a single protein can be targeted by many miRNAs. Thus it is plausible that

only a combination of miRNAs can feasibly produce a relevant physiological response and so the effects of miRNAs on their targets should be viewed in the context of a whole functional analysis (70). For example, Geekiyanage *et al* proposed that miR-137 regulated serine palmitoyltransferase and in turn Aβ in AD (71). However, examination of miR-137 according to Target Scan shows that this miRNA has 1305 predicted target transcripts while the serine palmitoyltransferase is targeted by 18 miRNAs. Thus, investigation of the total array of target proteins is necessary to provide a functional analysis including assessment of overlapping targets between miRNAs (70).

An additional important aspect is the probability of a miRNA binding to a 3′ UTR mRNA target. Agarwal *et al* established a scoring system based on 14 features (total context score) to permit determination of such a probability, and allows categorization of miRNAs into percentiles (63). This score represents the binding affinity of the miRNA for the mRNA without considering the number of transcripts or miRNAs. Applying this approach to Geekiyanage's paper and attempting to order the 1305 miR-137 target transcripts by the total context score, one sees that the targeting of serine palmitoyltransferase occupies the 291th position (i.e. in the 78th percentile). In other words, miR-137 would have a greater effect on 290 other transcripts thought to have higher binding affinities that it, and thus the effects on serine palmitoyltransferase may relate to those other transcripts. It has to be acknowledged that the number of genes expressed amongst these 1305 candidates will likely vary from tissue to tissue and cell type to cell type, so it is conceivable that serine palmitoyltransferase may indeed rank higher than the 291st position predicted, yet it also highlights that there is still likely to be significant competition between some targets for specific miRNAs.

Finally, the copy number of a miRNA expressed is important. MiR-124 and miR-128 are examples of highly expressed miRNAs (30,000 – 50,000 copies per neuron), whereas other miRNAs have been reported to be very low, e.g. 1 - 2 copies per neuron (52). Thus, in addition to the affinity of miRNAs for different target transcripts, the copy number is likely to have a modifying effect. It is rarely the case that all of these factors

are considered in the numerous studies of miRNAs in dementia to date, and most studies have assumed the rationale of single miRNA-protein interaction effect.

I propose a novel approach for the study of miRNAs in dementia considering multiple targets, previously reported number of copies of miRNAs, and the affinity for their targets in an attempt to overcome proposed caveats in miRNA research, previously described. Given that miRNAs are autocrine, paracrine and endocrine molecules necessary for physiological processes, I hypothesize that dysregulation of certain miRNAs might simultaneously affect different transcripts involved in the development of the two most common forms of dementia, AD and VaD.

Based on this approach, in Chapter 3, I have considered 35 gene transcripts suggested to be involved in some of the 'traditional' neuropathological processes thought to be important in the development of dementia. These transcripts were chosen on the basis of their participation in one or more of the following AD-related processes: amyloid production, transport of amyloid across the blood brain barrier and amyloid degrading enzymes, tau phosphorylation, BBB integrity and the glymphatic system.

In Chapter 6, a similar analysis was performed considering multiple transcripts involved in processes that are less commonly studied. These include transcripts involved in the renin angiotensin system (RAS), as well as vascular dysfunction and hypoxia inducible factors. This second analysis was modified in a way looking for functional or physiological impact. In this analysis, 164 combinations of overlapping targets were examined for miRNAs that were in common, and 14 of which were selected on the assumption that they might have a functional impact on the RAS by influencing vasoconstriction or vasodilation(45).

For both the first and second analyses, I also propose new approaches towards the measurement of these miRNAs and the selection of appropriate calibrators (Chapter 4), as well as an exploratory investigation of their presence in a cell culture model

(Chapter 7) to test the future viability of this as an experimental model for the future study of miRNAs.

While, the approach in this thesis argues the benefits for a broader approach to the study of miRNAs, I have also explored the possibility that single miRNA-protein relations could exist under certain restricted conditions (Chapter 6). For this analysis, I have chosen instances where polymorphisms in single nucleotides exist and have reported to increase the risk for dementia. In this regard, I have investigated if these variants could have a direct effect on miRNAs (e.g. either by creating or abolishing miRNA binding sites), which in turn trigger changes to proteins that could ultimately contribute to the pathogenesis of AD. Analysis of data from genome wide association studies (GWAS) was performed and will be described in Chapter 6.

Chapter 2.- Materials and methods

2.1 Study cohort

Human post-mortem brain tissue from controls, AD and VaD patients was obtained from the Human Tissue Authority (HTA) licensed South West Dementia Brain Bank (SWDBB), Southmead Hospital with approval from the local research ethics committee (REC reference number 08/H0106/28+5) and was handled according to good laboratory practice techniques. The cohort was increased from 66 to 84 cases in the second year of this project and is summarised in Table 2.1.

Diagnostic criteria was based on the National Institute on Aging and Reagan Institute (NIA-RI) consensus that combine the Consortium to Establish a Registry for Alzheimer's Disease (CERAD) score of neuritic plaques and the Braak and Braak (72) staging of neurofibrillary tangles (NFTs). The latter was used to distinguish three AD categories: I) AD with frequent neuritic plaques (CERAD definite) and abundant isocortical NFTs, Braak stage 5 and 6; II) intermediate probability with moderate neuritic plaques (CERAD probable) and NFTs in limbic regions, Braak 3 and 4, and III) low probability associated with infrequent neuritic plaques (CERAD possible) and NFTs restricted to the entorhinal cortex and/or hippocampus, Braak 1 and 2 (5).

The cases were matched where possible for gender, age at death (years) and post-mortem interval delay (hours – i.e. the time between time of death and the freezing of tissue following tissue processing of the brain donation). Cases with a post-mortem interval delay of below 48 hours were preferred; however 7 cases are between 48 and 68 hours. In addition, every effort was made to keep a proportion of cases with and without the presence of *APOE* ε4 allele given its status as a risk factor in AD. However, this was more challenging for controls given the normal lower prevalence of *APOE* ε4 compared to AD cases. Statistical analysis of the demographic data is included in Appendix 1. No statistically significant differences were found with respect to gender

or age. A significant difference was found in post-mortem interval delay between groups, ANOVA F=3.7 and p=0.01. Post hoc analysis with Tukey's test showed a significant difference between the AD group and controls ($p<0.05$) and EAC ($p<0.05$). Similarly, a significant difference was found in the proportion of cases with the presence of an ApoE4 allele, $x^2=30.7$ and $p<0.0001$.

Table 2.1 Demographic information of the cohort.

Diagnosis	Gender (Male/Female)	Age (σ)	PMI (σ)	ApoE4 (No/Yes)	Total
Control	11/13	80 (9.7)	35.4 (16.2)	21/1	24
Early Alzheimer Changes	11/9	85 (6)	36.5 (15)	14/4	20
Alzheimer's Disease	11/11	78 (7.2)	23.7 (13.4)	3/16	22
Vascular Dementia	9/9	83 (7.9)	34.7 (12.3)	9/4	18
Total	42/42	81.2 (8.1)	32.5 (15.1)	47/25	84

Demographic information of the cohort, age in years, post-mortem interval delay (PMI) in hours, standard deviation (σ).

2.2 Brain tissue dissection and homogenisation

Post-mortem brain tissue was dissected from frozen brain slices in collaboration with Dr. Taya Thomas of SWDBB. 300 mg of the posterior cingulate cortex (Brodmann areas 23, 31) was dissected from frozen samples using appropriate sterile techniques. The brain areas were identified with reference to the corpus callosum and ventricles. Tissue was homogenised in a Precellys 24 Homogeniser in 2 separate procedures for isolation of RNA and protein.

2.3 RNA isolation, quantification and standardisation

90-100 mg of frozen tissue were collected in 2 mL homogenate tubes and kept on ice during the process. MiRvana miRNA isolation kit (Ambion™ AM1560) was then used for RNA extraction and isolation. Manufacturer's instructions were followed and precautions were taken against RNAse contamination. Briefly, 900 µl of lysis/binding buffer were placed into the 2 mL homogenate tube on ice and 8 ceramic/silica beads

(2.3 mm) were added. Tissue was homogenised in a Precellys 24 Homogeniser using 2 cycles of 15 seconds bursts at 6,000 rpm. After homogenisation, samples were centrifuged at 4°C for 15 minutes at 12,470 g. 900 µl of supernatant from the homogenate were transferred to another 2 mL homogenate tube and the pellet was kept separate.

MiRNA homogenate additive (90 µl) was combined with the supernatant from the homogenate, then vortexed and stored on ice for 10 minutes. 900 µl of acid-phenol:chloroform was added and vortexed for 40 seconds to mix. The mixture was centrifuged at room temperature for 15 minutes at 12,470 g to separate the solution and the aqueous/upper phase and about 800 µl of the upper phase was transferred to a new tube without disturbing the lower phase.

Elution solution and nuclease free water were heated to 95°C to elute the RNA from the filter at the end of the procedure. 1 mL of 100% ethanol at room temperature was added to the aqueous phase. A filter cartridge was placed into a collection tube (included in the kit) and 700 µl of the lysate/ethanol mixture were pipetted onto the filter and centrifuged at 7,378 g for 15 seconds. The filtrate was discarded, and the procedure repeated with more lysate/ethanol mixture using 700 µl at a time until all the lysate/ethanol mixture passed through the filter.

MiRNA wash solution 1 mixed with ethanol (700 µl) was then applied to the filter cartridge and centrifuged for 10 seconds at 7,378 g. The filtrate from the collection tube was discarded and the filter reinserted into the same tube. 500 µl of the miRNA wash solution 2/3 was then applied and drawn through the filter by centrifugation as previously. Once completed, a further 500 µl of the miRNA wash solution 2/3 was applied, centrifuged, the filter carefully removed to allow the filtrate to be discarded. The filter was again replaced into the centrifuged for a final time for 1 minute at 7,378 g to remove residual fluid from the filter.

The filter cartridge was transferred into a new collection tube (supplied with the kit), 100 µl of pre-heated (95°C) elution solution was applied to the centre of the filter and centrifuged for 30 seconds at 7,378 g to recover the RNA. Similarly, 400 µl of pre-heated RNAse free water (95°C) was applied twice (200 µl each) and centrifuged as previously. The filtrate was collected (approximately 500 µl) and stored at -80°C for further use.

The RNA isolation procedure was modified for extractions from cell culture. After cells were detached and centrifuged, 500 µl of lysis/binding buffer were placed into the 2 mL homogenate tubes on ice and 8 ceramic/silica beads were added. The cells were homogenised and centrifuged as previously described. MiRNA homogenate additive (50 µl) was combined with the homogenate, then vortexed and stored on ice for 10 minutes. 500 µl of acid-phenol:chloroform were added and filtration steps were followed as described for brain tissue.

Quant-iT RiboGreen assay (Invitrogen™ R11490) was used for RNA quantification. Quant-iT RiboGreen RNA reagent was diluted in a 1:200 proportion. For a 96-well plate (Nunc™ F96 MicroWell™ Black Polystyrene Plate 237105) 50 µl of RNA reagent was diluted in 9,950 µl of RNAse free water (working solution A). To prepare the working solution B, 1 mL of 20X Tris EDTA (TE) buffer (200 mM Tris-HCl, 20 mM EDTA, pH 7.5 in DEPC-treated water) was diluted in 19 mL of RNAse free water to obtain a 1:20 dilution.

For the standard, ribosomal RNA standard was diluted in working solution B at different concentrations, the first measurement was based on a 10-fold serial dilution over 4 standards, i.e. 1000, 100, 10 and 1 ng/mL. Given the variability of low concentrations (1 and 10 ng/mL) over different plates, an extra standard was included and concentrations were changed to 100, 200, 400, 700 and 1000 ng/mL for further measurements.

Samples were prepared in triplicate at a 1:100 dilution at first instance i.e. 1 μl of RNA concentrate in 99 μl of RNAse free water. Similarly, the measurements were not reproducible and were highly variable across the initial plates. Thus, 5 μl of the RNA concentrate was diluted in 995 μl of RNAse free water and then different dilutions for RNA quantification were used to compare the reproducibility of the measurements 1:200, 1:100, 1:66.66 and 1:50. The latter two dilutions showed a coefficient of variability between replicates within a plate of 2.1% (σ=1.6) and the variability between plates using standards and sample repeats across all the plates was 2.9% (σ=1.8).

Homogenate samples were therefore diluted 1:66 and 1:50 in RNAse free water on a 96 well plate in triplicate, blanks were comprised of 100 μl of working solution B and standards were diluted as described in working solution B. 100 μl of working solution A was added to each well (samples, blanks and standards) and absorbance was read on a multi-detection plate reader (FLUOstar Optima, BMG Labtech). The absorbance of the standard and samples was measured compared to the blank at 485 nm excitation and 520 nm emission. RNA concentration was determined by the following formula and interpolated to standard values:

$$RNA\ concentration\ \left(\frac{ng}{mL}\right) = \frac{(Absorbance\ of\ sample)(Concentration\ of\ standard)}{Absorbance\ of\ standard}$$

All samples were standardised to a concentration of 400 ng/mL ± 10% in order to ensure 10 ng of RNA was present in 5 μl as recommended for the qRT-PCR test. The amount of RNA needed to reach a 400 ng/mL concentration was calculated according to this formula:

$$RNA\ to\ add\ (\mu l) = \frac{(RNA\ added\ \mu l)(400\ ng/mL)}{RNA\ concentration\ (ng/mL)} - RNA\ added\ (\mu l)$$

Once the RNA was added, all samples were again quantified, and the process was repeated until all samples were at a concentration of 400 ng/mL ± 10%. Where the RNA concentration increased more than calculated, RNAse free water was added and quantification was re-done until the appropriate concentration was obtained.

2.4 Homogenates and protein quantification

100 mg ± 10% of tissue were collected in 2 mL homogenate tubes and kept on ice during the process. Lysis buffer was prepared beforehand as follows: 0.1 M of NaCl, 0.01 M Tris-HCl pH 7.6, 1 μg/mL aprotinin (Sigma A6279), 10% SDS, 1 μM PMSF (Sigma 93482) and 43.42 ml of dH_2O. Proteinase inhibitors (aprotinin and PMSF) were added to the lysis buffer immediately before use and the buffer was added within 30 minutes. 1 mL of lysis buffer and 6 silica beads (2.3 mm) were added and the brain tissue was homogenised in a Precellys 24 Homogeniser using 2 cycles of 15 second bursts at 6,000 rpm. After homogenisation, samples were centrifuged at 4°C for 15 minutes at 12,470 g and the supernatant was separated and stored at -80°C.

Protein quantification was performed using a Coomasie protein assay kit (ThermoFisher 23200). All samples were diluted in a 1:20 proportion in 0.85% NaCl prior to protein quantification. Standards were made using bovine serum albumin and diluted at 9 different concentrations for the standard curve: 2 mg/mL, 1.5 mg/mL, 1 mg/mL, 0.75 mg/mL, 0.5 mg/mL, 0.25 mg/mL, 0.125 mg/mL, 0.025 mg/mL. From each diluted sample and standard, 5 μL were loaded into the plate in triplicate. Then, 250 μL of Coomasie reagent were added to all wells and the plate was read for absorbance on a multi-detection plate reader (Fluostar Optima, BMG Labtech) at 595 nm. Total protein was obtained by extrapolating data from the standard curve and then multiplied by the dilution factor of 20.

2.5 Simulation of postmortem delay

Previously dissected tissue was sourced from two human brain donations with the lowest post-mortem delay (5 hours) were selected, one with a definite diagnosis of AD and the other a non-demented control. From the already dissected tissue, 12 aliquots of 5 mg were taken for assessment of simulated post mortem delay on RNA. Individual aliquots were incubated for 0, 6, 12, 24, 48 or 72 hours at room temperature and at 4°C (intended to simulate with the average time window in which most brain donations

are received post-mortem). After incubation, samples were stored at -80°C. For experimentation, samples were retrieved; 5 mg samples were used for RNA isolation, quantification and standardisation.

2.6 Quantitative real time polymerase chain reaction

Quantitative real time polymerase chain reaction (qRT-PCR) was performed using TaqMan® microRNA assays. First, cDNA was reverse transcribed from total RNA samples using specific miRNA primers (stem-looped reverse transcriptase primers). PCR products were then amplified from cDNA samples and CT (cycle threshold) values established (i.e. the number of cycles required for the signal to cross the threshold for detection). This allows quantitative determination of the number of initial DNA molecules by use of a standard curve of absolute concentration. Each cycle represents a 2-fold change in expression.

First the reverse transcription (RT) reaction was performed to generate cDNA. Each 15 µl RT reaction assay consisted of 7 µl of master mix, 3 µl of RT primer and 5 µl of RNA (10 ng). First, in a 500 µl polypropylene tube the master mix was prepared as follows:

Table 2.2 Constituents of the reverse transcription reaction assay.

Component	Master mix volume (µl)	Volume 24 reactions + 10% (µl)
Nuclease free water	4.16	109.8
10 X RT buffer	1.5	39.6
RNase inhibitor (20 U/µl)	0.19	5
dNTP mix (100 mM total)	0.15	3.96
Multiscribe RT enzyme (50 U/µl)	1	26.4
Total	7 µl	184.8 µl

The master mix was centrifuged briefly without exceeding 295 g or 5 minutes as recommended by manufacturer. Eppendorf® PCR tubes (Sigma Z316121) were labelled and 7 µl of master mix was mixed with 5 µl of RNA. 3 µl of RT primer from each assay (8 assays) was transferred into the corresponding tubes as described.

Figure 2. 1 Example layout of qRT-PCR plates.

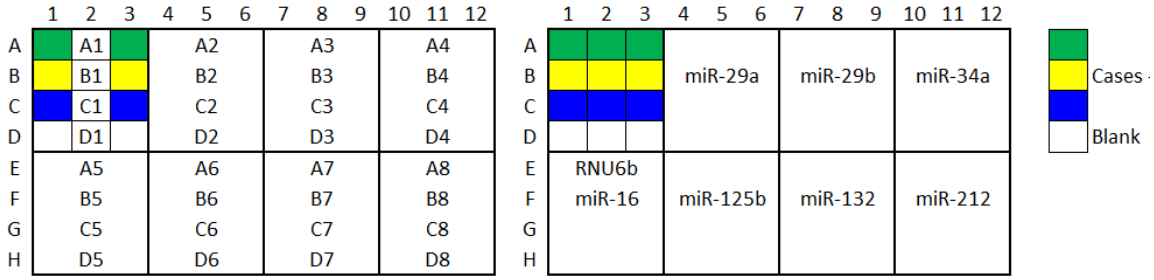

Example layout of qRT-PCR plates, miRNAs included are just examples of the 27 miRNAs investigated in this project.

Tubes were incubated on ice for at least 5 minutes. Using 9,600 emulation mode, the thermal cycler was programmed to hold steps of 30 minutes at 16°C, followed by 30 minutes at 42°C, 5 minutes at 85°C and finishing at 4°C. The reaction volume was set to 15 µl in the thermal cycler, tubes were loaded and the program was run.

For the PCR amplification step of the qRT-PCR, individual reactions were prepared for 32 polypropylene tubes on ice (8 assays for each of 3 cases and a blank-negative control). Volumes were scaled according to the following proportions and number of PCR reactions on a plate.

Table 2. 3 Components of the quantitative polymerase chain reaction.

Component	Volume (µl)	Triplicates + 10%
Nuclease-free water	7.67	25.31
TaqMan 2X Universal PCR master mix, No AmpErase	10	33
TaqMan microRNA assay (20X)	1	3.3
Product from RT reaction (minimum 1:15 dilution)	1.33	4.39
Total	20 µl	66 µl

For all 32 reactions, a total volume of 683.39 µl nuclease free water was transferred into a tube with 891 µl of TaqMan 2X Universal PCR master mix, No AmpErase Uracil-DNA glycosylase (UNG) (Applied Biosystems™ 4326614) were added, mixed and centrifuged. From the PCR master mix/water mixture, 58.3 µl was added into each of the 32 polypropylene tubes. 3.3 µl of each TaqMan microRNA assay was added into the corresponding tube as previously described. Subsequently, 4.4 µl of the RT product

was combined with the master mix and microRNA assay into the corresponding tube and RNAse free water for the blanks. A few samples were assayed in a higher dilution (1:20) but the CT values for miR-132 and miR-212 were higher than the recommended 36 cycles and thus not appropriate for analysis. Therefore, the minimum dilution (as recommended by manufacturer) of 1:15 was used.

Once all of the components for the PCR amplification were combined and mixed, a Fast Optical 96-Well Reaction Plate of 0.1 mL (Applied Biosystems™ 4346907) was prepared by dispensing 20 µl of the complete PCR mix into each of the wells. The plate was sealed with an optical adhesive cover and centrifuged briefly to spin down the content and eliminate air bubbles.

On a Viia7 PCR machine (Applied Biosystems™), the PCR plate was read using the following parameters:

Table 2. 4 PCR program used.

Parameter	Value			
Run mode	9600 emulation (Default)			
Sample volume	20 µl			
Thermal cycling parameters	**Step**	**AmpliTaq Gold enzyme activation**	**PCR**	
			Cycle (40 cycles)	
		HOLD	Denature	Anneal/extend
	Time	10 min	15 sec	60 sec
	Temp (˚C)	95 ˚C	95 ˚C	60 ˚C
Auto increment settings	Accept default values (Default is 0)			
Ramp rate settings	Accept default values (Default is Standard)			
Data collection	Accept default values (Default is 60 ˚C)			

Results from the Viia7 PCR machine were exported to Microsoft Excel and CT values were analysed to calculate variability within triplicates and to select samples to be repeated. Samples were repeated when the standard deviation of triplicates was higher than 0.1. In addition, given the similar sequence of some miRNAs assayed the specificity of the miRNA probes was also confirmed by interchanging probes for different amplimers (e.g. miR-29a quencher dye used with miR-29b RT products and vice versa) where no amplification would be expected.

Table 2. 5 Pre-designed primer sequences and assay IDs of requisition.

Name	Assay ID	Sequence
RNU43	001095	GAACTTATTGACGGGCGGACAGAAACTGTGTGCTG ATTGTCACGTTCTGATT
RNU44	001094	CCTGGATGATGATAGCAAATGCTGACTGAACATGA AGGTCTTAATTAGCTCTAACTGACT
RNU48	001006	GATGACCCCAGGTAACTCTGAGTGTGTCGCTGATG CCATCACCGCAGCGCTCTGACC
RNU6B	001093	CGCAAGGATGACACGCAAATTCGTGAAGCGTTCC ATATTTTT
miR-9-5p	000583	UCUUUGGUUAUCUAGCUGUAUGA
miR-9-3p	002231	AUAAAGCUAGAUAACCGAAAGU
miR-15a-5p	000389	UAGCAGCACAUAAUGGUUUGUG
miR-15b-5p	000390	UAGCAGCACAUCAUGGUUUACA
miR-16-5p	000391	UAGCAGCACGUAAAUAUUGGCG
miR-195-5p	000494	UAGCAGCACAGAAAUAUUGGC
miR-424-5p	000604	CAGCAGCAAUUCAUGUUUUGAA
miR-497-5p	001043	CAGCAGCACACUGUGGUUUGU
miR-29a-3p	002112	UAGCACCAUCUGAAAUCGGUUA
miR-29b-3p	000413	UAGCACCAUUUGAAAUCAGUGUU
miR-29c-3p	000587	UAGCACCAUUUGAAAUCGGUUA
miR-34a-5p	000426	UGGCAGUGUCUUAGCUGGUUGU
miR-34b-5p	000427	UAGGCAGUGUCAUUAGCUGAUUG
miR-34c-5p	000428	AGGCAGUGUAGUUAGCUGAUUGC
miR-449-5p	001030	UGGCAGUGUAUUGUUAGCUGGU
miR-125a-5p	002198	UCCCUGAGACCCUUUAACCUGUGA
miR-125b-5p	000449	UCCCUGAGACCCUAACUUGUGA
miR-132-3p	000457	UAACAGUCUACAGCCAUGGUCG
miR-212-3p	000515	UAACAGUCUCCAGUCACGGCC
miR-17-5p	002308	CAAAGUGCUUACAGUGCAGGUAG
miR-20a-5p	000580	UAAAGUGCUUAUAGUGCAGGUAG
miR-20b-5p	001014	CAAAGUGCUCAUAGUGCAGGUAG

miR-93-5p	001090	CAAAGUGCUGUUCGUGCAGGUAG
miR-106a-5p	002169	AAAAGUGCUUACAGUGCAGGUAG
miR-106b-5p	000442	UAAAGUGCUGACAGUGCAGAU

2.7 Analysis of qPCR using the $2^{(-\Delta\Delta CT)}$ method

The analytical method represents the relative quantity or fold-change of an expression target (in this case target miRNAs) in cases compared to a control, and normalised to a calibrator (i.e. a reference standard marker that is ordinarily thought to not be affected by disease pathology). The average CT of triplicate reactions was obtained for miRNAs of interest and calibrators.

First, the delta CT (ΔCT) value was obtained by subtracting the mean CT of the calibrator from the mean CT of the miRNA of interest. Then, the delta delta CT (ΔΔCT) value was calculated with respect to controls, ΔCT of sample minus ΔCT of controls. The fold change in the expression was calculated as $2^{(-\Delta\Delta CT)}$ (73).

Although this method has been widely used, its creators acknowledged in a subsequent paper that it is not appropriate to use when using patient samples, as compared to experimental treated versus untreated samples (74). In addition, given that the fold change is the result of an exponential equation, 2 to the power of –ΔΔCT (i.e. $2^{-\Delta\Delta CT}$), any value higher than one would increase to infinity and in contrast, any value lower than one would never decrease below zero, therefore it would affect its comparison to the control represented as one.

To validate the statement that any value higher than one would increase towards infinity and in contrast, any value lower than one would never decrease below zero, all $2^{-\Delta\Delta CT}$ values were plotted against ΔΔCT values to create a graph of fold change (Figure 2.2).

Figure 2. 2 Plot of $2^{-\Delta\Delta CT}$ values against ΔΔCT values and corresponding fold values of 2 points.

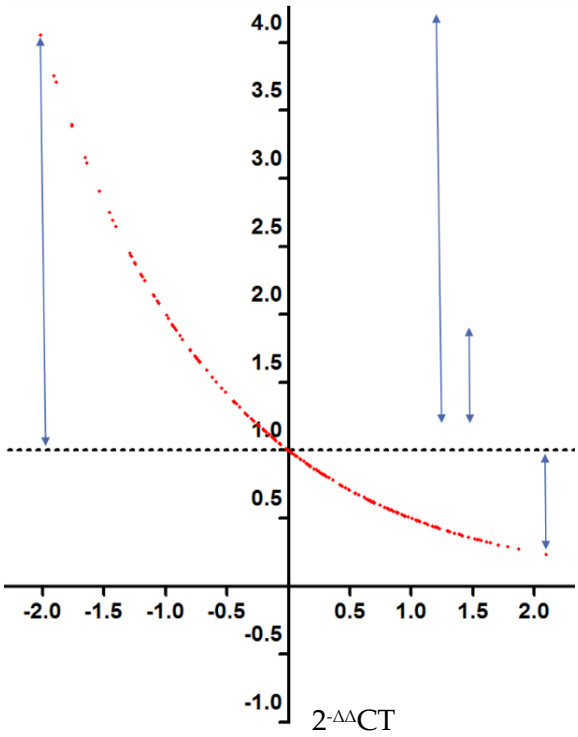

DDCT	RQ (2^{-DDCT})
-2.0202	4.0566
2.0918	0.2345

DDCT	RQ (2^{-DDCT})	Fold
-2.0202	4.0566	(4.05/1) 4.05
2.0918	0.2345	(1/0.23) 4.26

For example, 2 points were selected (blue arrows), both with a ΔΔCT of ±2. Given that one cycle of PCR represents a 2-fold change, both of them should represent a 4-fold change, which is not what the $2^{-\Delta\Delta CT}$ value shows. This exponential equation produces a multiplicative effect rather than an additive effect.

A new method using absolute values is proposed, referred as Delta (Δ) and represented as percentage of difference. By using absolute values, higher and lower values than zero will be exponentially elevated in a similar way (Figure 2.3). However, relative quantities of 2 and 0.5 (original $2^{(-\Delta\Delta CT)}$) would be expressed as +2 rather than +2 and -2. Thus, relative quantity was multiplied by its original symbol (+/-). Then, the percentage of difference with respect to -1 or +1 ($2^{(-\Delta\Delta CT)}$ of zero) was calculated.

$$\text{Delta} = \left(2^{|(\text{CTis}-\text{CTrs})-(\text{CTic}-\text{CTrc})|} - 1\right)\left(-\frac{(\text{CTis}-\text{CTrs})-(\text{CTic}-\text{CTrc})}{|(\text{CTis}-\text{CTrs})-(\text{CTic}-\text{CTrc})|}\right)$$

Where:

Δ = Delta (percentage of difference)

CTic = Cycle threshold of interest in controls

CTrc = Cycle threshold of reference in controls

CTis = Cycle threshold of interest in samples

CTrs = Cycle threshold of reference in samples

Figure 2. 3 Resulting values using the new formula termed Δ.

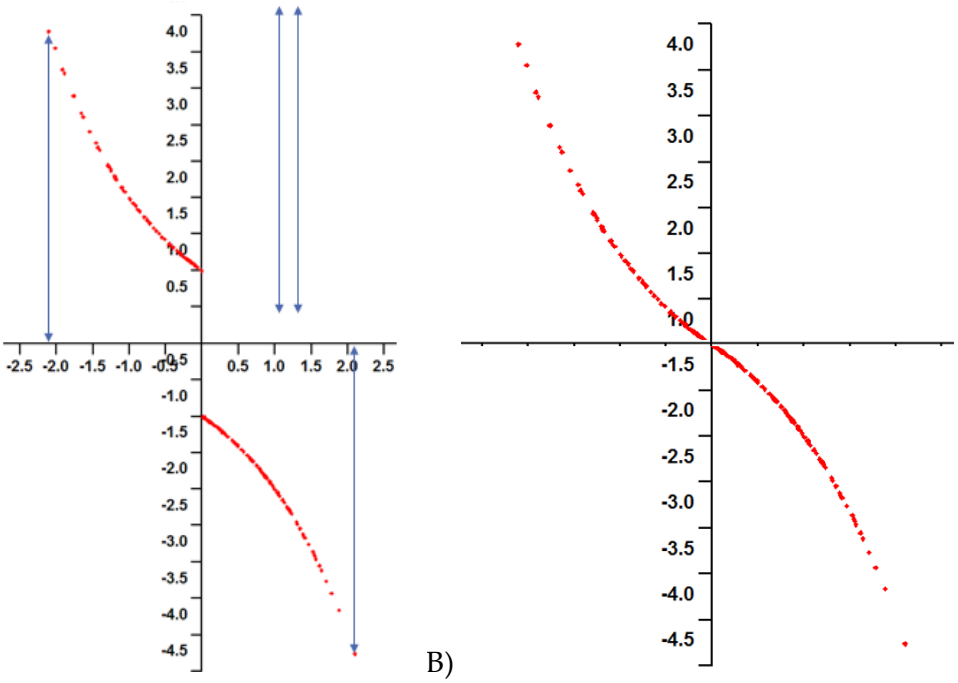

A) B)

Resulting values using the new formula termed Δ. By using absolute values, values higher and lower than zero are proportional but it creates a disjunction from -1 to +1 (A). By subtracting 1 and presenting the data as a percentage of difference, results are continuous with no points of inflection or disjunction (B).

Furthermore, a new formula is proposed to replace the use of geometric mean when calculating the reference CT from different calibrator genes. Vandesompele *et al* proposed the use of the geometric mean of calibrator genes for normalization of PCR results (75). However, the geometric mean does not consider some principles of PCR. First, the geometric mean does not consider that values derived from PCR are based on log2. Second, CT values obtained from PCR should be interpreted in an inverse manner, i.e. high values represent low quantities and vice versa. When using the

geometric mean, high values will have a contrary effect on the result of the geometric mean. The geometric mean might be applicable when a high number of CT values are used, however when using a few of them, high values can affect the result. The formula of geometric mean and a new formula are presented.

$$Geometric\ mean = \sqrt[n]{a_1 a_2 a_3 \dots a_n}$$

A formula is proposed considering the logarithmical base of the PCR method and the total cycles of the reaction.

$$Average\ CT\ of\ calibrator\ genes = 40 - \log_2\left(\frac{2^{40-CT1} + 2^{40-CT2} + \dots + 2^{40-CTn}}{n}\right)$$

Where:

CT= Cycle threshold of calibrator genes

n = Number of calibrator genes

2.8 miRNA repositories (miRbase, mirgeneDB and miRbase tracker)

Training was undertaken at the European Bioinformatics Institute with respect to data repositories available for research into miRNAs. Since miRNAs are still an emerging field, with hundreds still being discovered, it is therefore necessary to distinguish between authentic miRNA sequences from short RNA sequences, which are likely to be products of RNA degradation. Different online repositories exist to capture information on miRNA and each focuses on specific criteria. MiRbase and mirgeneDB were used in this project as the chosen miRNA repositories, whilst miRbase tracker was used for comparison and tracking of changes in miRNA nomenclature and recognition of miRNA sequences.

MiRbase (http://www.mirbase.org) is a widely used resource for miRNA cataloguing and nomenclature. It allows browsing and searching of miRNA sequences. In order to be recognized as a high confidence miRNA, a locus must meet the following criteria (76):

1. At least 10 reads must map to the two mature miRNAs derived from their precursor with no mismatches.
2. The most abundant reads must match the miRNA duplex with 0–4 nucleotides overhanging at the 3′ end.
3. At least 50% of reads of both mature miRNAs must have the same 5′ end.
4. The predicted hairpin structure (miRNA precursor) must have a folding free energy of <−0.2 kcal/mol/nt.
5. At least 60% of the bases in the mature sequences must be paired in the predicted hairpin structure.

Some changes have been made to these criteria over time. For instance, the first criteria in 2003 required a miRNA gene to be phylogenetically conserved; now it is known that different organisms present a wide range of miRNAs. However, only 20% of human miRNAs passed all these criteria when it was formulated in 2014.

Fromm *et al* (77) developed mirgeneDB (http://mirgenedb.org/) with different criteria for inclusion of *bona fide* miRNAs. Like miRbase, mirgeneDB allows browsing and searching of miRNAs but also includes the option to search for seed regions of miRNAs. To be recognized as a high confidence miRNA by mirgeneDB, a locus must meet the following criteria:

1. An RNA stem-loop consisting of two mature miRNAs with a median length of 22–23 nucleotides (range size from 20 - 26 nucleotides).
2. Complementary base pairing of both mature miRNAs in at least 16 nucleotides separated by a single-stranded loop of 8-40 nucleotides.

An average precursor miRNA forms a 22–23-nt duplex with 2-nucleotide offsets, a loop of 16-nucleotides in average and complementarity between the two mature miRNAs.

Although Fromm *et al* suggested that utilization of miRbase is problematic for both functional and evolutionary studies; both repositories were used.

Finally, miRbase tracker (http://www.mirbasetracker.org/) was used for tracking of changes made to miRNA annotation and as a comparative point for both repositories. miRbasetracker allows search of historical and current miRNA annotation in miRbase.

2.9 Genomic mapping (RNA central)

The online resource RNA central (https://rnacentral.org/) from the European Bioinformatics Institute and the Genome Browser (https://genome.ucsc.edu/) from the University of California Santa Cruz were used for verification of miRNA sequences, validation of binding sites and corroboration of single nucleotide polymorphisms (SNP rs6857 in Chapter 6). RNA central is a collection of 28 databases of non-coding RNA sequences, thus allowing a search and browse of RNA sequences and mapping to their genome localization.

2.10 miRNA-target predicting software

TargetScan (www.targetscan.org) and miRanda (www.microrna.org) are software that allow users to obtain predicted miRNAs binding at those transcripts and miRNAs with the highest number of overlapping transcripts were included. Official international gene symbol of transcripts and miRbase nomenclature of miRNAs are used in this thesis. miRNA selection was performed in 2 different approaches that are described in more detail in Chapters 3 and 6.

2.11 GWAS Catalog NHGRI-EBI

GWAS Catalog National Human Genome Research Institute (NHGRI) Catalog of Published Genome-Wide Association Studies (GWAS) European Molecular Biology

Laboratory-European Bioinformatics Institute (EMBL-EBI) (NHGRI-EBI). Training was undertaken from online courses from the European Bioinformatics Institute. The GWAS catalogue is a publicly available, manually curated resource of published GWAS and association results (7). For inclusion in the catalogue, studies and associations must meet certain criteria. Studies must include an array-based GWAS and analysis of >100 000 single nucleotide polymorphisms (SNPs) with genome-wide coverage and SNP-trait associations must have a p-value $<1\times10^{-5}$. The database was retrieved using the words ''Alzheimer'', ''Alzheimer's disease'', ''Alzheimer's'', ''vascular dementia'' and ''vascular cognitive impairment''. Initially, all SNP's reported were scrutinised, however, given the constraints on time, it was decided that there should be a concentration on 3'UTRs.

2.12 R software

Training was undertaken from an introductory course on R at the University of Bristol and subsequently using online courses from Johns Hopkins University. R is a free software and computational language developed for statistical computing and graphics. It also allows other functions such as data handling and storage, a set of operators for calculations, tools for data analysis, graphical facilities for data analysis and display, and programming language.

2.13 Software for analysis of target proteins (DAVID and PANTHER)

The Database for Annotation, Visualization and Integrated Discovery (DAVID) software (www.david.ncifcrf.gov/) version 6.8 was used for analysis of predicted target proteins of the selected miRNAs. This most recent version of DAVID software provides a comprehensive set of functional annotation tools to enable the understanding of the biological function behind a large list of genes. It facilitates discovery of enriched functional-related gene groups, by making clusters redundant annotation terms and correlating with gene ontology or BioCarta & Kyoto

Encyclopedia of Genes and Genomes (KEGG) pathway maps (78). Disease, gene ontology and pathways were considered for analysis.

Use of DAVID software in this study was carried out by initially uploading a list of predicted targets using the official internationally agreed gene symbol nomenclature for each target gene. The background was selected to be exclusive for genes specific for Homo sapiens. DAVID uses 5 predefined levels of stringency (lowest, low, medium, high and highest) for user selection. The default setting is medium; which was changed to the highest in this work. A higher level specificity (high stringency) is recommended for tight, clean and reduced number of clusters. For wider scope and larger number of clusters stringency can be lowered.

The Protein ANalysis THrough Evolutionary Relationships (PANTHER) software (www.pantherdb.org/) allows to analyse gene lists combining gene function, ontology, pathways and statistical analysis tools. The last version of PANTHER (v. 14) includes enrichment analysis using pathway classifications similar to KEGG pathway maps used in DAVID software (79).

Similar to DAVID software, lists of predicted target genes were uploaded using their official gene symbols, with selection of organism as Homo sapiens. Analysis was then performed using statistical overrepresentation test with PANTHER pathways, Fisher's exact test and Bonferroni correction for multiple testing.

2.14 Western blotting

Western blotting was used for measurement of the proteins RORA (retinoic acid related orphan receptor alpha) and MAP2 (microtubule associated protein 2) covered in Chapter 3 and 5. Running buffer and sample buffer were prepared beforehand. A dilution of 50 ml of 10x running buffer (30.3 g 0.25M Tris Base, 144 g 1.92M glycine, 900 ml distilled water and 10 g sodium dodecylsulfate (SDS)) was diluted in 450 ml of distilled water. Samples from homogenates were prepared with a concentration of 30

μg total protein per well and were incubated at 95°C for 5 minutes. Recombinant proteins for MAP2 and RORA were prepared at concentrations of 10, 1, 0.1 and 0.01 ng.

A Bio-Rad gel was assembled (4-20% Mini-PROTEAN TGX Gel, 10 well, 8.6 x 6.7 cm) for sample loading at 150V for 1 hour. After electrophoresis was complete, the gel was removed from the assembled cassette and placed into blotting buffer prepared as follows: 200 ml methanol, 700 ml distilled water and 100 ml of 10x blotting buffer (30.3 g 0.25M Tris Base, 144 g 1.92M glycine, 1 L distilled water) for 10-20 minutes prior to blot assembly. Concurrently, a nitrocellulose membrane (8.6 x 6.7 cm) and 2 filter papers (10 x 7.5 cm) were cut and soaked in blotting buffer for 15-20 minutes.

The gel sandwich cassette was assembled in the following order starting at the black side of the cassette: pre-wetted fibre pad, a filter paper on the base of the cassette, followed by the gel and nitrocellulose membrane, then a second filter paper and finally a second fibre pad at the clear side of the cassette. Any air bubbles between the layers were removed with a roller. Once the cassette was assembled, it was closed and placed into the tank with an ice pack, magnetic stir bar and the tank was filled with blotting buffer (as described above). The tank assembly was placed on a magnetic stirrer and connected to a power supply to blot for 1 hour at 100V. After transfer, the cassette was disassembled, and the membrane was placed in Tris-buffered saline with 0.05% Tween 20 (TTBS).

The membrane was blocked in blocking buffer (10% milk powder in TTBS) for 1 hour at room temperature prior to antibody incubation, the membrane was subsequently washed 3 times for 10 minutes in TTBS at room temperature. Antibody buffer was prepared using 5% milk powder in TTBS and antibodies were diluted in this at the concentrations shown in Table 2.6. The membrane was incubated with the antibody, overnight at 4°C.

Table 2. 6 Antibodies, requisition ID's, concentration and dilutions used.

Antibody	Concentration	Dilutions
Monoclonal mouse antibody IgG2A to human ROR alpha (RORA) R&D Cat no. PP-H3910-00	1 µg/µL	1:2000 1:1000
Polyclonal rabbit antibody to human RORA Abcam Cat no. ab70061	1 µg/µL	1:500
Monoclonal mouse antibody [MT-08] to (cow/human) MAP2 Abcam Cat no. ab118898	1 µg/µL	1:2000
Monoclonal mouse antibody to purified recombinant fragment of human MAP2 (AA: 24-123) expressed in E. Coli Novus Bio Cat no. NBP2-37734	1 µg/µL	1:500

The following day, the membrane was washed and incubated with a secondary antibody (anti-rabbit IgG–Peroxidase antibody produced in goat (Sigma Aldrich, A0545-1 mL)) at a concentration of 1:5000 and incubated for 1 hour at room temperature on shaker. After incubation the membrane was washed 6 times for 10 minutes each in TTBS at room temperature on shaker.

The membrane was incubated in Immobilon chemiluminescence horse radish peroxidase (HRP) substrate (Millipore, WBKL30500), a mixture of equal volumes of luminol reagent and peroxide solution in a clean container for 5 minutes. Finally, the membrane was placed in ChemiDoc XRS+ machine (BioRad) and an image of the membrane was obtained using Image Lab 5.0 software.

2.15 Cell culture

Cell culture work is undertaken in Chapter 7 to evaluate the suitability of cell culture for the study of miRNAs in dementia. Protocols for handling, subculture routine and culture media were obtained from the European Collection of Authenticated Cell Cultures (ECACC), a Culture Collection of Public Health England (PHE). Training was supervised by Mrs. Saranna Chipper-Keating (Translational Health Sciences, University of Bristol). Frozen SH-SY5Y cells were (ECACC 94030304) at passage 12 and were resuscitated in a water bath for 1 minute at 37°C until thawed.

Culture medium was prepared beforehand as follows, Ham's F12 (Sigma-Aldrich® N4888) : Eagle's Minimum Essential Medium (MEM) (Sigma-Aldrich® M2279) (1:1) plus 2mM Glutamine (Sigma-Aldrich® G7513), 1% Non Essential Amino Acids (NEAA) (Sigma-Aldrich® M7145) and 15% Foetal Bovine Serum (FBS) (Gibco® A31608-01). Resuscitated cells were incorporated into 5 ml of prepared culture medium and resuspended. A further 5 ml of culture medium were added to the resuspended cells in the solution and placed into a 75 cm^2 cell culture flask (Sigma-Aldrich® CLS3290) in the incubator at 37°C and 5% CO_2.

Subculture was performed at a confluency of 70-80% and cells were detached using trypsin-ethylenediaminetetraacetic acid (EDTA) (Lonza® CC-5012) and re-seeded at a concentration of 1,000 - 10,000 cells/cm^2. Once the first flask reached the determined confluency, 2 further flasks were seeded from this, and the rest of the cells were stored in -150 °C freezer in aliquots using DMSO (Sigma-Aldrich® D2650). Aliquots were labelled with the number of cells, passage, cell line and date of storage.

Cell counting was performed using a haemocytometer and 0.4% trypan blue stain in PBS. 100 µl of resuspended cells were combined with 100 µl of trypan blue (Sigma T8154 0.4%). An inverted microscope was used to observe and count cells, live cells appearance was bright and colourless whilst dead cells stained blue.

Retinoic acid (Sigma-Aldrich® R2625) was used at a concentration of 10 μM in culture media prepared with 98% Neurobasal® medium (Gibco® 21103-049) and 2% B27® supplement (Gibco® 17504-044). Treatment with retinoic acid was for 9 days with a change of medium on days 1, 4 and 7. Both treated and untreated cells were harvested at day 10. The number of samples considered for analysis are six samples for untreated cells and six samples for treated cells.

2.16 Statistical package Graph Pad Prism

Data was analysed with GraphPad Prism software version 5 for descriptive statistics (Shapiro Wilk and D'Agostino & Pearson omnibus normality tests) and based on the characteristics of the variables, unpaired t test and Mann-Whitney tests were performed for comparison of two groups and ANOVA and Kruskal Wallis for more than two groups. Correction for multiple testing was performed exclusively for pathway analysis in DAVID and PANTHER tables using the Benjamini-Hochberg procedure.

Chapter 3.- miRNAs related to classical histopathological hallmarks of Alzheimer's disease

3.1. Introduction

MiRNAs are posttranscriptional regulators of gene expression by repressing protein synthesis. Changes in several proteins have been implicated in the development of AD. Thus, proteins involved in processes relevant in AD pathology and their associated miRNAs are a primary research question in this project. miRNAs are able to target hundreds of proteins. This property can be used as an advantage in such a way that as increasing the number of proteins, miRNAs in common would be restricted. In other words, the number of miRNAs in common for a set of proteins will be lower than the number of miRNAs of each protein within the set.

In this Chapter, an investigation of miRNAs associated with 35 proteins (see Table 3.1) that have been proposed to be relevant in dementia are presented. The proteins described are mentioned in relation to biochemical processes they are linked to and with their corresponding gene name.

3.1. Alzheimer's disease-related proteins and their associated miRNAs

3.1.1. Amyloid and its production

Amyloid plaques and cerebral amyloid angiopathy (CAA) are caused by deposits of two isoforms of amyloid beta (Aβ) of different lengths (Aβ42 and Aβ40 respectively). Cleavage and processing of the amyloid precursor peptide (APP) can be performed either by α-secretase or by β-secretase (BACE), resulting in the secretion of two large soluble ectodomains, APPsα and APPsβ, respectively. α-secretases are members of the ADAM (A Disintegrin And Metalloprotease) family, including ADAM9, ADAM10

(Table 3.1) and ADAM17. Reduced levels of APPsα and ADAM10 in cerebrospinal fluid (CSF) are characteristic of AD (80). Similarly, β-secretase is comprised of either BACE1 or BACE2 (included in Table 3.1) which cleave APP to yield the precursor to Aβ peptide formation as part of the amyloidogenic pathway (80).

The production of APPsα is part of a non-amyloidogenic pathway, with growth promoting and neurotrophic properties. APPsβ is thought to have opposing effects, and subsequent cleavage of APPsβ by ɣ-secretase results in the production of Aβ, p3, and the APP intracellular domain (AICD) (80). ɣ-secretase is a complex composed by four different proteins, presenilin PSEN1 (included in Table 3.1) or PSEN2, nicastrin, APH-1 (anterior pharynx-defective phenotype) and PEN-2 (presenilin enhancer) (39). The site of cleavage on APPsβ by ɣ-secretase determines the length of resultant neurotoxic Aβ isoforms to complete the amyloidogenic pathway (19).

Presenilins are also important for development, differentiation of immune cells, intestinal goblet cells, and others by regulating Notch signalling (39). Some studies have shown that mutations in Presenilin 1 (PSEN1) and Presenilin 2 (PSEN2), which cause familial AD, can reduce Notch signalling (81). However, other studies have found that Notch1 expression is increased in sporadic AD (81). Dysregulation of Notch1 might play a role in AD (*NOTCH1* is included in Table 3.1) (81).

3.1.2. ApoE, ApoE receptors and lipidation of Aβ

Aβ metabolism is greatly influenced by apolipoprotein E (ApoE) (82). ApoE is a component of lipoprotein particles acting as a ligand in receptor-mediated endocytosis of lipoprotein particles, thus supporting lipid transport and injury repair in the brain.
The gene that encodes for ApoE (APOE) has polymorphic alleles (ε2, ε3 and ε4) that give rise to the ApoE isoforms ε2, ε3 and ε4 respectively. *APOE* ε4 is the greatest genetic risk factor for development of sporadic AD and VaD and will be covered in Chapter 6. The presence of the ApoE ε4 allele is also linked with increased risk of CAA and age-related cognitive decline in normal ageing (40).

ApoE is expressed throughout different organs in the body with a higher expression in the liver and the brain, mainly in astrocytes and to some extent in microglia (40,83), where ApoE is the most abundant lipoprotein and where it is secreted by astrocytes in high density lipoprotein (HDL) molecules (82). A related protein that works in conjunction with ApoE is the ATP Binding Cassette 1 protein (ABCA1 – Table 3.1). This is a cholesterol transporter protein that mediates the transport of phospholipids, cholesterol and is involved in the biogenesis of HDL (84).

Once produced by astrocytes, ApoE is lipidated by ABCA1 to form lipoprotein particles that promotes the binding of soluble Aβ in an allele-dependent manner and also in relation to lipidated levels of ApoE. ApoE E2 has the highest Aβ-binding efficiency, followed by E3 and lastly by E4. ApoE lipidation also appears to influence Aβ transport and Aβ plaque formation. When APP transgenic mice were crossed with *ABCA1* knockout mice, ApoE lipidation was decreased whilst amyloid deposition was increased (83).

ApoE is endocytosed into different cell types within the brain and by various members of the low density lipoprotein (LDL) receptor family, including LDLR, SORL1 and LRP1 (Table 3.1) (83). The low density lipoprotein receptor (LDLR) is a cell surface receptor that controls the amount of ApoE in the brain but may also be important in relation to Aβ. Basak et al found that overexpression of LDLR in cell cultured primary astrocytes enabled Aβ transport into lysosomes and increased intracellular Aβ degradation whereas deletion of LDLR caused a decrease in Aβ uptake (85).

Another ApoE receptor is the Sortilin Related Receptor 1 (SORL1 – Table 3.1) is a neuronal endocytic receptor of ApoE, which also mediates cellular uptake of Aβ in an ApoE isoform dependant manner (86). SORL1 also participates in the processing and trafficking of APP; retaining it to prevent Aβ production. Notably SORL1 and APP are expressed in nearly equimolar ratio (83). SORL1 levels have been found to be significantly decreased in AD brain with a positive correlation with Aβ accumulation (87). In agreement with this, a knockout mouse model for SORL1 showed higher

concentrations of Aβ (83). Inherited variants of *SORL1* have been associated with a higher risk to develop AD (83). Shen et al investigated the effects of genetic variants of *APOE* and *SORL1* on hippocampal resting-state functional connectivity (88). *APOE ε4* patients had decreased hippocampal connectivity with the precuneus/posterior cingulate cortex and subgenual anterior cingulate cortex. Risk associated G-allele carriers of SORL1 showed decreased connectivity between the hippocampus and middle temporal gyrus (88). Andersen et al suggested that reduced levels of SORL1 in AD is probably due to loss of protection of APP from processing (89), however, as some studies show, the loss of APP could similarly be suggested to be due to loss of SORL1 and thus the nature of the interaction between both still needs further clarification.

Similarly to LDLR, the Lipoprotein Receptor-related Protein 1 (LRP1 – Table 3.1) is a cell surface receptor that binds soluble Aβ and transports it from the interstitial fluid into the bloodstream at the abluminal side of the blood brain barrier (82). There is some evidence showing that LRP1 is reduced in brain capillaries of AD brains (83). Halliday et al found reduced LRP1 levels in pericytes and endothelial cells from AD brains (90). They also found a positive correlation between pericyte coverage and LRP1 levels. A conditional knockdown mouse model for LRP1 showed that reduction of LRP1 in astrocytes resulted in an increase in Aβ deposition by affecting Aβ clearance with no effect on Aβ production (91).

Whilst the efflux of cerebral Aβ into the circulation is thought to be performed mostly by LRP1, the Receptor for Advanced Glycation End products (RAGE – Table 3.1) also plays an important opposing role in Aβ clearance at the BBB. RAGE works as an important transporter by regulating influx of peripheral Aβ into the brain (92). RAGE is a cell surface receptor that binds to Aβ and increased levels of RAGE have been found in endothelial cells from AD brain and mice models (93). Donahue et al observed a stronger expression of RAGE in neurons compared to vascular cells in non-demented elderly; however, neuronal RAGE was significantly decreased in AD cases with an unexpected stronger RAGE immunoreactivity in vascular cells (94).

Other ApoE receptor members of the LDLR family, such as ApoER2 and VLDLR, are also thought to be involved in Aβ clearance and tau phosphorylation. ApoER2 and VLDLR are also receptors for Reelin (RELN – Table 3.1) (83). RELN is a signalling protein important in neurodevelopment, neuronal connectivity and synaptic function. RELN induces the cleavage of ApoER2 through processing of α- and γ-secretases, however, there is contradictory evidence about RELN levels in AD brain (95). Repression of *RELN*, *ApoER2* or *VLDLR* in mice was associated with reduced phosphorylation of the Glycogen Synthase Kinase 3β (GSK3B), which leads to disinhibition of this enzyme and subsequent hyperphosphorylation of tau (83).

Similar to LRP1, other important proteins at the BBB are the platelet-derived growth factor B (PDGFB), its receptors (PDGFRA and PDGFRB) and aquaporin 4 (AQP4 – all in Table 3.1). The platelet-derived growth factor (PDGF) family is composed of four ligands (A, B, C and D) that bind to two receptors (PDGFR-α and PDGFR-β). PDGF receptors are tyrosine kinases that can form three different conformations of dimers: $\alpha\alpha$, ββ and $\alpha\beta$ (96).

Platelet-derived growth factor B (PDGFB) derived from endothelial cells interacts with PDGFRB in pericytes, inducing pericyte recruitment. Pericytes and the end-feet of astrocytes are essential for a stable and impermeable BBB. PDGFB binds to heparan sulfate proteoglycans in the basement membrane, and regulates pericyte proliferation, migration, and recruitment to the vessel wall through PDGFRB in pericytes (97).

As mentioned, the end-feet of astrocytes, which express AQP4, contribute to the stability of the BBB. The glymphatic system allows clearance of interstitial solutes, including Aβ. Within the glymphatic system, the CSF flows through para-arterial spaces, and is then transported into the interstitial space by astrocytic AQP4 to be drained into the para-venous spaces, and finally diffuses into the subarachnoid CSF or enters the bloodstream through the vasculature (98). An AQP4 knockout mice model showed a reduction in the clearance of Aβ by approximately 55% (99). Furthermore,

the association of function with pericytes is itself notable given the increasing evidence of pericyte loss in AD (100).

In addition to Aβ clearance through the glymphatic system, phagocytosis and further degradation of Aβ occurs by astrocytes, macrophages and microglia (24,25). Toll-like receptors (TLRs) expressed in microglia are necessary for recognition of the immune response and further phagocytosis. Aβ binds to the TLR4 co-receptor CD14 (Table 3.1) and can induce microglia to produce nitric oxide, interleukin 6, and other inflammatory factors (25). Repression of CD14 in microglia impedes phagocytosis in response to Aβ, increases Aβ deposition and causes cognitive impairment (25).

Microglia interact with other cell types, including neurons through ligand–receptor pairs that support their interaction, including CD200 and its receptor CD200R. CD200 is expressed on several cell types including neurons whereas the CD200 receptor is particularly expressed in cells of the myeloid lineage, such as microglia and macrophages (101). Notably, Walker et al found a reduction in the levels of CD200 and CD200R in AD brain but the neuronal expression of CD200 was heterogeneous (102).

3.1.3. Proteolytic degradation of amyloid

Aβ clearance, besides being removed by phagocytosis, is due to proteolytic degradation that is a substantial determinant of cerebral Aβ levels (103). These include neprilysin (MME), endothelin converting enzyme 1/2 (ECE1, ECE2), angiotensin converting enzyme 1/2 (ACE1, ACE2), insulin degrading enzyme (IDE), several extracellular matrix metalloproteases (including MMP2, MMP14) and the extracellular matrix metalloproteinase inducer EMMPRIN (CD147) (all in Table 3.1).

Indeed there are more than 20 proteases reported to degrade Aβ, a number still to be fully elucidated and many with differing affinities for Aβ, according to different optimal pH conditions for function, as well as regional, cellular, and subcellular localizations. A number of these enzymes have been postulated as important

determinants of AD pathology, yet some Aβ degrading enzymes work cooperatively with each other. Some of these enzymes (e.g. ACE1, ACE2, ECE1, ECE2, and NEP) all have important functions in the production or cleavage of vasoactive peptides, and thus blood pressure regulation, which is in itself an important factor and pathological hallmark of AD. This collection of enzymes also works alongside other catabolic mechanisms to eliminate Aβ, and thus collectively influence total Aβ levels (103).

3.1.4. Tau phosphorylation

In addition to amyloid plaques and CAA; neurofibrillary tangles are a classical hallmark of AD. Neurofibrillary tangles are composed of hyperphosphorylated tau protein (MAPT in Table 3.1). The normal phosphorylation state of a protein occurs from the interplay between kinases and phosphatases. Thus imbalance between these systems can result in hyperphosphorylation of tau. Glycogen synthase kinase 3 (GSK3) proteins are serine/threonine kinases that function as regulatory enzymes in glucose metabolism. There are two isoforms, GSK3A and GSK3β (GSK3B in Table 3.1) (104).

The GSK3β isoform is abundant in the central nervous system and is able to phosphorylate tau. GSK3β phosphorylates tau in serine/threonine residues and its overactivity contributes to Aβ production and Aβ-mediated neuronal death (105). Similar to GSK3β, the Mitogen Activated Protein Kinase 1 (MAPK1) is also thought to play a role in tau hyperphosphorylation and has been found to be increased in the hippocampus of AD brains (106).

Protein phosphatase 2A (PP2A) enzyme family is composed of 96 serine/threonine phosphatases. This large family of enzymes is involved in tau phosphorylation as these enzymes are responsible for the majority of brain serine/threonine phosphatase activity, where tau phosphorylation occurs at serine/threonine residues. PP2A is a heterotrimeric complex composed by the catalytic C subunit (PPP2CA in Table 3.1), a scaffolding A subunit (PPP2R1A in Table 3.1) and a regulatory B subunit (107).

Changes in PP2A regulators and PP2A catalytic activity, PP2A methylation and/or phosphorylation, have been reported in AD (107). PP2A catalytic activity is regulated by endogenous ligands, such as metal cations, ceramides and polyamines that enhance the activity of PP2A enzymes. In contrast, PP2A phosphatase activity can be inhibited by endogenous nuclear inhibitors, such as I1PP2A (ANP32A in Table 3.1) and I2PP2A (SET in Table 3.1). PP2A enzymes can also associate with other protein kinases that have been linked to AD, such as glycogen synthase kinase 3B (in Table 3.1) (107).

Similar to PP2A, calcineurin is a serine/threonine phosphatase that phosphorylates tau. Calcineurin calmodulin-binding catalytic subunit A-beta (PPP3CB) is included in Table 3.1. Changes in calcineurin have been proposed to contribute to AD pathology by inhibiting synaptic function, modifying learning and memory affecting long-term potentiation and altering dendritic spine density and dendritic arbor branching. Karch et al observed that calcineurin protein levels inversely correlated with Braak stage in AD brains and that calcineurin activity is globally reduced in AD brains (108).

Finally, O-GlcNAc glycosylation is a posttranslational modification produced by O-GlcNAc transferase (OGT in Table 3.1) that has been associated in protein changes of neurodegenerative disorders such as α-synuclein, amyloid precursor protein, and tau. Knockout mice of OGT showed progressive neurodegeneration, loss of neurons, gliosis, an increase in hyperphosphorylated tau and Aβ−peptides and memory impairment (109).

This study recognises and explores one of the major challenges in miRNA research, which is that a miRNA has the potential to affect the production of hundreds of proteins. This property allows the possibility that some miRNAs could be involved in several pathways at the same time by affecting numerous proteins such as those described above. Selection of miRNAs of interest was therefore performed with consideration of previously proposed caveats in miRNA research.

3.2. Hypothesis

The null hypothesis is that there is no significant difference in the levels of selected miRNAs between diagnostic groups, AD, VaD, early AD changes (EAC) and non-demented controls.

3.3. Methods

3.3.1. Choice of miRNAs

A number of proteins were chosen on the basis that they have been implicated in amyloid production or clearance including transport of Aβ across the BBB, Aβ degrading enzymes, BBB integrity, proteins involved in the glymphatic system, immune response and tau phosphorylation. The software applications TargetScan (www.targetscan.org) and miRanda (www.microrna.org) were used to obtain predicted miRNAs binding to the transcripts of these genes and the miRNAs that appeared relevant to the highest number of target gene transcripts were included.

Table 3.1 lists the number of binding sites of each miRNA family that was predicted to bind to the target protein transcripts according to TargetScan. The probability with which they bind to the transcripts was also taken into account and all miRNAs selected were within the 15% with the highest ''total context score'', i.e. percentile 85 or higher. Only high confidence miRNAs (i.e. according to miRbase criteria) were further investigated, according to the average number of reads previously reported in miRbase (as produced by NGS data) and the number of predicted transcripts they bind to (Table 3.2). Ratios between the number of reads and the number of transcripts were calculated. Only miRNAs with a ratio higher than 1 were selected for actual screening, suggesting that at least 1 miRNA copy is able to bind at each predicted transcript.

Table 3. 1 Transcripts related to classical hallmarks of AD.

Gene name	miR-16	miR-29	miR-34	miR-125	miR-132/212	miR-216
ADAM10	2		2			
BACE1	2	2		1	2	1
BACE2	1			1		1
PSEN1		1	1	1		2
NOTCH1			2	1		
ABCA1			1		1	
LDLR			1		1	
LRP1				1	2	
AGER					2	
SORL1						1
RELN	2		1			
PDGFB		1	1			
PDGFRA		1	2		1	
PDGFRB		1	1			
AQP4	2	2				4
CD200			1			1
CD14			1			
CD200R1			1			5
MME	1				2	3
ECE1			2	2		
ECE2						1
ACE	1	2	3	1		
MMP2		1	1	1		
MMP14			1	1		
CD147				1		
IDE		1		2	1	1
GSK3B		1			2	
MAPK1		1	2		3	
MAPT			3		1	
PPP2CA	2	1		1		3
PPP2R1A		1		3		
ANP32A			1		1	
SET		2		1		
OGT	1				2	
PPP3CB	1					3

Transcripts involved in one or more of the following: amyloid production, transport across the blood brain barrier (BBB) and degradation enzymes; tau phosphorylation; BBB integrity; glymphatic system or immune response are listed with the corresponding number of binding sites for each of the six miRNA families.

Table 3. 2 Preselected miRNA families.

miRNA family	Confidence	Targets	Reads per million	Ratio reads/targets
miR-15	High	1508	3930	2.61
miR-29	High	1256	17090	13.61
miR-34	High	751	1130	1.50
miR-125	High	927	7470	8.06
miR-132/212	High	474	901	1.90
miR-216	High	372	195	0.52

Preselected miRNA families with confidence level (according to MiRbase criteria), number of predicted targets (according to miRanda), average reads per million and the ratio of the latter two.

3.3.2. Study cohort

The study cohort, as described in detail in Chapter 2 (Section 2.1) comprised brain tissue from 19 AD, 10 EAC, 18 VaD and 19 controls.

Table 3. 3 Demographic information of the cohort used in Chapter 3.

Diagnosis	Gender (Male/Female)	Age (σ)	PMI (σ)	ApoE4 (No/Yes)	Total
Control	10/9	80 (7.4)	30 (12)	19/0	19
Early AD changes	6/4	85 (6.2)	32 (13)	6/4	10
AD	8/11	76.6 (6.1)	23 (13.3)	3/16	19
VaD	9/9	82.6 (7.7)	34.8 (12)	9/4	18
Total	33/33	81 (7.6)	30 (13)	37/24	66

Demographic information of the cohort, post-mortem interval (PMI), standard deviation (σ).

3.3.3. Brain tissue dissection and homogenization

Brain tissue dissection and homogenization was undertaken on the cohort as described in Chapter 2 section 2.2.

3.3.4. RNA isolation, quantification and standardization

RNA isolation, quantification and standardization were performed as described in detail in Chapter 2 section 2.3.

3.3.5. Software for analysis of target proteins (DAVID and PANTHER)

DAVID and PANTHER software were used for analysis of predicted target proteins of the selected miRNAs as described in detail in Chapter 2 section 2.13.

3.3.6. Data collection and analysis

Data on selected calibrator genes was generated by quantitative polymerase chain reaction (qPCR) as described in Chapter 2 section 2.6. The analysis of the resultant data was undertaken using the new formula proposed in Chapter 2 section 2.7. Statistical analysis was performed using the statistical package Graph Pad Prism (Chapter 2 section 2.16).

3.4. Results

3.4.1. miR-16

D'Agostino & Pearson normality test showed that miR-16 levels were normally distributed across the whole cohort. However, Bartlett's test ($p=0.0124$) for homogeneity of variances found that the groups variances differed significantly. Thus, one-way ANOVA was inappropriate for analysis. Kruskal-Wallis test was used for analysis of the data. On comparison, the expression of miR-16 was significantly different across the groups (Figure 3.1), Kruskal-Wallis statistic $H=21.62$ and $p<0.0001$.

Dunn's multiple comparison test showed a significant increase in the AD group compared to controls (p=0.03), EAC (p=0.0051) and VaD (p<0.0001).

Figure 3. 1 Percentage of difference for miR-16.

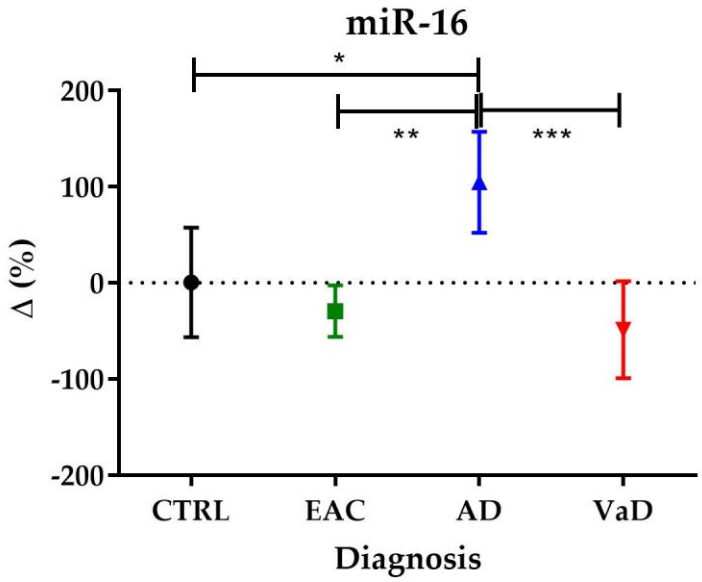

Figure shows the percentage of difference for miR-16 compared to controls, error bars show the 95% confidence interval and the average is depicted, * p<0.05, ** p<0.01 and *** p<0.001.

Analysis using DAVID software to further explore the potential impact of miR-16 changes was then undertaken. MiR-16 maps to an intron on chromosome 13q14.2 and it is part of the miR-15 gene family (with miR-15, miR-195, miR-424 and miR-497). According to TargetScan, 1508 transcripts are predicted to be targeted by miR-16. Significant enrichment scores were found with respect to Rho GTPase-activating protein domain (enrichment score of 2.72 and p=0.0014); voltage gated sodium channel and sodium ion transport (enrichment score of 1.68 and p=0.035); and regulation of postsynaptic membrane potential (enrichment score of 1.56 and p=0.025).

3.4.2. miR-29a/b

Both miR-29a and miR-29b are part of the miR-29 family in addition to miR-29c. miR-29a is encoded in an intron on chromosome 7q32.3. MiR-29b can be derived from two

precursors, 29b-1 and 29b-2 that are co-transcribed with miR-29a and miR-29c respectively. miR-29b-2 and miR-29c are mapped to chromosome 1. D'Agostino & Pearson normality test showed that both miR-29a and miR-29b levels were normally distributed across the whole cohort. However, Bartlett's test found that the variances between the groups were significantly non homogeneous (p=0.0050 for miR-29a and p=0.048 for miR-29b). Thus the data was analysed by Kruskal-Wallis test. Both miR-29a and miR-29b were significantly different across the groups (Kruskal-Wallis statistic H=11.86 and p=0.0079 for miR-29a; Kruskal-Wallis statistic of 12.33 and p=0.0063 for miR-29b). Dunn's post hoc test showed that miR-29a was significantly increase in AD versus EAC (p=0.033) and VaD (p=0.0189); whilst miR-29b was also significantly increased in AD versus EAC (p=0.0281) and VaD (p=0.0183).

Figure 3. 2 Percentage of difference for miR-29a.

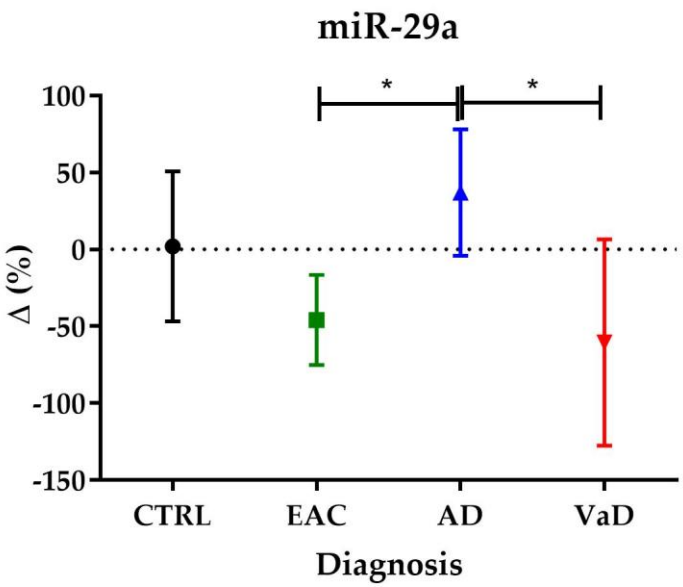

Figure show the percentage of difference for miR-29a compared to controls, error bars show the 95% confidence interval and the average is depictured, * p<0.05.

Figure 3. 3 Percentage of difference for miR-29b.

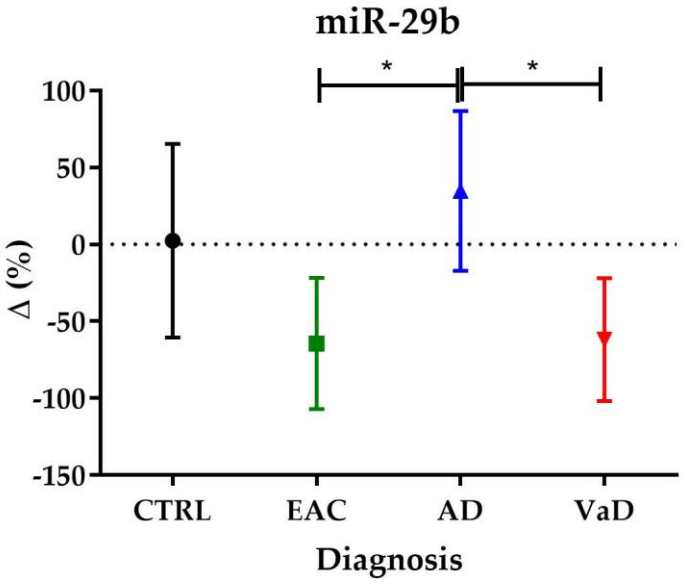

Figure show the percentage of difference for miR-29b compared to controls, error bars show the 95% confidence interval and the average is depictured, * $p<0.05$.

Analysis of the miR-29 family by TargetScan and DAVID revealed it to have 1256 predicted targets and significant enrichment scores in the angiotensin-converting enzyme 2 pathway (enrichment score of 3.53 and p=0.0027); platelet amyloid precursor protein pathway (enrichment score of 3.53 and p=0.0054); acute myocardial infarction (enrichment score of 3.53 and p=0.024); intrinsic prothrombin activation pathway (enrichment score of 3.53 and p=0.035); and apoptosis regulator BCL-2 (enrichment score of 1.67 and p=0.011).

3.4.3. miR-34a

The miR-34 family is composed of four miRNAs, miR-34a/34b/34c/449. miR-34a is transcribed from chromosome 1p36.22. D'Agostino & Pearson normality test showed that miR-34a was normally distributed across the whole cohort and this was confirmed by Bartlett's test (p=0.1196). Thus, the parametric tests one-way ANOVA and Tukey's post hoc were used. miR-34a was found to be differentially expressed between diagnostic groups, one-way ANOVA F=7.089 and p=0.0004. Tukey's post hoc testing showed an increase in AD versus EAC (p=0.03) and VaD (p=0.0002).

Figure 3. 4 Percentage of difference for miR-34a.

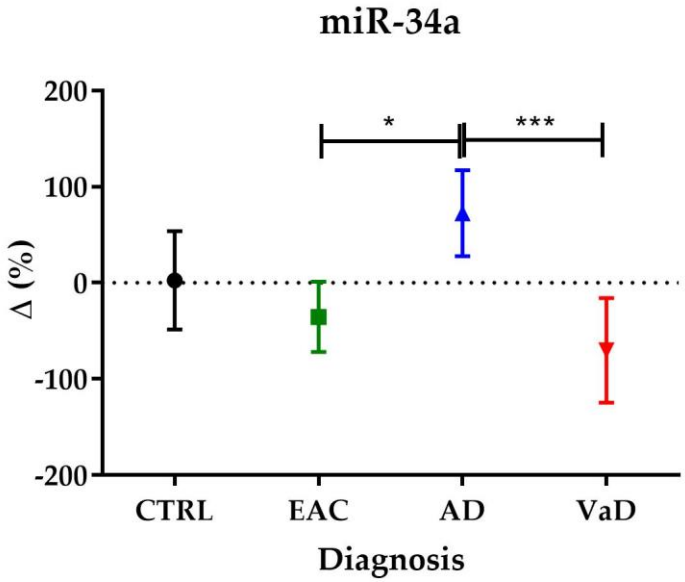

Figure shows the percentage of difference for miR-34a compared to controls, error bars show the 95% confidence interval and the average is depicted, * $p<0.05$ and *** $p<0.001$.

DAVID-assisted analysis showed that this miR-34 family has 751 predicted targets and significant enrichment scores were found in Notch signalling (enrichment score of 1.2 and p=0.046). Other clusters were identified with a possible relevance but were not significant, with respect to fatty acid transport (enrichment score of 0.68 and p=0.078); Rho GTPase-activating protein domain (enrichment score of 0.58 and p=0.23); gamma-aminobutyric acid A receptor (enrichment score of 0.35 and p= 0.22) and PPAR signalling pathway (enrichment score of 0.68 and p=0.75).

3.4.4. miR-125b

miR-125b is transcribed from chromosome 11q24.1, along with miR-125a both of them belong to the miR-125 family. D'Agostino & Pearson normality test showed that miR-125b was normally distributed, which was confirmed by Bartlett's test (p=0.0624). One-way ANOVA showed that miR-125b expression was significantly different between the groups (F=10.69 and $p<0.0001$) with Tukey's post hoc showing significant increases in AD compared to controls (p=0.0114), EAC (p=0.0006) and VaD ($p<0.0001$).

Figure 3. 5 Percentage of difference for miR-125b.

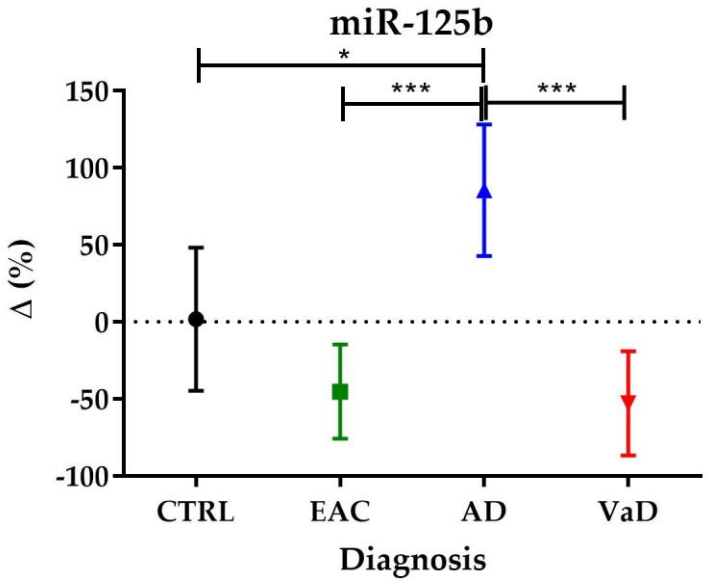

Figure shows the percentage of difference for miR-125b compared to controls, error bars show the 95% confidence interval and the average is depicted, * $p<0.05$ and *** $p<0.001$.

927 transcripts were predicted to be targeted by this miRNA family according to DAVID analysis and high enrichment scores were found in a number of pathways. These included the apoptosis regulator BCL-2 pathway (enrichment score of 2.09 and p=0.0046); fatty acid elongation, saturated, monounsaturated and polyunsaturated fatty acids (enrichment score of 1.34 and p=0.041); tyrosine protein kinase EGF/ERB/XmrK receptor (enrichment score of 1.34 and p=0.012); and furin-like cysteine-rich domain (enrichment score of 1.34 and p=0.038).

3.4.5. miR-132/212

This miRNA family is composed of miR-132 and miR-212, both genes are transcribed from chromosome 17p13.3. D'Agostino & Pearson normality test showed that both miR-132 and miR-212 were normally distributed, which was confirmed by Bartlett's test (p=0.47 for miR-132 and p=0.2993 for miR-212). Both miRNAs showed differences between diagnostic groups, for miR-132 (one-way ANOVA F=5.321 and p=0.0025) and miR-212 (one-way ANOVA F=5.645 and p=0.0017). Tukey's post hoc showed a

significant reduction of miR-132 in controls compared to AD (p=0.0396) and VaD (p=0.0014). Similarly, for miR-212, Tukey's post hoc showed a significant reduction in controls compared to AD (p=0.0189) and VaD (p=0.0014).

Figure 3. 6 Percentage of difference for miR-132.

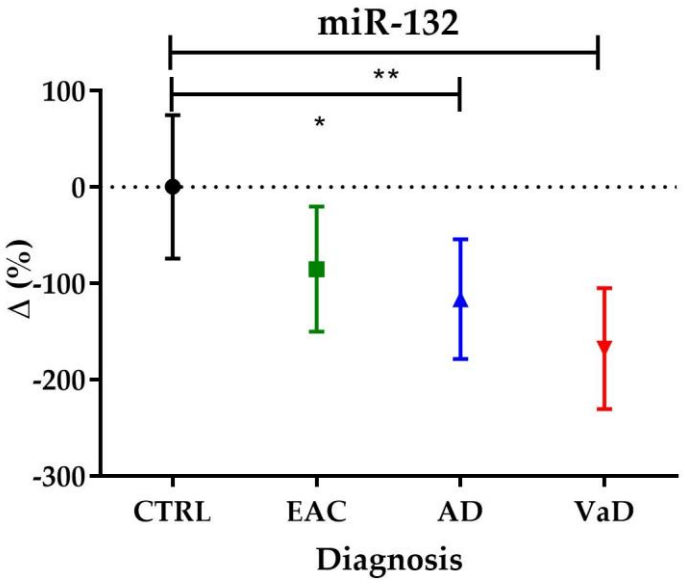

Figure represents the percentage of difference for miR-132 compared to controls, error bars show the 95% confidence interval and the average is depicted, * $p<0.05$ and ** $p<0.01$.

Figure 3. 7 Percentage of difference for miR-212.

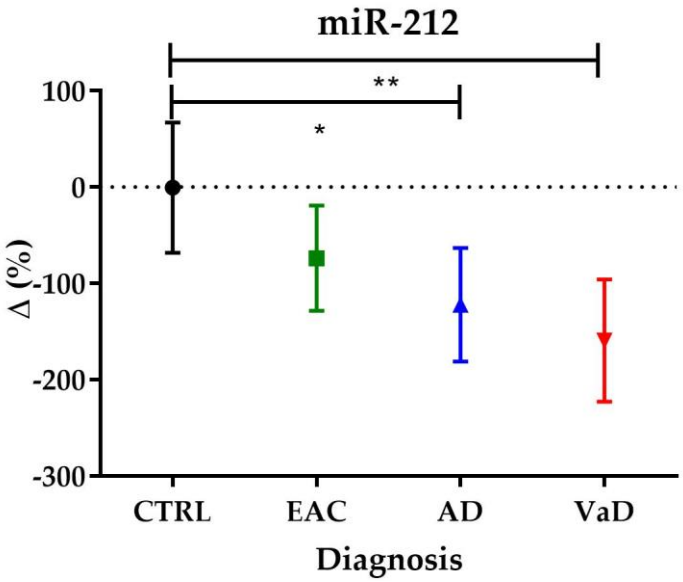

Figure 3.7 represents the percentage of difference for miR-212 compared to controls, error bars show the 95% confidence interval and the average is depicted, * $p<0.05$ and ** $p<0.01$.

This miRNA family has 474 predicted transcripts associated with it. According to DAVID significant enrichment scores were observed for TGF-beta receptor/activin receptor pathway (enrichment score of 2.12 and p=0.001); Rho GTPase pathway (enrichment score of 1.56 and p=0.024); voltage gated sodium channel and sodium ion transport (enrichment score of 1.19 and p= 0.023); and insulin/IGF-1 signalling pathway (enrichment score of 1.15 and p=0.05).

3.4.6. Analysis of miRNAs with comparable patterns

MiR-16, miR-29a/b, miR-34a and miR-125b were found to have a similar pattern of expression across groups, and in contrast to miR-132 and miR-212. Although not all demonstrated significant differences with respect to controls, it should be noted that a significant increase was found in Braak stage II that is considered as part of the controls. Examination of the expression pattern of the various miRNAs, in relation to Braak stage showed increases in these miRNAs in AD in Braak II and VI (miR-16, miR-29a, miR-34a, miR-125b with $p<0.001$ and miR-29b p=0.002), but no difference in VaD

(Figure 3.8). Thus, the baseline for controls might be increased by those cases corresponding to Braak stage II.

Figure 3. 8 Expression pattern of miRNAs according to Braak stage and VaD.

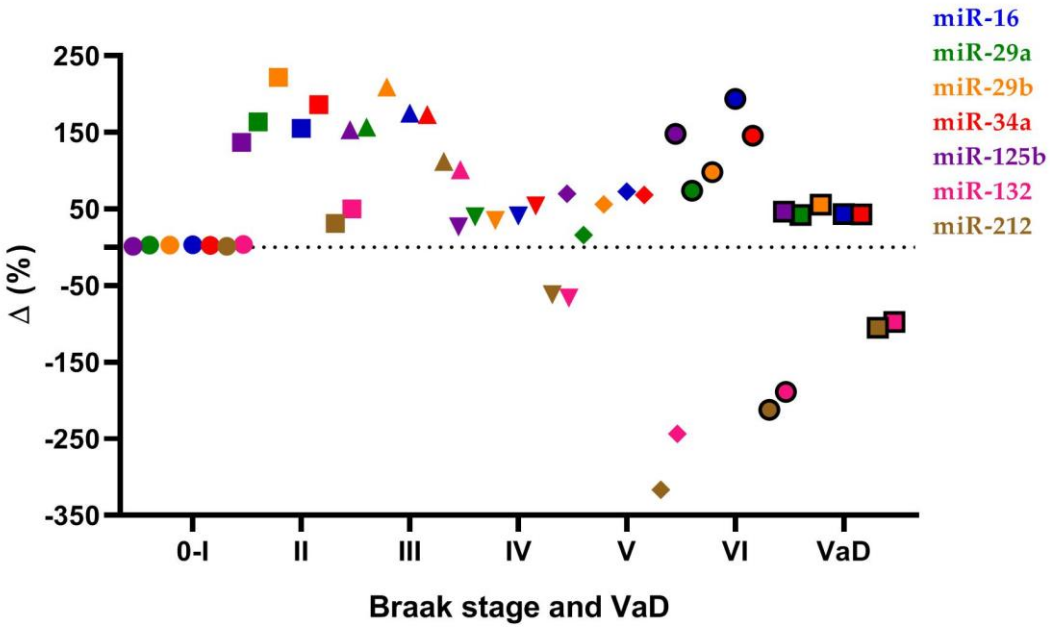

Figure shows patterns of expression for the different miRNAs across AD Braak stage and VaD. Different figures (circles, triangles, etc) are used for the different categories shown.

A further examination of the four miRNA families, with apparently similar behaviour were examined further to the extent in which they may have had similar targets, and these are represented in Figure 3.9. Analysis of the transcripts targeted by at least four of the miRNAs by DAVID software showed significant clusters that were involved in zinc, zinc metal binding and zinc-finger (enrichment score of 3.83 and p=0.00005); stem cell maintenance and development (enrichment score of 2.88 and p=0.0048); serine/threonine kinases and phosphatases (enrichment score of 0.99 and p=0.035); and another cluster, although not significant, was the neurotrophin signalling pathway (enrichment score of 0.99 and p=0.13).

Figure 3. 9 Overlapping targets of miRNA families.

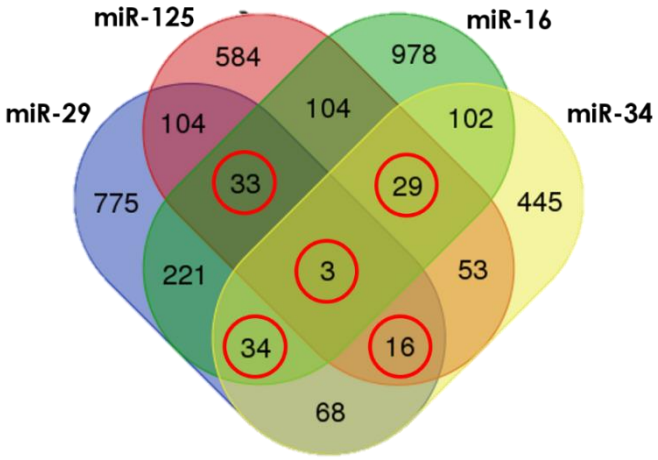

Figure shows miRNA families that showed a similar expression pattern according to Braak stage and their overlapping targets. Only those numbers in red circles were considered for further examination.

From this four-way comparison of shared targets, the four miRNA families were all found to have 3 transcripts in common. These were ELMSAN1 (ELM2 And Myb/SANT Domain Containing 1), RORA (Retinoic acid receptor-related orphan receptor alpha) and ONECUT2 (One cut homeobox 2).

Of the three targets shared across the four families, the most information is available on RORA, the retinoic acid receptor-related orphan receptor alpha. RORA is thought to regulate genes involved in lipid metabolism such as apolipoproteins (110) particularly apolipoprotein J, which is a second major lipoprotein in the brain that, unlike apolipoprotein E, easily transverses the blood-brain barrier and associates with HDL in the periphery (84). This is interesting given that previous pathway analyses of AD point to the important of lipid metabolism and cholesterol in AD (42) not to mention the long-standing and considerable body literature that points to the important of APOE in AD risk and aspects of pathology.

RORA is also involved in hypoxia, another pathway receiving increasing attention as a contributor to the early development and progression of dementia (111). In this case RORA promotes hypoxia-related changes in cell signalling by interacting with, and activating the transcriptional activity of, hypoxia-inducible factor 1-alpha (HIF1A).

RORA was also found to participates in peroxisome proliferator-activated receptor gamma (PPARγ) dependent adipogenesis through competition for DNA-binding (112). The association with PPARγ is also noteworthy for other reasons because of its association with Aβ and also that some drugs that reduce angiotensin II signalling and which are protective against AD-related pathology in animal models have partial PPARγ agonist properties (113). Moreover, the expression of RORA and the α-secretase ADAM10 (A disintegrin and metalloproteinase domain-containing protein 10) were significantly ($p<0.05$) correlated with both fractional anisotropy and gray matter thickness, measurements for water diffusion in the brain and white matter cerebral atrophy (114).

Other functions that have been attributed to RORA function is that it is also a negative regulator of the inflammatory response and regulates interleukin 6 in resting and reactive astrocytes (115,116). Finally, in genome-wide association studies (GWAS), a significant association was observed for the rs2456930 polymorphism and increased risk of AD (119). Other SNPs in RORA have also been implicated with increased risk of depression and a relationship between depression and AD has also been observed (117,118). A finding also more recently replicated by Baker et al were RORA was one of three genes found to be associated with AD, alongside PPARGC1A (a PPARγ related gene), and ZNF423 (a zinc finger gene) (119). While there is a limited, but very interesting literature related to RORA and a number of related mechanisms in AD, there is no literature thus far, describing any role or association between ELMSAN1 and ONECUT2 with AD.

3.5. Discussion and conclusions

These initial results suggest that miRNAs might act in a co-ordinated manner in some forms of dementia. While there is already studies reporting the role of single miRNAs in dementia (71,120,121), based on the current findings, it is reasonable to suggest that such associations are perhaps an over simplification of the possible involvement of

these molecules in AD. More likely, it is conceivable that combinations of miRNAs, given that some can share the same targets, will have a substantive physiological role in the development and/or progression of neurodegeneration. The findings here around the identification of changes to miRNAs that all share a property of the capacity to target the RORA gene may be one such example. Furthermore, this collection of miRNAs also have additional shared functions that are relevant to zinc metabolism, serine/threonine protein kinases and phosphatases, stem cell maintenance and development.

Zinc metabolism has been linked to the development of AD and several amyloid degrading enzymes are metalloproteinases dependant on zinc (122–124). Serine/threonine kinases and phosphatases are similarly particularly important due to the importance of phosphorylation of tau protein at serine/threonine residues and the contribution of this towards the formation of neurofibrillary tangles.

RORA represents an attractive candidate protein that participates in numerous processes linked to dementia, however empirical measurement of RORA levels in AD or VaD brains have not yet been described. Only one study has directly linked RORA to AD by analysis with computational node networks of the insulin pathway and brain derived neurotrophic factor (BDNF) (125). RORA also represents an intersection of changes observed in AD and VaD, in hypoxia, cholesterol metabolism and energy deficiency.

MiRNA expression fluctuates as the disease progresses and thus might represent compensatory mechanisms that under non-physiological conditions will affect other pathways. MiRNAs might target some transcripts that contribute to the development of dementia but at the same time target other transcripts that may act as counter-regulators. Therefore, under normal physiological conditions certain miRNAs, such as the miR-29 family, are able to repress the formation of Aβ by downregulating BACE1 or favouring vasodilation (and potentially aiding amyloid clearance) by repressing

angiotensin converting enzyme (ACE) expression and thus its role in the formation of the vasoconstrictor angiotensin II.

However, if a pathology-induced increased expression of miR-29 exceeds a given concentration threshold, the 'excess' miR-29, unless regulated might begin to affect other transcripts through low affinity binding to targets such as the platelet derived growth factor (PDGF) and its receptors, and aquaporin 4, important for BBB integrity and glymphatic clearance of amyloid.

Similarly, the very nature of how miRNAs function, particularly their sometimes wide substrate specificity, could explain why what appears to be non-linked processes tend to occur during the development of AD, or how there is some variation that gives rise to variable neuropathology for AD and VaD, or indeed even the variable extent to which some age-related pathologies accumulate. That miRNAs are autocrine, paracrine and endocrine molecules, which can be transported via exosomes poses a possibility that they could mediate their effects following a concentration gradient, where there might be a higher impact in the cells in which they are being produced, but with a reduced effect in neighbouring cells or in other organs.

From the seven miRNAs assessed in this chapter, five of them (miR-16, miR-29a, miR-29b, miR-34a and miR-125b) followed a similar pattern with differences between AD and VaD. Two of them (miR-132 and miR-212) decreased according to Braak stage and a similar reduction was found in both AD and VaD suggesting that although there might be specific pathways pathognomonic of AD, they also share other characteristics in common such as vascular changes. Analysis of a miRNA signature based on hypoxia inducible factors, responsive genes and the MTHFR (methylene tetrahydrofolate reductase) gene, variation in which is a risk factor for VaD (126), could help to identify more similarities between AD and VaD, for instance miR-132 and miR-212.

In studies of disease, in particular in post-mortem tissue, the pathological stage of the disease, the duration of post mortem delay prior to the availability of tissue and the

agonal state prior to death are also important factors to consider in the study of miRNAs, especially since the multi-functional functions of miRNAs measured could represent causal and/or responsive mechanisms. Indeed, during the natural history of a disease, miRNAs will likely fluctuate and their final expression signature might represent a retrospective picture of various attempts at protective mechanisms as well as the cause of various detrimental dysregulations. As observed, dysregulation of those miRNAs in Braak stage II (Figure 3.8) could support an early diagnosis before the manifestation of symptoms.

Analysis of the samples studied here by Braak stage also highlighted the importance of using adequate calibrators for the measurement of miRNAs (e.g. calibrators that are unlikely to be affected by disease status). RNU6B was found to be relatively stable from Braak stage 0 to V but then was observed to have a 3-fold reduction in Braak stage VI. The use of more stable calibrators, that would be unaffected by disease for any stage of the disease would provide more reliable results. Moreover, there was also a low number of cases in Braak stage 0-I as controls (5 cases), perhaps reflecting the rarity of the absence of some age-related pathology, even in controls. However, increasing the number of cases in Braak 0-I would be beneficial in provide a larger number of samples across the spectrum of Braak stages and in doing so allow strengthening of statistical power.

All of the seven miRNAs studied here were found to be significantly different between diagnostic groups. Of the seven studied, five (miR-16, miR-29a, miR-29b, miR-34a and miR-125b) were found to be increased and two (miR-132 and miR-212) found to be decreased. With these findings the null hypothesis proposed that there is no significant difference in the levels of selected miRNAs between diagnostic groups, can be rejected. However, given the observations of a lack of consistent expression across all Braak stages for the calibrator RNU6B, which has been a widely used calibrator in the study of miRNAs in AD to date, it does shed some doubt as to the reliability of my observations. This therefore prompted the need for a more thorough evaluation of commonly used calibrator genes, which will be described in Chapter 4, as a way to

progress this area and highlight if there are unreliable calibrators that have not been extensively studied for their robustness and reliability in the context of AD. This will provide a more robust footing on which to re-visit and investigate again whether the observations described in this chapter indeed have merit and strengthen the case for their candidature in future research in AD and VaD.

Chapter 4.- Advancing the reliability of miRNA measurement

4.1. A critical appraisal of techniques for miRNA measurement

4.1.1. Challenges in the measurement of miRNAs

As previously described, miRNAs are small non-coding RNA sequences of about 22 nucleotides in length, with a range from 16 to 27 nucleotides (127). The structure of which present a number of challenges that have a bearing on how they are researched. One of the first considerations in the characterization and measurement of miRNAs, is that the miRNA sequence is present in three contexts: the primary miRNA transcript, the miRNA precursor and the mature miRNA. Another consideration is that miRNAs are highly variable in the proportion of guanine/cytosine bases they contain. This results in a wide array of melting temperatures and this may in turn affect specificity and sensitivity of an assay.

Third, some miRNAs within the same family differ by just a single nucleotide. Thus, some methods, such as hybridization methods, may have limited specificity, which is notable given that early research in the miRNA field used the northern blot method. Given the various challenges summarized above, it is perhaps not surprising that the signals obtained from such earlier work could have inaccuracies, or a lack of precision, given that these signals could have been derived from each of the three forms in which the miRNA sequence exists (66,128).

The important need to distinguish between specific miRNAs will depend on the sequence of the mature miRNA. A mature miRNA sequence that is more enriched in guanine cytosine bases will bind more efficiently and with greater affinity to the detection probe. This interaction can also be manipulated further to increase binding affinity and specificity for probes by using Locked Nucleic Acids (LNA) (129). These

developments, contribute to why northern blots are less utilized, as well as other less satisfactory properties of northern blots that are time consuming and require larger amounts of RNA compared to other newer methods.

4.1.2. Newer approaches for measurement of miRNAs

miRNA detection with high sensitivity and specificity remains a challenge; however in more recent years three different methods have emerged that are used to varying extents to achieve this. The first is the amplification of miRNAs, allowing its measurement, using quantitative real time polymerase chain reaction (qPCR). The second is the use of microarrays and thirdly, sequencing by Next Generation Sequencing (NGS) technologies (66,129). Microarrays have the advantage of highest throughput allowing measurement of multiple miRNAs simultaneously. However, due to the different and critical binding affinities of miRNAs summarised, microarrays can be less specific in differentiating between individual miRNAs, and thus less suited where accurate and specific quantification is needed.

Recent NGS technologies have enabled considerable advances in miRNA research by allowing the specific detection of low copy number miRNAs. This has helped to identify new miRNAs and their relative abundance, and the collection of data that has emerged from various NGS experiments has helped to provide new criteria for the RNA sequences to be recognized as miRNAs. Despite these great advances of NGS experiments, it is recommended that the results derived from NGS experiments are also supported by an additional validation method, such as qPCR. Although there is still no formal consensus, qPCR has been extensively cited by many researchers as the 'gold standard' approach for miRNA research. This is due to its quantitative properties, the specificity it offers towards the differentiation between isomirs, and due to the use of stem-loop primers, also helps to discriminate between primary miRNAs, pre-miRNAs and degraded mRNA (66,68).

Perhaps the most comprehensive study of approaches to miRNA measurement was undertaken by Mestdagh et al. They compared 12 different technical platforms for the measurement of miRNAs in terms of reproducibility, sensitivity, accuracy, specificity and similarity of expression (130). They found that low reproducibility was associated with low-copy miRNAs and that such low-copy miRNAs differed in frequency among platforms. The low reproducibility observed is also potentiated by the low number of copies and proportion of mismatches. In terms of sensitivity, they found lower sensitivity for platforms using hybridization approaches. Accuracy was assessed by measuring certain miRNAs in specific samples and by measuring the detectability after miRNAs were ''spiked'' into reactions. Overall, they found that in general, qPCR generally accurately quantified low-abundant miRNAs.

Mestdagh et al also observed that most platforms showed high specificity between miRNAs that differed by only 3-4 nucleotides but there was higher cross-reactivity (i.e. lower specificity) between miRNAs when they differed from each other by only 1-2 nucleotides. Finally, with respect to their evaluation of the similarity of expression, they investigated into 66 miRNAs differentially expressed between 2 sample groups (130). Of the 66 miRNAs studied, only two were found to be differentially expressed by all platforms. Other studies evaluating similar characteristics of different assays have found that observed miRNA levels were dependent on the technical approach and also with differences between commercial kits of the same technique (i.e. amplification, hybridization or NGS) (128,131,132). Yet, qPCR appeared to perform the best overall with the widest dynamic range and highest accuracy and it has been on this basis that the method has been proposed as the gold standard for miRNA profiling (66,68).

4.2. A closer look at quantitative reverse transcription polymerase chain reaction

Polymerase chain reaction (PCR) is an enzymatic assay that allows the amplification of a specific sequence of nucleotides from a pool of DNA, or from RNA that has been produced through the use of reverse transcription (RT), also known as RT-PCR (133). 'Qualitative' PCR is another application where the method is used simply to detect the

absence or presence of a specific sequence. This is useful when PCR is performed with respect to checking the specificity of a PCR reaction for a target, or with respect to cloning purposes and validation of the existence of a cloned target or insert, or to identify or confirm the presence of a pathogen in a sample (e.g. in forensic or medical microbiological applications).

Quantitative real-time PCR (qPCR) provides more information than just specific detection of specific sequences (133). This accurately measures the amount of a specific DNA or RNA sequence present in a sample and allows for both detection and quantification of the PCR product in real-time, while it is being synthesized (133). Although qPCR has been recognized as the best technique for miRNA measurement (as outlined in 4.1.2), it still requires normalization to a reference (i.e also called calibrator) gene that is considered to have a constant level of expression for the sample type being investigated, and in the case of applications where disease association is being investigated, appears to be unchanged in the presence of the disease.

Unfortunately, there is currently no consensus nor systemic evaluation of the most commonly used and cited calibrator genes for miRNA profiling in human post-mortem brain tissue. This is because most studies have not investigated brain tissue. However, there is an important need to have robust calibrators unaffected by disease. With this in mind, there is a risk that calibrator genes previously tested and reported, for instance in cultured cell lines, or blood-derived samples (e.g. serum) or other peripheral tissues, are not appropriate for use universally or other tissue types (e.g. the brain).

Small nuclear/nucleolar RNAs (snRNAs) have been commonly used for miRNA normalization. This is because that have similar properties to miRNAs, they have comparable RNA-like stability, are of similar size, and are often abundantly expressed (134). The abundant expression of these small RNAs in different cell types, is attractive when being considered as a possible calibrator because they provide some flexibility for the measurement of miRNAs, and would be subject to similar cell-type specific expression (135,136). Yet, surprisingly these small RNAs, and their appropriateness as

calibrator genes, have not been investigated in any robust manner with respect to brain tissue, where their study is arguably most relevant with the development and progression of AD.

The importance of studying these snRNAs in a disease specific manner has been shown in other diseases. Gee et al showed that the commonly used snRNAs correlated with tumour pathology, breast cancer and head and neck squamous cell carcinoma. They also reported that low expression of these snRNAs correlated with markers of aggressive pathology, suggesting the importance of their evaluation in other specific pathologies (136). Similarly, Benz et al demonstrated that the most commonly used snRNA calibrator gene RNU6B was upregulated in patients with sepsis, but downregulated in patients with liver fibrosis, highlighting how the behaviour of snRNAs have both disease- and tissue-specific profiles of activity (135). Thus, if they are to be used as calibrator genes it is important to evaluate whether these small RNAs are affected by disease state in dementia.

In doing so, there is also a need to acknowledge that the size of such snRNAs is variable. The sequence length of commonly used and commercially available snRNAs was investigated (Table 4.1.) using manufacturer catalogue and the National Center for Biotechnology Information (https://www.ncbi.nlm.nih.gov/).

Table 4. 1 Commercially available snRNAs.

Small RNA	Nucleotides
RNU44	**61**
RNU43	**62**
RNU48	**63**
RNU38B	69
RNU49	71
RNU24	75
Z30	97
RNU6B	**106**

Table shows examples of commercially available assays for various snRNAs used for normalization with summary information regarding their size. Those in bold text are considered in this thesis for evaluation.

RNU6B has, thus far, been the most commonly used calibrator in miRNA screenings in dementia (137). However, it is important to note that its length is almost five times that of a more typical miRNA (22 nucleotides) which immediately raises questions regarding potential issues around comparability of assay kinetics with those for snRNAs. Furthermore, as per the findings in the previous chapter (3.5. Discussion and conclusions), despite its widespread use in dementia, its expression in human brain tissue was not uniform according to disease severity. I observed that in brain tissue determined to be Braak stage VI, the levels of RNU6B had a significant three-fold reduction compared to other less severe Braak stages, suggesting changes in the most severe cases of AD.

Another notable gene that has been used for calibrating miRNA expression is, miR-9-5p. This was used as calibrator gene in the largest study of miRNAs in AD (138). However, this study lacked information justifying its selection for this function and there was no information regarding the evaluation of its stability to support its validity for this function (138).

To explore the possible relevance of amplimer length with respect to chosen calibrator genes, I selected three snRNAs (RNU43, RNU44 and RNU48) with the shortest lengths (Table 4.1). RNU6B as the most commonly used, miR-9-5p as used in the largest study to-date (138) and its counterpart miR-9-3p, to evaluate their suitability as calibrator genes for the measurement of miRNAs in dementia. To do this I investigated them in two ways.

First, in terms of their potential variability with respect to disease state in dementia. Second, I was also interested to explore the potential impact, if any, of post-mortem delay, on their measured expression levels. For the latter, I undertook an experiment that simulated post-mortem delay (further details provided in the methods section 2.5 Simulation of postmortem delay) as a way to determine if levels of the proposed calibrators changed under different temperature and time conditions. This would

allow better contextualization and interpretations of further human tissue-based studies, particularly in dementia and where post-mortem delay is likely.

Different methods for selecting appropriate calibrator genes have been proposed in the literature but which have differences between them. A search was performed in Pubmed using the words ''qPCR microRNA'', ''normalization microRNA PCR'', ''calibrator gene microRNA PCR'' and combinations thereof. Twenty papers published to date were also examined closely in terms of the experimental methodology used. Similarly the various mathematical and analytical approaches used were scrutinized and will be summarised.

Chen et al compared the stability of 9 commonly used calibrator genes in human umbilical vein endothelial cells. This was using four widely used analytical methods involving the software applications *Genorm*, *NormFinder* and *BestKeeper* in addition to the comparative ΔCT method (139). Their results showed some consistency between conclusions drawn from *Genorm*, *NormFinder* and the ΔCT method with some minor differences between them; however *BestKeeper* was found to be less consistent with respect to the other methods. *NormFinder*, which performed the best, relies on the variation of the calibrator genes within the same group and between groups (intra and intergroup variation) which is the same principle of the statistical test analysis of variance, ANOVA (140).

The inventors of *NormFinder* have stated that the generally accepted criterion for selecting a calibrator gene is too simple (140). The criteria is that a gene should show no variation across the sample set, and that analysis of subgroups should be performed. On the basis of my initial results (Chapter 3), no significant differences were observed in the calibrator RNU6B between diagnostic groups. Yet, a three-fold reduction was observed in Braak stage VI compared to all the other Braak stages where no change was observed. Given that calibrator genes are used to standardize the measurement of target miRNAs within each individual sample, analysis of their stability by groups might disguise specific differences.

Genorm relies on pairwise analysis of calibrator genes and subsequent normalization to the geometric mean of calibrator genes that showed higher correlation between them (75). The authors also suggested that normalization by multiple calibrator genes is required for accurate measurement. Nevertheless, the fact that a subset of calibrator genes shows good correlation between each other does not necessarily prove that this is indicative of wider changes in miRNA expression overall. Such subsets could be involved in and very specific to certain pathologies, as could be represented by the two groups of miRNAs with similar patterns of expression across Braak stage. The three most stable calibrators identified in this chapter will be used for further normalisation of the miRNAs I am interested in.

BestKeeper showed less consistency than *Genorm*, *Normfinder* and the comparative ΔCT method (139). First described by Pfaffl et al and freely available, *BestKeeper* is an Excel-based tool that considers pair-wise correlations to the geometric mean of all evaluated calibrator genes. This comparative approach is to some extent, similar to Genorm but differs in that BestKeeper focuses in the standard deviation while the others consider other factors such as mean and coefficient of variation (141). Pfaffl et al showed that the reference value (derived from evaluation of all calibrator genes collectively) obtained with their tool performed better than individual calibrator genes.

However, it is conceivable that this approach could be subject to artefacts created by the mean of different calibrator genes regardless of its stable expression across all samples. For instance, one cycle of qPCR represents a two-fold difference in gene expression, thus the exponential nature of the method might affect the resultant geometric mean when a few but highly variable samples are included within the dataset. This might explain why BestKeeper was reported to be less consistent than the other methods evaluated by Chen et al.

Other methods have also been described in the literature. *ReadqPCR* and *NormqPCR* are packages based on the software 'R' for normalisation of qPCR (142). Software R is

further described in the methods section 2.12 R software. Both ReadqPCR and NormqPCR were explored for use in this work, however, on further exploration it was found that both methods rely on the same algorithm used by (and thus are in effect derivatives of) Genorm and thus were not further explored.

Finally, the comparative ΔCT method was also evaluated in this project. Whilst doing so it revealed that any ΔCT value higher than one would increase towards infinity, whilst in contrast, any ΔCT value lower than one would never decrease below zero. This exponential equation therefore produces a multiplicative effect rather than an additive effect. With this in mind, and these limitations, a modification of this method is proposed and described in the methods section. In summary, analysis of the variability of calibrator genes will be performed by the comparative ΔCT method using absolute values and plots of the data. In additional work to validate the calibrators for the current investigative context, the effect of a simulation of postmortem delay on brain tissue was explored to explore the stability of the qPCR signal of these calibrator genes over a period of 72 hours.

4.3. Hypothesis

The null hypothesis states that there is no significant difference in the levels of these small RNAs between stages of neuropathology, as denoted by Braak stage.

4.4. Methods

The methods used in this chapter have been described in detail in Chapter 2 and are as follows:

4.4.1 Study cohort

The study cohort comprised brain tissue from 22 AD, 20 EAC, 18 VaD and 24 controls, as described in Chapter 2.1.

Table 4. 2 Demographic information of the cohort used in Chapter 4.

Diagnosis	Gender (Male/Female)	Age (σ)	PMI (σ)	ApoE4 (No/Yes)	Total
Control	11/13	80 (9.7)	35.4 (16.2)	21/1	24
Early Alzheimer Changes	11/9	85 (6)	36.5 (15)	14/4	20
Alzheimer's Disease	11/11	78 (7.2)	23.7 (13.4)	3/16	22
Vascular Dementia	9/9	83 (7.9)	34.7 (12.3)	9/4	18
Total	42/42	81.2 (8.1)	32.5 (15.1)	47/25	84

Table shows the demographic information of the cohort, post-mortem interval (PMI), standard deviation (σ).

4.4.2. Brain tissue dissection and homogenization

Brain tissue dissection and homogenization was undertaken on the cohort as described in Chapter 2.2.

4.4.3. RNA isolation, quantification and standardization

RNA isolation, quantification and standardization were similarly performed as described in Chapter 2.3.

4.4.5. Simulation of postmortem delay.

Two cases with the lowest postmortem delay (5 hours) were selected, one with a definite diagnosis of AD and the other a non-demented control. From already dissected tissue, 60 mg of tissue were taken and divided into 12 aliquots of 5 mg. These aliquots were incubated for 0, 6, 12, 24, 48 or 72 hours at room temperature and at 4°C (resonating with the typical time window in which most brain banking seeks to recruit

within). After incubation, samples were stored at -80°C and once all samples were retrieved, RNA isolation, quantification and standardisation were performed as described. For RNA isolation, specific quantities were modified according to the proportion of tissue.

4.4.6 Data collection and analysis.

Data on selected calibrator genes was generated by quantitative polymerase chain reaction (qPCR) as described in Chapter 2.6. The analysis of the resultant data was undertaken using the new formula proposed in section 2.7. The $2^{(-\Delta\Delta CT)}$ method. Statistical analysis was performed using the statistical package Graph Pad Prism (section 2.16 Statistical package Graph Pad Prism).

4.5. Results

4.5.1. Investigation of snRNA expression across the whole sample cohort

4.5.1.1. RNU43

Figure 4.1 shows the variability of expression of RNU43 across the whole cohort (n=84) with differences in CT values from a maximum CT difference value (from the geometric mean) of 2.27 to a minimum difference of -1.69. The average percentage difference from the geometric mean was 105.40%.

Figure 4. 1 Plot of CT differences for RNU43 in individual samples of the cohort.

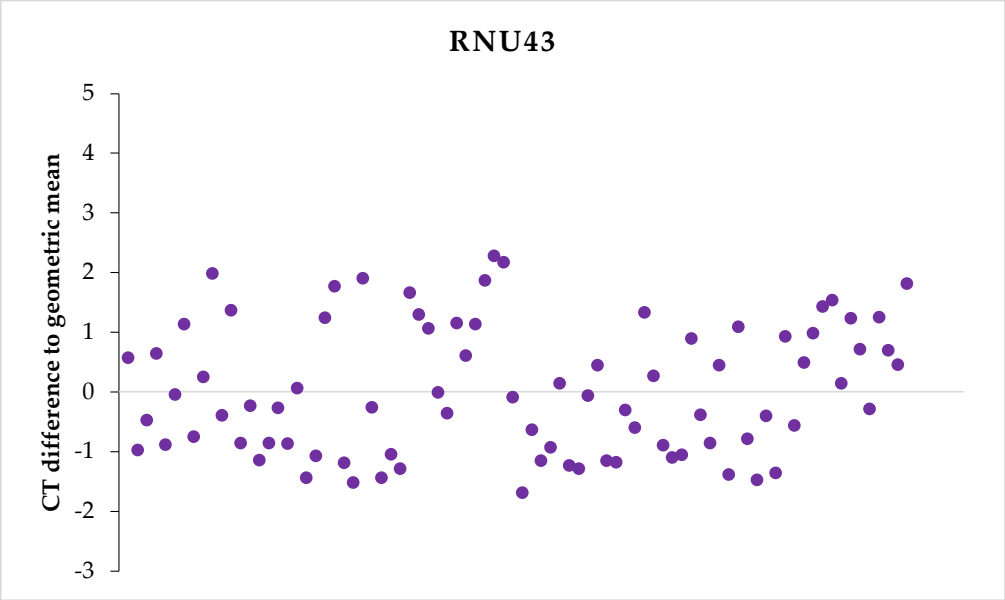

4.5.1.2. RNU44

Figure 4.2 shows the highly variable expression of RNU44 across the whole cohort (n=84) between a maximum CT difference of 4.27 and a minimum of -2.45. The average percentage of difference to the geometric mean was 188.62%.

Figure 4. 2 Plot of CT differences for RNU44 in individual samples of the cohort.

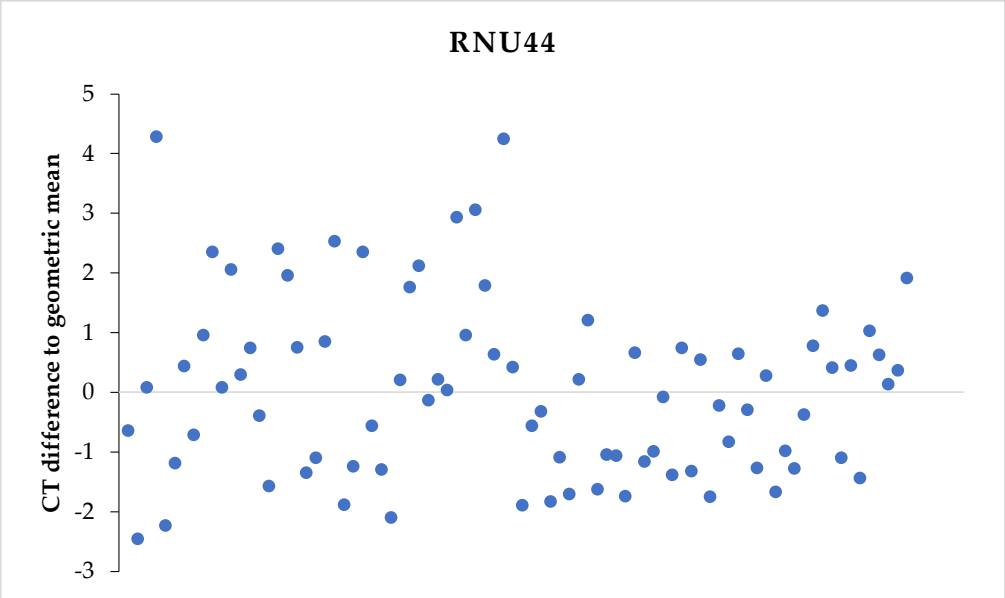

4.5.1.3. RNU48

The lesser variability of expression of RNU48 across the cohort (n=84) is shown in Figure 4.3, with values ranging from a maximum CT difference of 2.83 to a minimum of -1.57. The average percentage of difference to the geometric mean was 71.23%.

Figure 4. 3 Plot of CT differences for RNU43 in individual samples of the cohort.

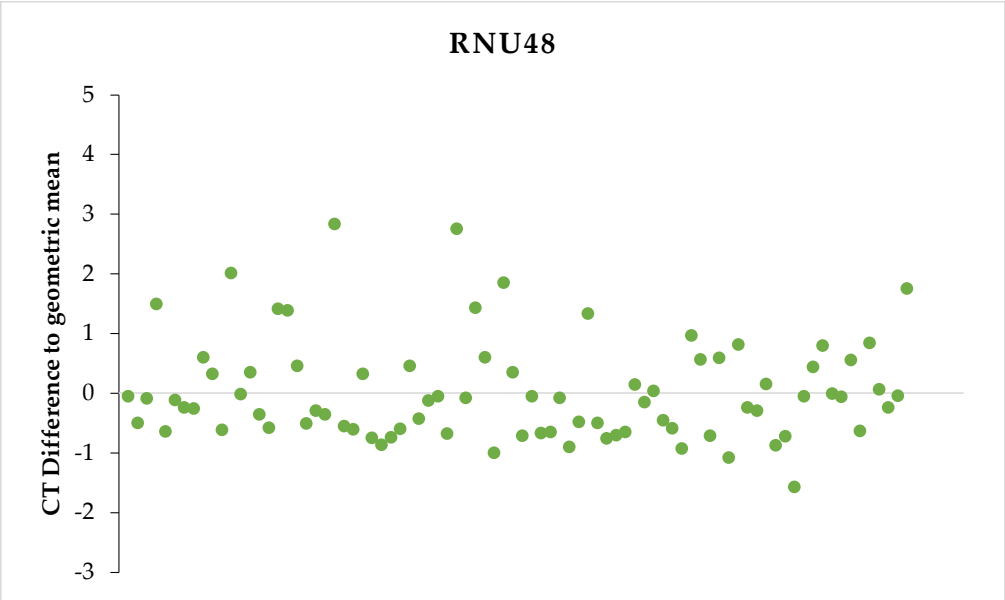

4.5.1.4. RNU6B

In addition to the significant differences in the levels of expression of RNU6B between states of neuropathology observed in Chapter 3, Figure 4.4 shows in more detail the variable expression of RNU6B across the cohort (n=84) with differences in the CT values from the geometric mean ranging from a maximum of 4.28 to a minimum of -2.39. The average percentage of difference to the geometric mean for RNU6B was 158.39%.

Figure 4. 4 Plot of CT differences for RNU6B in individual samples of the cohort.

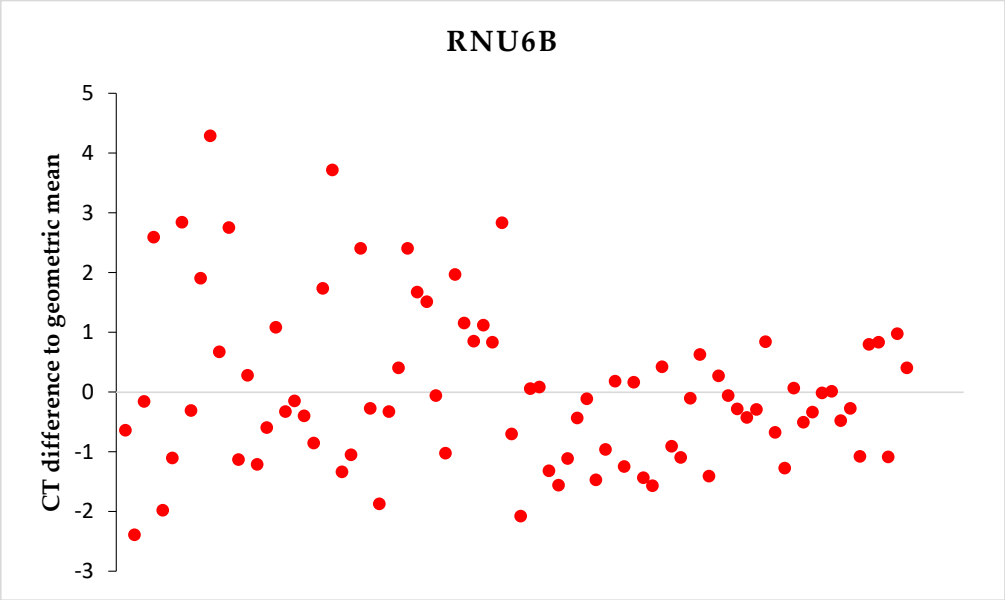

4.5.1.5. miR-9-5p

The variability in the expression of miR-9-5p across the cohort (n=84) is plotted in Figure 4.5, ranging from a maximum CT difference of 1.63 to a minimum of -0.87. The average percentage of difference to the geometric mean for miR-9-5p was 29.86%.

Figure 4. 5 Plot of CT differences for miR-9-5p in individual samples of the cohort.

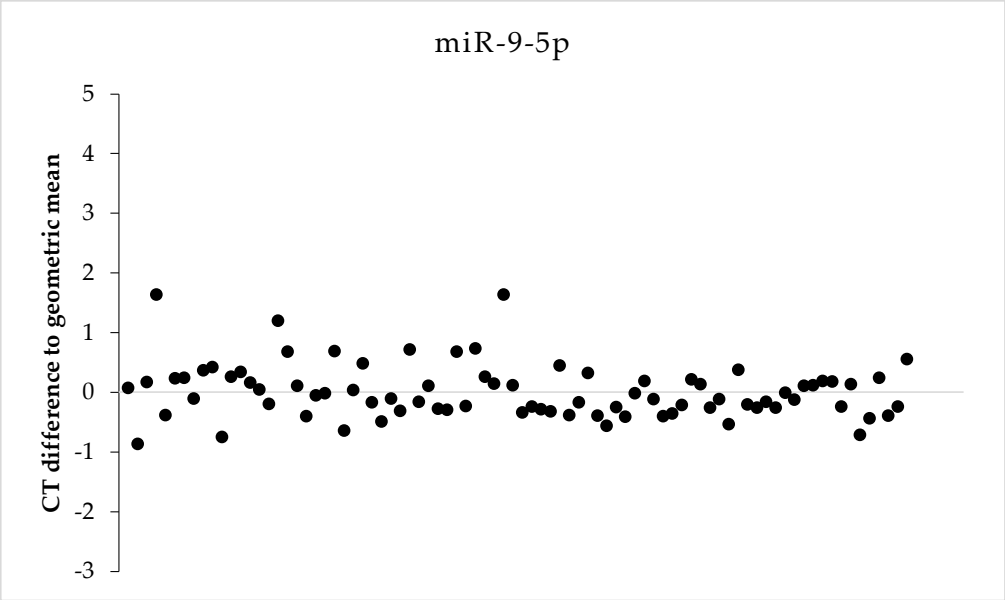

4.5.1.6. miR-9-3p

The variability in the expression of miR-9-3p across the cohort (n=84) is plotted in Figure 4.6, ranging from a maximum CT difference of 0.895 to a minimum of -1.019. The average percentage of difference to the geometric mean of miR-9-3p was 23.99%.

Figure 4. 6 Plot of CT differences for miR-9-3p in individual samples of the cohort.

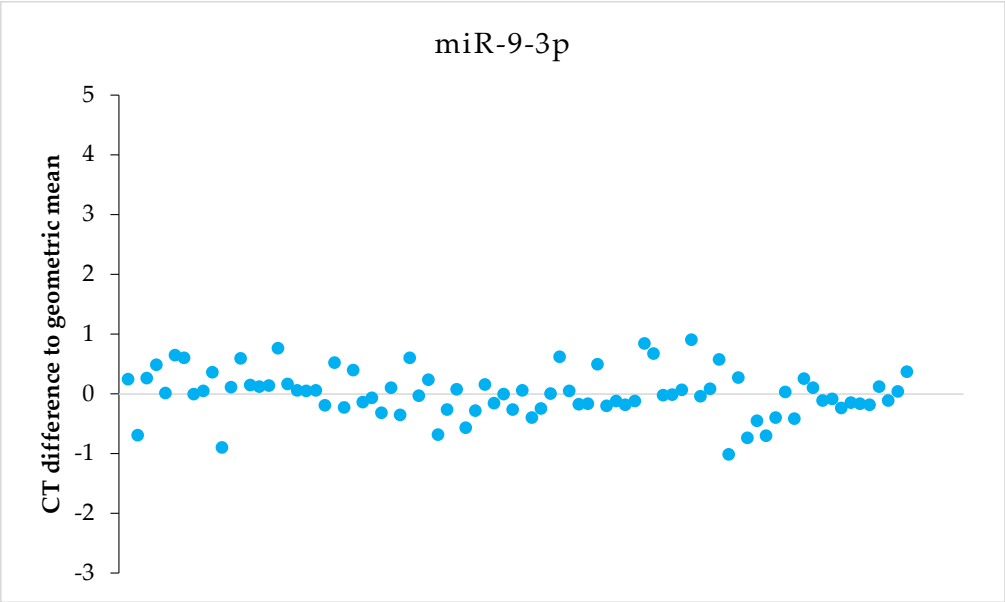

4.5.1.7 Rank-ordering of the calibrator genes related to CT value differences from the geometric mean.

Based on the above data, the rank order of the performance of calibrator genes studied, based on the size of average differences observed in CT values from the geometric means is as follows:

miR-9-3p > miR-9-5p > RNU48 > RNU43 > RNU6B > RNU44

4.5.2 Simulation of post-mortem delay

This experiment is to test the stability of the expression of all proposed calibrators in post mortem brain tissue. Given that most research using post mortem tissue may be subject to the effects on assays of unavoidable post mortem delays and possible changes to the tissue, it is important to try and assess if there are any changes to the levels of expression that can be measured in such samples. As described in the methods, this experiment, which is conducted in brain tissue with an initial short post-mortem delay from an AD patient and a control (no VaD brain tissue was available) tests the performance of each calibrator gene over a series of time points and temperatures to approximate the conditions that are relevant to brain tissue donation.

4.5.2.1. RNU43

RNU43 showed an approximate CT difference of 2 in the simulation of post-mortem delay (Figure 4.7). This CT difference suggests about a four-fold reduction in the levels of RNU43 for both samples (AD and control) at both temperatures (4°C and room temperature). After six hours, the four samples appeared to continue to degrade until 72 hours, resulting in an approximate 32 fold reduction in RNU43.

Figure 4. 7 CT difference of individual samples to the 0 hours sample for RNU43.

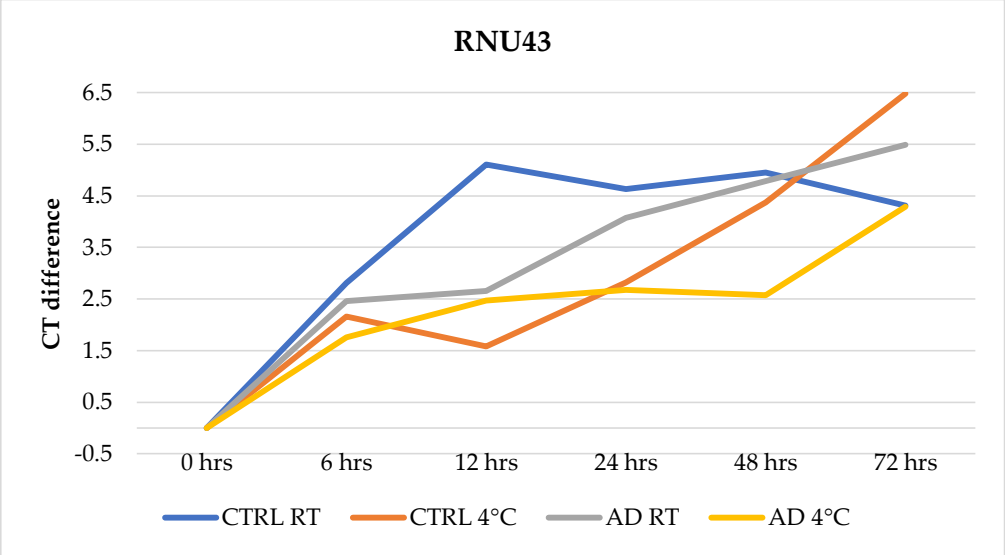

4.5.2.2. RNU44

In Figure 4.8, a CT difference of approximately 1.5 is observed after leaving the samples for six hours. This represents an almost three-fold reduction in RNU44 in the samples. A similar CT difference is observed for three of the four samples after 12 hours with the deviation being from the control room temperature (CTRL RT) sample. After this point, samples showed greater degradation with more heterogenous results. At 72 hours, two samples displayed a CT difference of three indicative of an eight-fold reduction in transcript levels whilst two other samples showed CT differences of 4.5 and around 6 suggesting a decrease of 22 and 64 folds respectively.

Figure 4. 8 CT difference of individual samples to the 0 hours sample for RNU44.

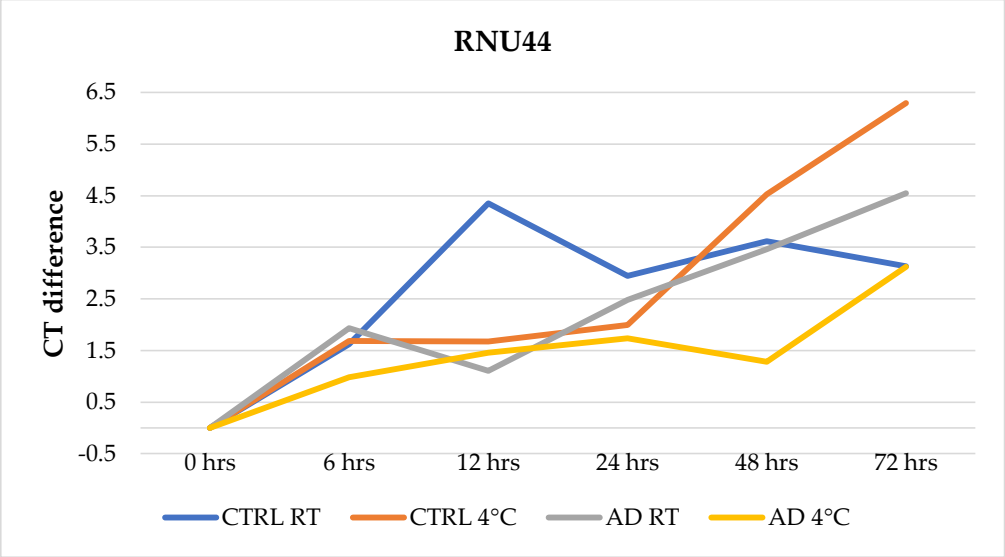

4.5.2.3. RNU48

As can be observed in Figure 4.9, RNU48 demonstrated reasonable similar and stable levels for the 2 tissue samples stored at 4°C until 24 hours. Some difference is later perceptible at 48 hours and 72 hours for these samples with CT differences between 0.5 and 1. A CT difference of 1 at 72 hours indicates a two-fold reduction for the calibrator gene RNU48. In contrast, the two samples stored at room temperature started to show a decrease in measurable signal (e.g. increased CT values) at 24 hours and ranging

from 1 to 3.5 up to 72 hours. This represents a reduction from a two-fold at 24 hours to an 11 fold decline in measurable RNU48 transcripts at 72 hours.

Figure 4. 9 CT difference of individual samples to the 0 hours sample for RNU48.

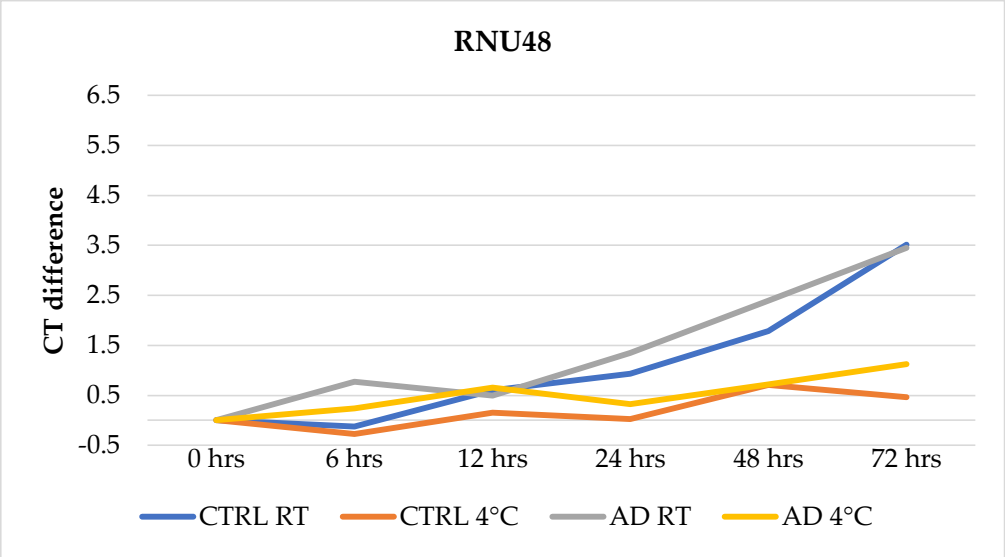

4.5.2.4. RNU6B

RNU6B shows a CT difference of nearly 1.5 for both samples stored at 4°C and approximately 2.5 for samples stored at room temperature (RT). This corresponds to a three-fold and almost six-fold drop in measurable transcript levels respectively (Figure 4.10). From 12 until 72 hours CT differences varied between 2.5 and 3.5 with some minor discrepancies. This represents a diminution in RNU6B transcript levels from six-fold to 11 fold at 72 hours.

Figure 4. 10 CT difference of individual samples to the 0 hours sample for RNU6B.

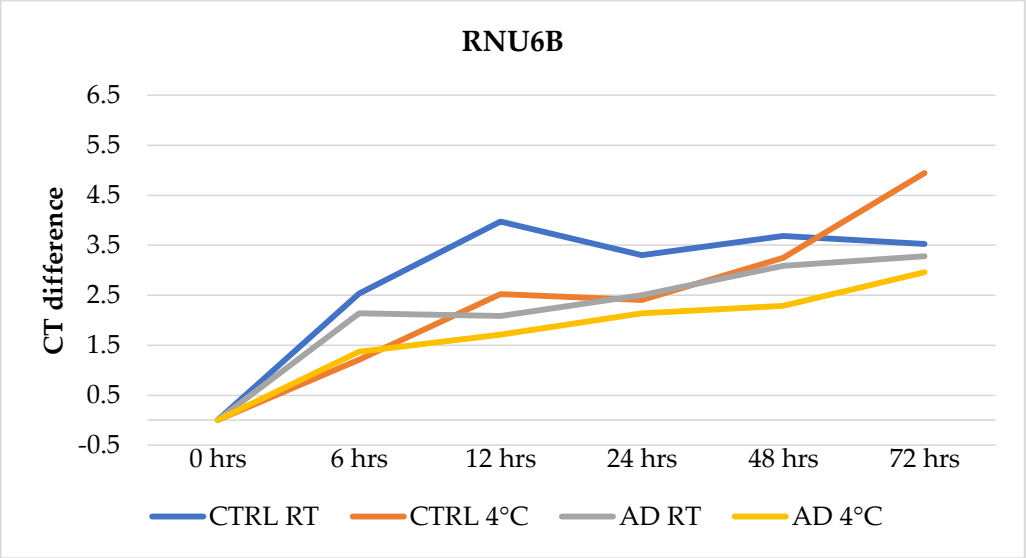

4.5.2.5. miR-9-5p

Samples stored at 4°C demonstrated steady transcript levels for miR-9-5p up to 72 hours in the simulation of post-mortem delay as observed in Figure 4.11. In the case of samples stored at room temperature, a CT difference of 2 is observable at 72 hours. This represents a four-fold drop for miR-9-5p at 72 hours.

Figure 4. 11 CT difference of individual samples to the 0 hours sample for miR-9-5p.

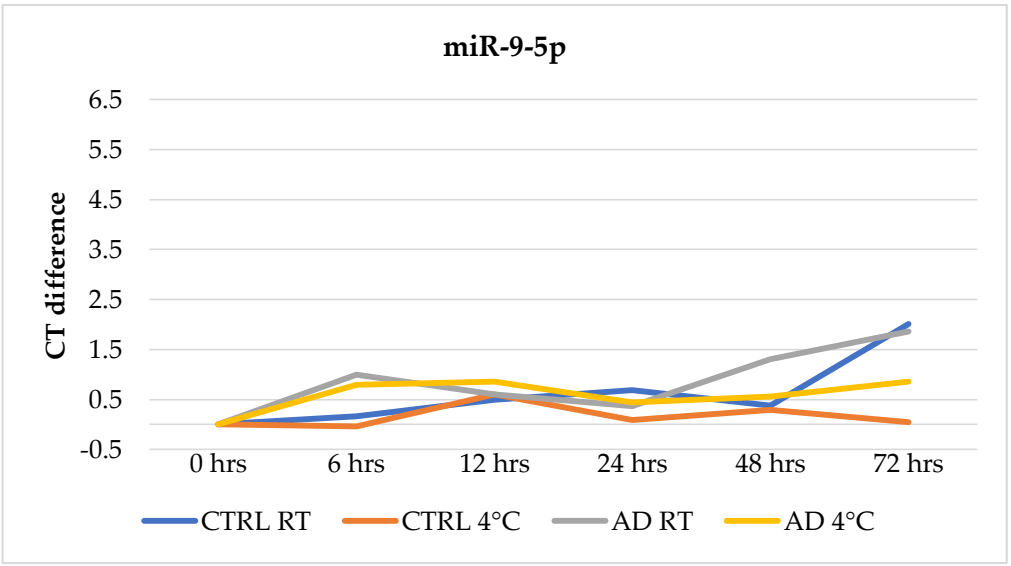

4.5.2.6. miR-9-3p

As observed in Figure 4.12, miR-9-3p shows very steady values for both samples at both temperatures. All CT differences are within a range of -0.5 to 0.5 to the geometric mean. This miRNA, along to its counterpart miR-9-3p are stable up to 72 hours.

Figure 4. 12 CT difference of individual samples to the 0 hours sample for miR-9-3p.

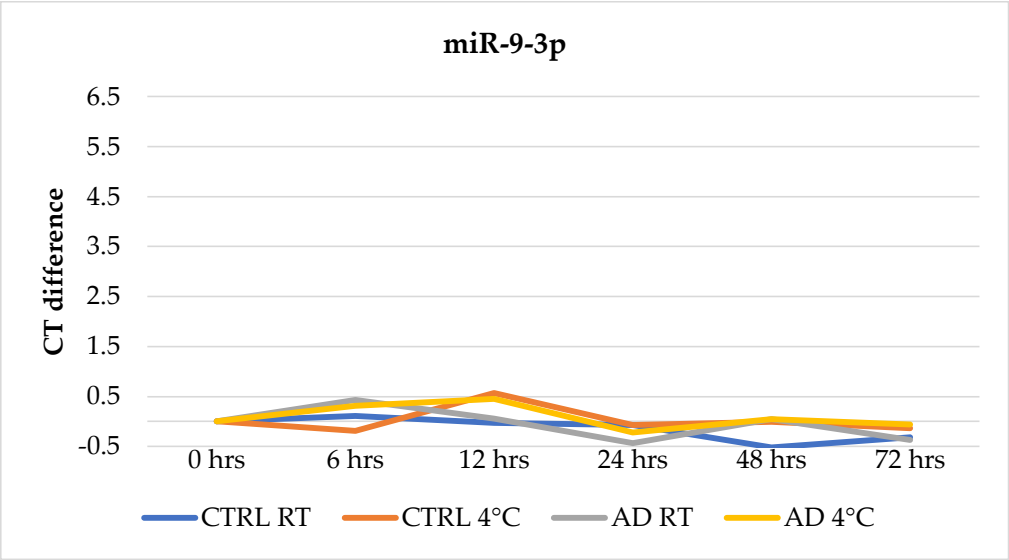

4.5.2.7 Comparison and rank-ordering of observed transcript stabilities for investigated calibrators.

For the 4°C incubation experiments, based on variations of CT value differences from the geometric mean, the performance of the various calibrators, in terms of highest to lowest apparent stability of transcripts over time are:

miR-9-3p > miR-9-5p > RNU48 > RNU6B > RNU44 > RNU43

For the RT incubation experiments, based on variations of CT value differences from the geometric mean, the performance of the various calibrators, in terms of highest to lowest apparent stability of transcripts over time are:

miR-9-3p > miR-9-5p > RNU48 > RNU44 > RNU6B > RNU43

4.5.3. Evaluation of calibrator genes according to disease pathology

In addition to the need to assess general patterns of expression of each of the calibrators across all individual samples, and to investigate the stability of calibrator transcripts under various simulated storage conditions, the final assessment needed to verify the suitability of a calibrator is to assess whether the expression of the calibrator genes is changed according to any phenotype or level of disease severity, as was noted in Chapter 3 for RNU6B highlighting its lack of suitability as a calibrator gene for the study of AD.

4.5.3.1. RNU43

The small nucleolar RNU43 (Official symbol *SNORD43*) is transcribed from chromosome 22q13.1. The average CT standard deviation between triplicates was 0.052 (252 triplicates in total) suggesting a good estimate for results (143). D'Agostino & Pearson normality test showed that RNU43 doesn't have a normal distribution. The expression of RNU43 with Braak stage score was not significantly different, as assessed by Kruskal-Wallis test H=5.09 and significance of p=0.4049 (Figure 4.13). The expression of RNU43 between diagnostic groups was not significantly different, as assessed by Kruskal-Wallis test H=4.604 and significance of p=0.2032 (Figure 4.14).

Figure 4. 13 Percentage of difference for RNU43 by Braak stages.

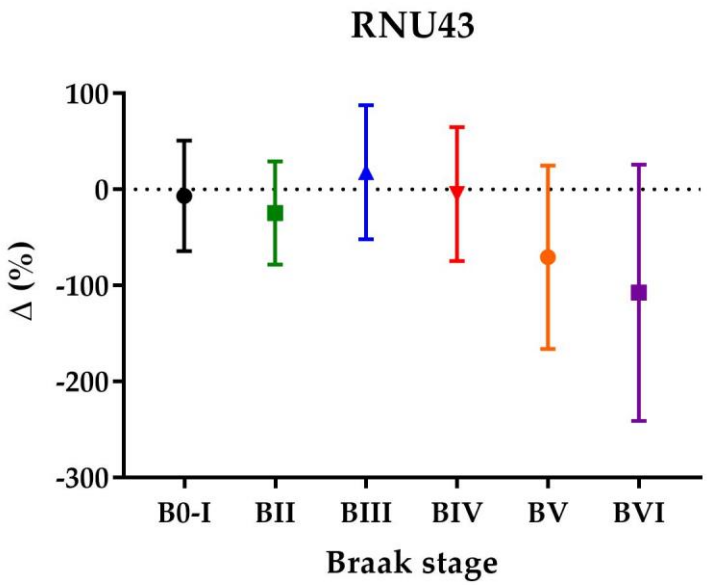

Figure shows the percentage of difference for RNU43 in Braak-related disease stages compared to samples with Braak stage 0 and I, error bars show the 95% confidence interval and average is depicted.

Figure 4. 14 Percentage of difference for RNU43 by diagnostic groups.

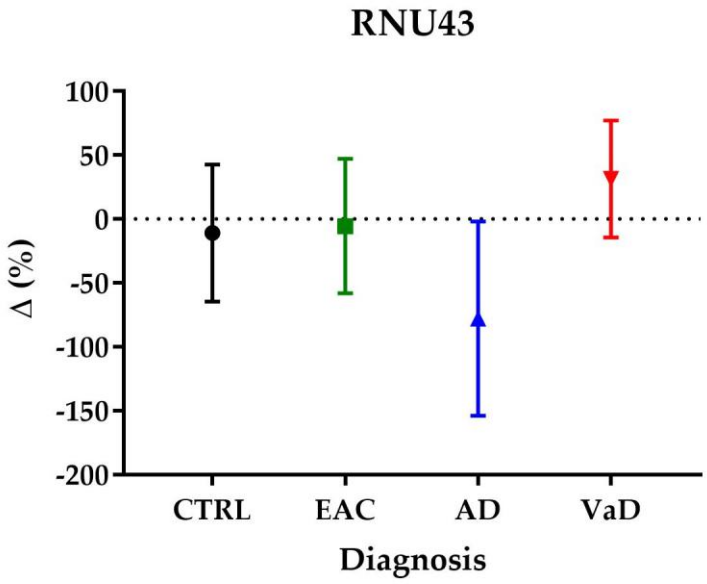

Figure shows the percentage of difference for RNU43 by diagnostic groups, error bars show the 95% confidence interval and average is depicted.

4.5.3.2. RNU44

The small nucleolar RNU44 (Official symbol *SNORD44*) is transcribed from chromosome 1q25.1. The average CT standard deviation between triplicates was 0.042 (255 triplicates in total) suggesting a good estimate for results (143). D'Agostino & Pearson normality test showed that RNU44 was not normally distributed. The expression of RNU44 with Braak stage score was significantly different, as assessed by Kruskal-Wallis test H=14.37 and significance of p=0.0134 (Figure 4.15). Dunn's post hoc test showed a significant difference between Braak stage VI and Braak stage 0-1 ($p<0.05$) and Braak stage III ($p<0.05$) (Figure 4.15). The expression of RNU44 between diagnostic groups was significantly different, as assessed by Kruskal-Wallis test H=15.4 and significance of p=0.0015 (Figure 4.16). Dunn's post hoc test showed a significant difference between AD and VaD ($p<0.01$) (Figure 4.16).

Figure 4. 15 Percentage of difference for RNU44 by Braak stages.

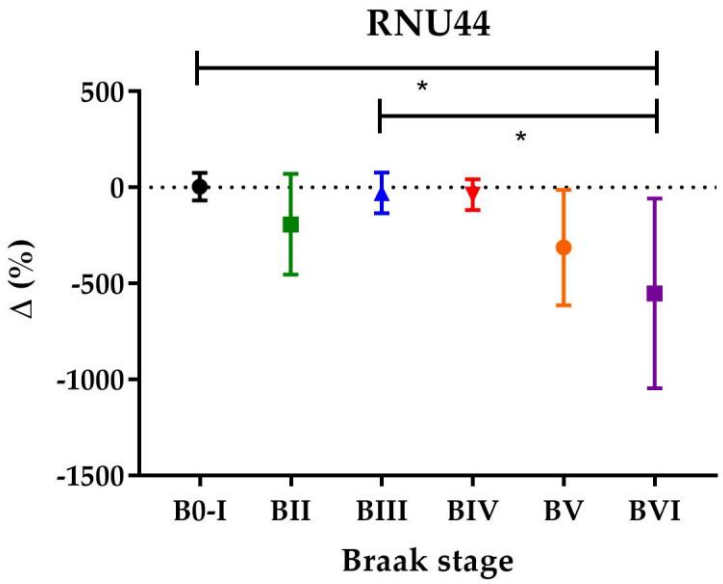

Figure 4.15 shows the percentage of difference for RNU44 in Braak-related disease stages compared to samples with Braak stage 0 and I, error bars show the 95% confidence interval and average is depicted, *$p<0.05$.

Figure 4. 16 Percentage of difference for RNU44 by diagnostic groups.

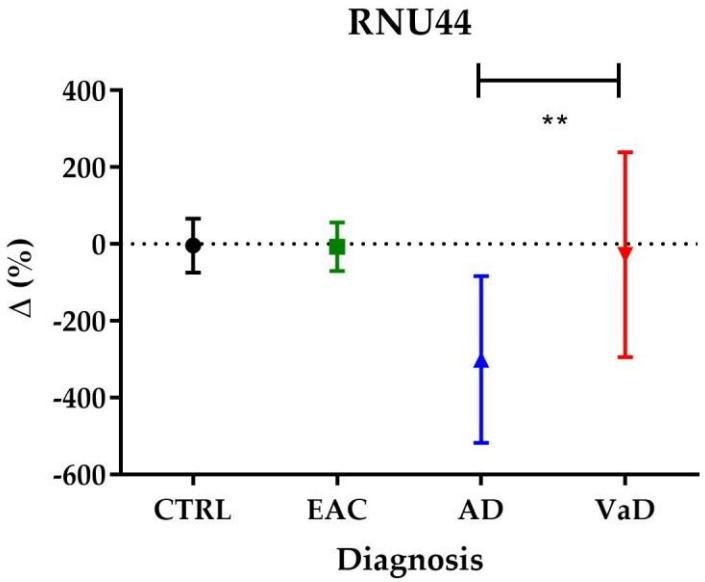

Figure shows the percentage of difference for RNU44 between diagnostic groups, error bars show the 95% confidence interval and average is depicted, **p<0.01.

4.5.3.3. RNU48

The small nucleolar RNU48 (Official symbol *SNORD48*) is transcribed from chromosome 6p21.33. The average CT standard deviation between triplicates was 0.032 (258 triplicates in total). D'Agostino & Pearson normality test showed that RNU48 was not normally distributed. The expression of RNU48 between Braak stages was not significantly different, Kruskal-Wallis statistic of H=4.43 and p=0.4893 (Figure 4.17). The expression of RNU48 between diagnostic groups was not significantly different, as assessed by Kruskal-Wallis test H=4.139 and significance of p=0.2468 (Figure 4.18).

Figure 4. 17 Percentage of difference for RNU48 by Braak stages.

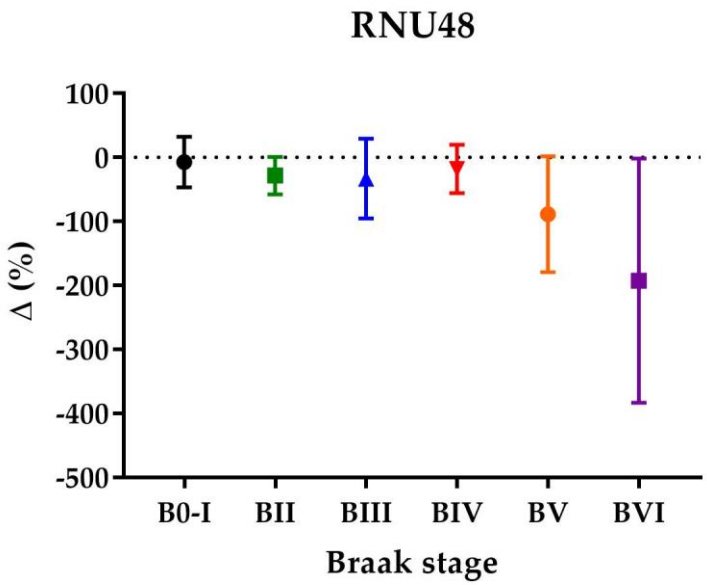

Figure shows the percentage of difference for RNU48 in Braak-related disease stages compared to samples with Braak stage 0 and I, error bars show the 95% confidence interval and average is depicted.

Figure 4. 18 Percentage of difference for RNU48 by diagnostic groups.

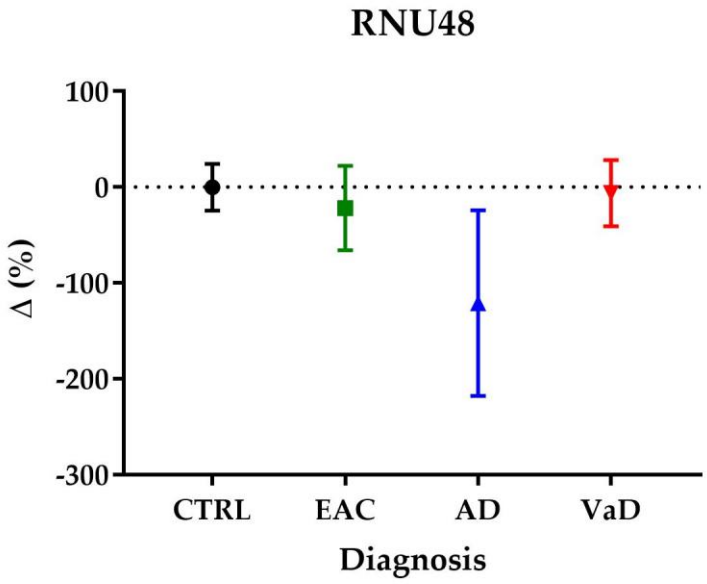

Figure shows the percentage of difference for RNU48 between diagnostic groups, error bars show the 95% confidence interval and average is depicted.

4.5.3.4. RNU6B

The small nuclear RNU6B (Official symbol *RNU6-6P*) maps from a pseudogene in chromosome 10p13. The average CT standard deviation between triplicates was 0.031 (252 triplicates in total). D'Agostino & Pearson normality test showed that RNU6B was not normally distributed. The expression of RNU6B across Braak stage and VaD was significantly different, Kruskal-Wallis statistic of 12.42 and p=0.0294. Dunn's multiple comparison test showed a significant difference between Braak stage VI and Braak stage III ($p<0.05$) (Figure 4.19). The expression of RNU6B between diagnostic groups was significantly different, as assessed by Kruskal-Wallis test H=12.37 and significance of p=0.0062 (Figure 4.20). Dunn's multiple comparison test showed a significant difference between AD and VaD ($p<0.05$) (Figure 4.20).

Figure 4. 19 Percentage of difference for RNU6B by Braak stages.

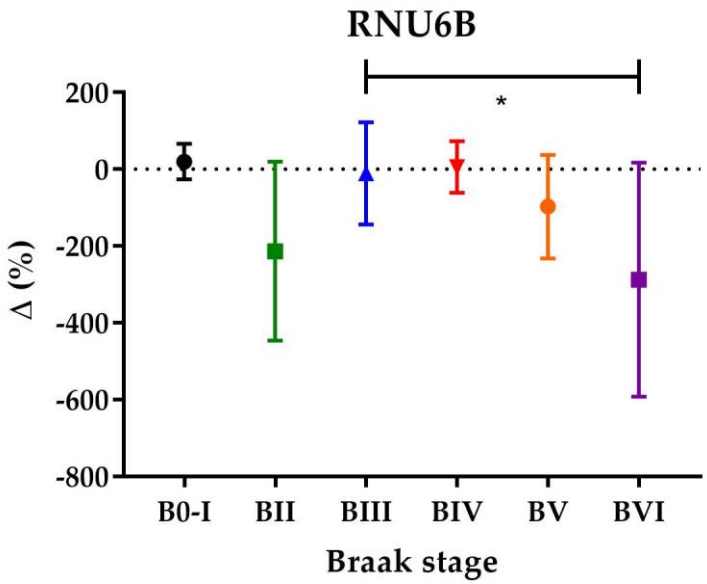

Figure shows the percentage of difference for RNU6B in Braak-related disease stages compared to samples with Braak stage 0 and I, error bars show the 95% confidence interval and average is depicted, *$p<0.05$.

Figure 4. 20 Percentage of difference for RNU6B by diagnostic groups.

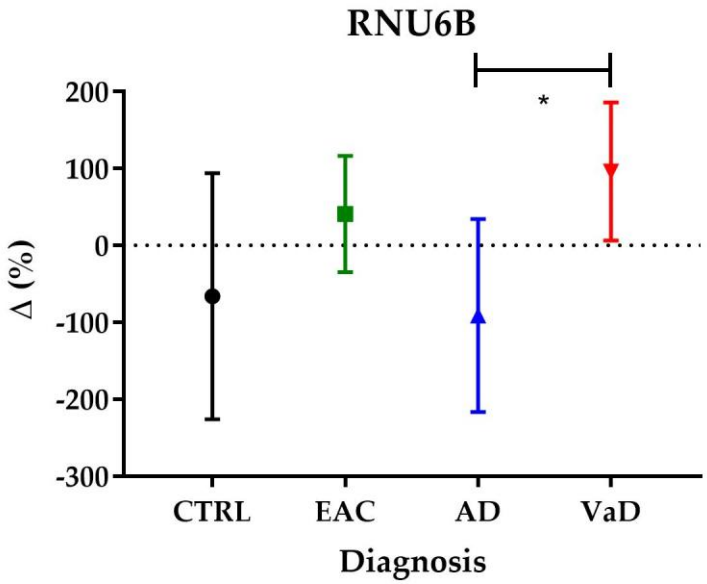

Figure shows the percentage of difference for RNU6B between diagnostic groups, error bars show the 95% confidence interval and average is depicted.

4.5.3.5. miR-9-5p

miR-9-5p derives from the miR-9 gene along with miR-9-3p located on chromosome 1q22. The average CT standard deviation between triplicates was 0.036 (252 triplicates in total). D'Agostino & Pearson normality test showed that miR-9-5p was not normally distributed. The expression of miR-9-5p across Braak stage and VaD was not significantly different, Kruskal-Wallis statistic of 7.284 and p=0.2003 (Figure 4.21). The expression of miR-9-5p between diagnostic groups was not significantly different, as assessed by Kruskal-Wallis test H=5.896 and significance of p=0.1168 (Figure 4.22).

Figure 4. 21 Percentage of difference for miR-9-5p by Braak stages.

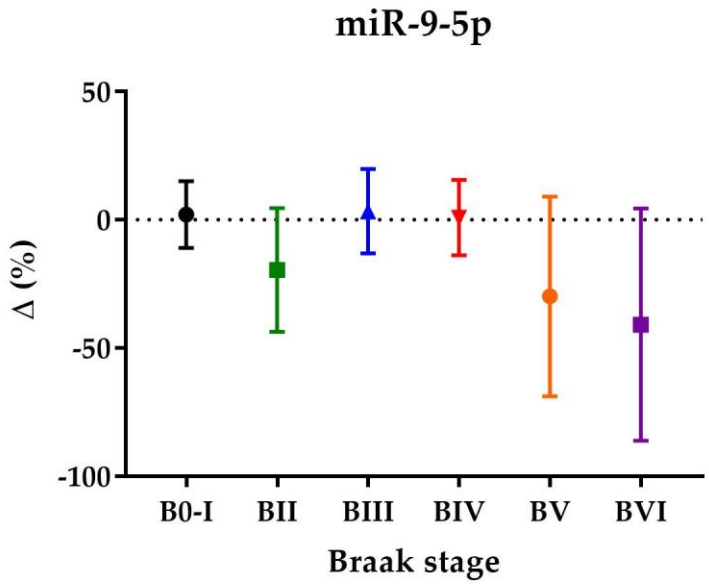

Figure shows the percentage of difference for miR-9-5p in Braak-related disease stages compared to samples with Braak stage 0 and I, error bars show the 95% confidence interval and average is depicted.

Figure 4. 22 Percentage of difference for miR-9-5p by diagnostic groups.

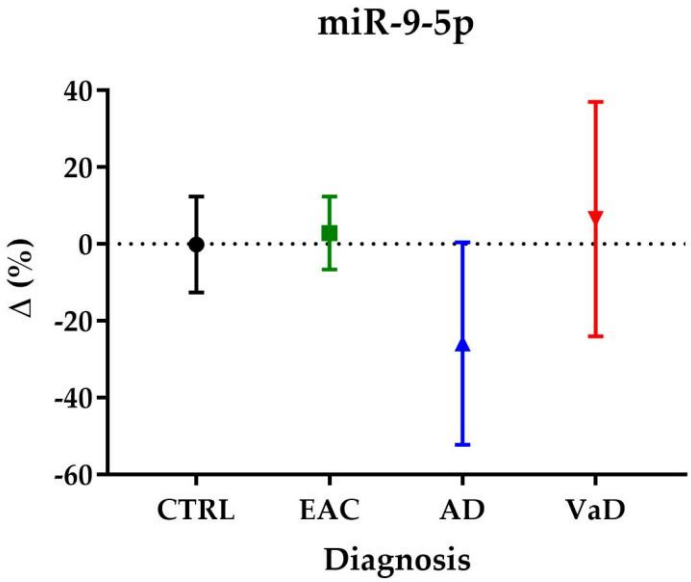

Figure shows the percentage of difference for miR-9-5p between diagnostic groups, error bars show the 95% confidence interval and average is depicted.

4.5.3.6. miR-9-3p

Similar to its counterpart (miR-9-5p), miR-9-3p derives from the miR-9 gene located on chromosome 1q22. The average CT standard deviation between triplicates was 0.042 (255 triplicates in total). D'Agostino & Pearson normality test showed that miR-9-3p was not normally distributed. The expression of miR-9-3p across Braak stage was not significantly different, Kruskal-Wallis statistic of 5.104 and p=0.4034 (Figure 4.23). The expression of miR-9-3p between diagnostic groups was not significantly different, as assessed by Kruskal-Wallis test H=1.581 and p=0.6637 (Figure 4.24).

Figure 4. 23 Percentage of difference for miR-9-3p by Braak stages.

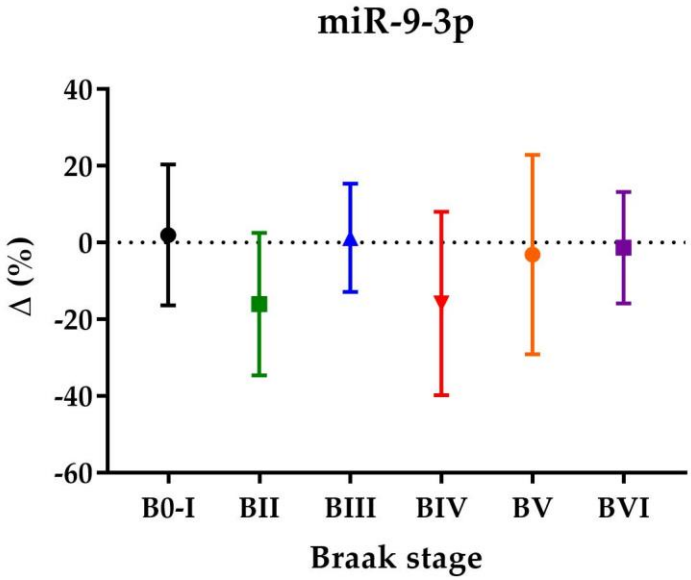

Figure shows the percentage of difference for miR-9-3p in Braak-related disease stages compared to samples with Braak stage 0 and I, error bars show the 95% confidence interval and average is depicted.

Figure 4. 24 Percentage of difference for miR-9-3p by diagnostic groups.

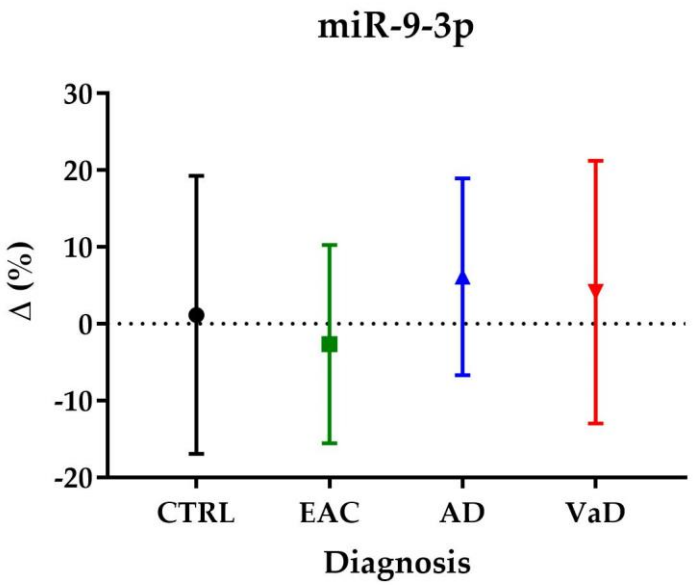

Figure shows the percentage of difference for miR-9-3p between diagnostic groups, error bars show the 95% confidence interval and average is depicted.

4.5.3.7. Ranking of calibrators according to expression in relation to neurodegenerative pathology and disease group

According to the comparisons of each of the calibrators in relation to markers of neurodegenerative pathology and diagnostic group, all but 2 of the calibrators showed no significant differences. As a calibrator no differences would be what is expected to be suited as a calibrator gene.

4.5.4. Overall ranking of small RNAs as calibrator gene

It is important to assess the performance of all the calibrators across all of the criteria in which they were tested in this chapter. This includes assessment of expression according to plots of the data across all the individual samples studied and the percentage of difference proposed previously. It also includes performance for their stability against the simulated post-mortem delay experiments, and the comparisons against neurodegenerative pathology and diagnosis.

A good calibrator gene should be one with low variance between individual samples, show little or no loss of stability according to post-mortem delay time and temperature conditions, and not be altered according to the disease phenotypes it is to be used in to measure changes of other target miRNAs.

Overall, miR-9-3p appeared to be the most consistent performer across all of these investigative tests and would appear to be the highest performing calibrator gene tested. On balance the second best performing calibrator was miR-9-5p. The third most stable calibrator gene found was RNU48, followed by RNU43 and RNU6B. Finally, RNU44 is the least stable calibrator gene evaluated.

4.6. Discussion and conclusions

4.6.1 Summary of findings

As stated, the null hypothesis posits that there would be no significant difference in the levels of these snRNAs between stages of neuropathology and disease, nominated by Braak stage and by type of dementia when compared to VaD. A statistically significant difference in the expression of RNU6B and RNU44 was found. Thus, the null hypothesis is rejected for these two calibrator genes. Although, the null hypothesis cannot be rejected for the rest of snRNAs evaluated, analysis of their stability by groups might disguise specific differences.

The alternative analysis using general plots of the data across all samples and the percentage of difference using absolute values showed equivalent results. These data showed that the most stable, and least variable of the snRNAs were miR-9-3p and miR-9-5p with only minor differences between them. There were greater levels of variance observed for RNU48, RNU43, RNU6B and RNU44 in that order.

Similar standardised testing of all the calibrators under simulated conditions of post-mortem delay showed a similar pattern of results, where the best performing calibrators were miR-9-3p and miR-9-5p with the other snRNAs performing less well and not to standards that might be deemed acceptable for use in post-mortem tissue studies. Finally, from comparisons with neurodegenerative pathology (according to Braak stage) and with disease type, there were no significant differences found for miR-9-3p, miR-9-5p, RNU48 and RNU43.

4.6.2. Next steps

miRNAs are much more resistant to RNA degradation than longer RNA sequences (66) and thus this chapter sought to test more appropriate snRNAs that were of more equivalent size to miRNAs as well as test the possible effect of sequence length as a variable in its own right with respect to being a calibrator gene.

My results showed that RNU48, miR-9-3p and miR-9-5p are all stable at 4°C in the period of 72 hours. This is in accordance to others reports in the literature, in related work, Ma et al analysed the effect of post-mortem delay on RNA degradation in rat brain tissue (144). They analysed the stability of 9 commonly used calibrators (including RNU6B, miR-9 and miR-125b) over a period of 144 hours with 12-time points and at different temperatures, including 4, 15, 25, and 35°C. They concluded, in this non-human, non-diseased tissue that miR-9 and miR-125b were not degraded up to 144 hours post-mortem even at 35°C and that the commonly used RNU6B is not suitable as an endogenous control. This is consistent with my findings where miR-9-5p and miR-9-3p were the best performing calibrators and RNU6B one of the worst performers.

In a subsequent publication, by the same group, they analysed the extent of RNA degradation in rat and human tissues from myocardium and liver, but not brain tissue (145). They showed in this study that miR-1 and miR-133a were stable over 5 days, even at 35°C. Similarly, Peiro-Chova et al analysed samples from patients with breast

cancer obtained after tumor resection that were stored using cryopreservation, frozen samples with several thawing processes and formalin-fixed paraffin-embedded samples (146). They studied the stability of several calibrators, including miR-21, miR-125b, miR-191 and like in this study, RNU6B. They concluded that miRNAs are strongly preserved irrespective of the quality of the tissue sample and that their levels were similar between different samples and with RNA integrity values ranging from 1.3 to 9.7 (147).

From my data, which has been validated against the tissue type and the disease context I am investigating, I have concluded that the best choice of calibrators for this work, miR-9-3p, miR-9-5p and RNU48, will be used henceforth as calibrator genes for the reinvestigation of the panel of miRNAs investigated in Chapter 3 and also to investigate other miRNAs as they are described in later chapters.

Chapter 5.- Evidence-based re-evaluation of examining miRNAs related to classical histopathological hallmarks of Alzheimer's disease

5.1 Introduction

A number of proteins postulated to play a role in the development of AD have been investigated and miRNAs predicted to target those proteins, have been considered as miRNAs of interest in the studies outlined in this thesis. Details of experiments to determine the involvement of miRNAs findings related to those proteins can be found in Chapter 3. Seven miRNAs from five miRNA families of interest were examined in Chapter 3, and some thought-provoking results were obtained.

A pattern of expression for five of the seven miRNAs was found to be associated with disease progression and significant differences were observed between the diagnostic groups EAC, AD, VaD and control. However, it was also found that such measurements lacked some precision. The calibrator gene used was not appropriate and this questioned preliminary results.

Thus, in Chapter 4, I evaluated six calibrator genes to explore their suitability as alternative calibrator genes that would be better suited to the study of miRNAs in AD. In doing so, I also scrutinised several methods in order to find the best way of analysing the variability of the reference genes. The intention of these studies was to identify the best performing calibrator genes to allow a more accurate re-evaluation of the miRNAs of interest in relation to the development of classical histopathological hallmarks of AD, first described in Chapter 3.

From the six calibrator genes analysed, two of them showed significant differences between subgroups. Whilst statistical analysis was undertaken between subgroups, it is possible that the use of subgroups can disguise specific differences and thus, I also examined variability of expression for each calibrator gene by plots of the data and a

proposed percentage of difference method using absolute values (described in Methods section 2.7).

To aid with the re-evaluation, the three best performing calibrator genes selected from Chapter 4 (miR-9-3p, miR-9-5p and RNU48) were used to re-examine previous miRNA families of interest but this time with the total number of miRNAs comprising such miRNA families. A summary of the miRNAs and the proteins previously described in Chapter 3 are presented in Table 5.1 for convenience. This re-evaluation is the central focus of this chapter.

Table 5. 1 Transcripts and miRNAs related to classical hallmarks of AD.

Gene name	miR-16	miR-29	miR-34	miR-125	miR-132/212	miR-216
ADAM10	2		2			
BACE1	2	2		1	2	1
BACE2	1			1		1
PSEN1		1	1	1		2
NOTCH1			2	1		
ABCA1			1		1	
LDLR			1		1	
LRP1				1	2	
AGER					2	
SORL1						1
RELN	2		1			
PDGFB		1	1			
PDGFRA		1	2		1	
PDGFRB		1	1			
AQP4	2	2				4
CD200			1			1
CD14			1			
CD200R1			1			5
MME	1				2	3
ECE1			2	2		
ECE2						1
ACE	1	2	3	1		
MMP2		1	1	1		
MMP14			1	1		
CD147				1		
IDE		1		2	1	1
GSK3B		1			2	
MAPK1		1	2		3	
MAPT			3		1	
PPP2CA	2	1		1		3
PPP2R1A		1		3		
ANP32A			1		1	
SET		2		1		
OGT	1				2	
PPP3CB	1					3

Table shows transcripts involved in one or more of the following: amyloid production, transport across the blood brain barrier (BBB) and degradation enzymes; tau phosphorylation; BBB integrity; glymphatic system or immune response are listed with the corresponding number of binding sites for each of the six miRNA families.

5.2 Hypothesis

The null hypothesis is that there is no significant difference in the levels of these miRNAs between diagnostic groups, AD, VaD, early AD changes (EAC) and non-demented controls.

5.3 Methods

5.3.1. Study cohort

The study cohort, as described in detail in Chapter 2 (Section 2.1) comprised brain tissue from 22 AD, 20 EAC, 18 VaD and 24 controls.

Table 5. 2 Demographic information of the cohort used in Chapter 5.

Diagnosis	Gender (Male/Female)	Age (σ)	PMI (σ)	ApoE4 (No/Yes)	Total
Control	11/13	80 (9.7)	35.4 (16.2)	21/1	24
Early Alzheimer Changes	11/9	85 (6)	36.5 (15)	14/4	20
Alzheimer's Disease	11/11	78 (7.2)	23.7 (13.4)	3/16	22
Vascular Dementia	9/9	83 (7.9)	34.7 (12.3)	9/4	18
Total	42/42	81.2 (8.1)	32.5 (15.1)	47/25	84

Table shows demographic information of the cohort, post-mortem interval (PMI), standard deviation (σ).

5.3.2. Brain tissue dissection and homogenization

Brain tissue dissection and homogenization was undertaken on the cohort as described in Chapter 2 section 2.2.

5.3.3. RNA isolation, quantification and standardization

RNA isolation, quantification and standardization were performed as described in detail in Chapter 2 section 2.3.

5.3.4. Software for analysis of target proteins (DAVID and PANTHER)

DAVID and PANTHER software were used for analysis of predicted target proteins of the selected miRNAs as described in detail in Chapter 2 section 2.13.

5.3.5. Data collection and analysis

Data on selected calibrator genes was generated by quantitative polymerase chain reaction (qPCR) as described in Chapter 2 section 2.6. The analysis of the resultant data was undertaken using the new formula proposed in Chapter 2 section 2.7. Statistical analysis was performed using the statistical package Graph Pad Prism (Chapter 2 section 2.16).

5.4 Results

This section will include the re-evaluation of all the miRNAs studied in Chapter 3, as well as the study of additional miRNAs that represent additional members of the main miRNA families that have been attributed to the characteristic hallmarks of AD pathology. Table 5.3 summarises the list of miRNAs studied here, according to the families they relate to and to highlight those that have been examined in Chapter 3 and repeated here, or investigated here for the first time.

Table 5. 3 miRNA families studied in Chapter 5.

miRNA family	miRNA members of the family
miR-16	miR-15a/15b/16/195/424/497
miR-29	miR-29a/29b/29c
miR-34	miR-34a/34b/34c/449
miR-125	miR-125a/125b
miR-132	miR-132/212

Table shows miRNA families studied in this chapter and their corresponding miRNA members.

5.4.1. miR-16 family

This miRNA family is composed by miR-15a/15b/16/195/424/497, all of which, as representative members were investigated, and the corresponding data is presented.

5.4.1.1. miR-15a

miR-15a is encoded on chromosome 13q14.2 (*MIR15A* gene). After the measurement of expression it was revealed by the D'Agostino & Pearson normality test that the miR-15a measurements were not normally distributed and thus the Kruskal-Wallis test was used. This revealed that there was a significant percentage of difference for miR-15a between diagnostic groups, Kruskal-Wallis test $H=9.55$ and $p=0.0228$ (Figure 5.1). Further analysis by Dunn's multiple comparison test showed a significant difference between EAC and AD ($p<0.05$), whereby there was a higher level of miR-15a expression in the AD group.

Figure 5. 1 Percentage of difference for miR-15a.

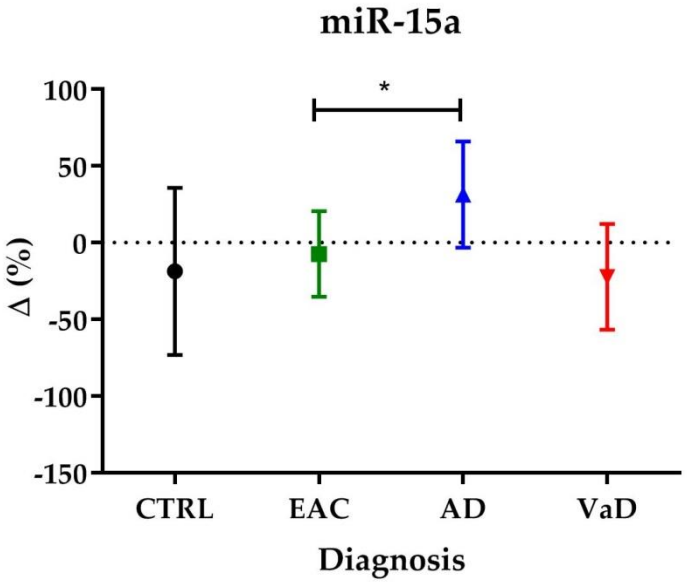

Figure shows the percentage of difference for miR-15a in different diagnostic groups compared to controls. Error bars show the 95% confidence interval and the average is depicted, * $p<0.05$.

5.4.1.2. miR-15b

miR-15b is encoded in chromosome 3q25.33 (*MIR15B* gene). The D'Agostino & Pearson normality test applied to the data showed that, like miR-15a, that the expression for miR-15b was not normally distributed and thus the Kruskal-Wallis test was used. This then showed the percentage of difference for miR-15b expression was significantly different between diagnostic groups, Kruskal-Wallis test $H=16.10$ and $p=0.0011$ (Figure 5.2). Dunn's multiple comparison test then revealed significant increases in miR-15b expression in AD compared to controls ($p<0.05$), EAC ($p<0.01$) and VaD ($p<0.05$).

Figure 5. 2 Percentage of difference for miR-15b.

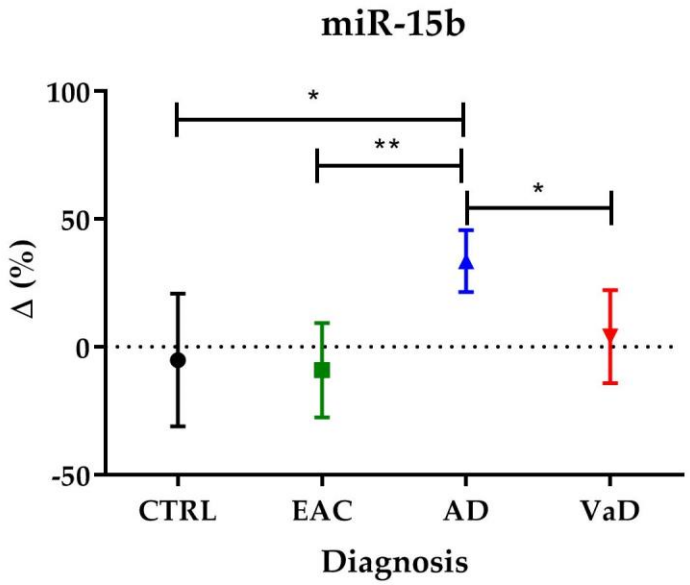

Figure shows the percentage of difference for miR-15b of all diagnostic groups compared to controls. Error bars show the average and the 95% confidence interval, * $p<0.05$ and ** $p<0.01$.

5.4.1.3. miR-16

Similar to miR-15a, miR-16 maps to chromosome 13q14.2 (*MIR16* gene), both genes are clustered within 0.5 kb. Application of the D'Agostino & Pearson normality test to the data showed that miR-16 was similarly not normally distributed (as with previous family members) and thus, the Kruskal-Wallis test was used. The Kruskal-Wallis test on miR-16 (Figure 5.3) revealed significant difference between diagnostic groups, (Kruskal-Wallis test $H=28.21$ and $p=0.0001$). Furthermore, application of Dunn's multiple comparison test showed a significant increase in miR-16 expression in AD compared to controls ($p<0.001$), EAC ($p<0.001$) and VaD ($p<0.0001$).

Figure 5. 3 Percentage of difference for miR-16.

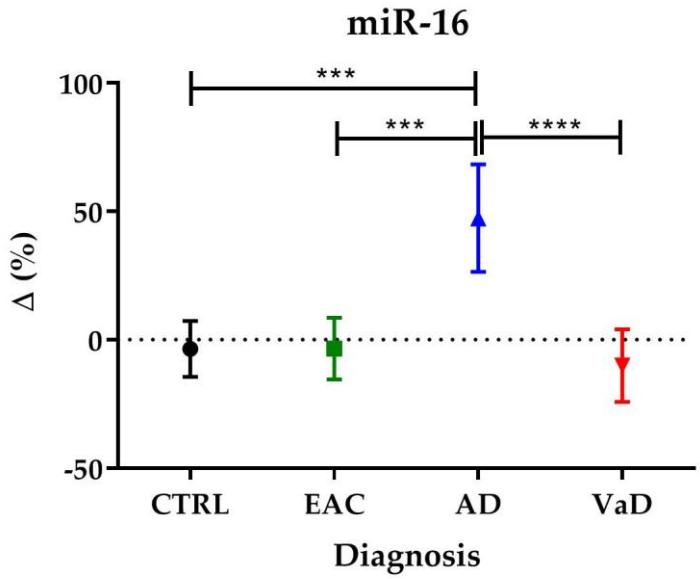

Figure 5.3 shows the percentage of difference for miR-16 of all diagnostic groups compared to controls. Error bars show the 95% confidence interval and the average is depicted, *** $p<0.001$ and **** $p<0.0001$.

5.4.1.4. miR-195

miR-195 is transcribed from chromosome 17p13.1 (*MIR195* gene). The D'Agostino & Pearson normality test, as for the other miRs in this family, showed that miR-195 was not normally distributed and thus, the Kruskal-Wallis test was used. In this analysis it revealed that the percentage of difference for miR-195 expression (Figure 5.4) was significantly different between diagnostic groups (Kruskal-Wallis test $H=23.76$ and $p<0.0001$). Moreover, Dunn's multiple comparison test found a significant increase in miR-195 expression in AD compared to controls ($p<0.01$), EAC ($p<0.0001$) and VaD ($p<0.05$).

Figure 5. 4 Percentage of difference for miR-195.

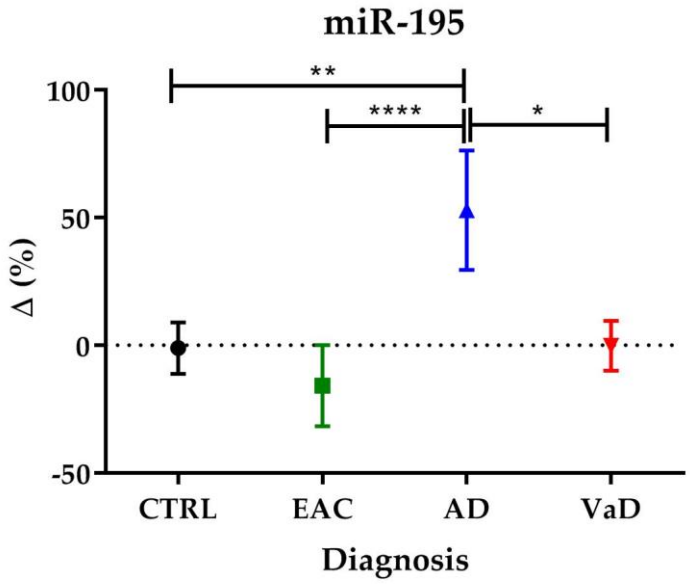

Figure shows the percentage of difference for miR-195 for all diagnostic groups compared to controls. Error bars show the 95% confidence interval and the average is depicted, * $p<0.05$, ** $p<0.01$ and **** $p<0.0001$.

5.4.1.4. miR-424

miR-424 is derived from chromosome Xq26.3 (*MIR424* gene). As with the previous miRNAs, the D'Agostino & Pearson normality test showed that miR-424 was not normally distributed and thus, the Kruskal-Wallis test was used. As seen for the other family members, miR-424 measurements were significantly different (Figure 5.5) between diagnostic groups (Kruskal-Wallis test H=10.42 and p=0.0153). Dunn's multiple comparison test similarly showed a significant difference between AD and EAC ($p<0.05$) in miR-424 expression.

Figure 5. 5 Percentage of difference for miR-424.

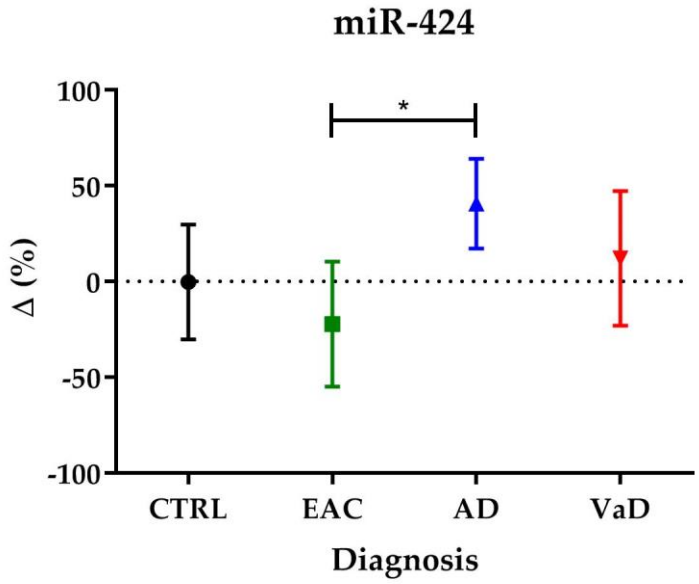

Figure shows the percentage of difference for miR-424 for all diagnostic groups compared to controls. Error bars show the 95% confidence interval and the average is depicted, * $p<0.05$.

5.4.1.5. miR-497

Similar to miR-195, miR-497 is also transcribed from chromosome 17p13.1 (*MIR497* gene). In contrast to all of the other family members, miR-497 expression was found to be normally distributed, which was confirmed by Bartlett's test ($p=0.269$). miR-497 was significantly different between diagnostic groups (Figure 5.6) ANOVA $F=3.01$ and $p=0.0347$. Furthermore, Tukey's multiple comparison test showed a significant increase in AD compared to EAC ($p<0.05$).

Figure 5. 6 Percentage of difference for miR-497.

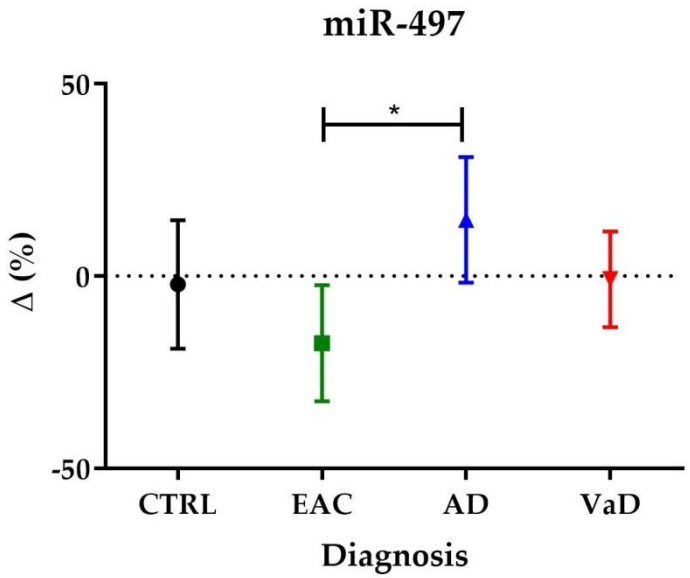

Figure shows the percentage of difference for miR-497 for all diagnostic groups compared to controls. Error bars show the 95% confidence interval and the average is depicted, * $p<0.05$.

5.4.1.5. Summary of miR-16 family results

All of the individual miRNA members of the miR-16 family showed relatively similar results. For some of them (miR-15b, miR-16 and miR-195) significant differences in their expression across all diagnostic groups with the greatest expression consistently shown in the AD group. For the remainder (miR-15a, miR-424 and 497) despite apparent significant differences across all groups, it was later found by Dunn's multiple comparison test, that the greatest effect appeared to be between the AD and EAC group.

5.4.1.6. Analysis of miR-16 family predicted target proteins

As these miRNAs share the seed region and predicted targets, and if they have influential effects on classical neuropathological hallmarks of AD, perhaps it is not unusual for all members of this family to demonstrate similar levels of expression.

With this in mind, it was deemed prudent for the predicted targets of these miRNAs to be analysed further.

Overall, this miRNA family has 1515 predicted targets according to TargetScan. Analysis of these predicted targets with DAVID software (May 2019) found 9 clusters that encapsulate particular pathways as defined by gene ontology terms. The clusters are annotated with their corresponding number of proteins involved in the pathway and the significance (p value) are shown in Table 5.4. The Benjamini value corresponds to the normal p-value (significance) adjusted to control for false discovery rate.

Table 5. 4 Analysis of predicted targets for miR-16 family by DAVID software.

DAVID pathways for miR-16 family	Protein count	Benjamini value
Cluster 1 enrichment score: 2.74		
Dicer pathway	4	0.48
RISC-loading complex	4	0.21
miRNA loading onto RISC involved in gene silencing by miRNA	4	0.5
Cluster 2 enrichment score: 1.3		
mRNA cleavage involved in gene silencing by siRNA	3	0.68
mRNA cleavage involved in gene silencing by miRNA	3	0.78
micro-ribonucleoprotein complex	3	0.51
Cluster 3 enrichment score: 1.18		
Phosphatidylinositol-5-phosphate binding	5	0.39
Phosphatidylinositol-3,5-bisphosphate binding	5	0.81
Phosphatidylinositol-3-phosphate binding	5	0.95
Cluster 4 enrichment score: 0.94		
Inositol-1,4,5-trisphosphate 5-phosphatase activity	3	0.76
Phosphatidylinositol-4,5-bisphosphate 5-phosphatase activity	3	0.85
Inositol-1,3,4,5-tetrakisphosphate 5-phosphatase activity	3	0.88
Cluster 5 enrichment score: 0.73		
Ubiquitin-like protein binding	3	0.76
Protein neddylation	3	0.99
Cullin family protein binding	3	0.97
Cluster 6 enrichment score: 0.51		
Voltage-gated chloride channel activity	3	0.95
Chloride ion binding	3	0.97
Regulation of anion transmembrane transport	3	1
Cluster 7 enrichment score: 0.3		

Inorganic anion transport	3	1
Inorganic anion exchanger activity	3	0.99
Anion transmembrane transport	3	1
Cluster 8 enrichment score: 0.28		
Nerve growth factor pathway	4	0.89
Epidermal growth factor signalling pathway	4	0.95
Platelet derived growth factor signalling pathway	4	0.96
Cluster 9 enrichment score: 0.04		
Proteasome	3	0.97
Regulation of cellular amino acid metabolic process	3	0.99
Antigen processing and presentation of exogenous peptide antigen via MHC class I, TAP-dependent	3	0.97

Table shows gene ontology and pathways related to proteins predicted to be targeted by the miR-16 family according to DAVID software analysis. The number of proteins that correspond to each pathway and the significance value (Benjamini value) are specified.

To further understand the possible biological relevance of changes observed in miR-16 family results, predicted targets for various miR-16 members were also analysed with PANTHER software (May 2019) and the summary results of these are shown in Table 5.5.

Table 5. 5 Analysis of predicted targets for miR-16 family by PANTHER software.

PANTHER pathways for miR-16 family	Protein count	Fold enrichment	P value
Cell cycle	9	5.65	0.0229
Insulin/insulin growth factor pathway-mitogen activated protein kinase cascade	13	5.28	0.0014
Alzheimer disease-amyloid secretase pathway	22	3.49	0.0004
Alzheimer disease-presenilin pathway	54	3.36	1.72 e-10
Fibroblast growth factor signalling pathway	26	2.99	0.0008
Cadherin signalling pathway	28	2.45	0.0133
Angiogenesis	30	2.28	0.0222
Wnt signalling pathway	49	2.13	0.0007
Gonadotropin-releasing hormone receptor pathway	45	2.09	0.0027

Table shows biological pathways related to proteins predicted to be targeted by miR-16 family members according to PANTHER software and presented in order of fold enrichment. The individual Panther pathways that were identified, the number of proteins targeted within that pathway, the corresponding fold enrichment and the corresponding p-values are specified.

According to the analysis done by PANTHER, nine pathways were identified that were statistically significant. These pathways involved variable numbers of predicted target proteins that ranged from 9 to 54 target proteins in any one pathway. These also had a range of fold enrichment scores that ranged from 5.65 to 2.09. On further examination of the pathways identified, it is evident that the Alzheimer-disease presenilin pathway has the highest target protein count and was the most highly significant (p=1.72 e-10), with an enrichment score of 3.36. Other pathways that were highly significant included the insulin/insulin growth factor pathway-mitogen activated protein kinase cascade (p=0.0014); Alzheimer disease-amyloid secretase pathway (p=0.0005); fibroblast growth factor signalling pathway (p=0.0008); Wnt signalling pathway (p=0.0007) and gonadotropin-releasing hormone receptor pathway (p=0.0027). There were also significant effects, although to a lesser extent for cell cycle (p=0.0229); cadherin signalling pathway (p=0.0133), and angiogenesis (p=0.0222).

5.4.2. miR-29 family

The miR-29 family is composed of the three members miR-29a/29b/29c, all of which were investigated and the data is now presented.

5.4.2.1. miR-29a

miR-29a is encoded on chromosome 7q32.3 (*MIR29A* gene). miR-29a expression when analysed by the D'Agostino & Pearson normality test showed that miR-29a was not normally distributed and thus, Kruskal-Wallis test was necessary. Application of the Kruskal-Wallis test showed that the percentage of difference for miR-29a (Figure 5.7) was significantly different between diagnostic groups (H=8.79 and p=0.032). Subsequent *post hoc* analysis by Dunn's multiple comparison test found that the previous association between all groups is perhaps due to a significant difference in miR-29a expression between the VaD and EAC groups such that the expression of the

VaD group was significantly lower than that of the EAC group ($p<0.05$), but which was not significantly different to the AD group.

Figure 5. 7 Percentage of difference for miR-29a.

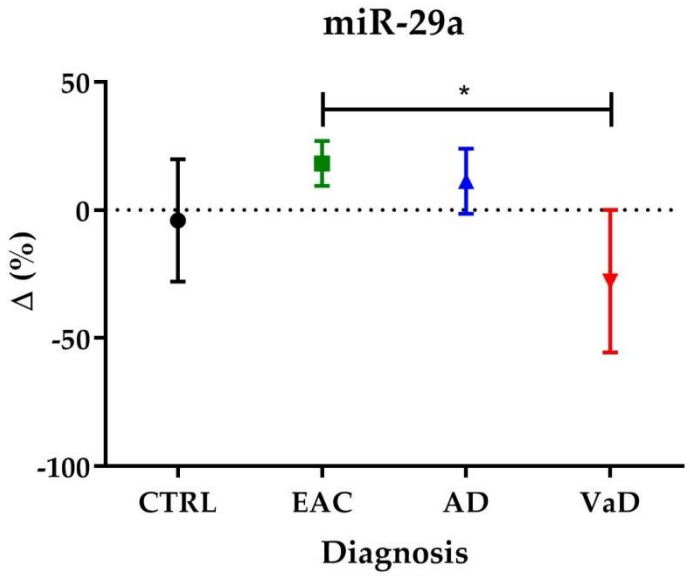

Figure shows the percentage of difference for miR-29a for all diagnostic groups compared to controls. Error bars show the 95% confidence interval and the average is depicted, * $p<0.05$.

5.4.2.2. miR-29b

MiR-29b can be derived from two precursors, miR-29b-1 (*MIR29B1* gene) and miR-29b-2 (*MIR29B2* gene) that are co-transcribed with miR-29a (chromosome 7q32.3) and miR-29c (chromosome 1q32.2) respectively. As for miR-29a, the D'Agostino & Pearson normality test showed that miR-29b was not normally distributed and thus, the Kruskal-Wallis test was used. On analysis it was revealed that measurements of miR-29b (Figure 5.8) were significantly different between diagnostic groups (Kruskal-Wallis test $H=12.77$ and $p=0.005$). Dunn's multiple comparison test showed a significant increase in AD compared to controls ($p<0.05$) and EAC ($p<0.01$).

Figure 5. 8 Percentage of difference for miR-29b.

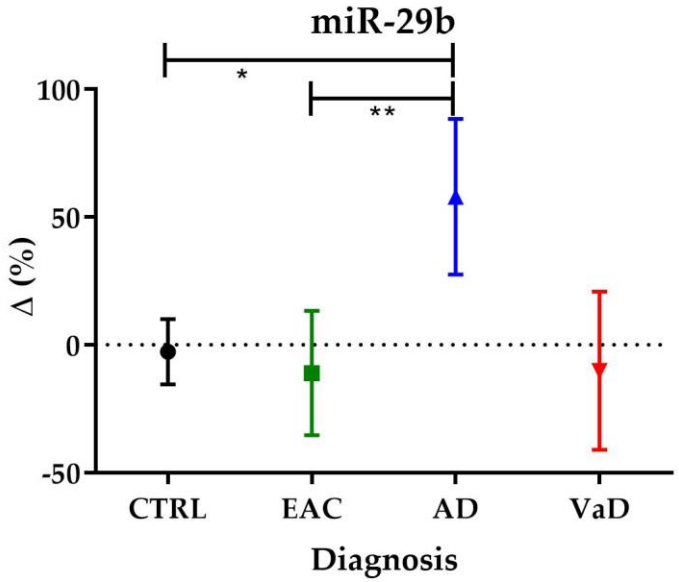

Figure shows the percentage of difference for miR-29b for all diagnostic groups compared to controls. Error bars show the 95% confidence interval and the average is depicted, * $p<0.05$ and ** $p<0.01$.

5.4.2.3. miR-29c

miR-29c is mapped to chromosome 1q32.2 (*MIR29C* gene). Initial analysis by the D'Agostino & Pearson normality test showed that miR-29c was normally distributed, which was then confirmed by Bartlett's test. In contrast to the other miR-29 family members, analysis by ANOVA showed that there was no significant difference for miR-29c expression (Figure 5.9) between diagnostic groups, ANOVA $F=1.167$ and $p=0.327$.

Figure 5. 9 Percentage of difference for miR-29c.

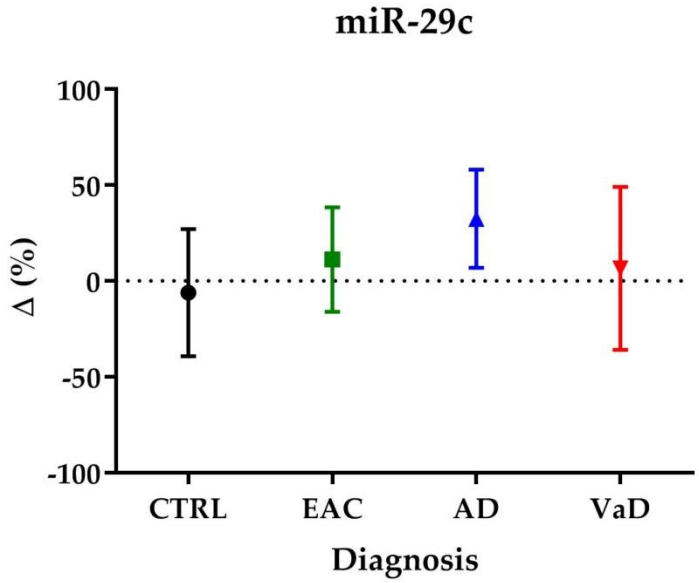

Figure shows the percentage of difference for miR-29c for all diagnostic groups compared to controls. Error bars show the 95% confidence interval and the average is depicted.

5.4.2.4. Summary of miR-29 family results

Only miR-29b showed a significant increase in AD cases, whilst miR-29c was found to have no statistical differences for AD, and miR-29a only had differences between EAC and VaD, but not compared to controls. It would seem that the majority of any involvement of the miR-29 family in AD may be reliant on miR-29b, and perhaps with some contribution from miR-29a. With this in mind additional pathway analysis was still deemed a worthy pursuit, to explore further the mechanisms which might be influenced by members of the miR-29 family.

5.4.2.5. Analysis of miR-29 family predicted target proteins

The miR-29 family was found to have 1265 predicted targets, according to TargetScan and analysis of them with both DAVID and PANTHER software's showed that these proteins are related to a number of pathways shown in Tables 5.6 and 5.7.

Table 5. 6 Analysis of predicted targets for miR-29 family by DAVID software.

DAVID pathways for miR-29 family	Protein count	Benjamini value
Cluster 1 enrichment score: 2.73		
Collagen type IV trimer	6	0.0009
Regulators of Bone Mineralization	6	0.065
Angiotensin-converting enzyme 2 regulates heart function	6	0.13
Platelet Amyloid Precursor Protein Pathway	6	0.2
Acute Myocardial Infarction	6	0.48
Intrinsic Prothrombin Activation Pathway	6	0.53
Cluster 2 enrichment score 1.45		
5-methylcytosine catabolic process	3	0.63
Sulfonate dioxygenase activity	3	0.54
C-19 gibberellin 2-beta-dioxygenase activity	3	0.54
C-20 gibberellin 2-beta-dioxygenase activity	3	0.54
2,4-dichlorophenoxyacetate alpha-ketoglutarate dioxygenase activity	3	0.54
Procollagen-proline dioxygenase activity	3	0.54
Methylcytosine dioxygenase activity	3	0.54
Hypophosphite dioxygenase activity	3	0.54
DNA-N1-methyladenine dioxygenase activity	3	0.72
Peptidyl-proline hydroxylation	3	0.97
Oxidative demethylation	3	0.98
Cluster 3 enrichment score 0.77		
L-alpha-amino acid transmembrane transport	3	0.96
L-amino acid transport	3	0.98
L-amino acid transmembrane transporter activity	3	0.92

Table shows gene ontology and pathways related to proteins targeted by miR-29 family, the number of proteins and Benjamini value are specified.

Analysis derived from DAVID software identified three clusters of pathways related to proteins predicted to be targeted by the miR-29 family. From them, only one pathway (collagen type IV trimer) within the cluster with the highest enrichment score (Cluster 1 enrichment score: 2.73) was found to be significant. Other pathways within this cluster did not reach significant levels.

Table 5. 7 Analysis of predicted targets for miR-29 family by PANTHER software.

PANTHER pathways for miR-29 family	Protein count	Fold enrichment	P value
Axon guidance mediated by netrin	10	4.58	0.0344
Insulin/insulin growth factor pathway-protein kinase B signalling cascade	13	4.47	0.0051
Phosphoinositide 3-kinase pathway	14	3.91	0.0089
Notch signalling pathway	14	3.85	0.0104
p53 pathway feedback loops	14	3.72	0.0141
Integrin signalling pathway	43	3.60	3.31 e-9
Alzheimer disease-presenilin pathway	40	2.97	2.06 e-6
Epidermal growth factor receptor signalling pathway	23	2.75	0.0071
Cadherin signalling pathway	26	2.71	0.0028
Cholecystokinin receptor signalling map	34	2.18	0.0153
Gonadotropin-releasing hormone receptor pathway	39	2.17	0.0039
Wnt signalling pathway	41	2.13	0.0041

Table shows pathways related to proteins targeted by miR-29 family, number of proteins targeted, fold enrichment and p values are specified.

After analysis of the target proteins with PANTHER, it was revealed that 12 pathways might be involved in miR-29 family function due to their statistically significant values. These 12 pathways include a number of proteins ranging from 10 to 41 target proteins in any one pathway. The range of enrichment scores for these pathways went from 2.13 to 4.58. On further inspection of the pathways identified, two of them presented higher significance. These pathways are the integrin signalling pathway (p=3.31 e-9) and the Alzheimer disease-presenilin pathway (p=2.06 e-6). Other statistically significant pathways include: axon guidance mediated by netrin (p=0.0344), insulin/insulin growth factor pathway-protein kinase B signalling cascade (p=0.0051), phosphoinositide 3-kinase pathway (p=0.0089), Notch signalling pathway (p=0.0104), p53 pathway feedback loops (p=0.0141), epidermal growth factor receptor signalling pathway (p=0.0071), cadherin signalling pathway (p=0.0028), cholecystokinin receptor signalling (p=0.0153), gonadotropin-releasing hormone receptor pathway (p=0.0039) and Wnt signalling pathway (p=0.0041).

5.4.3. miR-34 family

The miR-34 family is composed of four members miRNAs, miR-34a/34b/34c/449, which were all investigated here.

5.4.3.1. miR-34a

miR-34a is transcribed from chromosome 1p36.22 (*MIR34A* gene). Initial analysis by the D'Agostino & Pearson normality test showed that miR-34a was not normally distributed. Kruskal-Wallis test was therefore applied and showed that the percentage of difference for miR-34a was significantly different between diagnostic groups (H=20.45 and p=0.0001). Subsequent analysis by Dunn's multiple comparison test showed a reduction in miR-34a expression in VaD compared to EAC ($p<0.01$) and AD ($p<0.001$), but not between EAC and AD compared to controls (Figure 5.9)

Figure 5. 10 Percentage of difference for miR-34a.

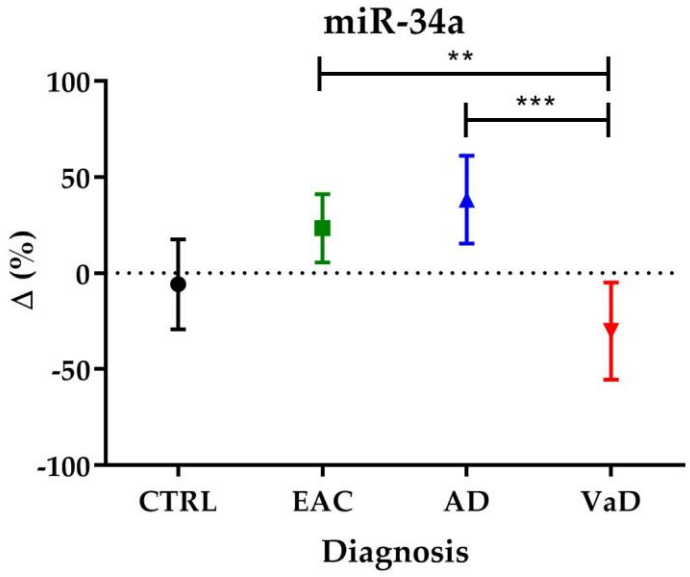

Figure 5.10 shows the percentage of difference for miR-34a for all diagnostic groups compared to controls. Error bars show the 95% confidence interval and the average is depicted, ** $p<0.01$ and *** $p<0.001$.

5.4.3.2. miR-34b

miR-34b is transcribed from chromosome 11q23.1 (*MIR34B* gene). As for miR-34a, the D'Agostino & Pearson normality test showed that miR-34b was not normally distributed. The percentage of difference for miR-34b expression was then found to be significantly different between diagnostic groups (Figure 5.11) using the Kruskal-Wallis test (H=11.92 and p=0.0076). A significant difference in miR-34b expression was then found between EAC and AD ($p<0.01$), but not between any of the diagnostic groups and controls by Dunn's multiple comparison test.

Figure 5. 11 Percentage of difference for miR-34b.

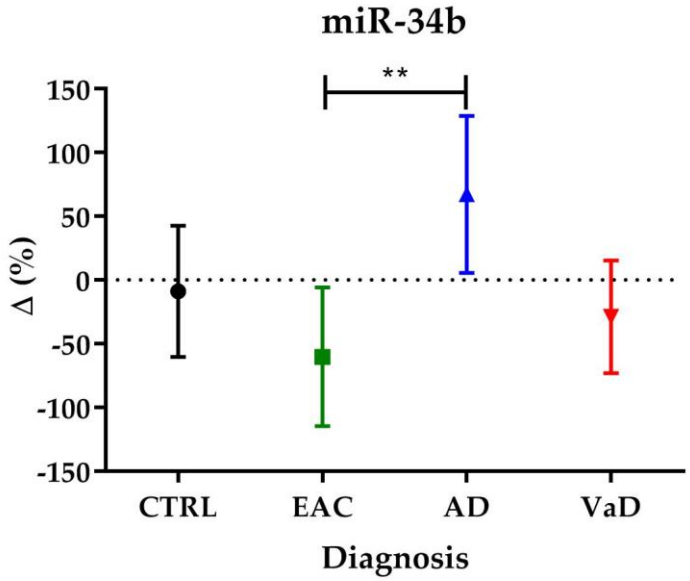

Figure shows the percentage of difference for miR-34b for all diagnostic groups compared to controls. Error bars show the 95% confidence interval and the average is depicted, ** $p<0.01$.

5.4.3.3. miR-34c

Similar to miR-34b, miR-34c also derives from chromosome 11q23.1 (*MIR34C* gene). Also similar to miR-34a and miR-34b, the D'Agostino & Pearson normality test showed that miR-34c was not normally distributed. Application of the Kruskal-Wallis test to miR-34c expression (Figure 5.12) revealed that there was significant difference between

diagnostic groups (H=12.17 and p=0.0068). Similar to miR-34b, Dunn's multiple comparison test showed a significant difference between EAC and AD (p<0.01), but none of the diagnostic groups individually differed from controls.

Figure 5. 12 Percentage of difference for miR-34c.

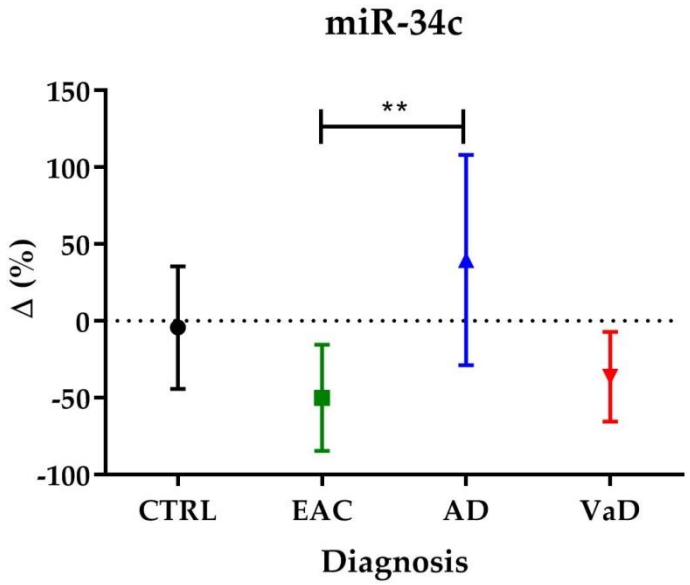

Figure shows the percentage of difference for miR-34c for all diagnostic groups compared to controls. Error bars show the 95% confidence interval and the average is depicted, ** p<0.01.

5.4.3.4. miR-449

miR-449 is encoded in chromosome 5q11.2 (*MIR449* gene). Unlike the other family members, the D'Agostino & Pearson normality test showed that miR-449 was normally distributed. However, Bartlett's test found that the variances between the groups were significantly non homogeneous (p=0.001) and thus, the data was analysed with Kruskal-Wallis test. There was no significant difference in miR-449 between diagnostic groups (Figure 5.13) Kruskal-Wallis test H=0.67 and p=0.88.

Figure 5. 13 Percentage of difference for miR-449.

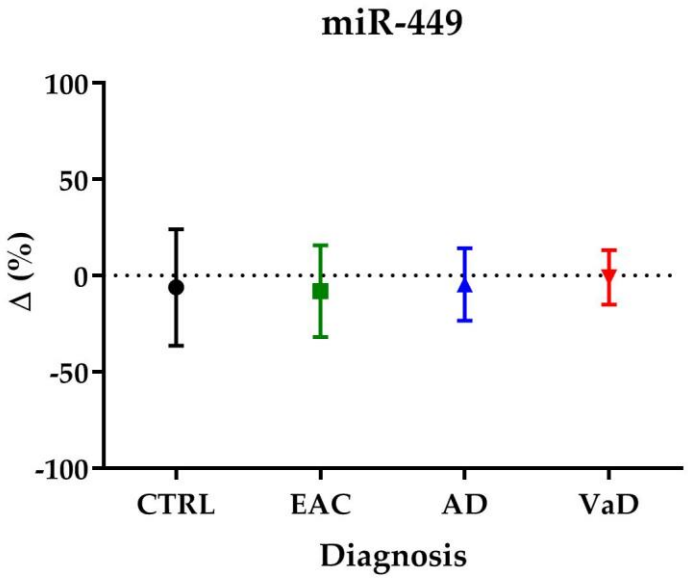

Figure shows the percentage of difference for miR-449 for all diagnostic groups compared to controls. Error bars show the 95% confidence interval and the average is depicted.

5.4.3.5. Summary of miR-34 family results

Neither miR-34a, -34b nor -34c, which did not have normal expression distributions, showed a significant difference between AD and controls, but there were some significant differences identified between levels of expression between various diagnostic groups in *post hoc* analysis. Similarly, miR-449, which had a normal distribution of expression, did not have any differences in expression across all groups. Acknowledging that there were no significant differences between various diagnostic group cases and controls, but that there were still some differences between diagnostic groups, it is worthwhile exploring what pathways this miRNA family is related to, which might inform some of the observations.

5.4.3.6. Analysis of miR-34 family predicted target proteins

An initial examination using TargetScan showed that the miR-34 family has 754 predicted targets. A further analysis (May 2019) of the pathways related to these predicted target proteins is shown according to analysis by DAVID software (Table 5.8) and PANTHER software (Table 5.9).

Table 5. 8 Analysis of predicted targets for miR-34 family by DAVID software.

DAVID pathways for miR-34 family	Protein count	Benjamini value
Cluster 1 enrichment score 1.05		
Semaphorin receptor binding	4	0.76
Negative regulation of axon extension involved in axon guidance	4	0.92
Chemorepellent activity	4	0.81
Negative chemotaxis	4	0.97
Cluster 2 enrichment score 0.94		
Positive regulation of cytoplasmic mRNA processing body assembly	3	0.82
Poly (A)-specific ribonuclease activity	3	0.82
RNA phosphodiester bond hydrolysis, exonucleolytic	3	1
Nuclear-transcribed mRNA poly(A) tail shortening	3	1
Cluster 3 enrichment score 0.74		
Fatty acid transport	3	0.91
Long chain fatty acid-coA ligase activity	3	0.82
Long chain fatty acid metabolic process	3	0.98
Peroxisome proliferator activated receptor signalling pathway	3	0.92
Cluster 4 enrichment score 0.6		
Diacylglycerol kinase activity	3	0.76
Protein kinase C-activating G-protein couple receptor signalling pathway	3	1
Glycerolipid metabolism	3	0.88
Cluster 5 enrichment score 0.58		
nuRD complex	3	0.71
ATP-dependent chromatin remodelling	3	0.99
Nucleosomal DNA binding	3	0.99
Cluster 6 enrichment score 0.19		
tRNA export from nucleus	3	1
Regulation of glucose transport	3	1
mRNA export from nucleus	3	1

Viral transcription	3	1
Protein sumoylation	3	1

Table shows gene ontology and pathways related to proteins targeted by miR-34 family, the number of proteins and Benjamini value are specified.

None of the pathways identified by DAVID software reached levels of significance. Nevertheless, when analysed with PANTHER, five pathways were found to be statistically significant (Table 5.9).

Table 5. 9 Analysis of predicted targets for miR-34 family by PANTHER software.

PANTHER pathways for miR-34 family	Protein count	Fold enrichment	P value
Notch signalling pathway	17	7.94	1.24 e-7
Metabotropic glutamate receptor group II pathway	9	5.37	0.0179
5-hydroxytryptamine-2 type receptor mediated signalling pathway	10	4.18	0.0468
Transforming growth factor-beta signalling pathway	15	3.62	0.0072
Alzheimer disease-presenilin pathway	25	3.16	0.0002

Table shows pathways related to proteins targeted by miR-34 family, number of proteins targeted, fold enrichment and p values are specified.

According to the analysis done with PANTHER, these five pathways include variable number of predicted target proteins that range from 9 to 25 proteins in any one pathway. Notably, the pathway with the highest significance (p=1.24 e-7) and fold enrichment score (7.94) is the Notch signalling pathway. Other pathways retrieved are Metabotropic glutamate receptor group II pathway (p=0.0179), 5-hydroxytryptamine-2 type receptor mediated signalling pathway (p=0.0468), transforming growth factor-beta signalling pathway (p=0.0072), and Alzheimer disease-presenilin pathway (p=0.0002). Interestingly presenilins, part of the ɣ-secretase, regulate Notch signalling and are both present in the analysis of miR-29 and miR-34 families.

5.4.4. miR-125 family

The miR-125 family has two members miR-125a and miR-125b, both of which are investigated here.

5.4.4.1. miR-125a

miR-125a is transcribed from chromosome 19q13.41 (*MIR125A* gene). Initial analysis by the D'Agostino & Pearson normality test showed that miR-125a was not normally distributed. The percentage of difference for miR-125a was significantly different between diagnostic groups (Figure 5.14) using the Kruskal-Wallis test (H=7.992 and p=0.046). Further analysis was then performed with Dunn's multiple comparison test showing a significant difference in miR-125a expression between EAC and AD ($p<0.05$).

Figure 5. 14 Percentage of difference for miR-125a.

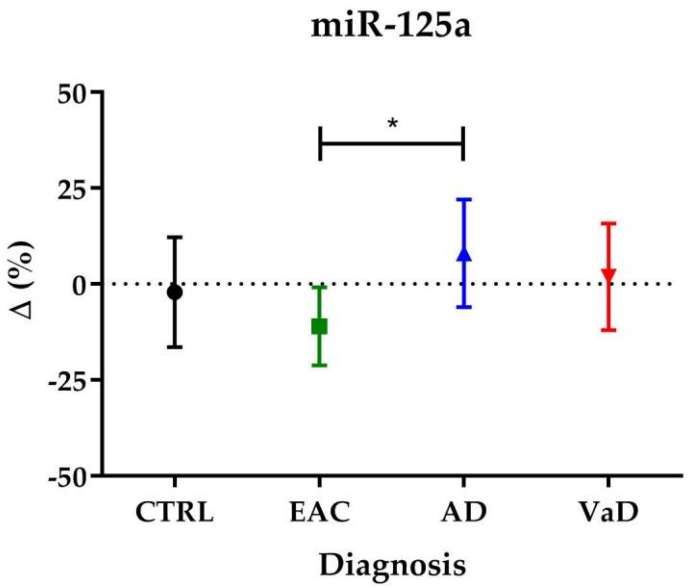

Figure shows the percentage of difference for miR-125a for all diagnostic groups compared to controls. Error bars show the 95% confidence interval and the average is depicted, * $p<0.05$.

5.4.4.2. miR-125b

miR-125b is transcribed from chromosome 11q24.1 (*MIR125B* gene). The D'Agostino & Pearson normality test applied to the data showed that miR-125b was not normally distributed and thus the Kruskal-Wallis test was used. This then showed that the percentage of difference for miR-125b was significantly different between diagnostic groups (Figure 5.15), Kruskal-Wallis test H=27.61 and p<0.0001. Dunn's multiple comparison test then revealed a significant increase in miR-125b expression in AD compared to controls (p<0.01), EAC (p<0.001) and VaD (p<0.0001).

Figure 5. 15 Percentage of difference for miR-125b.

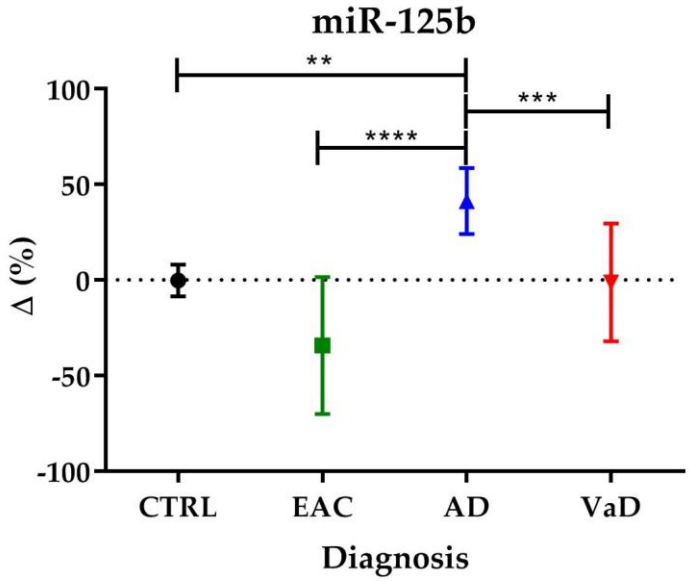

Figure shows the percentage of difference for miR-125b for all diagnostic groups compared to controls. Error bars show the 95% confidence interval and the average is depicted, ** p<0.01, *** p<0.001, **** p<0.0001.

5.4.4.3. Summary of miR-125 family results

Despite the fact that miR-125a did not reach a significant difference between AD and controls, miR-125b expression appeared to be more greatly altered between AD cases and controls, but also between AD and the other diagnostic groups. In contrast, miR-125a was only significantly different between EAC and AD. Given these observed

differences with controls and between groups for miR-125 family members, it is worth exploring what pathways and target proteins have been attributed to miR-125 activity, to further explore what effects they may have on AD pathology.

5.4.4.4. Analysis of miR-125 family predicted target proteins

Assessment of this miRNA family on TargetScan shows that it may have 931 predicted target proteins. The analysis of the pathways (May 2019) related to these proteins is shown for both DAVID software (Table 5.10) and PANTHER software (Table 5.11).

Table 5. 10 Analysis of predicted targets for miR-125 by DAVID software.

DAVID pathways for miR-125 family	Protein count	Benjamini value
Cluster 1 enrichment score 1.72		
2,4-dichlorophenoxyacetate alpha-ketoglutarate dioxygenase activity	3	0.35
Procollagen-proline dioxygenase activity	3	0.35
Hypophosphite dioxygenase activity	3	0.35
Sulfonate dioxygenase activity	3	0.35
C-19 gibberellin 2-beta-dioxygenase activity	3	0.35
C-20 gibberellin 2-beta-dioxygenase activity	3	0.35
DNA-N1-methyladenine dioxygenase activity	3	0.58
Peptidyl-proline hydroxylation	3	0.94
Cluster 2 enrichment score 1.32		
3-oxo-cerotoyl-CoA synthase activity	3	0.58
3-oxo-arachidoyl-CoA synthase activity	3	0.58
3-oxo-lignoceronyl-CoA synthase activity	3	0.58
Fatty acid elongase activity	3	0.58
Fatty acid elongation, monounsaturated fatty acid	3	0.86
Fatty acid elongation, polyunsaturated fatty acid	3	0.86
Fatty acid elongation, saturated fatty acid	3	0.86
Very long-chain fatty acid biosynthetic process	3	0.96
Cluster 3 enrichment score 1.11		
Dicer pathway	3	0.64
RISC-loading complex	3	0.51
miRNA loading onto RISC involved in gene silencing by miRNA	3	0.86
Production of miRNAs involved in gene silencing by miRNA	3	0.89

RISC complex	3	0.67
Double-stranded RNA binding	3	1
Cluster 4 enrichment score 1.06		
Neuropilin binding	4	0.53
Semaphorin receptor binding	4	0.8
Semaphorin-plexin signalling pathway	4	0.99
Cluster 5 enrichment score 0.91		
Voltage-gated sodium channel activity involved in cardiac muscle cell action potential	3	0.44
Voltage-gated sodium channel complex	3	0.71
Cardiac muscle cell action potential involved in contraction	3	0.98
Sodium channel regulator activity	3	0.98
Cluster 6 enrichment score 0.79		
Magnesium ion transport	3	0.96
Magnesium ion transmembrane transport	3	0.98
Magnesium ion transmembrane transporter activity	3	0.90
Cluster 7 enrichment score 0.72		
Inorganic anion exchanger activity	4	0.75
Regulation of intracellular pH	4	0.99
Bicarbonate transport	4	1
Cluster 8 enrichment score 0.7		
G-protein activated inward rectifier potassium channel activity	3	0.76
Inward rectifier potassium channel activity	3	0.93
Potassium ion import	3	1
Cluster 9 enrichment score 0.53		
Antigen Processing and Presentation	3	0.86
Proteasome core complex	3	0.83
Threonine-type endopeptidase activity	3	0.94
Proteolysis involved in cellular protein catabolic process	3	1

Table shows gene ontology and pathways related to proteins targeted by miR-125 family, the number of proteins and Benjamini value are specified.

Similar to previous miRNA families analysed, none of the pathways identified with DAVID software reached levels of significance. Nonetheless, when analysed with PANTHER, five pathways were found to be statistically significant (Table 5.11).

Table 5. 11 Analysis of predicted targets for miR-125 by PANTHER software.

PANTHER pathways for miR-125 family	Protein count	Fold enrichment	P value
p38 mitogen-activated protein kinase pathway	9	4.8	0.0427
Transforming growth factor-beta signalling pathway	20	3.86	0.0002
Epidermal growth factor receptor signalling pathway	23	3.73	5.91e-5
Ras pathway	12	3.63	0.0444
Fibroblast growth factor signalling pathway	18	3.36	0.0038

Table 5.10 Pathways related to proteins targeted by miR-125 family, number of proteins targeted, fold enrichment and p values are specified.

According to the analysis done by PANTHER, five pathways were identified that were statistically significant. These pathways involved variable numbers of predicted target proteins that ranged from 9 to 23 target proteins in any one pathway. These also had a range of fold enrichment scores that ranged from 3.36 to 4.8. On further examination of the pathways identified, the highest significance value was observed for the epidermal growth factor receptor signalling pathway with an enrichment score of 3.73 and also the highest target protein count. Other pathways that were statistically significant included the p38 mitogen-activated protein kinase pathway (p=0.0427), transforming growth factor-beta signalling pathway (p=0.0002), Ras pathway (p=0.0444) and fibroblast growth factor signalling pathway (p=0.0038).

5.4.5. miR-132/212 family

This miRNA family is composed by miR-132 and miR-212, both genes are clustered within 0.5 kb on chromosome 17p13.3.

5.4.5.1. miR-132

Application of the D'Agostino & Pearson normality test to the data found that the expression of miR-132 was not normally distributed and thus Kruskal-Wallis test was used. The percentage of difference for miR-132 expression, as found by Kruskal-Wallis

test was significantly different between diagnostic groups (H=30.37 and p<0.0001). Furthermore, application of Dunn's multiple comparison test showed a significant decrease in miR-132 expression in AD in comparison with controls (p<0.0001), EAC (p<0.01) and VaD (p<0.05), but no differences between EAC and VaD compared to controls.

Figure 5. 16 Percentage of difference for miR-132.

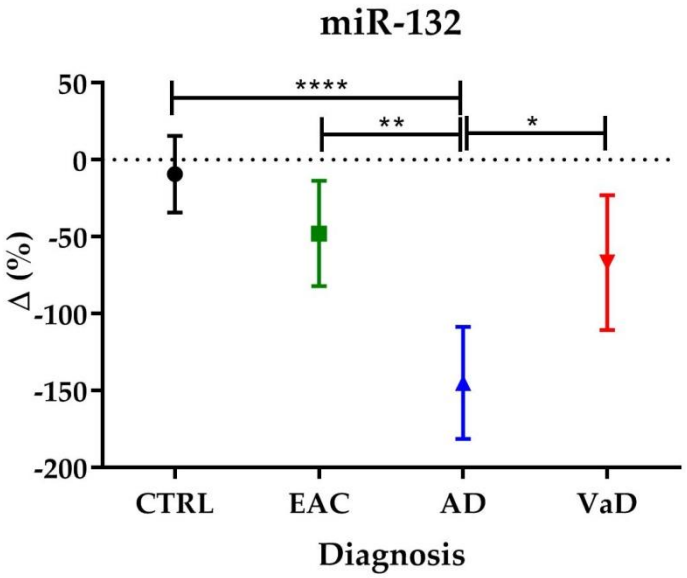

Figure shows the percentage of difference for miR-132 for all diagnostic groups compared to controls. Error bars show the 95% confidence interval and the average is depicted, * p<0.05, ** p<0.01 and **** p<0.0001.

5.4.5.2. miR-212

As with previous miRNAs, the percentage of difference for miR-212 was not normally distributed according to D'Agostino & Pearson normality test. Then, analysis by the Kruskal-Wallis test revealed that miR-212 levels were significantly different between diagnostic groups, (H=28.54 and p<0.0001). Furthermore, application of Dunn's multiple comparison test showed a significant decrease in AD in comparison with controls (p<0.0001) and EAC (p<0.01), but no differences between EAC and VaD and controls were found.

Figure 5. 17 Percentage of difference for miR-212.

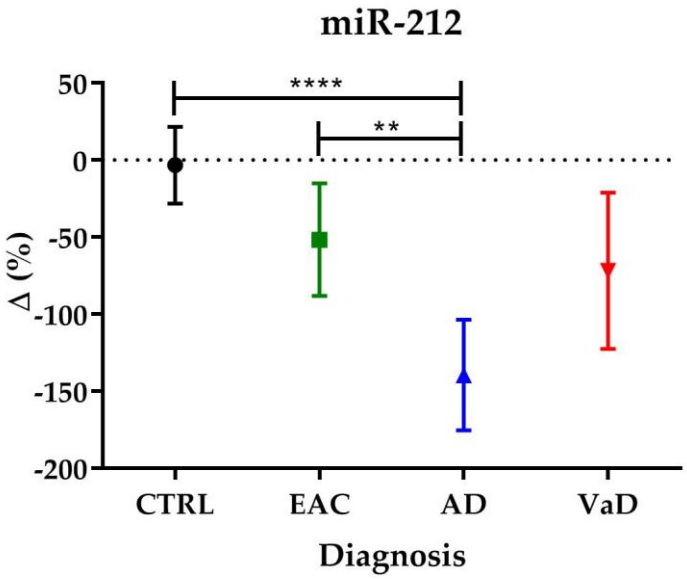

Figure shows the percentage of difference for miR-212 for all diagnostic groups compared to controls. Error bars show the 95% confidence interval and the average is depicted, ** $p<0.01$ and **** $p<0.0001$.

5.4.5.3. Summary of miR-132 family results

Both miR-132 and miR-212 demonstrated a significant reduction in AD cases compared to controls and also with respect to the EAC group. Whilst miR-132 reached significance for a difference between the AD and the VaD groups, this was not observed for miR-212. To further understand the possible biological relevance of the reduction observed in miR-132 and miR-212 in AD it was prudent to analyse the predicted target proteins regulated by this miRNA family.

5.4.5.4. Analysis of miR-132 family predicted target proteins

An initial examination using TargetScan showed that the miR-132 family has 474 predicted target proteins. A further analysis (May 2019) of the pathways related to these predicted target proteins is shown according to analysis by DAVID software (Table 5.12) and PANTHER software (Table 5.13).

Table 5. 12 Analysis of predicted targets for miR-132 family by DAVID software.

DAVID pathways for miR-132/212 family	Protein count	Benjamini value
Cluster 1 enrichment score 1.15		
Insulin growth factor-1 signalling pathway	4	0.37
Insulin signalling pathway	4	0.37
Thrombopoietin signalling pathway	4	0.41
Epidermal growth factor signalling pathway	4	0.47
Cluster 2 enrichment score 0.93		
Multiple antiapoptotic pathways from IGF-1R signalling lead to BAD phosphorylation	4	0.4
Transcription factor CREB and its extracellular signals	4	0.47
IL-2 Receptor Beta Chain in T cell Activation	4	0.66
Cluster 3 enrichment score 0.91		
Voltage-gated sodium channel complex	3	0.51
Voltage-gated sodium channel activity	3	0.67
Neuronal action potential	3	0.91
Membrane depolarization during action potential	3	0.91
Ion channel activity	3	0.91
Cluster 4 enrichment score 0.72		
T-cell anergy	3	0.98
Dorso-ventral axis formation	3	0.4
Links between Pyk2 and Map Kinases	3	0.79

Table shows gene ontology and pathways related to proteins targeted by miR-132/212 family, the number of proteins and Benjamini value are specified.

As with previous miRNA families analysed, none of the pathways identified with DAVID software reached levels of significance. Nevertheless, when analysed with PANTHER, five pathways were found to be statistically significant (Table 5.13).

Table 5. 13 Analysis of predicted targets for miR-132 family by PANTHER software.

PANTHER pathways for miR-132/212 family	Protein count	Fold enrichment	P value
Insulin/insulin growth factor pathway-protein kinase B signalling cascade	8	7.34	0.0048
p53 pathway feedback loops 2	10	7.10	0.0006
Transforming growth factor-beta signalling pathway	17	6.45	1.05e-6
Phosphoinositide 3 kinase pathway	8	5.97	1.79e-2
B cell activation	9	5.5	1.2e-2
Epidermal growth factor receptor signalling pathway	17	5.42	1.06e-5

p53 pathway	13	5.4	0.0004
Gonadotropin-releasing hormone receptor pathway	34	5.04	1.9e-11
Fibroblast growth factor signalling pathway	13	4.77	0.0013
Parkinson disease	11	4.7	0.0074
Angiogenesis	16	3.87	0.0015
Cholecystokinin receptor signalling map	21	3.6	0.0002
Wnt signalling pathway	22	3.05	0.0013

Table shows pathways related to proteins targeted by miR-132/212 family, number of proteins targeted, fold enrichment and p values are specified.

According to the analysis done by PANTHER, 13 pathways were identified to be statistically significant. These pathways involved variable numbers of predicted target proteins that ranged from 8 to 34 target proteins in any one pathway. These also had a range of fold enrichment scores that ranged from 3.05 to 7.34. On further examination of the pathways identified, three of them showed a high significant value, the gonadotropin-releasing hormone receptor pathway (p=1.9e-11), the transforming growth factor-beta signalling pathway (p=1.05e-6) and the epidermal growth factor receptor signalling pathway (p=1.06e-5). Other pathways that were highly significant included the insulin/insulin growth factor pathway-protein kinase B signalling cascade (p=0.0048), the p53 pathway feedback loops 2 (p=0.0006), the phosphoinositide 3 kinase pathway (p=1.79e-2), B cell activation (p=1.2e-2), p53 pathway (p=0.0004), fibroblast growth factor signalling pathway (p=0.0013), Parkinson disease (p=0.0074), angiogenesis (p=0.0015), cholecystokinin receptor signalling map (p=0.0002) and Wnt signalling pathway (p=0.0013).

5.5 Discussion and conclusions

The null hypothesis was that there is no significant difference in the levels of these miRNAs between diagnostic groups, AD, VaD, early AD changes (EAC) and non-demented controls. The null hypothesis is rejected for 15 of the 17 miRNAs measured. Although some miRNAs showed significant differences between diagnostic groups, only seven of them (miR-15b, miR-16, miR-195, miR-29b, miR-125b, miR-132 and miR-

212) were found to be significantly different in the AD group compared to controls. In order to understand the possible impact that miRNAs might have in disease, several factors should be considered.

In Chapter 3, a pattern of expression for five miRNAs (miR-16, miR-29a, miR-29b, miR-34a, miR-125b) was found with respect to Braak stage. The initial interesting finding in Chapter 3, that there was apparent increase in some of these miRNAs in AD, not VaD in Braak stage II disappeared when the size of the cohort was increased and they were re-evaluated with the three unchanging calibrator genes identified in Chapter 4. This highlights the importance of sample size and the use of rigorously verified calibrator genes.

Indeed, according to the data of re-assessed miRNAs in this chapter, and comparison with their corresponding data in Chapter 3 highlights that, the most commonly used calibrator gene, RNU6B (137) is questionable as a reliable calibrator for brain tissue studies of neurodegenerative disease. Most notable in this conclusion is that RNU6B was not stable after only 6 hours in the simulation of post-mortem delay experiment. This lack of stability might give rise to high RNU6B variability in various cohorts and thus increase the likelihood of false associations. By using three different calibrator genes, that have been demonstrated to have low variability and high stability to degradation rates, it gives greater confidence as to the accuracy of the results shown in this chapter compared to those presented in Chapter 3, which were based on what were approaches (using certain calibrators) more regularly used in the scientific literature.

From other studies, downregulation of the miR-132/212 family across different brain areas has been the only consistent finding so far in AD (64), which the data presented here agrees with. Whilst in Chapter 3, using a less reliable calibrator, miR-132/212 was found to be significantly reduced in AD and VaD for both miRNAs. In this Chapter, similar but statistically more significant (indicating greater confidence) reductions were found for both AD and VaD, but also for early AD changes (EAC). Other

miRNAs here examined have been found in the literature with inconsistent results that likely relate to the techniques used and brain regions analysed. Similar to the results here shown, miR-15a, miR-29b, miR-34a, miR-125a and miR-125b have been found to be increased in AD brain (148) whilst contradictorily some of these miRNAs (miR-15a and miR-29b) have also been found to be decreased in AD by others in the literature (121,149).

In Chapter 3, a similar analysis of predicted targets for the miR-132/212 family was undertaken that showed that these proteins are related to the TGF-beta receptor/activin receptor pathway, Rho GTPase pathway, voltage gated sodium channel and sodium ion transport and insulin/IGF-1 signalling pathway. The Rho GTPase pathway and the voltage gated sodium channel pathways in particular might be more relevant in the function of this miRNA family as it is highly expressed in dendrites and synapses (150). However, in the corresponding pathway analysis performed in this chapter, the Rho GTPase pathway was not found by DAVID nor PANTHER software despite prior evidence as to its importance in the function of this miRNA family. This highlights another important challenge in the study of miRNAs, and potentially in the use of bioinformatics in general, whereby similar analyses over a period of time can provide differences due to changing availability of data that can be updated, refined and in some cases revised or corrected. Thus, as a standard practice, with respect to any analyses and publication of results for any analysis using publicly available software and databases, the times at which the analyses were performed are strongly advised. Another implication of this is with respect to the effect it could give rise to false positives findings. For instance, the miR-29 targets were seen to be related to the platelet amyloid precursor protein pathway with a change in the p-value from 0.0052 (March 2017) as identified for work conducted in Chapter 3 to a non-significant p-value of 0.2 (May 2019) as was identified for the work in this chapter. This presents an important challenge for miRNA research and demonstrates the need for any ongoing project that the rationale by which they have been previously identified may require regular review to assess whether the findings and assumed involvement in disease remain consistent.

Another consideration and potential limitation, which the use of both DAVID and PANTHER here is designed to mitigate against, is that, the use of a single software can introduce bias towards the results. For example, using the preliminary data shown in Chapter 3 that was only analysed with DAVID software, when two types of software were applied to the same family, as was undertaken in this chapter, the results obtained from both DAVID and PANTHER software can differ. On one hand, even though the data might differ, that they both might yield results that point to related or converging pathways can still support the function. For instance, miR-29 target proteins relate to angiotensin-converting enzyme 2 regulation of heart function, platelet amyloid precursor protein pathway, Notch signalling pathway and Alzheimer disease-presenilin pathway, all of them relevant for dementia. However, it may also be conceivable, that instead of showing supportive converging results, it could have the potential to lead to contradictory information, thereby making interpretation of the role of target miRNAs a significant challenge.

Furthermore, several pathways can be found to relate to targets for a particular miRNA, however, if such pathways are being represented by a reduced number of proteins, for instance three proteins from hundreds of predicted targets, the final effect of the miRNA can be minimal and it could be similar to a single miRNA-protein relation. In addition, other factors such as the spatiotemporal expression of a miRNA should be considered.

No patterns of expression were found in this analysis. Yet, the RORA protein represents an attractive target for the multiple points at which intersects with characteristics observed in dementia. Similarly, with respect to the miR-132/212, the MAP2 protein could provide more information about the role of this miRNA family in synaptic loss. Both proteins were attempted to be measured and are presented in Appendix 2. This chapter covered classical histopathological hallmarks of AD. A slightly different approach and considering proteins that might be relevant to vascular factors and hypoxic conditions is presented in Chapter 6.

Chapter 6.- miRNAs related to vascular factors and the renin angiotensin system

6.1. Introduction

AD is histopathologically characterised by extracellular amyloid plaques, intracellular neurofibrillary tangles, astrogliosis and reactive microglia. Similar to VaD, many cases of AD also demonstrate varying degrees of vascular changes such as cortical microinfarcts, lacunar infarcts in the basal ganglia and cortical petechial microbleeds, which are linked to cerebral amyloid angiopathy (CAA) (5).

As mentioned in the introduction of this thesis, cerebral microinfarcts are caused by occlusion of cerebral blood flow and microbleeds are caused by extravasation of blood into the brain parenchyma. Interestingly, post-mortem microinfarcts have been associated with ante-mortem microbleeds in an odds ratio (OR) of 8.6. The authors of the study suggested that the 8-fold association of increased risk of microinfarcts in the presence of microbleeds could be due to the vascular damage and BBB disruption caused by CAA pathology (23).

Both microinfarcts and microbleeds are common findings at postmortem, the prevalence of microinfarcts has been reported as 16-48% of all brains studied whilst for microbleeds it is around 23.5% (23,151). Microinfarcts and microbleeds are also both associated with cognitive decline regardless of the presence or not of dementia (31,32).

Extravasation of blood into the brain parenchyma is neurotoxic. Haemorrhage triggers the formation of cerebral oedema in the tissue surrounding the haemorrhage. First, cytotoxic oedema is produced by glutamate accumulation. Then, vasogenic oedema is produced by exudation of serum proteins, including thrombin. Thrombin activates microglia and downregulates tight-junction proteins in endothelial cells through secretion of tumor necrosis factor alpha (TNFα) and interleukin 1β (IL-1β) (152).

This results in BBB disruption and opening. Moreover, haemoglobin (derived from blood extravasation) degrades into methaemoglobin and free iron. Methaemoglobin is a ligand for the toll like receptor 4 (TLR4) and is able to activate microglial secretion of TNFα and inflammation. Free iron causes reactive oxygen species production, matrix metalloproteinase 9 activation and BBB disruption (152).

Microinfarcts are caused by CAA, arteriolosclerosis, microemboli and hypoperfusion (31). Cortical microinfarcts but not subcortical microinfarcts are associated with cognitive impairment, in particular amongst individuals with risk factors for dementia (32). Arvanitakis *et al* examined the brains of 1,066 individuals looking at the relationship between microinfarcts and cerebral vessel pathology. Atherosclerosis was present in 41% of the individuals, arteriosclerosis in 36% and CAA in 35% of them. Interestingly, they found that atherosclerosis and arteriosclerosis were associated with subcortical microinfarcts whilst CAA was associated with cortical microinfarcts (153).

Although these associations do not necessarily imply a causal relationship, the findings highlight the importance of topographical location of vessel pathology that might contribute to differences in underlying aetiology. Remarkably, the specific association between cortical microinfarcts, CAA and cognitive decline still remains unclear. This might be explained by relating the normal physiology of CAA and localization of microinfarcts in the cortex. As described in the introduction of this thesis, Aβ accumulates directly in relation to the amount of synaptic activity (154).

Further research is necessary to fully elucidate the relationship between microinfarcts, microbleeds, CAA and cognitive decline. As suggested by Damasceno (32), the most relevant factor for the development of microinfarcts is CAA, where Aβ is deposited in the capillaries with subsequent occlusion and decrease in blood flow. This causes chronic cerebral hypoperfusion with hypoxia, oxidative stress and inflammation, also observed in microbleeds (32).

Poels *et al* examined the prevalence and determinants of microbleeds in a cohort of 3,979 individuals. The presence of microbleeds was detectable in middle age and strongly increased with age. They also found a robust association between cardiovascular factors (such as systolic blood pressure, hypertension and smoking) and microbleeds in subcortical regions. Interestingly, they found that strictly lobar microbleeds (markers of CAA) were significantly more often present in carriers of the *APOE* ε4 allele (155).

Alongside vascular changes, AD and VaD also present other similarities, such as risk factors. The greatest genetic risk factor for the development of dementia is the presence of the *APOE* ε4 allele, which is also associated with increased risk of CAA and CAA-related haemorrhages, normal aging-related cognitive decline, hyperlipidaemia, hypercholesterolemia, atherosclerosis, cardiovascular and cerebrovascular disorders (40).

ApoE, which is encoded for by *ApoE*, is a cholesterol carrier that supports lipid metabolism and injury repair in the brain (40). Presence of two copies of the *ApoE* ε4 has been reported to increase the risk for dementia up to as much 15-fold (40). Furthermore, differences in risk have been observed between different genetic backgrounds, for example carriers of *ApoE* ε4 having an odds ratio (OR) of 5.7 in African American individuals, OR 2.2 in Hispanic individuals, OR 33.1 in Japanese individuals (40). Yet, the importance of disturbance to pathways associated with cholesterol metabolism has been strongly associated with the development of dementia in general. Genome wide association studies have also highlighted the involvement of multiple genes involved in cholesterol metabolism and immune response (42).

Interestingly, cholesterol derivatives are able to upregulate the brain renin angiotensin system, an important system for the control of blood pressure and which is also implicated in other cardiovascular and cerebrovascular disorders (156). Hypertension (Stage 1: systolic/diastolic blood pressure of ≥ 140/90), and even prehypertension (Stage 2: blood pressure of 130-139/80-89), considered as a systolic blood pressure <140 mmHg

have been widely reported as a risk factor for the development of dementia (22). Several studies have shown cognitive decline in late-life (≥70 years) when individuals had high blood pressure in middle life. Hypertension induces stiffening of large arteries and this in turn reduces cerebral blood flow. Its effect is also observed in small vessels where hypertension may result in degenerative changes to the vessel wall that can result in haemorrhages which are another risk factor for AD, and also for some forms of VaD (22).

Hypertension, which can be induced by excess angiotensin II (Ang II)-mediated signalling, causes neurovascular dysfunction, mediated by central and peripheral effects on cerebral blood vessels (22). Such effects can include modulation of cerebral blood flow by vasoconstrictors such as Ang II, and also endothelin, but also vasodilators such as bradykinin and adenosine. Notably, the vasopressor effect of Ang II is also counter-regulated by other angiotensin ligands that bind through different RAS receptors in the brain (65).

Thus, an analysis of miRNAs involved in the RAS was performed, reviewed in (65), where 368 different miRNA families were found that target RAS elements, with the majority of these elements sharing gene transcripts. Table 6.1 summarizes the total number of miRNAs and unique miRNAs that have thus far been attributed to RAS elements, but where some also have other targets outside the RAS. For example, Angiotensin IV receptor (also known as AT4R or IRAP) has 252 miRNA families associated with it, making it the highest amongst the RAS, but also perhaps not surprising because the receptor is also involved in a number of metabolic pathways, including insulin transport, as well as oxytocin and vasopressin-related functions, in addition to downstream signalling in RAS that has been reported to be important in cognitive function.

Figure 6. 1 The renin angiotensin system and its components.

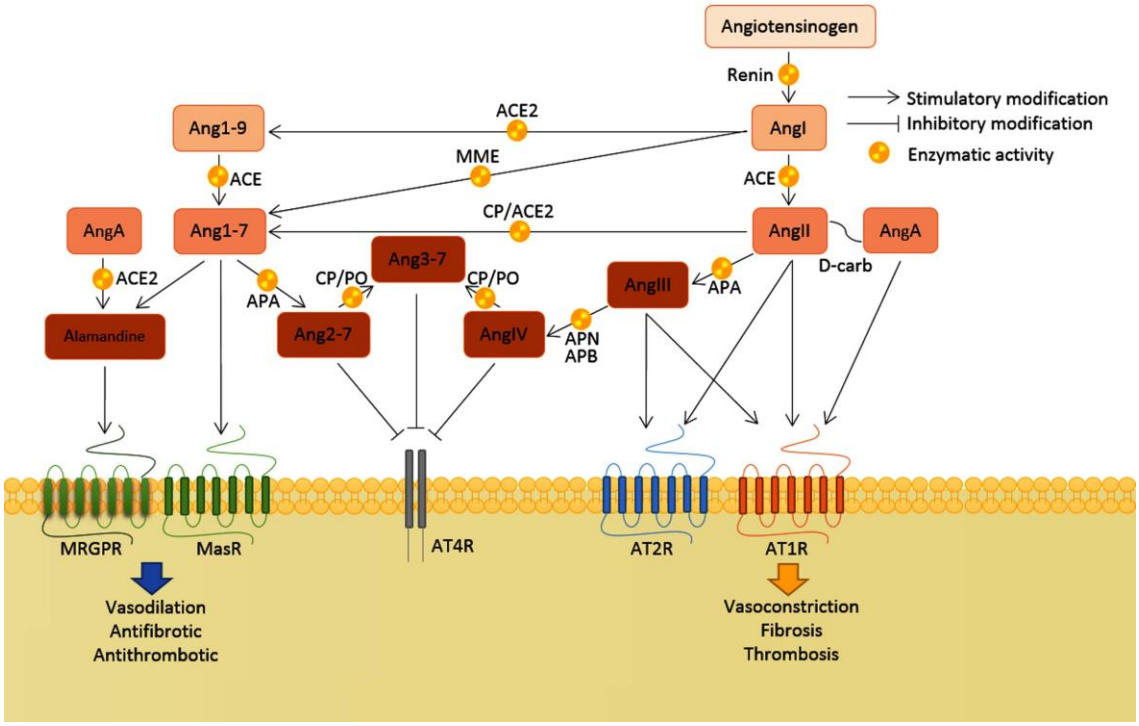

Figure shows the renin angiotensin system (RAS) and its components. RAS has two main axes: the pressor axis (tending towards an increase in blood pressure) comprising AngII, ACE and AT1Rs and the counter-regulatory axis comprising Ang(1–7), ACE2 and MasR. Angiotensin I (AngI), angiotensin II (AngII), angiotensin III (AngIII), angiotensin IV (AngIV), aminopeptidase A (APA), aminopeptidase N (APN), carboxypeptidase P (CP), prolyl oligopeptidase (PO), angiotensin 3-7 (Ang3-7), angiotensin 1-7 (Ang1-7), carboxypeptidase P (CP).

In contrast, the MAS receptor (MasR), a receptor involved in Ang-(1-7) signalling has only five miRNAs known to be associated, suggesting tightly regulated homeostatic expression, although other post-transcriptional modifications are also likely to be involved in its regulation. The MAS receptor, activated by the ligand Ang 1-7, functions as counterbalance to the angiotensin II type 1 receptor, thus MAS receptor favours vasodilation and has anti-inflammatory effects (157).

Table 6. 1 RAS elements with their total amount of miRNAs.

RAS element	Gene name	Total miRNAs	Overlapping miRNAs	Unique miRNAs
Angiotensin converting enzyme	ACE	59	55	4
Angiotensin converting enzyme 2	ACE2	54	50	4
Angiotensinogen	AGT	85	74	11
Angiotensin II type 1 receptor	AGTR1	46	45	1
Angiotensin II type 2 receptor	AGTR2	78	73	5
Aminopeptidase N	ANPEP	31	27	4
Dipeptidyl peptidase	DPP3	32	32	0
Aminopeptidase A	ENPEP	158	145	13
Angiotensin IV receptor (IRAP) *	LNPEP	252	224	28
Mas receptor	MAS1	5	4	1
Neprilysin	MME	151	143	8
Renin	REN	21	19	2
Aminopeptidase B	RNPEP	29	29	0

Table shows RAS elements with their total amount of miRNAs, the number of overlapping miRNAs with respect to other elements of the RAS and number of unique miRNAs for each RAS component. * denotes the fact that the complex molecule IRAP has both enzymatic as well as receptor functions, also been referred to in the literature by a number of other names such as: Oxytocinase, Vasopressinase, Insulin Regulated Aminopeptidase (IRAP), Angiotensin type IV receptor (AT4) (158).

A more detail of RAS-associated miRNAs, according to their functional impact in the RAS physiology is shown in Table 6.2. From a total of 164 combinations (Appendix 3) of overlapping targets and miRNAs in common, 14 were selected since these might have a functional impact in the RAS as they targeted multiple RAS components. Of these, 12 of them if increased would promote vasoconstriction and two would increase vasodilation.

6.1.1. A brief introduction to multi-functional miRNAs in RAS

miR-125-5p, which is listed, was also notably included in the first panel of miRNAs discussed in this thesis that investigated miRNAs involved in amyloid and tau processing. miR-670-3p is an interesting miRNA having 550 predicted targets, yet only 26 copies have been previously reported in miRbase. Based on this apparent discrepancy, particularly the low copy number, it is likely that changes in miR-670-3p

are unlikely to have any meaningful effect and thus will not be considered further as a miRNA of interest.

Table 6. 2 Combinations of RAS components and miRNAs in common.

RAS components	miRNA families in common	
ACE ACE2 ANPEP ENPEP LNPEP	1	miR-125-5p
ANPEP DPP3 ENPEP LNPEP	1	miR-670-3p
AGTR2 DPP3 LNPEP MME	1	miR-17-5p/20-5p/93-5p/106-5p/519-3p
ACE2 ENPEP LNPEP MME	3	miR-9-5p, miR-200-3p/429, miR-942-5p
AGTR2 LNPEP MAS1	1	miR-23-3p
ENPEP LNPEP MME	17	miR-26-5p, miR-30-5p, miR-132-3p/212-3p, miR-194-5p, miR-204-5p/211-5p, miR-216-5p, miR-376-3p, miR-376c-3p, miR-378-3p, miR-450b-5p, miR-518d-5p/519-5p, miR-522-3p, miR-580-3p, miR-653-5p, miR-1269, miR-3942-5p, miR-4766-3p
ACE2 ENPEP LNPEP	4	miR-374-5p/655-3p, miR-543, miR-4424, miR-1306-5p
ACE2 LNPEP MME	3	miR-374a-3p, miR-3194-3p, miR-5691
DPP3 LNPEP MME	5	miR-146-5p, miR-183-5p.1, miR-589-5p, miR-876-5p, miR-2355-5p
ACE2 DPP3 LNPEP	1	miR-329-3p/362-3p
ACE2 ENPEP MME	1	miR-140-3p.1
ENPEP LNPEP	17	miR-9-3p, miR-19-3p, miR-29-3p, miR-34b-5p/449c-5p, miR-105-5p, miR-122-5p, miR-144-3p, miR-320, miR-323-3p, miR-323b-3p, miR-382-3p, miR-494-3p, miR-514a-5p, miR-515-5p/519e-5p, miR-642a-5p, miR-3146, miR-5579-3p
DPP3 ENPEP	1	let-7-5p/98-5p
MAS1	1	miR-143-3p
ACE AGTR1 DPP3	1	miR-34-5p/449-5p

Table shows a detailed list of miRNAs that have various combinations of RAS components in common.

In contrast, the miR-17 family is an abundant miRNA with 7,380 copies reported in miRbase and 1,384 predicted targets. Thus, changes in the miR-17 family might have a more relevant impact. In addition to the RAS components, miR-17 also targets hypoxia-inducible factors and hypoxia-inducible genes such as the genes ANGPT2, EPAS1, HIF1A, SERPINE1 and VEGFA (159), which is notable given that hypoxia and

oxidative stress are also prominent features of the pathogenesis of AD and VaD, and likely some other forms of dementia.

miR-9-5p is another miRNA that was prominent in the examination of RAS miRNAs, it has previously been used as a calibrator in the largest screening of miRNAs in dementia (138). Furthermore, as is evident from Chapter 4 this miRNA was also considered for evaluation as both a calibrator and as a miRNA of interest. miR-9-3p, which is processed from the same precursor as miR-9-5p, similarly targets aminopeptidase A and the angiotensin IV receptor, as does miR-9-5p and targets a similar number of RAS components.

It is assumed that while one of these mature miRNA binds to a 3'UTR, its counterpart is degraded, nevertheless there is no report in the literature about the relation between these two miRNAs derived from the same precursor. Therefore the novel findings presented in Chapter 4 provide some update on these two miRNAs where they have been demonstrated to be robust calibrators for measurements to be undertaken in this chapter.

Although I have been critical of single miRNA-protein relationships in this project, given that the Mas receptor is regulated by only five miRNAs, it is possible that fluctuations in just one of them might have an important effect on MasR protein levels. Thus, I have included these as part of the 14 miRNAs of interest and an additional assessment of these MasR miRNAs was done.

This assessment was based on criteria previously described, that consider what is reported regarding binding affinity, number of copies previously reported, number of gene transcripts targeted and the ratio between the latter two referred to as the reads/target ratio (Table 6.3).

Table 6. 3 Assessment of Mas receptor miRNAs.

miRNA	Confidence	Targets	Reads per million	Ratio reads/targets
miR-143	High	487	24700	50.72
miR-23	High	1332	16900	12.69
miR-224	N/A	440	620	1.41
miR-448	N/A	685	24.7	0.03
miR-651	High	3719	168	0.05

Table shows the assessment of Mas receptor miRNAs. The confidence value is derived from miRbase catalogue. The reads/target ratio is an indicator of the number of miRNA copies that are likely to bind at each target.

Of the 5 MasR-targeting miRNAs, miR-143 was the miRNA with the highest affinity for MasR according to TargetScan. In addition, miR-143 is the most abundant of these miRNAs with the highest ratio between targets and previously reported copies (i.e. the reads/target ratios suggests that at least 50 miRNA copies are able to bind to each of predicted target gene transcripts). Thus, MasR protein levels could be explained by changes in miR-143, given its high affinity, abundancy and low number of predicted targets.

Moreover, changes in this miRNA might be specific to MasR in terms of the RAS system as the other 4 miRNAs targeting the MasR also target other RAS components. Following this assumption, it is feasible that an inverse relationship occurs between miR-143 and MasR levels. Such an assumption then lends itself to the possibility that single miRNA-protein relations could exist under specific conditions, for instance, polymorphisms in single nucleotides.

6.1.2. miRNAs and single nucleotide polymorphisms

Numerous single nucleotide polymorphisms (SNPs) have been proposed to increase the risk for dementia. Yet, hypothetically, any SNP could still have a direct effect over protein levels. That is, if a SNP is not in a coding or promoter region of any gene, a SNP could have an effect on a protein, if the SNP altered the sequence of a miRNA that

targeted it. This could occur, for example by affecting the seed region by which a miRNA binds to the 3'UTR of a gene transcript, by creating miRNA binding sites on gene transcripts or by modifying or abolishing a miRNA gene.

I undertook an exploratory examination of SNPs located at 3'UTR of genes reported to be associated with AD was performed using the catalogue for genome wide association studies (GWAS), updated in June 2019 (Appendix 4). No miRNA binding sites that could be abolished by these SNPs were found; however the creation of a miRNA binding site for miR-320e at the SNP rs6857 was found using mirgeneDB and manually corroborated.

Then, to further evaluate the relevance of this SNP, a search was performed in the GWAS catalogue for associated traits to this SNP. This SNP is associated to cerebral amyloid angiopathy, verbal declarative memory performance in nondemented older people, body fat percentage, type 2 diabetes, age-related macular degeneration and frontotemporal dementia. Although this miRNA binding site has been reported by others in the literature, its levels in brain tissue remain elusive (160,161).

The *PVRL2* gene codes for Poliovirus receptor-related 2, an endothelial adhesion molecule, which was discovered in 1998 (162). This protein is also known as nectin-2 or CD112. PVRL2 knockout mice show a tendency to develop atherosclerosis and altered trans endothelial migration with infiltration of leukocytes (163). Furthermore, it is a cholesterol responsive gene in both humans and mice more strongly expressed in endothelial cells and at lower levels in leukocytes (163).

A SNP can act in different ways, affecting the tertiary form of a protein, altering function, transport, etc. This particular SNP (rs6857) however, is located in the 3'UTR of the *PVRL2* gene where miR-320e is able to bind at it, thus possibly affecting protein levels of PVRL2. In doing so, it would affect cellular adhesion of endothelial cells and thus increase BBB permeability, which in turn might be a risk factor for cerebral amyloid angiopathy. Yashin *et al* suggested that PVRL2 is influenced by *APOE* (the

highest genetic risk factor for AD) and *TOMM40* (another AD-associated SNP) (164). Thus, *PVRL2* not only represents an important risk factor by itself but also as a polygenic risk with *APOE* and *TOMM40*. This chapter will explore the miR-17 family, miR-143 and miR-320e because of their relevance in RAS and possible relation with the SNP rs6857.

6.2. Hypotheses

First, the null hypothesis is that there is no significant difference in the levels of the member of the miR-17 family and miR-143 between diagnostic groups, AD, VaD, early AD changes (EAC) and controls.

6.3. Methods

6.3.1. Study cohort

The study cohort, as described in detail in Chapter 2 (Section 2.1) comprised brain tissue from 22 AD, 20 EAC, 18 VaD and 24 controls.

Table 6. 4 Demographic information of the cohort used in Chapter 6.

Diagnosis	Gender (Male/Female)	Age (σ)	PMI (σ)	ApoE4 (No/Yes)	Total
Control	11/13	80 (9.7)	35.4 (16.2)	21/1	24
Early Alzheimer Changes	11/9	85 (6)	36.5 (15)	14/4	20
Alzheimer's Disease	11/11	78 (7.2)	23.7 (13.4)	3/16	22
Vascular Dementia	9/9	83 (7.9)	34.7 (12.3)	9/4	18
Total	42/42	81.2 (8.1)	32.5 (15.1)	47/25	84

Table shows demographic information of the cohort, post-mortem interval (PMI), standard deviation (σ).

6.3.2. Brain tissue dissection and homogenization

Brain tissue dissection and homogenization was undertaken on the cohort as described in Chapter 2 section 2.2.

6.3.3. RNA isolation, quantification and standardization

RNA isolation, quantification and standardization were performed as described in detail in Chapter 2 section 2.3.

6.3.4. Software for analysis of target proteins (DAVID and PANTHER)

DAVID and PANTHER software were used for analysis of predicted target proteins of the selected miRNAs as described in detail in Chapter 2 section 2.13.

6.3.5. GWAS Catalog NHGRI-EBI

Examination of SNPs located at 3'UTR of genes reported to be associated with AD was performed using the GWAS Catalog NHGRI-EBI as described in detail in Chapter 2 section 2.11.

6.3.6. Data collection and analysis

Data on selected calibrator genes was generated by quantitative polymerase chain reaction (qPCR) as described in Chapter 2 section 2.6. The analysis of the resultant data was undertaken using the new formula proposed in Chapter 2 section 2.7. Statistical analysis was performed using the statistical package Graph Pad Prism (Chapter 2 section 2.16).

6.4. Results

6.4.1. miR-17 family

The miR-17 family is composed of six members miR-17/20a/20b/93/106a/106b, all of which were investigated and the data is now presented.

6.4.1.1. miR-17

miR-17 is transcribed from chromosome 13q31.3 (*MIR17* gene). mir-17 expression when analysed by the D'Agostino & Pearson normality test showed that miR-17 was not normally distributed and thus, Kruskal-Wallis test was necessary. Application of the Kruskal-Wallis test showed that the percentage of difference for miR-17 was significantly different (Figure 6.2) between diagnostic groups ($H=33.74$ and $p=0.0001$). Subsequent *post hoc* analysis by Dunn's multiple comparison test found that the previous association between all groups is perhaps due to a significant increase in the AD group compared to controls ($p<0.0001$), EAC ($p<0.0001$) and VaD ($p<0.01$).

Figure 6. 2 Percentage of difference for miR-17.

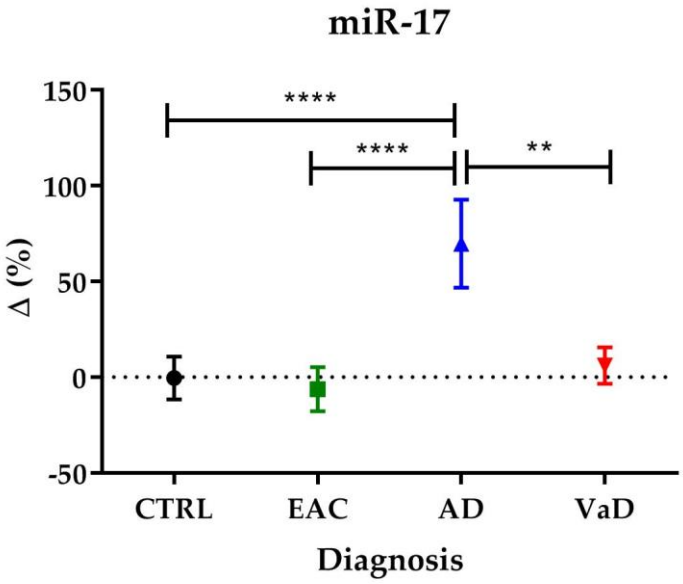

Figure shows the percentage of difference for miR-17 for all diagnostic groups compared to controls. Error bars show the 95% confidence interval and the average is depicted, ** p<0.01 and **** p<0.0001.

6.4.1.2. miR-20a

Similar to miR-17, miR-20a is co-transcribed from chromosome 13q31.3 (*MIR20A* gene). Initial analysis by the D'Agostino & Pearson normality test showed that miR-20a was normally distributed. However, Bartlett's test (p=0.0354) for homogeneity of variances found that the groups variances differed significantly. Thus, one-way ANOVA was inappropriate for analysis. Kruskal-Wallis test showed that the percentage of difference for miR-20a was significantly different (Figure 6.3) between diagnostic groups, (H=21.93 and p<0.0001). Application of Dunn's multiple comparison test showed an increase in AD compared to controls (p<0.01), EAC (p<0.001) and VaD (p<0.01).

Figure 6. 3 Percentage of difference for miR-20a.

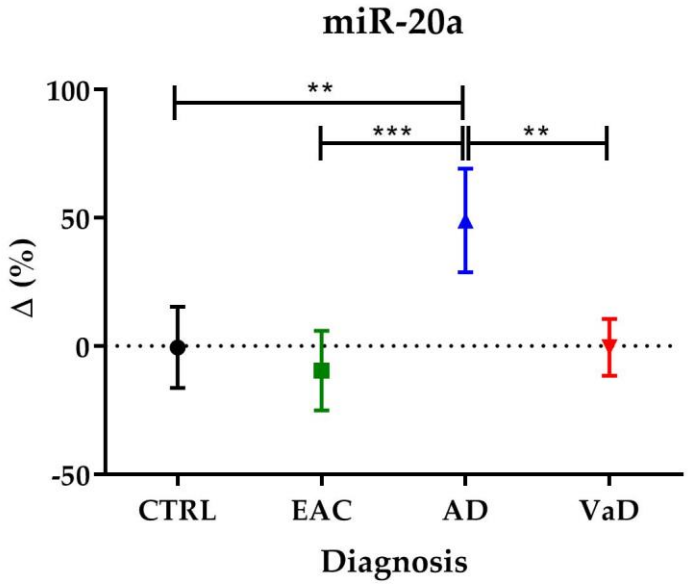

Figure shows the percentage of difference for miR-20a for all diagnostic groups compared to controls. Error bars show the 95% confidence interval and the average is depicted, ** $p<0.01$ and *** $p<0.001$.

6.4.1.3. miR-20b

miR-20b is transcribed from chromosome Xq26.2 (*MIR20B* gene). As for miR-20a, the D'Agostino & Pearson normality test showed that miR-20b was normally distributed, which was then confirmed by Bartlett's test ($p=0.25$). On analysis it was revealed that measurements of miR-20b (Figure 6.4) were significantly different between diagnostic groups (ANOVA $F=15.41$ and $p<0.0001$). Further analysis with Tukey's multiple comparison test showed an increase in AD compared to controls ($p<0.0001$), EAC ($p<0.0001$) and VaD ($p<0.0001$).

Figure 6. 4 Percentage of difference for miR-20b.

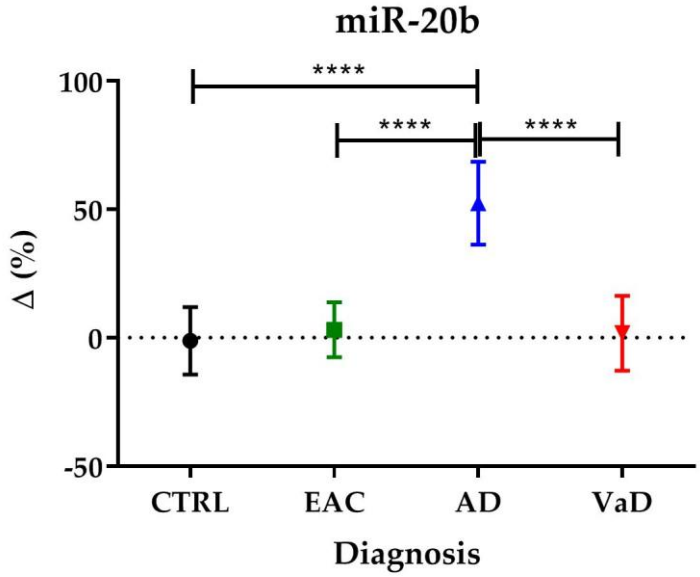

Figure shows the percentage of difference for miR-20b for all diagnostic groups compared to controls. Error bars show the 95% confidence interval and the average is depicted, **** p<0.0001.

6.4.1.4. miR-93

miR-93 is transcribed from chromosome 7q22.1 (*MIR93* gene). miR-93 expression when analysed by the D'Agostino & Pearson normality test showed that miR-93 was not normally distributed. Therefore, Kruskal-Wallis test was implemented. Application of the Kruskal-Wallis test showed that the percentage of difference for miR-93 (Figure 6.5) was significantly different between diagnostic groups (H=19.27 and p=0.0002). Subsequent *post hoc* analysis by Dunn's multiple comparison test found that the previous difference between groups is perhaps due to a significant increase in miR-93 expression in the AD group compared to controls (p<0.05), EAC (p<0.05) and VaD (p<0.001).

Figure 6. 5 Percentage of difference for miR-93.

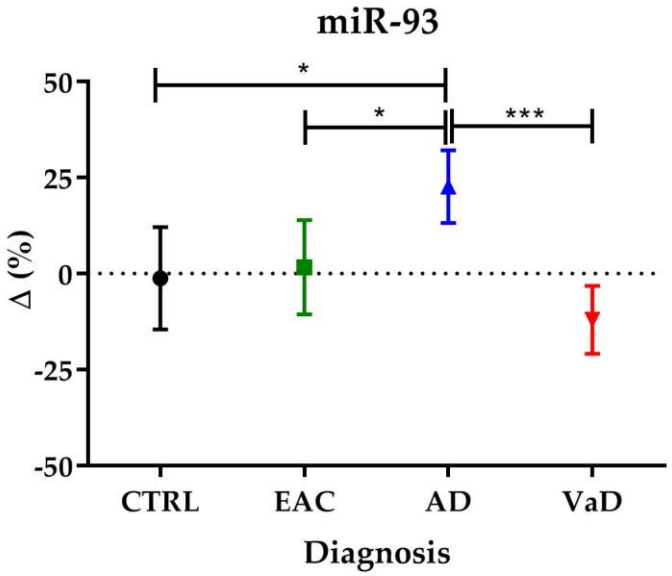

Figure shows the percentage of difference for miR-93 for all diagnostic groups compared to controls. Error bars show the 95% confidence interval and the average is depicted, *p<0.05 and *** p<0.001.

6.4.1.5. miR-106a

miR-106a is co-transcribed with miR-20b from chromosome Xq26.2 (*MIR106A* gene). D'Agostino & Pearson normality test showed that miR-106a was not normally distributed. The percentage of difference for miR-106a was significantly different between diagnostic groups, Kruskal Wallis test H=20.69 and p=0.0001 (Figure 6.6). Dunn's multiple comparison test showed an increase in AD compared to controls (p<0.001), EAC (p<0.01) and VaD (p<0.001).

Figure 6. 6 Percentage of difference for miR-106a.

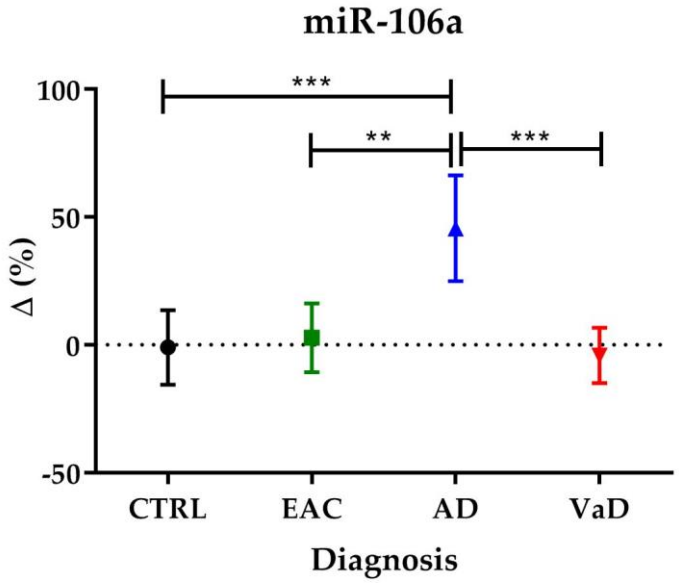

Figure shows the percentage of difference for miR-106a for all diagnostic groups compared to controls. Error bars show the 95% confidence interval and the average is depicted, **p<0.01 and *** p<0.001.

6.4.1.6. miR-106b

miR-106b is co-transcribed with miR-93 from chromosome 7q22.1 (*MIR106B* gene). Initial analysis by the D'Agostino & Pearson normality test showed that miR-106b was normally distributed, which was then confirmed by Bartlett's test (p=0.0811). Application of the one way ANOVA test found that the percentage of difference for miR-106b (Figure 6.7) was significantly different between diagnostic groups (F=7.11 and p=0.0003). Subsequent analysis by Tukey's multiple comparison test showed an increase in miR-106b expression in AD compared to controls (p<0.05), EAC (p<0.01) and VaD (p<0.001).

Figure 6. 7 Percentage of difference for miR-106b.

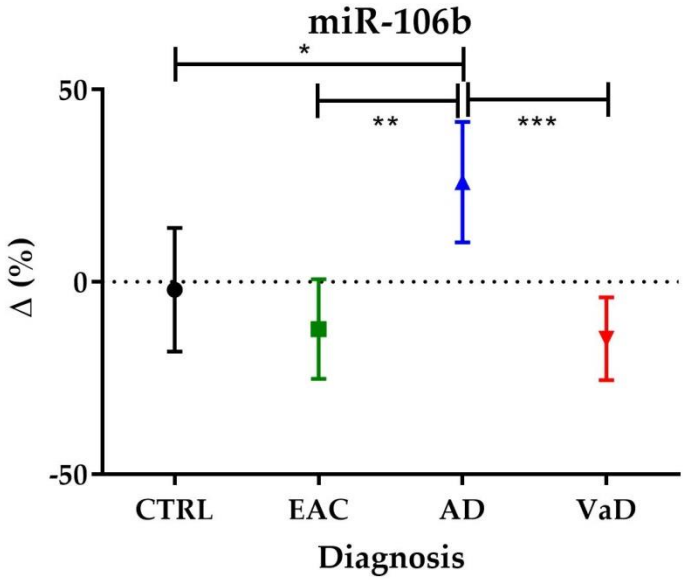

Figure shows the percentage of difference for miR-106b for all diagnostic groups compared to controls. Error bars show the 95% confidence interval and the average is depicted, *p<0.05, **p<0.01 and *** p<0.001.

6.4.1.7. Summary of miR-17 family results

All of the individual miRNA members of the miR-17 family showed relatively similar results. All of them demonstrated a significant difference between diagnostic groups. Further analysis with *post hoc* tests showed that all members of this miRNA family presented higher levels for the AD group in comparison to controls, EAC and VaD.

6.4.1.8. Analysis of miR-17 family predicted target proteins

As these miRNAs share the seed region and predicted targets, perhaps it is not unusual for all members of this family to demonstrate similar levels of expression. With this in mind, it was deemed prudent for the predicted targets of these miRNAs to be analysed further. Overall, this miRNA family has 1385 predicted target proteins according to TargetScan, analysis of the pathways related to these proteins is shown in Tables 6.5 and 6.6.

Table 6. 5 Analysis of predicted targets for miR-17 family by DAVID software.

DAVID pathways for miR-17 family	Protein count	Benjamini value
Cluster 1 enrichment score 1.3		
5-methylcytosine catabolic process	3	0.48
Sulfonate dioxygenase activity	3	0.46
C-20 gibberellin 2-beta-dioxygenase activity	3	0.46
C-19 gibberellin 2-beta-dioxygenase activity	3	0.46
Hypophosphite dioxygenase activity	3	0.46
Procollagen-proline dioxygenase activity	3	0.46
Methylcytosine dioxygenase activity	3	0.46
2,4-dichlorophenoxyacetate alpha-ketoglutarate dioxygenase activity	3	0.46
DNA-N1-methyladenine dioxygenase activity	3	0.71
Peptidyl-proline hydroxylation	3	0.97
Oxidative demethylation	3	0.98
DNA demethylation	3	1
Cluster 2 enrichment score 1.25		
Ganglioside biosynthetic process	5	0.69
Sialyltransferase activity	5	0.55
Oligosaccharide metabolic process	5	0.91
Cluster 3 enrichment score 0.76		
Histone methyltransferase activity (H3-K4 specific)	4	0.83
Histone H3-K4 methylation	4	0.97
Histone methyltransferase complex	4	0.78
Cluster 4 enrichment score 0.53		
Cytokine Receptors	3	0.88
Insulin signalling	3	0.99
LAT couples T-cell receptor	3	0.99
Cluster 5 enrichment score 0.53		
Semaphorin receptor binding	4	0.93
Negative regulation of axon extension involved in axon guidance	4	0.99
Semaphorin-plexin signalling pathway	4	1
Cluster 6 enrichment score 0.34		
Palmitoyltransferase activity	3	0.98
Protein palmitoylation	3	1
Protein-cysteine S-palmitoyltransferase activity	3	1

Table shows gene ontology and pathways related to proteins targeted by miR-17 family, the number of proteins and Benjamini value are specified.

None of the pathways identified with DAVID software reached levels of significance. However, analysed performed with PANTHER found seven pathways to be statistically significant (Table 6.6).

Table 6. 6 Analysis of predicted targets for miR-17 family by PANTHER software.

PANTHER pathway for miR-17 family	Protein count	Fold enrichment	P value
Cadherin signalling pathway	31	2.96	0.0001
Alzheimer disease-amyloid secretase pathway	17	2.94	0.0350
Transforming growth factor-beta signalling pathway	22	2.86	0.0067
Platelet derived growth factor signalling pathway	26	2.59	0.0078
Angiogenesis	28	2.32	0.0211
Alzheimer disease-presenilin pathway	32	2.17	0.0029
Wnt signalling pathway	45	2.13	0.0021

Table shows pathways related to proteins targeted by miR-17 family, number of proteins targeted, fold enrichment and p values are specified.

According to the analysis done by PANTHER, nine pathways were identified that were statistically significant. These pathways involved variable numbers of predicted target proteins that ranged from 17 to 45 target proteins in any one pathway. These also had a range of fold enrichment scores that ranged from 2.13 to 2.96. On further examination of the pathways identified, the cadherin signalling pathway has the highest enrichment score and was the most highly significant (0.0001), with an enrichment score of 2.96. Other pathways that were highly significant included the Alzheimer disease-amyloid secretase pathway (p=0.035), the transforming growth factor-beta signalling pathway (p=0.0067), the platelet derived growth factor signalling pathway (p=0.0078), angiogenesis (p=0.0211), the Alzheimer disease-presenilin pathway (p=0.0029) and Wnt signalling pathway (p=0.0021).

6.4.2. miR-143

miR-143 is transcribed from chromosome 5q32 (*MIR143* gene). According to the D'Agostino & Pearson normality test, measurements of miR-143 were not normally distributed. Thus, Kruskal-Wallis test was used for analysis of the data. The percentage

of difference for miR-143 was significantly different between diagnostic groups, Kruskal-Wallis test H=11.03 and p=0.011 (Figure 6.8). Subsequent *post hoc* analysis by Dunn's multiple comparison test showed an increase in AD compared to EAC ($p<0.05$).

Figure 6. 8 Percentage of difference for miR-143.

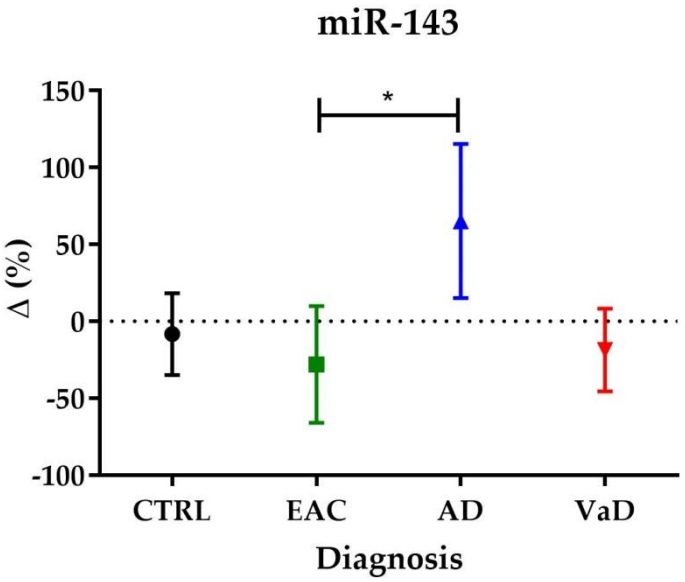

Figure shows the percentage of difference for miR-143 for all diagnostic groups compared to controls. Error bars show the 95% confidence interval and the average is depicted, *$p<0.05$.

6.4.2.1. Analysis of miR-143 predicted target proteins

In addition to the MAS receptor, miR-143 has another 497 predicted targets according to TargetScan; analysis of the pathways related to these proteins with DAVID and PANTHER software is shown in Tables 6.7 and 6.8.

Table 6. 7 Analysis of predicted targets for miR-143 by DAVID software.

DAVID pathways for miR-143	Protein count	Benjamini value
Cluster 1 enrichment score 0.59		
Integrin affinity modulation	3	0.45
Endometrial cancer	3	0.74
Non-small cell lung cancer	3	0.77
Fc epsilon RI signalling pathway	3	0.84
Hepatitis C	3	0.98
Cluster 2 enrichment score 0.57		
fMLP induced chemokine gene expression in HMC-1 cells	4	0.98
Fc Epsilon Receptor I Signalling in Mast Cells	4	0.98
NFAT and Hypertrophy of the heart (Transcription in the broken heart)	4	1
Cluster 3 enrichment score 0.45		
Role of MEF2D in T-cell Apoptosis	3	0.98
Neuropeptides VIP and PACAP inhibit the apoptosis of activated T cells	3	0.98
BCR Signalling Pathway	3	1
Signalling Pathway from G-Protein Families	3	1
T Cell Receptor Signalling Pathway	3	1

Table shows gene ontology and pathways related to proteins targeted by miR-143, the number of proteins and Benjamini value are specified.

As with previous miRNAs, none of the pathways identified with DAVID software obtained significant levels. Nonetheless, when analysed with PANTHER, it revealed that only one pathway came up to be statistically significant (Table 6.8). This pathway is the gonadotropin-releasing hormone receptor pathway with a protein count of 21, fold enrichment score of 2.96 and significance of p=0.0032.

Table 6. 8 Analysis of predicted targets for miR-143 by PANTHER software.

PANTHER pathways for miR-143	Protein count	Fold enrichment	P value
Gonadotropin-releasing hormone receptor pathway	21	2.96	0.0032

Table 6.8 Pathway related to proteins targeted by miR-143, number of proteins targeted, fold enrichment and p values are specified.

6.4.3. miR-320e

miR-320e is transcribed from chromosome 19q13.32 (*MIR320E* gene). The D'Agostino & Pearson normality test showed that miR-320e was normally distributed. It was not possible to perform genotyping of the SNP rs6857, thus analysis was performed using diagnostic groups. The percentage of difference for miR-320e was significantly different between diagnostic groups, ANOVA F=3.84 and p=0.026 (Figure 6.8). Tukey's multiple comparison test showed an increase in AD compared to controls ($p<0.05$) and EAC ($p<0.05$).

Figure 6. 9 Percentage of difference for miR-320e.

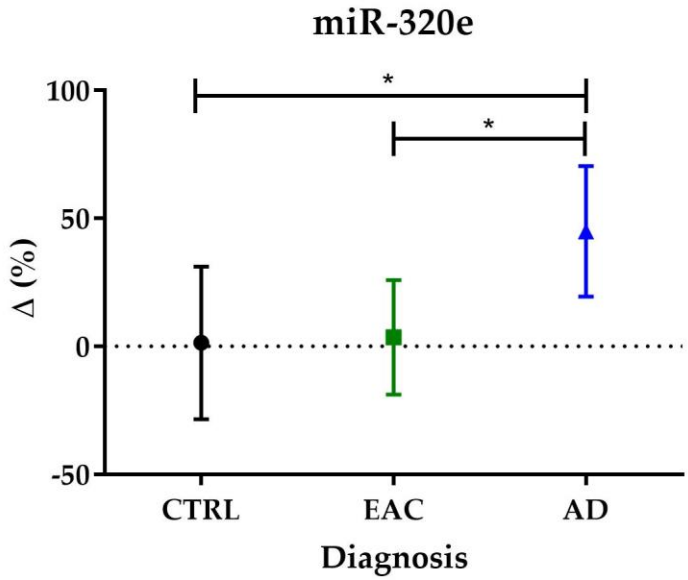

Figure shows the percentage of difference for miR-320e for all diagnostic groups compared to controls. Error bars show the 95% confidence interval and the average is depicted, *$p<0.05$.

6.4.3.1. Analysis of miR-320e predicted target proteins

In addition to the binding site created at the SNP rs6857 at the PVRL2 gene, miR-320e has 4219 predicted targets; analysis of the pathways related to these proteins with DAVID and PANTHER software is shown in Tables 6.9 and 6.10.

Table 6. 9 Analysis of predicted targets for miR-320e by DAVID software.

DAVID pathways for miR-320e	Protein count	Benjamini value
Cluster 1 enrichment score 1.23		
Actin cortical patch	3	0.82
Actin cortical patch localization	3	0.99
Actin cortical patch assembly	3	0.99
Cluster 2 enrichment score 0.66		
N-formyl peptide receptor activity	3	0.98
Complement receptor activity	3	0.99
Complement receptor mediated signalling pathway	3	1
Cluster 3 enrichment score 0.5		
Glycerol channel activity	4	1
Cellular water homeostasis	4	1
Glycerol transport	4	1
Water channel activity	4	1
Cluster 4 enrichment score 0.44		
Proton-transporting two-sector ATPase complex	3	0.91
Proton-transporting V-type ATPase, V1 domain	3	0.95
Proton-transporting ATPase activity, rotational mechanism	3	1
Cluster 5 enrichment score 0.36		
Pointed-end actin filament capping	3	1
Striated muscle thin filament	3	0.98
Myofibril assembly	3	1
Cluster 6 enrichment score 0.3		
Voltage-gated sodium channel complex	3	0.95
Voltage-gated sodium channel activity	3	1
Regulation of postsynaptic membrane potential	3	1
Cluster 7 enrichment score 0.25		
Potassium: proton antiporter activity	3	1
Sodium: proton antiporter activity	3	1
Sodium ion import across plasma membrane	3	1

Table shows gene ontology and pathways related to proteins targeted by miR-320e, the number of proteins and Benjamini value are specified.

As with previous miRNAs, none of the pathways identified with DAVID software reached levels of significance. Nonetheless, when analysed with PANTHER, two pathways were found to be statistically significant (Table 6.8). These pathway are the cadherin signalling pathway (p=0.0032) with a protein count of 46 and fold enrichment score of 2.06, and the Wnt signalling pathway (p=0.0294) with a protein count of 74 and fold enrichment score of 1.65.

Table 6. 10 Analysis of predicted targets for miR-320e by PANTHER software.

PANTHER pathway for miR-320e	Protein count	Fold enrichment	P value
Cadherin signalling pathway	46	2.06	0.0064
Wnt signalling pathway	74	1.65	0.0294

Table shows pathways related to proteins targeted by miR-320e, number of proteins targeted, fold enrichment and p values are specified.

6.5 Discussion and conclusions

The null hypothesis was that there is no significant difference in the levels of miR-17 family and miR-143 between diagnostic groups, AD, VaD, early AD changes (EAC) and non-demented controls. In the case of miR-320e, the null hypothesis was that there is no significant difference between diagnostic groups, AD, early AD changes (EAC) and non-demented controls. The null hypothesis is rejected for the eight miRNAs measured. Seven of them showed a significant difference between diagnostic groups, and specifically a significant increment was found in AD with respect to controls. miR-143 that targets the MASR was found to be significantly different between the AD group and the EAC group. As mentioned previously, it could be possible that such miRNAs have an impact in disease; however there are several factors that need to be considered.

Unexpectedly, no change was observed in theses miRNAs for the VaD group. The transcripts considered were based in elements of the renin angiotensin system and others related to hypoxic conditions. However, it should be noted that there is a high disparity in the number of considered transcripts compared to the number of transcripts targeted by these miRNAs, 1385 target proteins for miR-17 family and 497 target proteins for miR-143.

In the case of miR-17 family, all miRNAs were found to be significantly increased in the AD group compared to other diagnostic groups. Interestingly, PANTHER software showed that this miRNA family target proteins related to amyloid secretase and the

presenilin pathway, which are implicated in AD, but also to angiogenesis, transforming growth factor (TGF), platelet derived growth factor (PDGF) and cadherin signalling pathways. However, similar to the results obtained in Chapter 5, there was almost no concordance between the results obtained from DAVID and PANTHER software. This puts in doubt whether or not these pathways are indeed related to the miR-17 family.

Before making any assumptions about the role of any miRNAs examined in this thesis some factors such as the location of the miRNA in the brain should be considered. Using *in situ* hybridization, miR-17 family has been found to be expressed at high levels in paediatric high-grade gliomas (165). It has also been found to be highly expressed in medulloblastoma (166). Unfortunately, the normal expression of the miR-17 family in the human brain and whether differences exist across brain areas in unknown. However, interestingly the authors found a specific miRNA pattern in paediatric high-grade glioma, which reinforces the idea that miRNA signatures exist (165).

Combinations of miRNAs are likely to have a more relevant role in disease. Although single miRNA–protein relations have been criticised in this project, it could be possible that under certain restricted conditions such relations exist. The analysis of miRNAs for the MAS receptor showed that only five miRNAs are able to bind at it. miR-143 is the miRNA with the highest affinity for binding at MAS receptor and also an abundant miRNA with respect to the other four miRNAs that bind at this receptor. miR-143 was found to be significantly increased in the AD cases in comparison to the early AD changes (EAC) group. Nevertheless, the MAS receptor is only one of the 497 predicted targets for miR-143. The location of miR-143 should also be investigated and whether it co-localizes with the MAS receptor.

Another important factor in miRNA research is to validate the binding site at which the miRNA binds and thus, may cause a reduction in protein levels. This has exceptionally importance for experiments where the predicted binding site is not

supported by target predicting software. For instance, Zhao *et al* suggested that a binding site at the mRNA of TREM2 exists for miR-34 and thus its expression is regulated by miR-34a. This was performed using independent bioinformatics algorithms (69). However, when analysed by TargetScan and MiRanda miRNA binding predicting software, no binding sites are found.

Along these lines, the SNP at rs6857 creates a binding site for miR-320e. Although the existence of this binding site has been reported already in the literature, the results shown in this thesis suggest that the levels of miR-320e are increased in AD brain (160,161). Yet, it would be even more interesting to know the levels of this miRNA in relation to the presence of the SNP rs6857. Also, to relate such findings in relation with the protein levels of the *PVRL2* gene.

The protein levels of PVRL2 are not only relevant for this miRNA but also as a marker of blood brain barrier dysfunction. The *PVRL2* gene is an endothelial adhesion molecule important for cell adhesion and adherens junction (162). Knockout mice of this gene has shown a tendency to develop atherosclerosis and altered trans endothelial migration with infiltration of leukocytes (163). This is also relevant as the most common form of amyloid accumulates in the brain as CAA.

Indeed, individuals who carry the *APOE* ε4 allele are in a higher risk to present CAA-related microbleeds and age related cognitive decline (40). Where age and the presence of the *APOE* ε4 allele are the highest risk factors to develop dementia. The *APOE* gene is located within the AD linkage region at chromosome 19, specifically the cytogenetic band 19q13.32. Interestingly, miR-320e is also encoded at 19q13.32 along *TOMM40* and the *PVRL2* genes. Yashin et al suggested the PVRL2 is influenced by APOE and TOMM40 and that APOE, APOC1, TOMM40 and NECTIN2 (all encoded at 19q13.32) might influence AD acting in concert (164). miR-320e might also work synergistically with these proteins or might be influenced by APOE.

Based on this, a further research question would be the effect of APOE status in relation to miR-320e levels. This was not possible to analyse in this cohort given the proportions of *APOE* ε4 carriers with respect to other carriers within the diagnostic groups. There is only one *APOE* ε4 carrier in the control group (N=24), four carriers in the EAC group (N=20) and 16 carriers in the AD group (N=22). Yet, the effect of *APOE* status in miR-320e levels remains an interesting research question. This could also be associated with PVRL2 protein levels once the validation of the binding site is performed.

Validation of miRNA binding sites is a supportive tool in order to extrapolate results from miRNA binding software into functionality. Cell culture is a useful tool for experimentation of changes derived from observational studies. Causal versus consequential effects can be investigated using cell culture. Validation of miRNA binding sites is being performed using luciferase assays. However, luciferase assays are not able to differentiate between canonical and non-canonical binding sites, neither if the effects are a result of direct miRNA binding to the transcript or via changes in other miRNAs that also affect the transcript (65).

In adittion, miRNAS have certain characteristics that should be considered, and it is necessary to first evaluate the suitability of cell culture as a model for study of dementia. Some miRNAs are cell-type and brain-area specific (167,168). Given the cytoarchitectural and functional differences between Brodmann areas of the brain, it is possible that different brain areas exhibit cellular populations with characteristic miRNA signatures. These properties and the location of miRNAs previously examined will be explored in Chapter 7.

Chapter 7.- Evaluation of cell culture as an experimental model for the study of miRNAs in dementia

7.1 Introduction

This part of the study aims to investigate whether there is a cellular association between miRNAs of the same family. This is of importance because the origin of the miRNAs informs us as to the origin of the changes which are occurring in a disease state. In order to address this question, a cell culture approach has been used to determine if, with induced differentiation of SH-SY5Y cells, localisation of certain miRNA families develops.

It is important first however, to consider the knowledge we have so far as to the cellular location of different miRNA families .As described in Chapter 6, the presence of a miRNA is not sufficient to assume its effect, but the location of the miRNA and whether it co localizes with its targets is critical. The importance of *in situ* localization of miRNAs and how this differs between cell types, has also been emphasized by Kent *et al* (169). Kent *et al* reviewed the role of both miR-143 (this miRNA is discussed in Chapter 6) and miR-145 as tumour suppressors. These miRNAs have been found to be highly expressed in the colon and are consistently reported as being downregulated in colorectal and other cancers.

However, it came to light that miR-143 and miR-145 are not expressed in colonic epithelial cells; although highly expressed in mesenchymal cells such as fibroblasts and smooth muscle cells. Several studies were performed without considering that multiple different cell types, each with unique miRNA signatures, make up each tissue. As mentioned above, without knowing the origin of the miRNAs it is impossible to evaluate why it has changed. The authors also examined other examples of miRNAs being investigated in a non-biological manner, which is a common tendency in miRNA research (170).

The localisation of the 25 miRNAs previously measured in this thesis is summarised in Table 7.1. Most of them are unknown. Mellios *et al* performed *in situ* hybridization of a set of miRNAs in the prefrontal cortex of subjects aged 15-84 years (171). They found lamina-specific expression patterns for several miRNAs. miR-16 was expressed from layer III to layer VI with a stronger expression in layer V whilst miR-195 was expressed in layers II to V with strongest expression in layers II and III. Interestingly, miR-103 was similarly expressed across all layers and also in white matter. miR-103 was not considered for analysis in this thesis. However, this finding suggests that this miRNA might be important for instance in differentiation of brain cells from the ectoderm. The localisation of other members of the miR-16 family in the human brain is unknown.

Similarly, the localisation of miR-29 family is also unknown. Wang *et al* found this miRNA family to be enriched in cultured glial preparations (172). Nevertheless, its presence in vitro could be just inherent of the particular cell type. The in situ location of miR-29 across brain areas would be necessary in order to relate to the functional attributes found previously using pathways software. In the same way, miR-34 family localisation in the human brain is also unknown.

Liu *et al* suggested that miR-34b upregulation was associated with astrocyte apoptosis in mice. Yet, this upregulation of miR-34b could be specific for apoptosis regardless of the cellular population. It could also be exclusive to mice or specific to the area analysed (hippocampus). Interestingly, although the study used mice tissue, Kasai *et al* performed *in situ* hybridization of miR-34a and found its specific expression in GABAergic interneurons across the thalamic reticular nucleus, the globus pallidus and the entopeduncular nucleus (173).

Thus, the findings reinforce the idea of the specificity for miRNAs in cellular populations, in this case within a neuronal subgroup (GABAergic interneurons). In contrast, using laser microdissection and human brain tissue, Rao *et al* observed that miR-34a and miR-449 (both members of the miR-34 family) were expressed in astrocytes, together with other miRNAs considered in this project such as miR-125b

and miR-143 (174). However, the study focused on astrocytes and it is possible that those miRNAs might be expressed at even higher levels in other cell types. Determination of the *in situ* location of the miRNAs is therefore fundamental before considering any further suggestions as described by Kent *et al* (60).

Table 7. 1 In-situ location of previously measured miRNAs in the human brain.

miRNA family	miRNA	Human brain location	Cellular population
miR-16	miR-15a	Unknown	Unknown
	miR-15b	Unknown	Unknown
	miR-16	Prefrontal cortex Layers III-VI	Pyramidal neurons
	miR-195	Prefrontal cortex Layers II-V	Pyramidal neurons
	miR-424	Unknown	Unknown
	miR-497	Unknown	Unknown
miR-29	miR-29a	Unknown	Unknown
	miR-29b	Unknown	Unknown
	miR-29c	Unknown	Unknown
miR-34	miR-34a	Unknown	Unknown
	miR-34b	Unknown	Unknown
	miR-34c	Unknown	Unknown
	miR-449	Unknown	Unknown
miR-125	miR-125a	Unknown	Unknown
	miR-125b	Unknown	Unknown
miR-132	miR-132	?	Neurons Synapses and dendrites
	miR-212	?	Neurons Synapses and dendrites
miR-17	miR-17	Unknown	Unknown
	miR-20a	Unknown	Unknown
	miR-20b	Unknown	Unknown
	miR-93	Unknown	Unknown
	miR-106a	Unknown	Unknown
	miR-106b	Unknown	Unknown
miR-143	miR-143	Unknown	Unknown
miR-320e	miR-320e	Unknown	Unknown

Location of the miR-125 family in the human brain is also unknown. Pogue *et al* found miR-125b to be expressed in cell culture of astrocytes (175). Along these lines, Rao *et al* observed that miR-125b was undetected in deeper grey matter astrocytes, whereas white matter astrocytes expressed this miRNA. Rao *et al* focused on analysing astrocytic miRNAs, thus it still remains unknown as to whether miR-125b is also present in other cellular populations (e.g. like neurons) and how they compare to reported levels of astrocytic miR-125b.

In contrast to previously described miRNAs, there is more evidence about the miR-132/212 family. Downregulation of this miRNA family in different brain areas is the only consistent finding according to a meta-analysis of profiling studies in AD (64). The miR-132/212 family is highly expressed in dendrites and synapses, and is regulated by neuronal activity (150,176). Zhu *et al* observed the expression of miR-132 in neurons of the nucleus basalis of Meynert (177). They also found a significant positive correlation with choline acetyltransferase (ChAT) expression and that ChAT expression showed a significantly negative correlation with hyperphosphorylated tau.

Functional attributes of this miRNA family in the brain have been found by Hansen *et al* (176,178). These studies provided insight into the function of this miRNA family using a combination of conditional knockout and transgenic mouse models of miR-132/212. They corroborated that miR-132 is upregulated by neuronal activity and that induction of miR-132 expression was sufficient to modulate cognitive capacity in a dose-dependent manner (176). Likewise, miR-132 levels correlated with spine density and interestingly, expression of miR-132 over and above physiological levels led to excessive spine density and cognitive deficits (176).

Hansen *et al* also, used Illumina sequencing to show that miR-132/-212 deletion increased the expression of hundreds of genes. Functional gene ontology analysis of those genes revealed significant enrichment scores related to synaptic transmission, neuronal proliferation and morphogenesis (178). Interestingly, in Chapter 3, the

analysis of predicted targets for the miR-132/212 also found significant enrichment scores for the Rho GTPase signalling pathway, important for neurogenesis.

Another miRNA family (discussed in Chapter 6) that has been proposed to contribute to neurogenesis is the miR-17 family (179). Jin *et al* suggested that the miR-17 family have a significant impact on neurogenesis in mice as well as in depression and anxiety. However, the localisation of members of the miR-17 family in the human brain is unknown. Similarly, the location of miR-143 and miR-320e is also unknown. As described before, several attributes can be suggested from each of the transcripts that a miRNA binds to. However, the effect of the miRNA will be related to the number of transcripts that it targets and whether they are co-localised in the brain.

miRNAs have an important role in cell fate and differentiation (180,181). Laser microdissection of human astrocytes showed miRNA signatures specific to brain regions, subcortical astrocytes, cortical astrocytes and differences were even observed between layers of the cortex (174). A proportion of their evaluated miRNAs was present in all astrocytes suggesting that these miRNAs might be important for functions common to all astrocytes.

In addition, this study also found that not only the presence but also the levels of a miRNA might be relevant as some changes were observed when a miRNA was present in surrounding neuronal and other glial cells. The results suggest that some miRNAs might be important for the coordination of a microenvironment between cellular populations. In this way, a combination of miRNAs might be determinant in the proteome landscape expressed by different cell types and brain areas in order to direct specific functions and to respond to external stimuli.

Similarly, the levels of a miRNA might also change during the differentiation of a cell. miR-128 and miR-124 are examples of abundant miRNAs in the adult brain (52). miR-124 expression is undetectable or expressed at low levels during neurogenesis in progenitor cells whilst it is upregulated in differentiating and post mitotic neurons

(181). Le *et al* also observed that miR-124 expression increased after differentiation of the human neuroblastoma cell line SH-SY5Y into neuronal-like cells. They then overexpressed miR-124 in SH-SY5Y cells and found a significant increase in the percentage of differentiated cells with neurite outgrowth (182).

Similarly, using HeLa cells (cervical cancer cells), overexpression of miR-124 caused a decrease in several non-neuronal genes, showing a gene expression program that resembles neuronal cells (181). In accordance with this, it has been shown that pluripotent stem cells demonstrate exclusive miRNA patterns, the levels of which decrease following differentiation (180). Indeed, an important function of miRNAs in human embryonic stem cells is to regulate cell cycle progression (180). If such miRNAs are able to modify cellular phenotype, experimentation of miRNAs in cell culture and its extrapolation from observational studies should be taken with caution as every cellular population will show specific miRNA signatures.

For instance, Sarkar *et al* observed that miR-34a is increased in brain regions of AD patients and that this miRNA was also overexpressed in a mouse model for AD (183). The authors postulated miR-34a as a potential therapeutic target for AD. Similarly, Zovoilis *et al* found increased levels of miR-34c in the hippocampus of AD patients and also in mouse models for AD. The authors suggested that targeting miR-34c could be used as a therapeutic approach (184).

However, despite the promise of an intervention, the complexity of therapeutic manipulation of miRNAs in the brain should not be under-estimated. Indeed, miR-34 and miR-125 have been found to be able to differentiate SH-SY5Y cells into neuronal-like phenotype (182,185). Le *et al* overexpressed miR-125b in SH-SY5Y cells and observed that miR-125b was both sufficient and necessary to induce neurite and dendritic outgrowth and in doing so affected 164 target genes (182). In contradiction to this, Zhang *et al* found that overexpression of miR-125b in the brains of mice resulted in decreased dendritic spine density (186).

Zhang *et al* also observed that overexpression of miR-125b *in vitro* caused hyperphosphorylation of tau. miR-125b has also been associated with cognitive deficits *in vivo* and hyperphosphorylation of tau *in vitro* by others in the literature (120,187). The contradictory evidence might be explained by the fact that some miRNAs are cell-type and brain-area specific (167,168). Given the cytoarchitectural and functional differences between Brodmann areas of the brain, it is possible that different brain areas exhibit cellular populations with characteristic miRNA signatures.

Yet, experimentation of miRNAs in cell culture could be used to investigate certain properties of miRNAs, such as their regulation. Little is known about expression of miRNAs of the same miRNA family in relation to each other. miRNAs within the same family share the seed region by which they bind to the mRNAs and eventually remodel the proteome. It is known that miRNAs that are clustered within 50 kilobases from each other show common expression patterns (52). However, it is also clear, as was shown in chapter 6 that different members of the same miRNA family can reside on different chromosomes. So it remains the question as to whether miRNAs of the same family show similar expression despite their genomic location and similarly whether this is altered under circumstances of differentiation of a cell type. The research question covered in this chapter is ''Is there an association between miRNAs of the same family over differentiation of SH-SY5Y cells into neuronal-like cells?''

7.2 Hypothesis

The null hypothesis is that there is no correlation in the expression between miRNAs of the same family over differentiation of SH-SY5Y cells into neuronal-like cells.

7.3 Methods

7.3.1. RNA isolation, quantification and standardization

RNA isolation, quantification and standardization were similarly performed as described in Chapter 2.3.

7.3.2. Cell culture

The SH-SY5Y cell line is human-derived. Originally, a bone marrow biopsy was taken from a metastatic bone tumour of a four-year-old female and this formed the SK-N-SH cell line; SH-SY5Y was subcloned from this. The cells are epithelial-like but addition of retinoic acid causes them to produce dendrites and thus are termed 'neuron-like'. They are adrenergic but can also have markers similar to those found in dopaminergic, cholinergic and glutamatergic neurons (188).

Protocols for handling, subculture routine and culture media were obtained from the European Collection of Authenticated Cell Cultures (ECACC), a Culture Collection of Public Health England and practical training was supervised by Mrs. Saranna Chipper-Keating. Frozen SHSY5Y cells were acquired (ECACC 94030304) at passage 12 and were resuscitated on a water bath until thawed.

Culture medium was prepared beforehand as follows, Ham's F12 (Sigma-Aldrich® N4888) : Minimum Essential Medium Eagle (MEM) (Sigma-Aldrich® M2279) (on a proportion of 1:1) plus 2mM Glutamine (Sigma-Aldrich® G7513), 1% Non Essential Amino Acids (Sigma-Aldrich® M7145) and 15% Foetal Bovine Serum (Gibco® A31608-01). Resuscitated cells were incorporated into 5 ml of prepared culture medium and resuspended. 5 ml of culture medium was added to the resuspended cells in the solution and placed into a 75 cm^2 cell culture flask (Sigma-Aldrich® CLS3290) in the incubator at 37°C and 5% CO_2.

Subculture was performed at a confluency of 70-80% and cells were detached using trypsin-EDTA (ethylenediaminetetraacetic acid) (Lonza® CC-5012) and re-seeded at a concentration of 1,000 - 10,000 cells/cm^2. Once the first flask reached the determined confluency, two flasks were seeded, and the rest of the cells were stored in aliquots using DMSO (Sigma-Aldrich® D2650). Aliquots were labelled with the number of cells, passage, cell line and date of storage.

Cell counting was performed using a haemocytometer and 0.4% trypan blue stain in phosphate buffered saline (PBS). 100 µl of resuspended cells were combined with 100 µl of trypan blue. An inverted microscope was used to observe and count cells, live cells appearance was bright and colourless whilst dead cells stained blue.

Retinoic acid (Sigma-Aldrich® R2625) was used at a concentration of 10 µM in culture media prepared with 98% Neurobasal® medium (Gibco® 21103-049) and 2% B27® supplement (Gibco® 17504-044). The time period of retinoic acid treatment was nine days with three points for medium change at day 1, 4 and 7. Both treated and untreated cells were harvested at day 10. The number of samples considered for analysis is six samples for untreated cells and six samples for treated cells.

7.3.3. Data collection and analysis.

Data on selected calibrator genes was generated by quantitative polymerase chain reaction (qPCR) as described in Chapter 2.6. The analysis of the resultant data was undertaken using the new formula proposed in section 2.7. Statistical analysis was performed using the statistical package Graph Pad Prism (section 2.16 Statistical package Graph Pad Prism).

7.4. Results

7.4.1. Selection of calibrator gene

All miRNAs measured in this chapter were evaluated for use as a calibrator gene. Six miRNAs were found to be not significantly different between untreated and treated cells, miR-15a, miR-16, miR-497, miR-34a, miR-125a and miR-125b. D'Agostino & Pearson omnibus normality test showed that the percentage of difference for these miRNAs was normally distributed but not for miR-34a. The data was analysed using Mann-Whitney test for miR-34a and unpaired t test for the remainder. Figures 7.1 to 7.6 show the percentage of difference between untreated and treated cells.

Figure 7. 1 Percentage of difference for miR-15a in SH-SY5Y cells.

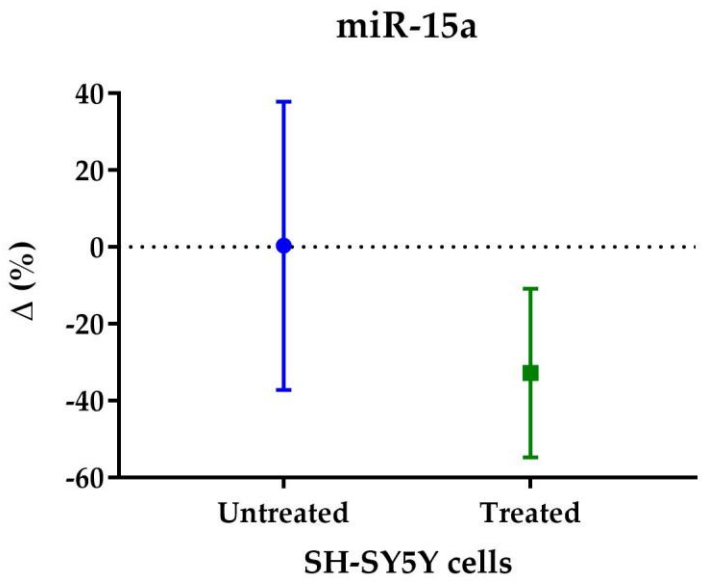

Figure shows the percentage of difference for miR-15a between untreated and treated cells, error bars show the 95% confidence interval and the average is depicted.

Figure 7. 2 Percentage of difference for miR-16 in SH-SY5Y cells.

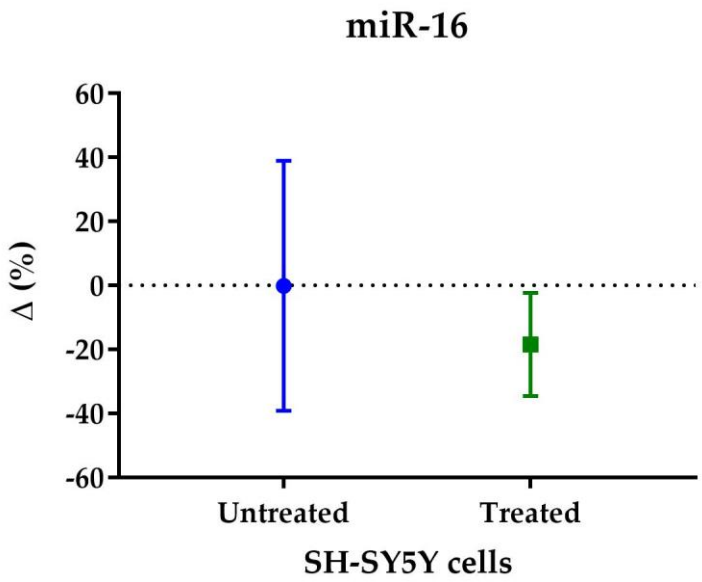

Figure shows the percentage of difference for miR-16 between untreated and treated cells, error bars show the 95% confidence interval and the average is depicted.

Figure 7. 3 Percentage of difference for miR-497 in SH-SY5Y cells.

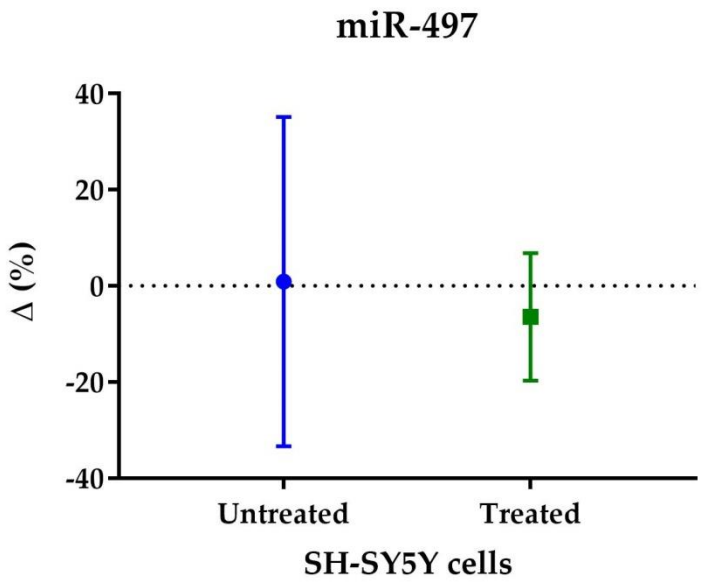

Figure shows the percentage of difference for miR-497 between untreated and treated cells, error bars show the 95% confidence interval and the average is depicted.

Figure 7. 4 Percentage of difference for miR-34a in SH-SY5Y cells.

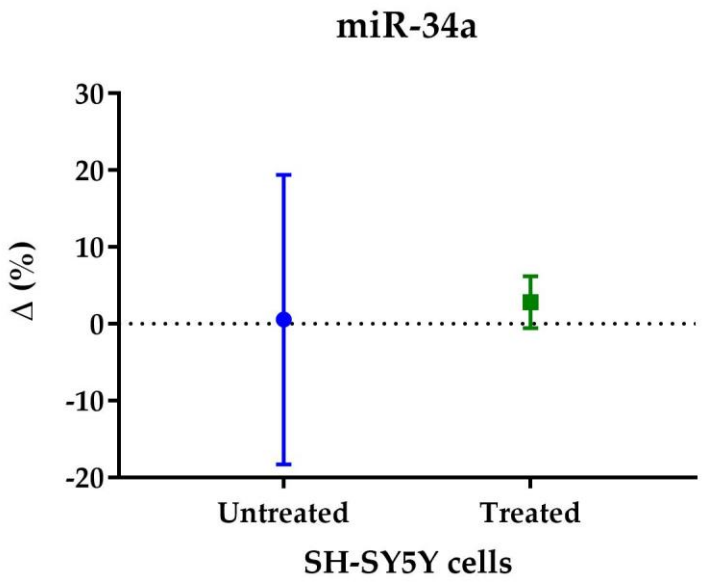

Figure shows the percentage of difference for miR-34a between untreated and treated cells, error bars show the 95% confidence interval and the average is depicted.

Figure 7. 5 Percentage of difference for miR-125a in SH-SY5Y cells.

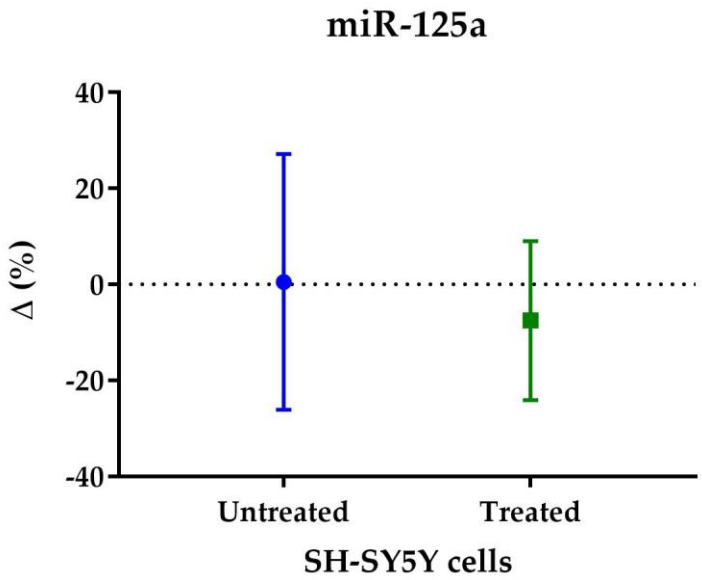

Figure shows the percentage of difference for miR-125a between untreated and treated cells, error bars show the 95% confidence interval and the average is depicted.

Figure 7. 6 Percentage of difference for miR-125b in SH-SY5Y cells.

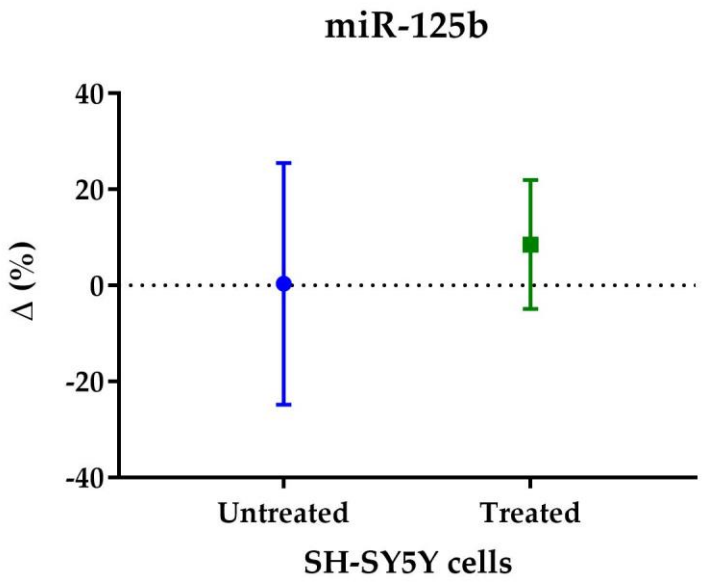

Figure shows the percentage of difference for miR-125b between untreated and treated cells, error bars show the 95% confidence interval and the average is depicted.

No significant difference was found with respect to levels of expression between untreated and treated cells for miR-15a, miR-16, miR-497, miR-34a, miR-125a and miR-125b. Therefore, these miRNAs were used as calibrator genes to help calculate the average CT value with a new formula proposed in section 2.7. After selection of calibrator genes, calculation of miRNA changes and correlation analysis for each of the miRNA families covered in this thesis was performed.

7.4.2. miR-16 family

The miR-16 family is composed of miR-15a/15b/16/195/424/497. miR-15a and miR-16 map to an intron in chromosome 13q14.2, both genes are clustered within 0.5 kb. miR-15b is encoded in chromosome 3q25.33. miR-195 and miR-497 are both transcribed from chromosome 17p13.1, whilst miR-424 is derived from chromosome Xq26.3. Figure 7.7 shows the percentage of difference for miR-16 family between untreated and treated cells, no statistical test was performed.

Figure 7. 7 Percentage of difference for miR-16 family in SH-SY5Y cells.

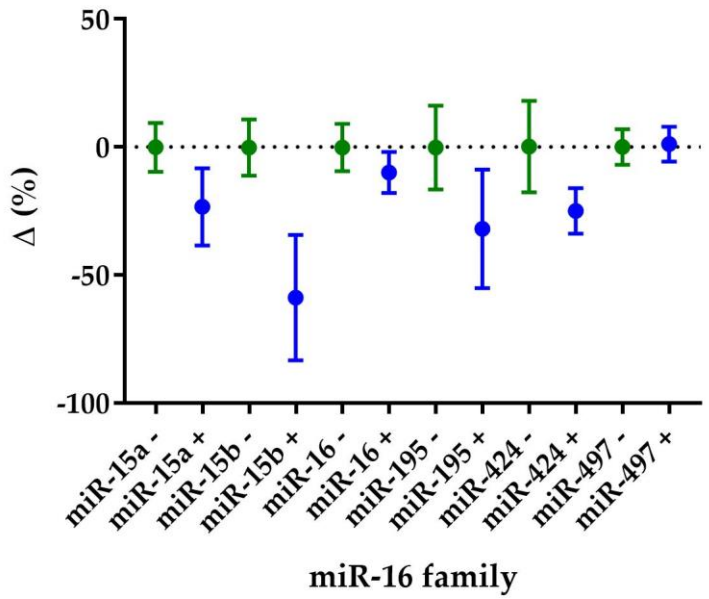

Figure shows the percentage of difference for miR-16 family between untreated (''-'') (green) and treated (''+'') (blue) cells, error bars show the 95% confidence interval and the average is depicted.

Association between miRNAs of the miR-16 family was performed using Spearman correlation test and is shown in Table 7.2. Only miR-15b was found to significantly correlate with miR-15a, miR-195 and miR-424. No correlation was found between miRs that are coded within 50 kilobases from each other, such as miR-15a and miR-16, miR-195 and miR-497.

Table 7. 2 Spearman correlation test for members of the miR-16 family.

	miR-15a	miR-15b	miR-16	miR-195	miR-424	miR-497
miR-15a	r=1	r=0.8462 p=0.001***	r=0.5779 p=0.053	r=0.4965 p=0.104	r=0.5289 p=0.080	r=0.0876 p=0.787
miR-15b		r=1	r=0.4799 p=0.116	r=0.6993 p=0.014*	r=0.8196 p=0.002**	r=0.1331 p=0.678
miR-16			r=1	r=0.3257 p=0.299	r=0.2246 p=0.479	r=0.0737 p=0.820
miR-195				r=1	r=0.5359 p=0.076	r=-0.0701 p=0.829
miR-424					r=1	r=0.4246 p=0.169
miR-497						r=1

7.4.3. miR-29 family

As described in Chapter 5, the miR-29 family is composed of miR-29a/29b/29c. miR-29a is encoded in an intron from chromosome 7q32.3. MiR-29b can be derived from two precursors, miR-29b-1 and miR-29b-2 that are co-transcribed with miR-29a and miR-29c respectively. miR-29b-2 and miR-29c are mapped to chromosome 1q32.2. Figure 7.8 shows the percentage of difference for miR-29 family between untreated and treated cells, no statistical test was performed.

Figure 7. 8 Percentage of difference for miR-29 family in SH-SY5Y cells.

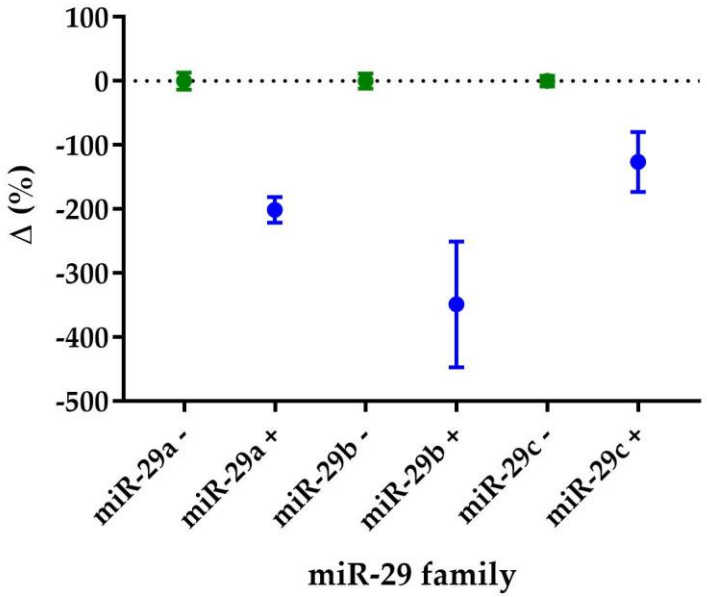

Figure shows the percentage of difference for miR-29 family between untreated (''-'') (green) and treated (''+'') (blue) cells, error bars show the 95% confidence interval and the average is depicted.

Examination of the level of co-expression between miRNAs of the miR-29 family was performed using Spearman correlation test and is shown in Table 7.3. The three members of this miRNA family were found to significantly correlate with each other.

Table 7. 3 Spearman correlation test for members of the miR-29 family.

	miR-29a	miR-29b	miR-29c
miR-29a	r=1	r=0.783 p=0.004**	r=0.727 p=0.010**
miR-29b		r=1	r=0.930 p=4.1e10^{-5}***
miR-29c			r=1

7.4.4. miR-34 family

miR-34 family is composed of 4 miRNAs, miR-34a/34b/34c/449. miR-34a is transcribed from chromosome 1p36.22. miR-34b and miR-34c are transcribed from chromosome 11q23.1. miR-449 is encoded in chromosome 5q11.2. Figure 7.9 shows the percentage of difference for miR-34 family between untreated and treated cells, no statistical test was performed.

Figure 7. 9 Percentage of difference for miR-34 family in SH-SY5Y cells.

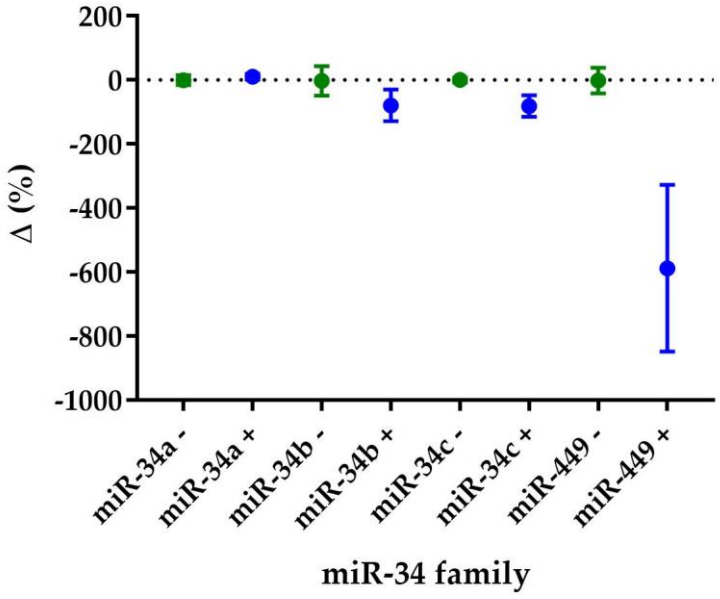

Figure shows the percentage of difference for miR-29 family between untreated (''-'') (green) and treated (''+'') (blue) cells, error bars show the 95% confidence interval and the average is depicted.

Association between miRNAs of the miR-34 family was performed using Spearman correlation test and is shown in Table 7.3. Only miR-34c was found to significantly correlate with miR-449. No correlation was found with the rest of miRNAs.

Table 7. 4 Spearman correlation test for members of the miR-34 family.

	miR-34a	miR-34b	miR-34c	miR-449
miR-34a	r=1	r=0.084 p=0.800	r=-0.294 p=0.355	r=-0.343 p=0.276
miR-34b		r=1	r=0.559 p=0.063	r=0.524 p=0.084
miR-34c			r=1	r=0.706 p=0.013*
miR-449				r=1

7.4.5. miR-125 family

This miRNA family is composed by miR-125a and miR-miR-125b. Whilst miR-125a is transcribed from chromosome 19q13.41, miR-125b is transcribed from chromosome 11q24.1. Figure 7.10 shows the percentage of difference for miR-125 family between untreated and treated cells, no statistical test was performed.

Figure 7. 10 Percentage of difference for miR-125 family in SH-SY5Y cells.

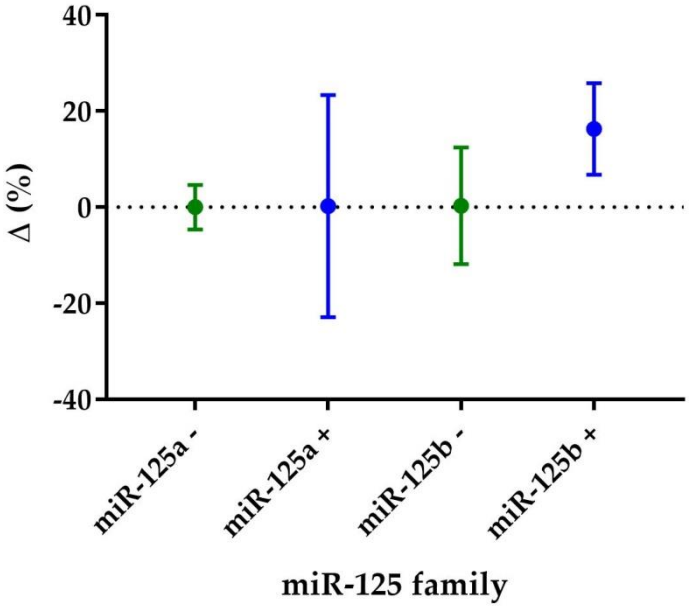

Figure shows the percentage of difference for miR-125 family between untreated (''-'') (green) and treated (''+'') (blue) cells, error bars show the 95% confidence interval and the average is depicted.

Pearson correlation test was used to evaluate the association between miR-125a and miR-125b. No correlation was found between members of the miR-125 family (R=0.164 and p=0.611).

7.4.6. miR-132/212 family

This miRNA family is another small family composed of miR-132 and miR-212, both genes are clustered within 0.5 kb on chromosome 17p13.3. Figure 7.11 shows the percentage of difference for miR-132 family between untreated and treated cells, no statistical test was performed.

Figure 7. 11 Percentage of difference for miR-132 family in SH-SY5Y cells.

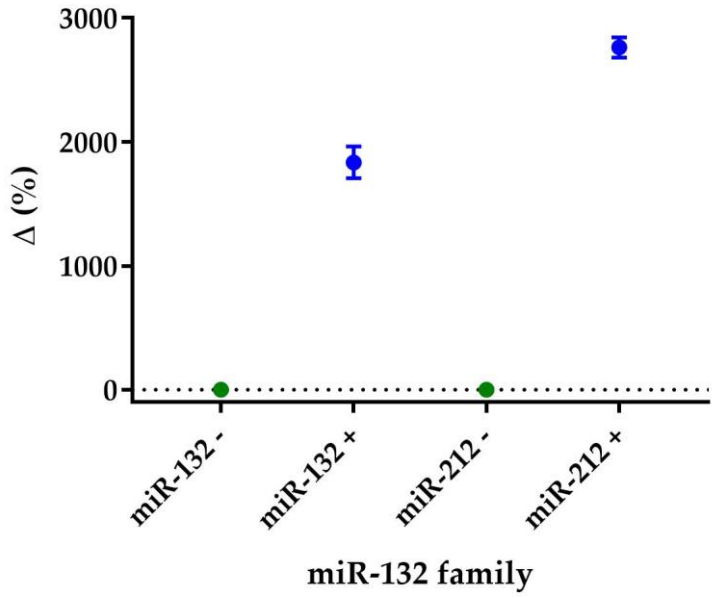

Figure shows the percentage of difference for miR-132 family between untreated (''-'') (green) and treated (''+'') (blue) cells, error bars show the 95% confidence interval and the average is depicted.

Association between miRNAs of the miR-132 family was performed using Spearman correlation test. miR-132 and miR-212 were found to be significantly correlated (r=0.881 and p=0.0003).

7.4.7. miR-17 family

miR-17 family was examined in Chapter 6 and is composed of miR-17/20a/20b/93/106a/106b. miR-17 and miR-20a are co-transcribed from chromosome 13q31.3. miR-20b and miR-106a are co-transcribed from chromosome Xq26.2. miR-93 and miR-106b are co-transcribed from chromosome 7q22.1. Figure 7.12 shows the percentage of difference for miR-17 family between untreated and treated cells, no statistical test was performed.

Figure 7. 12 Percentage of difference for miR-17 family in SH-SY5Y cells.

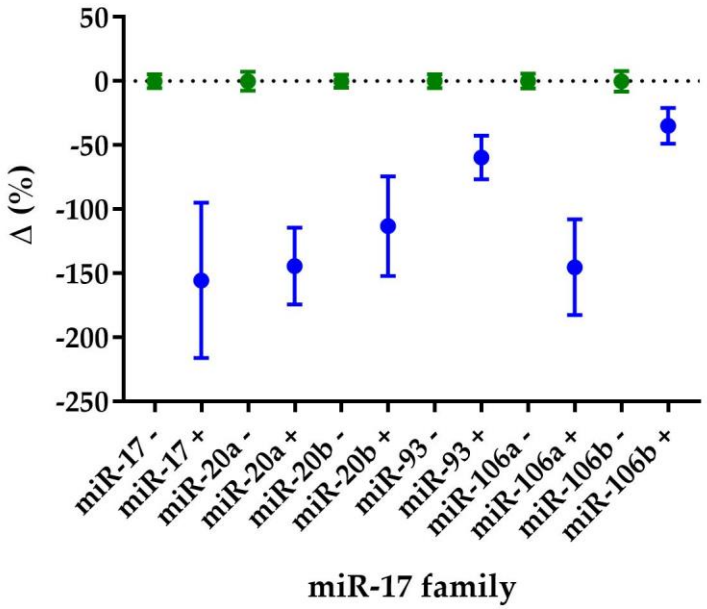

Figure shows the percentage of difference for miR-17 family between untreated (''-'') (green) and treated (''+'') (blue) cells, error bars show the 95% confidence interval and the average is depicted.

Spearman correlation test was used to evaluate the association between members of the miR-17 family. All miRNAs were found to significantly correlate with each other (Table 7.5).

Table 7. 5 Spearman correlation test for members of the miR-17 family.

	miR-17	miR-20a	miR-20b	miR-93	miR-106a	miR-106b
miR-17	r=1	r=0.979 p=6.7e^{-7}***	r=0.769 p=0.005**	r=0.718 p=0.011*	r=0.762 p=0.006**	r=0.706 p=0.013*
miR-20a		r=1	r=0.727 p=0.010**	r=0.669 p=0.020*	r=0.741 p=0.008**	r=0.657 p=0.024*
miR-20b			r=1	r=0.918 p=7.0e^{-5}***	r=0.874 p=4.1e^{-4}***	r=0.916 p=8.3e^{-5}***
miR-93				r=1	r=0.900 p=1.5e^{-4}***	r=0.991 p=7.5e^{-8}***
miR-106a					r=1	r=0.916 p=8.3e^{-5}***
miR-106b						r=1

7.5 Discussion and conclusions

The null hypothesis was that there is no correlation between the expression of miRNAs of same family. miR-29, miR-132/212 and miR-17 families showed significant correlation between miRNAs of the same family. Following investigation, the null hypothesis could be rejected for these three miRNA families. However, not all members of the miR-16, miR-34 and miR-125 families showed some correlations in expression amongst individual members of their family.

Within the miR-16 family, only the expression of miR-15b was found to significantly correlate with miR-15a, miR-195 and miR-424. Similarly, only miR-34c expression was found to significantly correlate with miR-449 as part of the miR-34 family. No correlation was found within the miR-125 family, indeed no change was observed between treated and untreated cells for both miR-125a and miR-125b.

Interestingly, there was no significant correlation between the expression of some miRNAs that are encoded within 50 kilobases of each other. O'Carrol *et al* stated that miRNAs that are clustered within 0.1–50 kilobases from each other display common expression patterns. This was based on observations from work of Baskerville and Bartel in 2005. Baskerville and Bartel profiled the expression of 175 miRNAs from 24 different human tissues and HeLa cells. The authors observed a higher correlation between miRNAs encoded within 50 kilobases overall. However, their data also shows some pairs of miRNAs (within the 50 kilobase range) with correlation values ranging from 0.2 up to 1.

Similar to my results, there might be exceptions to this phenomenon as observed also in Baskerville and Bartel's results. The authors mentioned that some miRNAs fall within the 50 kilobases but they are not correlated, including miR-23b and miR-24 (correlation of 0.19). Another possible factor that could explain why some miRNAs didn't correlate with each other is the variable affinity of miRNAs within the same

family for their targets. miRNAs of the same family share the seed region by which they bind to the 3'UTR of their targets, however, their affinity is variable.

Hansen *et al* used a combination of conditional knockout and transgenic mouse models for miR-132 and miR-212 (178). Using RNA sequencing they explored the possible differential effects that each of these miRNAs could have on the whole transcriptome of mice hippocampus. They found that there was some overlap between downregulated transcripts when each of these miRNAs was overexpressed. However, they found that there were substantively more downregulated transcripts for overexpression of miR-132 than miR-212.

Although both miRNAs share the same seed region they have some different nucleotides in the rest of their sequence (189). This would give different binding affinity for transcripts and would affect in turn the levels of the miRNA (189). miRNA binding to the 3'UTR of a target is followed by recruitment of the RISC complex and eventually mRNA cleavage of the target. This reaction destabilizes the association of the RISC complex and the 3' end of the miRNA, thus promoting its degradation and affecting the miRNA levels (190,191).

This effect could explain why some miRNAs did not show correlation between miRNAs of the same family as most of the miRNAs within a family showed similar trends after treatment of SH-SY5Y cells. Furthermore, a similar effect was observed particularly for the miR-132/212 family. These miRNAs are simultaneously transcribed (189), yet miR-132 showed an increase of approximately 18-fold and a 27-fold for miR-212. The difference in their levels could be explained by their predominance over certain transcripts. This is in accordance with the described above work of Hansen *et al* (178).

Hansen *et al* found that there were substantively more downregulated transcripts when miR-132 was overexpressed than when miR-212 was overexpressed. The effect of miR-132 in downregulating such transcripts would in turn also reduce the levels of

miR-132 despite being co-transcribed with miR-212. However, it should be noted that this higher effect of miR-132 would depend on the transcriptome expressed at a cell in a certain time. Yet, miR-132 and miR-212 showed correlation between them and their levels after differentiation of SH-SY5Y cells into neuronal like cells are generally known to be high in comparison with other miRNA changes.

Similar to my results, Meseguer and colleagues performed differentiation of SH-SY5Y into neuronal like cells (192). They found a significant increase in 26 microRNAs, including miR-132 and miR-212. Likewise, Skalsky and Cullen observed that after treatment of SH-SY5Y cells with retinoic acid, cells change their morphology, express neuronal markers and up regulated several brain-specific miRNAs including miR-128, miR-124 and miR-132 (193).

Magill *et al* also found that both miR-132 and miR-212 were increased after differentiation of SH-SY5Y into neuronal like cells (194). The same effect has been observed by others when inducing neurite outgrowth in PC12 and SH-SY5Y cells (195). This is in accordance to the literature as miR-132 and miR-212 are highly expressed in dendrites and synapses, and are regulated by neuronal activity (150,176). These miRNAs have a prominent role in neuronal morphogenesis, dendritic plasticity and neuronal differentiation (189,195).

Conversely, using hippocampal neurons from rat embryos, overexpression of miR-132 increased dendritic spine width whilst knockdown of miR-132 showed a reduction in dendritic complexity (196). Dendritic outgrowth was also induced by miR-132 overexpression in neuronal primary cell culture (197). Using olfactory bulb neurons, overexpression of miR-132 led to a more complex dendritic tree with more synaptic connections (198). Reduced spine density and dendritic complexity was observed when reducing miR-132 levels (198).

In vivo experiments using transgenic mouse models have shown that induction of miR-132 expression was sufficient to modulate cognitive capacity in a dose-dependent

manner (176). Likewise, miR-132 levels correlated with spine density and interestingly, expression of miR-132 over and above physiological levels led to excessive spine density and cognitive deficits (176). *In vivo* experimentation by Magill, *et al* have demonstrated that the degree of neuronal dendritic growth and arborisation depends on the levels of miR-132 and miR-212 (194). Similarly, *in vivo* inhibition of miR-132 resulted in reduced spine density and more immature spines, characterised by a reduced percentage of mushroom spines and increased proportion of immature filopodia (199).

The miR-132/212 family has attracted marked examination as downregulation of this miRNA family is the only consistent finding according to a meta-analysis of profiling studies of miRNAs in dementia (64). Nevertheless, miRNA changes can be particular to the different brain areas analysed and the consistent downregulation of miR-132/212 across different brain areas might be explained by a widespread synaptic loss.

Another miRNA that has attracted attention in dementia research is miR-29. Hebert *et al* showed that miR-29a/b-1 was significantly decreased in AD patients showing high BACE1 protein (121). This finding was replicated in primary neuronal culture and they suggested a relationship between miR-29a/b-1 expression and amyloid production (121). Certainly, miR-29 might have a strong effect on BACE1 as it is the miRNA with the highest affinity for BACE1 according to TargetScan (63).

A knockout mouse model of miR-29 showed that members of the microRNA 29 family are strongly expressed in neurons of the olfactory bulb, hippocampus and Purkinje cells of the cerebellum (200). The mice showed motor impairment and ataxia by affecting cerebellar Purkinje cells (200). This effect was also observed by others when delivering miR-29 inhibitors to the mouse brain using a neurotropic peptide (201). While miR-29 expression in mice is observed in neurons, particularly in the cerebellum, its expression in humans is unknown but might be accentuated in glial cells (172). Interestingly, in the results here shown, SH-SY5Y cells differentiated into neuronal like cells demonstrated a decrease in all members of the miR-29 family.

The evidence reinforces some important aspects to be considered in miRNA research: the need for *in situ* localization of miRNAs in the human brain and the possible differential expression of a miRNA between species, cell types and even brain areas. The same effect of cell type miRNAs is also observed for target validation of miRNAs in cell culture.

Varendi *et al* reviewed the effect of 21 miRNAs that target BDNF using luciferase assays (202), which are commonly used for target validation but usually with inconsistent results. Some miRNAs showed an effect on protein levels while others had no effect, all of them predicted to target the 3'UTR. Some studies included, where 2 forms of the 3'UTR were cloned (short and long), showed that there were even differences between different forms of the same 3'UTR. Other studies showed that the same miRNA had different effects in different cell lines, causing no effect, increasing or reducing BDNF protein levels (202). Although there was inconsistency between the studies, this phenomenon is expected as part of normal miRNA biology.

miRNAs are already present under physiological conditions and the proteome in a certain cell type at a certain time is already remodelled by the miRNAs expressed. Thus, assumptions derived from experimentation of miRNAs in cell culture should be taken with caution as every cellular population will show specific miRNA signatures. Instead, miRNAs are a useful tool to identify changes in hundreds of proteins and as biomarkers given its resistance to changes in temperature, pH and the effect of RNases (66).

Chapter 8.- General discussion and conclusions

8.1 Recapitulation of chapters

In Chapter 1, I proposed a novel approach for the study of miRNAs in dementia. This involved how one should consider multiple targets, previously reported number of copies of miRNAs, and the affinity for their targets in an attempt to overcome proposed caveats, previously described in miRNA research. I hypothesized that dysregulation of certain miRNAs might simultaneously affect different transcripts involved in the development of the two most common forms of dementia, AD and VaD.

Chapter 3 described an investigation of miRNAs that were chosen because they targeted proteins involved in amyloid production, transport and amyloid degrading enzymes, tau phosphorylation, BBB integrity, glymphatic system and immune response, and therefore should be important in the pathogenesis of AD. Some significant results were found between diagnostic groups, and an interesting pattern of expression was found across Braak stages for five miRNAs that had three targets in common. One of these targets, the RORA protein represents an attractive target for the multiple points at which it is associated with characteristics observed in dementia.

Despite the interesting results, a major methodological issue was identified. I found that the most commonly used calibrator gene in the scientific literature was significantly reduced by three-fold in AD cases of Braak stage VI. Given that a key property of a reliable calibrator gene is that it is not altered in circumstances of pathology then this calibrator was no longer useful to perform this role in studies of AD. Therefore, it was necessary to first identify new calibrators and evaluate their appropriateness for use in this project.

Chapter 4 described the identification and evaluation of six different calibrators. This chapter describes the assessment of these calibrators with respect to their variability across the cohort and their stability in a simulation of post-mortem delay. Three of the six calibrators (RNU48, miR-9-5p and miR-9-3p) showed lower variability across the cohort and greater stability with simulation of post-mortem delay.

Although miR-9-5p and miR-9-3p showed a greater degree of stability in the various investigations undertaken, it must be acknowledged that their localisation in human brain is still unknown. Furthermore, overall changes seen may be a result of the sum of both increases and decreases in homogenised tissue comprising different cell types. In addition, the use of a single calibrator gene can introduce bias in the results. Thus, RNU48, miR-9-5p and miR-9-3p were used as calibrators for the evaluation of miRNAs of interest in Chapters 5 and 6.

A re-examination of previously measured miRNAs in Chapter 3 and additional miRNAs from the same families are presented in Chapter 5. Some significant results were found between diagnostic groups; however no patterns of expression were found like those first observed in Chapter 3. This would prompt one to suggest that the similar patterns of expression seen in Chapter 3 were perhaps the result of inappropriate calibrators, that would have been used throughout, rather than a disease-related phenomenon.

What remains problematic is that downregulation of the miR-132/212 family across different brain areas has been the only consistent finding so far in AD (64), which the data presented in Chapter 3 agrees with. Indeed, similar but statistically more significant reductions were found for both AD and VaD, but also for early AD (EAC) changes. However, as was mentioned, the problematic calibrators identified here were also commonly used in the literature, so it is possible they are all reflecting the same problematic issue with the calibrators rather than disease-related changes in miRNAs.

To reinforce the reproducibility of the measurements reported in this study, the three new calibrators were also measured in the whole cohort (n=84) at three different times. The CT difference between each of the three measurements to the CT average of them was 0.008 for RNU48, 0.028 for miR-9-5p and 0.018 for miR-9-3p. The average percentage of difference was 0.61% for RNU48, 2.42% for miR-9-5p and 1.86% for miR-9-3p. Although the results found in Chapter 5 are less interesting from the point of view of identifying disease-associated miRNAs, compared to what was observed in Chapter 3, the data is arguably more robust in terms of reproducibility and also in relation to the literature.

In Chapter 6, a similar approach was considered but this time in a way looking for a functional or physiological impact. This analysis was performed considering multiple transcripts involved in the renin angiotensin system and hypoxia inducible factors that might be relevant for both AD and VaD. Unexpectedly, no change was observed in the VaD group, despite obvious links with relevant factors, and only significant changes were observed in the AD group. Chapter 6 also included a nested study of miR-320e that binds to a created binding site due to the SNP rs6857 at the PVRL2 gene. A significant increase in miR-320e was found in AD with respect to the other diagnostic groups. Although it could be argued that this would only have an effect on those carriers of the SNP rs6857, miRNAs are able to bind with imperfect mismatch. This creates a bulge that reduces the affinity by which the miRNA binds to the 3'UTR of the mRNA. Chapters 5 and 6 also considered some important aspects for miRNA research such as the location of miRNAs.

Chapter 7 involved an exploration of the literature as to suggestions that miRNA changes derived from experimentation might be specific to cellular populations. It also helped to explore, using cell culture, whether miRNAs of the same family show similar expression patterns in the differentiation of a cell type, as well as exploring whether miRNAs that are co-located have similar patterns of expression. Most of the miRNAs within a family showed a significant correlation between them, although not all

reached statistical significance, whilst others showed similar trends to other miRNAs within the family.

In summary, Chapter 4 proposed and evaluated a number of prospective calibrators for the accurate measurement of miRNAs of interest. Three calibrators were confirmed and subsequently used due to their low variability across the cohort and their resistance to RNA degradation. Chapter 3 and 5 investigated proteins related to classical histopathological hallmarks of AD. Some of the miRNAs measured showed significant differences between diagnostic groups. Chapter 6 also considered proteins related to the renin angiotensin system and hypoxia inducible genes that might be relevant for both AD and VaD. Unexpectedly, no changes were observed in the VaD group. Only significant differences were found in the AD group. Chapter 6 also investigated miR-320e that bound to the endothelial adhesion protein PVRL2. Finally, Chapter 7 evaluated cell culture for its use in miRNA research in dementia and investigated whether miRNAs of the same family show common expression patterns.

Each of the miRNAs analysed in this project could have an impact in AD or VaD. However, the impact of a miRNA would relate to the number of proteins it targets and to the number of miRNAs that regulate a protein. Combinations of miRNAs are more likely to have a meaningful impact by reducing the number of proteins being affected at a higher degree (i.e. by several miRNAs at the same time). An interesting pattern of expression for a combination of miRNAs was found in Chapter 3, however no patterns of expression were subsequently found once the data was appropriately measured with more reliable calibrators. These findings and the identification of new calibrators highlights that a number of previously reported calibrators used in dementia-related research may be inappropriate and need validation, but equally further research also needs to further validate the calibrators reported here.

The functions of single miRNA-protein relations have been questioned in this project. However, the creation of a binding site in the *PVRL2* gene sequence opened the possibility that under certain conditions such miRNA-protein relations may exist. Yet,

other factors should be considered such as co-localisation of the miRNA with the protein of interest and validation of binding site. Furthermore, other posttranscriptional modifications might also be involved. This thesis attempted to demonstrate evidence for a more biologically relevant role of miRNAs.

8.2 Strengths of this study

This is the first study of miRNA research in dementia that considers several factors for selection of miRNAs of interest. Those factors are the selection of miRNAs based on the fact that they have multiple targets, their affinity for these targets and the number of copies of miRNAs that have been reported. Tens of publications in the study of dementia follow the rationale of single miRNA-protein relationship without consideration of these additional factors, which while perhaps demonstrable in a single cell experimental system may not be valid or translatable in the context of more complex experimental systems, multi-cellular systems and whole organisms. Witwer and Halushka have described that the applied and translational miRNA research is subject to many pitfalls and claims that many previous studies are neither scientifically rigorous nor reproducible (203). The approach taken in this study is therefore an attempt to conduct miRNA research in a more robust manner and with more biologically relevant results.

In terms of methodology used, I have used the recommended gold standards, such as TargetScan for the selection of miRNAs of interest and qPCR for accurate measurement of them (66,204). Additionally, two novel formulas are proposed in order to improve accuracy and statistical analysis of the data. One formula is to calculate the percentage of difference rather than the relative quantity for miRNAs of interest and a second formula to calculate the average CT value for different calibrators.

Furthermore, this is the first study that has investigated miRNA changes in the posterior cingulate cortex. The majority of publications have used other brain areas

such as the temporal, prefrontal, parietal cortexes and the hippocampus (64). The posterior cingulate gyrus shows a reduced metabolic rate and is able to predict progression from mild cognitive impairment to dementia with an accuracy of 94% (205–207). In addition, evaluation of this brain area in cognitively normal patients, shows a similar metabolic reduction in those patients with the *APOE* ε4 allele, which is the highest risk factor for AD and it is also reduced with increasing age (208).

8.3 Weaknesses of this study

The cohort presented in this study represents only 84 individuals with a common genetic (ethnic) background that (as a sample of more elderly cases) are not representative of the general population, although they are intended for study of an aged related disorder. The cohort could be further improved by increasing the number in particular to change the proportion of carriers with the *APOE* ε4 allele. There is only one APOE ε4 carrier in the control group (N=24), four carriers in the EAC group (N=20) and 16 carriers in the AD group (N=22), which limited some further investigations, although the cohort size is still larger than many studies conducted to-date.

With respect to the methodology used, previously reported number of copies of a miRNA were used as a reference of their abundance. However, previously reported copies are derived from different experiments using RNA sequencing deposited in miRbase. Such experiments have used different organs and miRNAs can highly fluctuate between organs, cell types and even between multiple cultures of the same cell type (209). Similarly, the results are presented as a percentage of difference with respect to controls. However, it would be much more informative to know the absolute quantification of miRNAs.

8.4 Recommendations for future research

The understanding of the role of miRNAs in dementia research has so far been restricted to single miRNA-protein relations. However, the impact of a single miRNA via a specific protein is related to the total number of different transcripts it targets and also by the number of other miRNAs that regulates the same protein (65). In addition, numerous miRNAs have been found to be dysregulated in AD brain with inconsistent results. Inconsistencies are likely to relate partly to the size, stratification and analysis of investigated cohorts; the profiling techniques used including hybridization methods lacking specificity; use of inaccurate miRNA calibrators; and the study of different brain areas. Some of these aspects have already been acknowledged and addressed by others in the literature (64,66,138).

This thesis did not find a combination or signature of miRNAs for AD or VaD. However, miRNA signatures have been reported to exist by others. Lau *et al* found 41 microRNAs dysregulated in the prefrontal cortex that were grouped in four different clusters according to their expression patterns (138). Combinations of miRNAs, particularly those simultaneously targeting similar proteins and pathways are likely to produce a more relevant physiological response. By analysing such combinations of miRNAs it is possible to identify proteins that are more affected than others by being targeted by more miRNAs.

Yet, in the case of particular miRNAs, the co-localisation of a miRNA with a target should be strongly recommended as well as the validation of the binding site to confirm interactions. The localisation of numerous miRNAs has been omitted by several in the literature and remains elusive for many miRNAs. Halushka and colleagues suggested that miRNA research particularly with respect to biomarker and functional studies has been affected by this (210). There was not scope within this project to look at this in detail.

miRNA research in dementia is still in its early stages and it is necessary to expand the conception of miRNA function. miRNAs are part of an evolutionary process and they are expressed under physiological conditions. The transcriptome present in cellular populations is constantly remodelled by already present miRNAs, some of which might be cell type specific that are in abundance and others with more precise levels that work to fine tune gene expression to respond to external stimuli. The biological impact of miRNAs is likely to be determined by their combinatorial signature, the number of miRNA copies, their affinity for different targets, and the existing transcriptome available for remodelling which fluctuates over time.

Appendix 1

Human post-mortem brain tissue was obtained from South West Dementia Brain Bank (SWDBB), Southmead Hospital with approval from the local research ethics committee (REC reference number 08/H0106/28+5). Statistical analysis of the demographic data is presented:

Diagnosis	Gender (Male/Female)	Age (σ)	PMI (σ)	ApoE4 (No/Yes)
Control	11/13	80 (9.7)	35.4 (16.2)	21/1
Early Alzheimer changes	11/9	85 (6)	36.5 (15)	14/4
Alzheimer's Disease	11/11	78 (7.2)	23.7 (13.4)	3/16
Vascular Dementia	9/9	83 (7.9)	34.7 (12.3)	9/4
Statistical test	Chi-square x^2=0.36 p=0.94	ANOVA F=2.59 p=0.06	ANOVA F=3.70 p=0.01	Chi-square x^2=30.7 p<0.0001

Demographic information of the cohort, age in years, post-mortem interval delay (PMI) in hours, standard deviation (σ).

Appendix 2

In Chapter 3, seven miRNAs were measured and an interesting pattern of expression was found across Braak stages for five miRNAs (miR-16, miR-29a/b, miR-34a and miR-125b) that had three targets in common. One of these targets, RORA, represents an attractive candidate protein that participates in numerous processes linked to dementia. On the other side, the remainder two miRNAs (miR-132 and miR-212) showed a reduction along progression of Braak stages. These two miRNAs (described in detail in Chapter 7) are present in dendrites and synapses, regulated by synaptic activity and have been associated with cognition. Further evidence of the role of the miR-132/212 family in dementia could be provided by measurement of the miR-132/212 family in post-mortem brain tissue in conjunction with protein levels of the microtubule associated protein 2 (MAP2), an essential protein for neuritogenesis. Thus, both proteins, RORA and MAP2 were attempted to be measured. Training was received from Dr. Hannah Tayler.

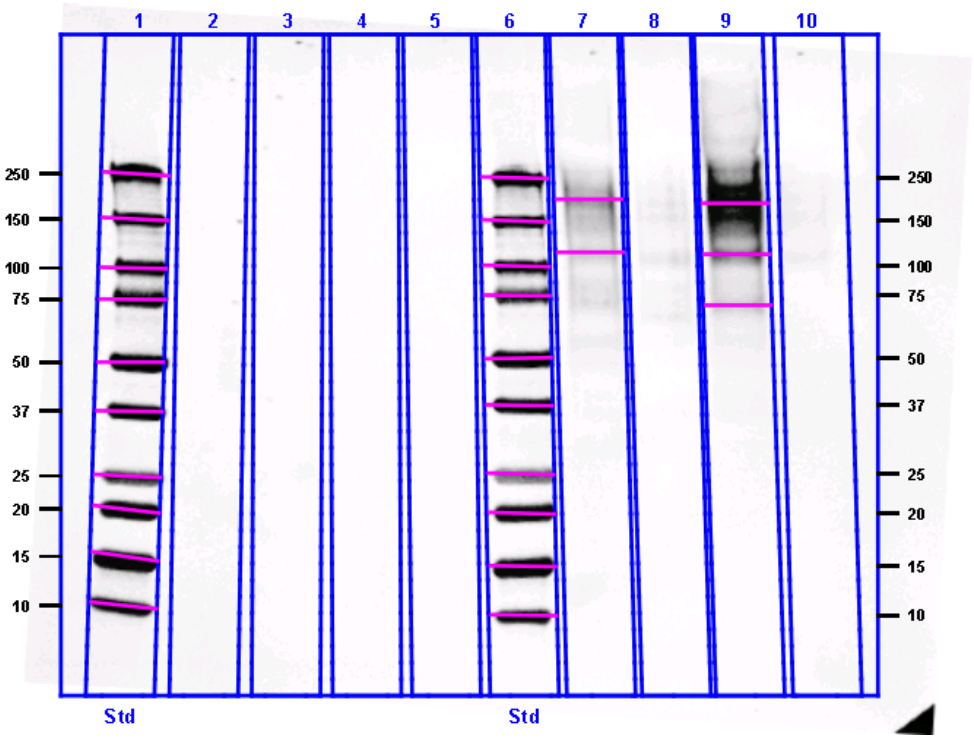

Western blotting for MAP2 (lines 7-10) and RORA (lines 2-5) protein as described in Chapter 2 section 2.14.

Appendix 3

Analysis of RAS-associated microRNAs according to their functional impact in the RAS physiology. From a total of 164 combinations (Appendix 3) of overlapping targets and miRNAs in common, 14 of them were selected (Chapter 6 Table 6.2) since these might have a functional impact in the RAS as they targeted multiple RAS components.

RAS components	miRNAs
AGT AGTR1 AGTR2 DPP3 ENPEP LNPEP MME RNPEP	miR-3163
AGT AGTR1 ENPEP LNPEP MME REN RNPEP	miR-2467-3p
ACE ACE2 AGT ANPEP ENPEP LNPEP MME	miR-670-5p
AGTR1 AGTR2 ENPEP LNPEP MME RNPEP	miR-944
ACE2 AGTR1 AGTR2 ENPEP MME RNPEP	miR-4766-5p
ACE AGTR2 ENPEP LNPEP MME RNPEP	miR-495-3p
AGT AGTR1 AGTR2 ENPEP LNPEP MME	miR-513b-5p
AGTR1 AGTR2 DPP3 ENPEP LNPEP MME	miR-512-3p miR-302-3p/372-3p/373-3p/520-3p
ACE AGT AGTR2 ENPEP LNPEP MME	miR-142-5p
ACE AGT ANPEP LNPEP RNPEP	miR-665 miR-24-3p
AGTR2 ENPEP LNPEP MME RNPEP	miR-541-5p
AGT ENPEP LNPEP MME RNPEP	miR-129-5p
ACE ENPEP LNPEP MME RNPEP	miR-185-5p
ACE DPP3 ENPEP LNPEP RNPEP	miR-3150b-3p
ACE ACE2 LNPEP REN RNPEP	miR-3909
AGTR2 ANPEP ENPEP LNPEP REN	miR-676-3p
AGT ANPEP ENPEP LNPEP	miR-2355-3p

REN	
ACE ACE2 ANPEP ENPEP LNPEP	miR-125-5p
ACE2 AGT ANPEP ENPEP MME	miR-149-5p
ACE AGT ANPEP ENPEP MME	miR-3612
AGT AGTR2 ENPEP LNPEP MAS1	miR-224-5p
AGTR1 AGTR2 DPP3 ENPEP LNPEP	miR-431-5p miR-889-3p
ACE2 AGTR1 AGTR2 LNPEP MME	miR-371-5p
AGTR2 ENPEP LNPEP MME REN	miR-330-3p
ACE AGTR2 ENPEP LNPEP MME	miR-302c-3p.2/520-3p
ACE2 AGT AGTR2 DPP3 LNPEP	miR-483-3p.2
ACE2 AGT AGTR2 ENPEP MME	miR-525-5p
AGTR1 DPP3 ENPEP LNPEP MME	miR-624-5p
ACE AGTR1 DPP3 ENPEP LNPEP	miR-148-3p/152-3p
AGT AGTR1 LNPEP MME REN	miR-605-3p
ACE2 AGT AGTR1 LNPEP MME	miR-513c-5p/514b-5p
ACE2 AGT ENPEP LNPEP MME	miR-218-5p miR-760
ACE ACE2 LNPEP MME REN	miR-326
AGTR2 ANPEP MME RNPEP	miR-874-3p
AGT ANPEP REN RNPEP	miR-423-5p
AGTR2 LNPEP MME RNPEP	miR-2115-3p
ACE AGT AGTR1 RNPEP	miR-7-5p
ACE ENPEP LNPEP RNPEP	miR-3150a-3p
AGT LNPEP MME RNPEP	miR-2278
AGTR1 ANPEP ENPEP LNPEP	miR-299-3p
ANPEP ENPEP LNPEP MME	miR-552-3p
ACE2 ANPEP ENPEP LNPEP	miR-345-3p
ACE ANPEP ENPEP LNPEP	miR-513a-5p
ANPEP DPP3 ENPEP LNPEP	miR-670-3p
AGT ANPEP LNPEP MME	miR-1197

ACE ANPEP LNPEP REN	miR-378g
AGTR1 AGTR2 LNPEP MME	miR-493-5p
ACE2 AGTR1 AGTR2 LNPEP	miR-1277-5p
AGTR2 ENPEP LNPEP MME	miR-656-3p miR-128-3p miR-369-3p miR-3121-3p miR-3145-3p miR-4640-3p miR-186-5p miR-488-3p miR-126-5p miR-374-5p miR-202-5p miR-337-3p
AGTR2 ENPEP LNPEP REN	miR-28-5p/708-5p
AGT AGTR2 ENPEP LNPEP	miR-330-3p.2 miR-3690
AGTR2 DPP3 LNPEP MME	miR-17-5p/20-5p/93-5p/106-5p/519-3p
AGT AGTR2 ENPEP MME	miR-506-5p
ACE2 AGTR2 ENPEP MME	miR-335-5p
AGTR1 ENPEP LNPEP MME	miR-410-3p miR-3140-3p miR-802 miR-511-3p
AGT AGTR1 ENPEP LNPEP	miR-375
AGT AGTR1 LNPEP MME	miR-4739 miR-181-5p
ACE2 AGTR1 LNPEP MME	miR-505-3p.2
AGTR1 DPP3 LNPEP MME	miR-3164
ACE2 ENPEP LNPEP MME	miR-9-5p miR-200-3p/429 miR-942-5p
ACE ENPEP LNPEP MME	miR-27-3p miR-1252-5p miR-221-3p/222-3p
DPP3 ENPEP LNPEP MME	miR-379-5p
ACE ENPEP LNPEP REN	miR-138-5p
ACE2 AGT ENPEP LNPEP	miR-1278
ACE DPP3 ENPEP LNPEP	miR-340-5p
ACE2 AGT LNPEP MME	miR-421 miR-873-3p
ACE AGT LNPEP MME	miR-766-5p
ACE2 AGT DPP3 LNPEP	miR-1301-3p
ACE2 AGT ENPEP MME	miR-141-3p/200-3p
ACE DPP3 ENPEP MME	miR-1294
ACE AGT DPP3 MME	miR-339-5p
AGTR2 ANPEP RNPEP	miR-3173-5p
AGT ANPEP RNPEP	miR-5194
LNPEP MAS1 RNPEP	miR-448
AGTR1 LNPEP RNPEP	miR-455-3p.1
ACE LNPEP RNPEP	miR-491-5p
ENPEP MME RNPEP	miR-668-3p
AGT MME RNPEP	miR-545-3p
AGTR2 ANPEP LNPEP	miR-383-5p.2
ANPEP ENPEP LNPEP	miR-3200-3p miR-361-3p
AGT ANPEP LNPEP	miR-873-5p.1
AGT ANPEP MME	miR-642-3p
AGTR2 LNPEP MAS1	miR-23-3p
AGTR2 ENPEP MAS1	miR-651-5p
AGTR2 ENPEP LNPEP	miR-576-5p miR-384 miR-524-5p
AGTR2 LNPEP MME	miR-361-5p miR-6509-5p miR-483-3p.1 miR-380-3p miR-892-5p
AGT AGTR2 LNPEP	miR-556-3p miR-532-5p miR-577 miR-520g-3p

ACE AGTR2 LNPEP	miR-516b-5p
AGTR2 ENPEP MME	miR-409-3p
AGT AGTR2 MME	miR-15-5p/16-5p/195-5p/424-5p/497-5p
ACE AGTR2 MME	miR-654-3p
ACE AGTR2 DPP3	miR-203a-3p.1
AGTR1 ENPEP LNPEP	miR-155-5p miR-641/3617-5p miR-223-3p
AGTR1 LNPEP MME	miR-545-5p miR-33-5p miR-134-5p miR-579-3p
ACE2 AGTR1 LNPEP	miR-381-3p
AGTR1 ENPEP MME	miR-2681-5p
AGT AGTR1 MME	miR-103-3p/107
ACE AGTR1 DPP3	miR-34-5p/449-5p
ENPEP LNPEP MME	miR-376c-3p miR-30-5p miR-3942-5p miR-132-3p/212-3p miR-204-5p/211-5p miR-1269 miR-450b-5p miR-216-5p miR-518d-5p/519-5p miR-378-3p miR-194-5p miR-26-5p miR-376-3p miR-653-5p miR-580-3p miR-522-3p miR-4766-3p
AGT ENPEP LNPEP	miR-193-3p miR-4428 miR-1245b-5p miR-377-3p miR-5581-3p
ACE2 ENPEP LNPEP	miR-4424 miR-1306-5p miR-374-5p/655-3p miR-543
ACE ENPEP LNPEP	miR-432-5p miR-3605-5p miR-4731-5p
DPP3 ENPEP LNPEP	miR-197-3p
LNPEP MME REN	miR-3200-5p
AGT LNPEP MME	miR-3924 miR-31-5p miR-758-3p
ACE2 LNPEP MME	miR-5691 miR-3194-3p miR-374a-3p
ACE LNPEP MME	miR-873-5p.2 miR-3126-5p
DPP3 LNPEP MME	miR-876-5p miR-2355-5p miR-146-5p miR-183-5p.1 miR-589-5p
AGT LNPEP REN	miR-6720-5p
ACE LNPEP REN	miR-214-3p/3619-5p
ACE2 AGT LNPEP	miR-3611 miR-212-5p miR-769-5p
AGT DPP3 LNPEP	miR-196-5p
ACE ACE2 LNPEP	miR-3187-3p miR-4677-3p miR-346 miR-582-5p
ACE2 DPP3 LNPEP	miR-329-3p/362-3p
ACE DPP3 LNPEP	miR-3179
ACE2 ENPEP MME	miR-140-3p.1
ACE2 AGT ENPEP	miR-489-3p
ACE ACE2 ENPEP	miR-642b-5p miR-331-3p
ACE MME REN	miR-3918
AGTR2 RNPEP	miR-129-3p
LNPEP RNPEP	miR-153-3p
ENPEP RNPEP	miR-383-5p.1
AGT RNPEP	miR-3194-5p
AGTR2 ANPEP	miR-193a-5p
AGT ANPEP	miR-328-3p
ACE ANPEP	miR-1908-5p

AGTR2 LNPEP	miR-556-5p miR-154-3p/487-3p miR-539-3p miR-3622a-5p miR-1276 miR-299-5p miR-561-5p
AGTR2 ENPEP	miR-629-5p
AGTR2 MME	miR-493-3p
ACE AGTR2	miR-425-5p
AGTR1 LNPEP	miR-140-3p.2 miR-205-5p miR-96-5p/1271-5p
AGTR1 MME	miR-182-5p
ACE2 AGTR1	miR-1266-3p
ACE AGTR1	miR-5000-3p
ENPEP LNPEP	miR-320 miR-515-5p/519e-5p miR-122-5p miR-323-3p miR-323b-3p miR-382-3p miR-5579-3p miR-34b-5p/449c-5p miR-144-3p miR-9-3p miR-19-3p miR-642a-5p miR-29-3p miR-494-3p miR-105-5p miR-514a-5p miR-3146
LNPEP MME	miR-452-5p/892-3p miR-411-5p.1 miR-325 miR-190-5p miR-582-3p miR-542-3p miR-885-5p miR-599 miR-3171 miR-411-5p.2 miR-433-3p miR-150-5p miR-130-3p/301-3p/454-3p miR-411-3p
AGT LNPEP	miR-345-5p miR-4637 miR-584-5p miR-625-5p miR-1323 miR-5010-5p
ACE2 LNPEP	miR-188-5p miR-7151-5p miR-574-5p
ACE LNPEP	miR-101-3p.2 miR-1270
DPP3 LNPEP	miR-5009-3p miR-324-3p/1913
ENPEP MME	miR-3064-5p miR-1911-5p miR-1295a miR-1296-5p miR-498
ENPEP REN	miR-136-5p miR-4761-3p
AGT ENPEP	miR-496.2 miR-145-5p
ACE ENPEP	miR-214-5p
DPP3 ENPEP	let-7-5p/98-5p
AGT MME	miR-2116-3p
ACE2 MME	miR-362-5p/500b-5p
ACE MME	miR-1286 miR-671-5p
DPP3 MME	miR-628-5p
AGT REN	miR-338-3p
ACE REN	miR-4640-5p
ACE2 AGT	miR-588
ACE AGT	miR-6509-3p miR-22-3p
ANPEP	miR-627-5p miR-151-3p miR-3622b-5p miR-3944-3p
MAS1	miR-143-3p
AGTR2	miR-6746-5p miR-2114-3p miR-888-5p miR-490-3p miR-770-5p
AGTR1	miR-1-3p/206
LNPEP	miR-101-3p.1 miR-137 miR-552-5p miR-532-3p miR-455-3p.2 miR-519-3p miR-4661-5p miR-147a miR-518-3p miR-135-5p miR-18-5p miR-374b-3p miR-142-

	3p.1 miR-1287-5p miR-875-5p miR-3614-5p miR-28-3p miR-3144-3p miR-324-5p miR-5687 miR-1343-3p miR-499b-5p miR-21-5p/590-5p miR-624-3p miR-501-3p/502-3p miR-99-5p/100-5p miR-183-5p.2 miR-1247-5p
ENPEP	miR-877-5p miR-451 miR-1185-5p miR-409-5p miR-219-5p miR-142-3p.2 miR-508-3p miR-526b-5p miR-371a-3p miR-133a-3p.1 miR-496.1 miR-133a-3p.2/133b miR-5094
MME	miR-139-5p miR-10-5p miR-342-3p miR-500a-3p miR-25-3p/32-5p/92-3p/363-3p/367-3p miR-4662-5p miR-1251-5p miR-625-3p
REN	miR-3127-5p miR-5586-5p
AGT	miR-2114-5p miR-219a-2-3p miR-2277-5p miR-486-5p miR-151-5p miR-124-3p.2/506-3p miR-370-3p miR-132-5p miR-184 miR-124-3p.1 miR-199-3p
ACE2	miR-514a-3p miR-505-3p.1 miR-144-5p miR-1179
ACE	miR-654-5p miR-3180-3p miR-199-5p miR-1180-5p

Appendix 4

Pubmed ID	Initial sample size	Replication sample size	Region	Gene	SNP	P value
27770636	1,825 African American ancestry cases, 3,784 African American ancestry controls		13q32.1	GPR180	rs187295598-T	6.00E-06
27770636	1,825 African American ancestry cases 3,784 African American ancestry controls		7q34	TAS2R5	rs2234017-C	7.00E-06
30636644	952 European ancestry male cases 1,789 European ancestry female cases 6,337 European ancestry male controls 8,402 European ancestry female controls	NA	19q13.32	TOMM40	rs405697	1.00E-13
30636644	952 European ancestry male cases 1,789 European ancestry female cases 6,337 European ancestry male controls 8,402 European ancestry female controls	NA	19q13.32	TOMM40	rs405697	1.00E-08
30636644	952 European ancestry male cases	NA	19q13.32	NECTIN2	rs6859-A	6.00E-13

	1,789 European ancestry female cases 6,337 European ancestry male controls 8,402 European ancestry female controls					
30636644	952 European ancestry male cases 1,789 European ancestry female cases 6,337 European ancestry male controls 8,402 European ancestry female controls	NA	19q13.32	NECTIN2	rs6859-A	1.00E-09
30636644	952 European ancestry male cases 1,789 European ancestry female cases 6,337 European ancestry male controls 8,402 European ancestry female controls	NA	19q13.32	NECTIN2	rs6859-A	2.00E-21
23419831	555 European ancestry individuals	NA	19q13.32	AC011481.2 NECTIN2	rs6857-T	1.00E-10
22005931	1,190 European ancestry cases 1,032 cases	NA	12q24.22	HRK	rs17429217	3.00E-06
23535033	303 European ancestry cases		2q14.3	LIMS2	rs78022502	2.00E-06
23535033	303 European ancestry cases		5q33.2	SAP30L	rs148763909	1.00E-08
23535033	303 European ancestry cases		7p15.3	CYCS	rs1861525	2.00E-07
26830138	2,478 European ancestry cases	NA	6q25.3	TULP4	rs116886320-A	3.00E-07

	979 ancestry controls					
26830138	2,478 European ancestry cases 979 ancestry controls	NA	7q36.3	INSIG1	rs191603973-C	7.00E-07
26830138	2,478 European ancestry cases 979 ancestry controls	NA	16p12.2	SDR42E2	rs145049847-C	8.00E-09
26830138	2,478 European ancestry cases 979 ancestry controls both from the same	NA	19p13.2	AC011472.2, TSPAN16, RAB3D, AC011472.3	rs148273964-A	8.00E-07
26830138	2,478 European ancestry cases 979 ancestry controls both from the same	NA	4q31.1	SETD7	rs72728723-A	2.00E-07
22159054	513 African American cases 496 African American controls	NA	19q13.32	NECTIN2	rs6859-A	5.00E-07
20885792	931 cases 1,104 controls	1,338 cases 2,003 controls	19q13.32	NECTIN2	rs6859-A	1.00E-07
18823527	1,082 European ancestry cases 1,239 European ancestry controls	1,400 controls	19q13.32	NECTIN2	rs6859-A	6.00E-14
29274321	190 European ancestry cases	NA	20p13	RSPO4	rs62187521-T	5.00E-07
29777097	42,034 British ancestry with parental AD history 272,244 British ancestry with no parental AD history	NA	19q13.32	NECTIN2	rs6859	1.00E-155

	25,580 Alzheimer's disease cases 48,466 controls					
29777097	42,034 British ancestry with parental AD history 272,244 British ancestry with no parental AD history 25,580 Alzheimer's disease cases 48,466 controls	NA	19q13.32	TOMM40	rs405697	5.00E-08
29777097	42,034 British ancestry with parental AD history 272,244 British ancestry with no parental AD history 25,580 Alzheimer's disease cases 48,466 controls	NA	19q13.32	TOMM40	rs141864196	5.00E-08
29777097	42,034 British ancestry with parental AD history 272,244 British ancestry with no parental AD history 25,580 Alzheimer's disease cases 48,466 controls	NA	19q13.32	MARK4, AC005779.1, AC005779.2	rs12463049	5.00E-08
28183528	13,100 European ancestry cases 13,220 European ancestry controls 1,472 African American cases 3,511 African American controls	5,813 European ancestry cases 20,474 European ancestry controls	19q13.32	AC011481.2, NECTIN2	rs6857-T	6.00E-07

	951 Japanese ancestry cases 894 Japanese ancestry controls 51 Israeli-Arab ancestry cases 64 Israeli-Arab ancestry controls					
28183528	13,100 European ancestry case 13,220 European ancestry controls 1,472 African American cases 3,511 African American controls 951 Japanese ancestry cases 894 Japanese ancestry controls 51 Israeli-Arab ancestry cases 64 Israeli-Arab ancestry controls	5,813 European ancestry cases 20,474 European ancestry controls	19q13.32	AC011481.2, NECTIN2	rs6857-T	7.00E-18
30617256	24,087 European ancestry late-onset AD cases 47,793 European ancestry with family history of AD 383,378 European ancestry controls	NA	19q13.32	NECTIN2	rs6859-A	1.00E-152
30617256	24,087 European ancestry late-onset AD cases 47,793 European ancestry with family history of AD 383,378 European ancestry controls	NA	19q13.32	BCAM	rs142092405-G	6.00E-12
30617256	24,087 European ancestry late-onset AD cases	NA	19q13.32	TOMM40	rs141864196-A	3.00E-10

	47,793 European ancestry with family history of AD 383,378 European ancestry controls					
30617256	24,087 European ancestry late-onset AD cases 47,793 European ancestry with family history of AD 383,378 European ancestry controls	NA	1q23.3	ADAMTS4	rs4575098-A	2.00E-10
25778476	7,184 cases, 26,968 controls	718 European ancestry cases, 1,699 European ancestry controls	8p21.2	PTK2B	rs2271920-A	8.00E-06
30820047	21,982 European ancestry cases 41,944 European ancestry controls	13,292 European ancestry cases 17,219 European ancestry controls	6p21.1	OARD1	rs114812713-C	2.00E-13

References

1. World Health Organization. Priority diseases and reasons for inclusion. Alzheimer disease and other dementias. 2013 . Available from: http://www.who.int/medicines/areas/priority_medicines/BP6_11Alzheimer.pdf?ua=1
2. Selkoe D, Mandelkow E, Holtzman D. Deciphering alzheimer disease. Cold Spring Harb Perspect Med. 2012;2(1).
3. Tarawneh R, Holtzman DM. The clinical problem of symptomatic Alzheimer disease and mild cognitive impairment. Cold Spring Harb Perspect Med. 2012;2(5).
4. Reitz C, Mayeux R. Alzheimer disease: Epidemiology, diagnostic criteria, risk factors and biomarkers. Biochem Pharmacol. 2014;88(4):640–51.
5. Serrano-Pozo A, Frosch MP, Masliah E, Hyman BT. Neuropathological alterations in Alzheimer disease. Cold Spring Harb Perspect Med. 2011;1(1):1–23.
6. Mandelkow EME. Biochemistry and cell biology of Tau protein in neurofibrillary degeneration. Cold Spring Harb Perspect Biol. 2011;3:1–25.
7. MacArthur J, Bowler E, Cerezo M, Gil L, Hall P, Hastings E, et al. The new NHGRI-EBI Catalog of published genome-wide association studies (GWAS Catalog). Nucleic Acids Res. 2017;45(D1):D896–901.
8. Morris M, Maeda S, Vossel K, Mucke L. The many faces of tau. Neuron. 2011 May 12;70(3):410–26.
9. Avila J, Lucas JJ, Pérez M, Hernández F. Role of Tau Protein in Both Physiological and Pathological Conditions. Physiol Rev. 2004 Apr;84(2):361–84.
10. Zhou F, Zhu X, Castellani RJ, Stimmelmayr R, Perry G, Smith MA, et al. Hibernation, a model of neuroprotection. Am J Pathol. 2001 Jun [cited 2019 Jan 12];158(6):2145–51.
11. Le Freche H, Brouillette J, Fernandez-Gomez F-J, Patin P, Caillierez R, Zommer

N, et al. Tau Phosphorylation and Sevoflurane Anesthesia. Anesthesiology. 2012;116(4):779–87.

12. Lee HG, Perry G, Moreira PI, Garrett MR, Liu Q, Zhu X, et al. Tau phosphorylation in Alzheimer's disease: Pathogen or protector? Trends Mol Med. 2005;11(4):164–9.
13. León-Espinosa G, García E, García-Escudero V, Hernández F, Defelipe J, Avila J. Changes in tau phosphorylation in hibernating rodents. J Neurosci Res. 2013;91(7):954–62.
14. Andresen M, Gazmuri JT, Marín A, Regueira T, Rovegno M. Therapeutic hypothermia for acute brain injuries. Scand J Trauma Resusc Emerg Med. 2015 Jun 5;23:42.
15. Härtig W, Stieler J, Boerema AS, Wolf J, Schmidt U, Weißfuß J, et al. Hibernation model of tau phosphorylation in hamsters: Selective vulnerability of cholinergic basal forebrain neurons - Implications for Alzheimer's disease. Eur J Neurosci. 2007;25(1):69–80.
16. Arendt T, Stieler J, Strijkstra AM, Hut RA, Rüdiger J, Van der Zee EA, et al. Reversible paired helical filament-like phosphorylation of tau is an adaptive process associated with neuronal plasticity in hibernating animals. J Neurosci. 2003 Aug 6;23(18):6972–81.
17. Arendt T, Stieler J, Holzer M. Brain hypometabolism triggers PHF-like phosphorylation of tau, a major hallmark of Alzheimer's disease pathology. J Neural Transm. 2015;122(4):531–9.
18. Masters CL, Selkoe DJ, Mayeux R, Stern Y, Johnson KA, Fox NC, et al. Biochemistry of Amyloid b-Protein and Amyloid. Cold Spring Harb Perspect Med. 2012;
19. Holtzman DM, Mandelkow E, Selkoe DJ, Tanzi RE, Laferla FM, Green KN, et al. Trafficking and Proteolytic Processing of APP. Cold Spring Harb Perspect Med. 2012;
20. Reinhard C, Hébert SS, De Strooper B. The amyloid-beta precursor protein: integrating structure with biological function. EMBO J. 2005 Dec 7;24(23):3996–4006.

21. Shankar GM, Li S, Mehta TH, Garcia-Munoz A, Shepardson NE, Smith I, et al. Amyloid-beta protein dimers isolated directly from Alzheimer's brains impair synaptic plasticity and memory. Nat Med. 2008 Aug;14(8):837–42.
22. Iadecola C, Gottesman RF. Compendium on the Pathophysiology and Treatment of Hypertension Neurovascular and Cognitive Dysfunction in Hypertension Epidemiology, Pathobiology, and Treatment. 2019;124:1025–44.
23. Lauer A, Van Veluw SJ, William CM, Charidimou A, Roongpiboonsopit D, Vashkevich A, et al. Microbleeds on MRI are associated with microinfarcts on autopsy in cerebral amyloid angiopathy. Neurology. 2016;87(14):1488–92.
24. Banerjee G, Carare R, Cordonnier C, Greenberg SM, Schneider JA, Smith EE, et al. The increasing impact of cerebral amyloid angiopathy: essential new insights for clinical practice. J Neurol Neurosurg Psychiatry. 2017 Nov 1;88(11):982–94.
25. Wyss-Coray T, Rogers J. Inflammation in Alzheimer disease-A brief review of the basic science and clinical literature. Cold Spring Harb Perspect Med. 2012;2(1).
26. Sarlus H, Heneka MT. Microglia in Alzheimer's disease. J Clin Invest. 2017 Sep 1;127(9):3240–9.
27. Heneka MT, Carson MJ, El Khoury J, Landreth GE, Brosseron F, Feinstein DL, et al. Neuroinflammation in Alzheimer's disease. Lancet Neurol. 2015 Apr;14(4):388–405.
28. Jessen NA, Munk ASF, Lundgaard I, Nedergaard M. The Glymphatic System: A Beginner's Guide. Neurochem Res. 2015;40(12):2583–99.
29. Rodriguez-Vieitez E, Saint-Aubert L, Carter SF, Almkvist O, Farid K, Schöll M, et al. Diverging longitudinal changes in astrocytosis and amyloid PET in autosomal dominant Alzheimer's disease. Brain. 2016;139(3):922–36.
30. Rodriguez-Vieitez E, Ni R, Gulyás B, Tóth M, Häggkvist J, Halldin C, et al. Astrocytosis precedes amyloid plaque deposition in Alzheimer APPswe transgenic mouse brain: a correlative positron emission tomography and in vitro imaging study. Eur J Nucl Med Mol Imaging. 2015;42(7):1119–32.
31. van Veluw SJ, Shih AY, Smith EE, Chen C, Schneider JA, Wardlaw JM, et al. Detection, risk factors, and functional consequences of cerebral microinfarcts.

Lancet Neurol. 2017;16(9):730–40.

32. Damasceno BP. Relationship between cortical microinfarcts and cognitive impairment in Alzheimer's disease. Dement Neuropsychol. 2012;6(3):131.
33. Weintraub S, Wicklund A, Salmon D. The neuropsychological profile of Alzheimer disease. Cold Spring Harb Perspect Med. 2012;2(4).
34. Sacuiu SF. Dementias. Handb Clin Neurol. 2016;138:123–51.
35. Association Alzheimer. 2018 Alzheimer's Disease facts and figures. Alzheimer's Dement. 2018;14(3):367–429.
36. Lourida I, Hannon E, Littlejohns TJ, Langa KM, Hyppönen E, Kuzma E, et al. Association of Lifestyle and Genetic Risk With Incidence of Dementia. JAMA. 2019 Aug 6;322(5):430.
37. Kamboh MI, Demirci FY, Wang X, Minster RL, Carrasquillo MM, Pankratz VS, et al. Genome-wide association study of Alzheimer's disease. Transl Psychiatry. 2012;2(5):1–7.
38. Tanzi RE. The Genetics of Alzheimer Disease. Cold Spring Harb Perspect Med. 2012;55(3):294.
39. De Strooper B, Iwatsubo T, Wolfe MS. Presenilins and γ-secretase: Structure, function, and role in Alzheimer disease. Cold Spring Harb Perspect Med. 2012;2(1).
40. Liu CC, Kanekiyo T, Xu H, Bu G. Apolipoprotein e and Alzheimer disease: Risk, mechanisms and therapy. Nat Rev Neurol. 2013;9(2):106–18.
41. Lambert JC, Ibrahim-Verbaas CA, Harold D, Naj AC, Sims R, Bellenguez C, et al. Meta-analysis of 74,046 individuals identifies 11 new susceptibility loci for Alzheimer's disease. Nat Genet. 2013;45(12):1452–8.
42. Jones L, Holmans PA, Hamshere ML, Harold D, Moskvina V, Ivanov D, et al. Genetic evidence implicates the immune system and cholesterol metabolism in the aetiology of Alzheimer's disease. PLoS One. 2010;5(11).
43. Finder VH. Alzheimer's disease: A general introduction and pathomechanism. J Alzheimer's Dis. 2010;22(3):5–19.
44. Pákáski M, Kálmán J. Interactions between the amyloid and cholinergic mechanisms in Alzheimer's disease. Neurochem Int. 2008 Nov 1;53(5):103–11.

45. Kehoe PG. The Coming of Age of the Angiotensin Hypothesis in Alzheimer's Disease: Progress Toward Disease Prevention and Treatment? J Alzheimer's Dis. 2018 Mar 13;62(3):1443–66.
46. Bartel DP. Review MicroRNAs: Genomics, Biogenesis, Mechanism, and Function. Cell. 2004;116:281–97.
47. Bartel DP. MicroRNAs: Target Recognition and Regulatory Functions. Cell. 2009 Jan 23;136(2):215–33.
48. Miyoshi K, Miyoshi T, Siomi H. Many ways to generate microRNA-like small RNAs: Non-canonical pathways for microRNA production. Mol Genet Genomics. 2010;284(2):95–103.
49. Winter J, Jung S, Keller S, Gregory RI, Diederichs S. Many roads to maturity: microRNA biogenesis pathways and their regulation. Nat Cell Biol. 2009 Mar 1;11(3):228–34.
50. Pelechano V, Steinmetz LM. Gene regulation by antisense transcription. Nat Rev Genet. 2013;14(12):880–93.
51. Mohr A, Mott J. Overview of MicroRNA Biology. Semin Liver Dis. 2015 Jan 29;35(01):003–11.
52. O'Carroll D, Schaefer A. General principals of miRNA biogenesis and regulation in the brain. Neuropsychopharmacology. 2013;38(1):39–54.
53. Baskerville S, Bartel DP. Microarray profiling of microRNAs reveals frequent coexpression with neighboring miRNAs and host genes. RNA. 2005 Jan 20;11(3):241–7.
54. Meunier J, Lemoine F, Soumillon M, Liechti A, Weier M, Guschanski K, et al. Birth and expression evolution of mammalian microRNA genes. Genome Res. 2013 Jan 1;23(1):34–45.
55. Berezikov E. Evolution of microRNA diversity and regulation in animals. Nat Rev Genet. 2011 Dec 1;12(12):846–60.
56. Afonso Guerra-Assunção J, Enright AJ. Large-scale analysis of microRNA evolution. BMC Genomics. 2012;13:1.
57. Gregory RI, Yan K, Amuthan G, Chendrimada T, Doratotaj B, Cooch N, et al. The Microprocessor complex mediates the genesis of microRNAs. Nature. 2004

Nov 11;432(7014):235–40.

58. Ameres SL, Zamore PD. Diversifying microRNA sequence and function. Nat Rev Mol Cell Biol. 2013;14(8):475–88.

59. Kai ZS, Pasquinelli AE. MicroRNA assassins: Factors that regulate the disappearance of miRNAs. Nat Struct Mol Biol. 2010;17(1):5–11.

60. Liu J, Valencia-Sanchez MA, Hannon GJ, Parker R. MicroRNA-dependent localization of targeted mRNAs to mammalian P-bodies. Nat Cell Biol. 2005 Jul 5;7(7):719–23.

61. Braun JE, Huntzinger E, Fauser M, Izaurralde E. GW182 Proteins Directly Recruit Cytoplasmic Deadenylase Complexes to miRNA Targets. Mol Cell. 2011 Oct 7;44(1):120–33.

62. Friedman RC, Farh KK, Burge CB, Bartel DP. Most mammalian mRNAs are conserved targets of miRNAs. Genome Res. 2009;(19):92–105.

63. Agarwal V, Bell GW, Nam JW, Bartel DP. Predicting effective microRNA target sites in mammalian mRNAs. Elife. 2015;4:1–38.

64. Lau P, Sala Frigerio C, De Strooper B. Variance in the identification of microRNAs deregulated in Alzheimer's disease and possible role of lincRNAs in the pathology: The need of larger datasets. Ageing Res Rev. 2014 Sep 1;17:43–53.

65. Gerardo-Aviles J, Allen S, Kehoe PG. Renin-Angiotensin System MicroRNAs, Special Focus on the Brain. In: Renin-Angiotensin System - Past, Present and Future. InTech; 2017.

66. Pritchard CC, Cheng HH, Tewari M, Division B, Hutchinson F, Health P, et al. MicroRNA profiling: approaches and considerations Colin. Nat Rev Genet. 2015;13(5):358–69.

67. Benes V, Castoldi M. Expression profiling of microRNA using real-time quantitative PCR, how to use it and what is available. Methods. 2010;50(4):244–9.

68. Hunt EA, Broyles D, Head T, Deo SK. MicroRNA Detection: Current Technology and Research Strategies. Annu Rev Anal Chem. 2015;8(1):217–37.

69. Zhao Y, Lukiw WJ. TREM2 signaling, miRNA-34a and the extinction of phagocytosis. Front Cell Neurosci. 2013;7:131.

70. Garzon R, Marcucci G, Croce CM. Targeting microRNAs in cancer: Rationale,

strategies and challenges. Vol. 9, Nature Reviews Drug Discovery. 2010. 775–89.

71. Geekiyanage H, Chan C. MicroRNA-137/181c Regulates Serine Palmitoyltransferase and In Turn Amyloid , Novel Targets in Sporadic Alzheimer's Disease. J Neurosci. 2011 Oct 12;31(41):14820–30.
72. Braak H, Braak E. Neuropathological stageing of Alzheimer-related changes. Acta Neuropathol. 1991;82(4):239–59.
73. Livak KJ, Schmittgen TD. Analysis of relative gene expression data using real-time quantitative PCR and the 2 Delta Delta CT method. Methods. 2001;25(3):402–8.
74. Schmittgen TD, Livak KJ. Analyzing real-time PCR data by the comparative CTmethod. Nat Protoc. 2008;3(6):1101–8.
75. Vandesompele J, De Preter K, Pattyn F, Poppe B, Van Roy N, De Paepe A, et al. Accurate normalization of real-time quantitative RT-PCR data by geometric averaging of multiple internal control genes. Genome Biol. 2002;50:1–30.
76. Kozomara A, Griffiths-Jones S. miRBase: annotating high confidence microRNAs using deep sequencing data. Nucleic Acids Res. 2014 Jan;42(D1):D68–73.
77. Fromm B, Billipp T, Peck LE, Johansen M, Tarver JE, King BL, et al. A uniform system for the annotation of human microRNA genes and the evolution of the human microRNAome. Annu Rev Genet. 2015;23(49):213–42.
78. Huang DW, Sherman BT, Lempicki Richar. Systematic and integrative analysis of large gene lists using DAVID bioinformatics resources. Nat Protoc. 2009;4(1):44–8.
79. Mi H, Muruganujan A, Huang X, Ebert D, Mills C, Guo X, et al. Protocol Update for large-scale genome and gene function analysis with the PANTHER classification system (v.14.0). Nat Protoc. 2019 Mar 25;14(3):703–21.
80. Müller UC, Zheng H. Physiological functions of APP family proteins. Cold Spring Harb Perspect Med. 2012;2(2):1–17.
81. Brai E, Alina Raio N, Alberi L. Notch1 hallmarks fibrillary depositions in sporadic Alzheimer's disease. Acta Neuropathol Commun. 2016 Dec 1;4(1):64.
82. Kim J, Basak JM, Holtzman DM. The Role of Apolipoprotein E in Alzheimer's

Disease. 2011;63(3):287–303.

83. Holtzman DM, Herz J, Bu G. Apolipoprotein E and apolipoprotein E receptors: Normal biology and roles in Alzheimer disease. Cold Spring Harb Perspect Med. 2012;2(3).

84. Hirsch-Reinshagen V, Zhou S, Burgess BL, Bernier L, McIsaac SA, Chan JY, et al. Deficiency of ABCA1 impairs apolipoprotein E metabolism in brain. J Biol Chem. 2004 Sep 24;279(39):41197–207.

85. Basak JM, Verghese PB, Yoon H, Kim J, Holtzman DM. Low-density lipoprotein receptor represents an apolipoprotein E-independent pathway of Aβ uptake and degradation by astrocytes. J Biol Chem. 2012 Apr 20;287(17):13959–71.

86. Yajima R, Tokutake T, Koyama A, Kasuga K, Tezuka T, Nishizawa M, et al. ApoE-isoform-dependent cellular uptake of amyloid-β is mediated by lipoprotein receptor LR11/SorLA. Biochem Biophys Res Commun. 2015 Jan 2;456(1):482–8.

87. Yin R-H, Yu J-T, Tan L. The Role of SORL1 in Alzheimer's Disease. Mol Neurobiol. 2015 Jun 16;51(3):909–18.

88. Shen J, Qin W, Xu Q, Xu L, Xu J, Zhang P, et al. Modulation of APOE and SORL1 genes on hippocampal functional connectivity in healthy young adults. Brain Struct Funct. 2017 Aug 22;222(6):2877–89.

89. Andersen OM, Rudolph I-M, Willnow TE. Risk factor SORL1: from genetic association to functional validation in Alzheimer's disease. Acta Neuropathol. 2016 Nov 16;132(5):653–65.

90. Halliday MR, Rege S V, Ma Q, Zhao Z, Miller CA, Winkler EA, et al. Accelerated pericyte degeneration and blood-brain barrier breakdown in apolipoprotein E4 carriers with Alzheimer's disease. J Cereb Blood Flow Metab. 2016 Jan;36(1):216–27.

91. Liu C-C, Hu J, Zhao N, Wang J, Wang N, Cirrito JR, et al. Astrocytic LRP1 Mediates Brain Aβ Clearance and Impacts Amyloid Deposition. J Neurosci. 2017;37(15):4023–31.

92. Cai Z, Liu N, Wang C, Qin B, Zhou Y, Xiao M, et al. Role of RAGE in Alzheimer's Disease. Cell Mol Neurobiol. 2016 May 15;36(4):483–95.

93. Sagare AP, Bell RD, Zlokovic B V, Tanzi RE, Nixon R, Aisen PS, et al. Neurovascular Dysfunction and Faulty Amyloid. Spring. 2012;
94. Donahue JE, Flaherty SL, Johanson CE, Duncan JA, Silverberg GD, Miller MC, et al. RAGE, LRP-1, and amyloid-beta protein in Alzheimer's disease. Acta Neuropathol. 2006 Sep 28;112(4):405–15.
95. Cuchillo-Ibañez I, Mata-Balaguer T, Balmaceda V, Arranz JJ, Nimpf J, Sáez-Valero J. The β-amyloid peptide compromises Reelin signaling in Alzheimer's disease. Sci Rep. 2016;6:31646.
96. Sweeney MD, Ayyadurai S, Zlokovic B V. Pericytes of the neurovascular unit: Key functions and signaling pathways. Nat Neurosci. 2016;19(6):771–83.
97. Zhao Z, Nelson AR, Betsholtz C, Zlokovic B V. Establishment and Dysfunction of the Blood-Brain Barrier. Cell. 2015;163(5):1064–78.
98. Ueno M, Chiba Y, Murakami R, Matsumoto K, Kawauchi M, Fujihara R. Blood–brain barrier and blood–cerebrospinal fluid barrier in normal and pathological conditions. Brain Tumor Pathol. 2016;33(2):89–96.
99. Jessen NA, Munk ASF, Lundgaard I, Nedergaard M. The Glymphatic System: A Beginner's Guide. Neurochem Res. 2015 Dec;40(12):2583–99.
100. Miners JS, Schulz I, Love S. Differing associations between Aβ accumulation, hypoperfusion, blood–brain barrier dysfunction and loss of PDGFRB pericyte marker in the precuneus and parietal white matter in Alzheimer's disease. J Cereb Blood Flow Metab. 2018 Jan 2;38(1):103–15.
101. Lynch MA. The impact of neuroimmune changes on development of amyloid pathology; relevance to Alzheimer's disease. Immunology. 2014 Mar;141(3):292–301.
102. Walker DG, Dalsing-Hernandez JE, Campbell NA, Lue L-F. Decreased expression of CD200 and CD200 receptor in Alzheimer's disease: a potential mechanism leading to chronic inflammation. Exp Neurol. 2009 Jan;215(1):5–19.
103. Holtzman DM, Mandelkow E, Selkoe DJ, Tanzi RE, Nixon R. Proteolytic Degradation of Amyloid beta Protein. Cold Spring Harb Perspect Med. 2012;
104. Hur EM, Zhou FQ. GSK3 signalling in neural development. Nat Rev Neurosci. 2010;11(8):539–51.

105. Hooper C, Killick R, Lovestone S. The GSK3 hypothesis of Alzheimer's disease. J Neurochem. 2008 Mar;104(6):1433–9.
106. Gerschütz A, Heinsen H, Grünblatt E, Wagner AK, Bartl J, Meissner C, et al. Neuron-Specific Alterations in Signal Transduction Pathways associated with Alzheimer's Disease. J Alzheimer's Dis. 2014 Mar 10;40(1):135–42.
107. Sontag J-M, Sontag E. Protein phosphatase 2A dysfunction in Alzheimer's disease. Front Mol Neurosci. 2014;7:16.
108. Karch CM, Jeng AT, Goate AM. Calcium phosphatase calcineurin influences tau metabolism. Neurobiol Aging. 2013 Feb;34(2):374–86.
109. Wang AC, Jensen EH, Rexach JE, Vinters H V, Hsieh-Wilson LC. Loss of O-GlcNAc glycosylation in forebrain excitatory neurons induces neurodegeneration. Proc Natl Acad Sci U S A. 2016;113(52):15120–5.
110. Lau P, Nixon SJ, Parton RG, Muscat GEO. RORα regulates the expression of genes involved in lipid homeostasis in skeletal muscle cells: Caveolin-3 and CPT-1 are direct targets of ROR. J Biol Chem. 2004;279(35):36828–40.
111. Kim EJ, Yoo YG, Yang WK, Lim YS, Na TY, Lee IK, et al. Transcriptional activation of HIF-1 by RORα and its role in hypoxia signaling. Arterioscler Thromb Vasc Biol. 2008;28(10):1796–802.
112. Boukhtouche F, Mariani J, Tedgui A. The "CholesteROR" Protective Pathway in the Vascular System. Arterioscler Thromb Vasc Biol. 2004;24(4):637–43.
113. Kehoe PG. The coming of age of the angiotensin hypothesis in Alzheimer's disease: Progress toward disease prevention and treatment? J Alzheimer's Dis. 2018;62(3):1443–66.
114. Kochunov P, Glahn DC, Nichols TE, Winkler AM, Hong EL, Holcomb HH, et al. Genetic analysis of cortical thickness and fractional anisotropy of water diffusion in the brain. Front Neurosci. 2011;5:1–15.
115. Journiac N, Jolly S, Jarvis C, Gautheron V, Rogard M, Trembleau A, et al. The nuclear receptor RORα exerts a bi-directional regulation of IL-6 in resting and reactive astrocytes. Proc Natl Acad Sci. 2009;106(50):21365–70.
116. Delerive P, Monté D, Dubois G, Trottein F, Fruchart-Najib J, Mariani J, et al. The orphan nuclear receptor RORα is a negative regulator of the inflammatory

response. EMBO Rep. 2001;2(1):42–8.

117. Ming Q, Wang X, Chai Q, Yi J, Yao S. Retinoid-related orphan receptor alpha (RORA) gene variation is associated with trait depression. Psychiatry Res. 2015;229(1–2):629–30.

118. Terracciano A, Tanaka T, Sutin A, Sanna S, Deiana B, Lai S, et al. Florida State University Libraries Genome-Wide Association Scan of Trait Depression. Biol Psychiatry. 2010;68(9):811–7.

119. Baker E, Sims R, Leonenko G, Frizzati A, Harwood J, Grozeva D, et al. Gene based Analysis in HRC Imputed Genome Wide Association Data Identifies Three Novel Genes for Alzheimer's Disease. bioRxiv. 2018 Jul 23;374876.

120. Banzhaf-Strathmann J, Benito E, May S, Arzberger T, Tahirovic S, Kretzschmar H, et al. MicroRNA-125b induces tau hyperphosphorylation and cognitive deficits in Alzheimer's disease. EMBO J. 2014 Aug 1;33(15):1667–80.

121. Hebert SS, Horre K, Nicolai L, Papadopoulou AS, Mandemakers W, Silahtaroglu AN, et al. Loss of microRNA cluster miR-29a/b-1 in sporadic Alzheimer's disease correlates with increased BACE1/ -secretase expression. Proc Natl Acad Sci. 2008;105(17):6415–20.

122. Craddock TJA, Tuszynski JA, Chopra D, Casey N, Goldstein LE, Hameroff SR, et al. The Zinc Dyshomeostasis Hypothesis of Alzheimer's Disease. Gong C-X, editor. PLoS One. 2012 Mar 23;7(3):e33552.

123. Li L-B, Wang Z-Y. Disruption of brain zinc homeostasis promotes the pathophysiological progress of Alzheimer's disease. Histol Histopathol. 2016 Jun;31(6):623–7.

124. Ventriglia M, Brewer GJ, Simonelli I, Mariani S, Siotto M, Bucossi S, et al. Zinc in Alzheimer's Disease: A Meta-Analysis of Serum, Plasma, and Cerebrospinal Fluid Studies. J Alzheimer's Dis. 2015 May 7;46(1):75–87.

125. Acquaah-Mensah GK, Agu N, Khan T, Gardner A. A regulatory role for the insulin- and BDNF-Linked RORA in the hippocampus: Implications for Alzheimer's disease. J Alzheimer's Dis. 2015;44(3):827–38.

126. Dwyer R, Skrobot OA, Dwyer J, Munafo M, Kehoe PG. Using Alzgene-Like Approaches to Investigate Susceptibility Genes for Vascular Cognitive

Impairment. J Alzheimer's Dis. 2013 Feb 6;34(1):145–54.

127. Fang Z, Du R, Edwards A, Flemington EK, Zhang K. The Sequence Structures of Human MicroRNA Molecules and Their Implications. PLoS One. 2013 Jan 18;8(1):e54215.

128. Benes V, Castoldi M. Expression profiling of microRNA using real-time quantitative PCR, how to use it and what is available. Methods. 2010 Apr;50(4):244–9.

129. Van Rooij E. The art of MicroRNA research. Circ Res. 2011;108(2):219–34.

130. Mestdagh P, Hartmann N, Baeriswyl L, Andreasen D, Bernard N, Chen C, et al. Evaluation of quantitative mirnA expression platforms in the micrornA quality control (mirQC) study. Nat Methods. 2014;11(8):809–15.

131. Mestdagh P, Van Vlierberghe P, De Weer A, Muth D, Westermann F, Speleman F, et al. A novel and universal method for microRNA RT-qPCR data normalization. Genome Biol. 2009;10(6).

132. Redshaw N, Wilkes T, Whale A, Cowen S, Huggett J, Foy CA. A comparison of miRNA isolation and RT-qPCR technologies and their effects on quantification accuracy and repeatability. Biotechniques. 2013;54(3):155–64.

133. Garibyan L, Avashia N. Polymerase chain reaction. J Invest Dermatol. 2013 Mar;133(3):1–4.

134. Schwarzenbach H, Silva AM da, Calin G, Pantel K. Which is the accurate data normalization strategy for microRNA quantification? Clin Chem. 2015;61(11):1333–42.

135. Benz F, Roderburg C, Cardenas DV, Vucur M, Gautheron J, Koch A, et al. U6 is unsuitable for normalization of serum miRNA levels in patients with sepsis or liver fibrosis. Exp Mol Med. 2013;45(9):1–9.

136. Gee HE, Buffa FM, Camps C, Ramachandran A, Leek R, Taylor M, et al. The small-nucleolar RNAs commonly used for microRNA normalisation correlate with tumour pathology and prognosis. Br J Cancer. 2011 Mar 29;104(7):1168–77.

137. Geekiyanage H, Jicha GA, Nelson PT, Chan C. Blood serum miRNA: Non-invasive biomarkers for Alzheimer's disease. Exp Neurol. 2012 Jun;235(2):491–6.

138. Lau P, Bossers K, Janky R, Salta E, Frigerio CS, Barbash S, et al. Alteration of the

microRNA network during the progression of Alzheimer's disease. EMBO Mol Med. 2013 Oct;5(10):1613–34.

139. Chen G, Zhao L, Feng J, You G, Sun Q, Li P, et al. Validation of Reliable Reference Genes for Real-Time PCR in Human Umbilical Vein Endothelial Cells on Substrates with Different Stiffness. PLoS One. 2013;8(6):1–9.
140. Andersen CL. Normalization of Real-Time Quantitative Reverse Transcription-PCR Data: A Model-Based Variance Estimation Approach to Identify Genes Suited for Normalization, Applied to Bladder and Colon Cancer Data Sets. Cancer Res. 2004;64(15):5245–50.
141. Pfaffl MW. Determination of most stable housekeeping genes, differentially regulated target genes and sample integrity: BestKeeper© - Excel spreadsheet tool using a Repeated Pair-wise Correlation. Biotechnol Lett. 2004;26:509–15.
142. Perkins JR, Dawes JM, McMahon SB, Bennett DLH, Orengo C, Kohl M. ReadqPCR and NormqPCR: R packages for the reading, quality checking and normalisation of RT-qPCR quantification cycle (Cq) data. BMC Genomics. 2012;13(1).
143. Kitchen RR, Kubista M, Tichopad A. Statistical aspects of quantitative real-time PCR experiment design. Methods. 2010;50(4):231–6.
144. Ma J, Pan H, Zeng Y, Lv Y, Zhang H, Xue A, et al. Exploration of the R code-based mathematical model for PMI estimation using profiling of RNA degradation in rat brain tissue at different temperatures. Forensic Sci Med Pathol. 2015;11(4):530–7.
145. Lv YH, Ma JL, Pan H, Zeng Y, Tao L, Zhang H, et al. Estimation of the human postmortem interval using an established rat mathematical model and multi-RNA markers. Forensic Sci Med Pathol. 2017;13(1):20–7.
146. Peiró-Chova L, Peña-Chilet M, López-Guerrero JA, García-Giménez JL, Alonso-Yuste E, Burgues O, et al. High stability of microRNAs in tissue samples of compromised quality. Virchows Arch. 2013;463(6):765–74.
147. Nagy C, Maheu M, Lopez J, Vaillancourt K, Cruceanu C, Gross J, et al. Effects of Postmortem Interval on Biomolecule Integrity in the Brain. J Neuropathol Exp Neurol. 2015;74(5):459–69.

148. Cogswell JP, Ward J, Taylor IA, Waters M, Shi Y, Cannon B, et al. Identification of miRNA changes in Alzheimer's disease brain and CSF yields putative biomarkers and insights into disease pathways. J Alzheimers Dis. 2008 May;14(1):27–41.
149. Nunez-Iglesias J, Liu C-C, Morgan TE, Finch CE, Zhou XJ. Joint Genome-Wide Profiling of miRNA and mRNA Expression in Alzheimer's Disease Cortex Reveals Altered miRNA Regulation. Maas S, editor. PLoS One. 2010 Feb 1;5(2):e8898.
150. Bicker S, Lackinger M, Weiß K, Schratt G. MicroRNA-132, -134, and -138: a microRNA troika rules in neuronal dendrites. Cell Mol Life Sci. 2014;71(20):3987–4005.
151. Martinez-Ramirez S, Greenberg SM, Viswanathan A. Cerebral microbleeds: overview and implications in cognitive impairment. Alzheimers Res Ther. 2014;6(3):33.
152. Stokum JA, Gerzanich V, Simard JM. Molecular pathophysiology of cerebral edema. J Cereb Blood Flow Metab. 2016;36(3):513–38.
153. Arvanitakis Z, Capuano AW, Leurgans SE, Buchman AS, Bennett DA, Schneider JA. The Relationship of Cerebral Vessel Pathology to Brain Microinfarcts. Brain Pathol. 2017;27(1):77–85.
154. Cirrito JR, Yamada KA, Finn MB, Sloviter RS, Bales KR, May PC, et al. Synaptic activity regulates interstitial fluid amyloid-beta levels in vivo. Neuron. 2005 Dec 22;48(6):913–22.
155. Poels MMF, Vernooij MW, Ikram MA, Hofman A, Krestin GP, van der Lugt A, et al. Prevalence and Risk Factors of Cerebral Microbleeds: An Update of the Rotterdam Scan Study. Stroke. 2010 Oct 1;41(10, Supplement 1):S103–6.
156. Mateos L, Ismail MAM, Gil-Bea FJ, Schüle R, Schöls L, Heverin M, et al. Side chain-oxidized oxysterols regulate the brain renin-angiotensin system through a liver X receptor-dependent mechanism. J Biol Chem. 2011;286(29):25574–85.
157. Romero CA, Orias M, Weir MR. Novel RAAS agonists and antagonists: Clinical applications and controversies. Nat Rev Endocrinol. 2015;11(4):242–52.
158. Elkins EA, Walti KA, Newberry KE, Lema SC. Identification of an

oxytocinase/vasopressinase-like leucyl-cystinyl aminopeptidase (LNPEP) in teleost fish and evidence for hypothalamic mRNA expression linked to behavioral social status. Gen Comp Endocrinol. 2017 Sep 1;250:58–69.

159. Wigerup C, Påhlman S, Bexell D. Therapeutic targeting of hypoxia and hypoxia-inducible factors in cancer. Pharmacol Ther. 2016 Aug 1;164:152–69.
160. Han Z, Huang H, Gao Y, Huang Q. Functional annotation of Alzheimer's disease associated loci revealed by GWASs. PLoS One. 2017;12(6).
161. Ghanbari M, Ikram MA, De Looper HWJ, Hofman A, Erkeland SJ, Franco OH, et al. Genome-wide identification of microRNA-related variants associated with risk of Alzheimer's disease. Sci Rep. 2016;6(June):1–9.
162. Lopez M, Aoubala M, Jordier F, Isnardon D, Gomez S, Dubreuil P. The human poliovirus receptor related 2 protein is a new hematopoietic/endothelial homophilic adhesion molecule. Blood. 1998;92(12):4602–11.
163. Rossignoli A, Shang MM, Gladh H, Moessinger C, Foroughi Asl H, Talukdar HA, et al. Poliovirus Receptor-Related 2: A Cholesterol-Responsive Gene Affecting Atherosclerosis Development by Modulating Leukocyte Migration. Arterioscler Thromb Vasc Biol. 2017;37(3):534–42.
164. Yashin AI, Fang F, Kovtun M, Wu D, Duan M, Arbeev K, et al. Hidden heterogeneity in Alzheimer's disease: Insights from genetic association studies and other analyses. Exp Gerontol. 2018;107(October):148–60.
165. Miele E, Buttarelli FR, Arcella A, Begalli F, Garg N, Silvano M, et al. High-throughput microRNA profiling of pediatric high-grade gliomas. Neuro Oncol. 2014 Jan;16(2):228–40.
166. Northcott PA, Fernandez-L A, Hagan JP, Ellison DW, Grajkowska W, Gillespie Y, et al. The miR-17/92 polycistron is up-regulated in sonic hedgehog-driven medulloblastomas and induced by N-myc in sonic hedgehog-treated cerebellar neural precursors. Cancer Res. 2009 Apr 15;69(8):3249–55.
167. Londin E, Loher P, Telonis AG, Quann K, Clark P, Jing Y, et al. Analysis of 13 cell types reveals evidence for the expression of numerous novel primate- and tissue-specific microRNAs. Proc Natl Acad Sci. 2015;112(10):E1106–15.
168. Lipovich L, Hou Z-C, Jia H, Sinkler C, McGowen M, Sterner KN, et al. High-

throughput RNA sequencing reveals structural differences of orthologous brain-expressed genes between western lowland gorillas and humans. J Comp Neurol. 2016 Feb 1;524(2):288–308.

169. Kent OA, McCall MN, Cornish TC, Halushka MK. Lessons from miR-143/145: The importance of cell-type localization of miRNAs. Nucleic Acids Res. 2014;42(12):7528–38.
170. Witwer KW, Halushka MK. Toward the promise of microRNAs – Enhancing reproducibility and rigor in microRNA research. RNA Biol. 2016;13(11):1103–16.
171. Mellios N, Huang HS, Grigorenko A, Rogaev E, Akbarian S. A set of differentially expressed miRNAs, including miR-30a-5p, act as post-transcriptional inhibitors of BDNF in prefrontal cortex. Hum Mol Genet. 2008;17(19):3030–42.
172. Wang WX, Danaher RJ, Miller CS, Berger JR, Nubia VG, Wilfred BS, et al. Expression of miR-15/107 family microRNAs in human tissues and cultured rat brain cells. Genomics, Proteomics Bioinforma. 2014;12(1):19–30.
173. Kasai A, Kakihara S, Miura H, Okada R, Hayata-Takano A, Hazama K, et al. Double In situ Hybridization for MicroRNAs and mRNAs in Brain Tissues. Front Mol Neurosci. 2016;9:126.
174. Rao VTS, Ludwin SK, Fuh SC, Sawaya R, Moore CS, Ho MK, et al. MicroRNA expression patterns in human astrocytes in relation to anatomical location and age. J Neuropathol Exp Neurol. 2016;75(2):156–66.
175. Pogue AI, Cui JG, Li YY, Zhao Y, Culicchia F, Lukiw WJ. Micro RNA-125b (miRNA-125b) function in astrogliosis and glial cell proliferation. Neurosci Lett. 2010 May 26;476(1):18–22.
176. Hansen KF, Karelina K, Sakamoto K, Wayman GA, Impey S, Obrietan K. miRNA-132: a dynamic regulator of cognitive capacity. Brain Struct Funct. 2013 May 16;218(3):817–31.
177. Zhu Q-B, Unmehopa U, Bossers K, Hu Y-T, Verwer R, Balesar R, et al. MicroRNA-132 and early growth response-1 in nucleus basalis of Meynert during the course of Alzheimer's disease. Brain. 2016 Mar 1;139(3):908–21.
178. Hansen KF, Sakamoto K, Aten S, Snider KH, Loeser J, Hesse AM, et al. Targeted

deletion of miR-132/-212 impairs memory and alters the hippocampal transcriptome. Learn Mem. 2016 Feb;23(2):61–71.

179. Jin J, Kim S-N, Liu X, Zhang H, Zhang C, Seo J-S, et al. miR-17-92 Cluster Regulates Adult Hippocampal Neurogenesis, Anxiety, and Depression. Cell Rep. 2016 Aug 9;16(6):1653–63.

180. Gangaraju VK, Lin H. MicroRNAs: Key regulators of stem cells. Nat Rev Mol Cell Biol. 2009;10(2):116–25.

181. Shi Y, Zhao X, Hsieh J, Wichterle H, Impey S, Banerjee S, et al. microRNA regulation of neural stem cells and neurogenesis. 2011;30(45):14931–6.

182. Le MTN, Xie H, Zhou B, Chia PH, Rizk P, Um M, et al. MicroRNA-125b Promotes Neuronal Differentiation in Human Cells by Repressing Multiple Targets. Mol Cell Biol. 2009;29(19):5290–305.

183. Sarkar S, Jun S, Rellick S, Quintana DD, Cavendish JZ, Simpkins JW. Expression of microRNA-34a in Alzheimer's disease brain targets genes linked to synaptic plasticity, energy metabolism, and resting state network activity. Brain Res. 2016 Sep 1;1646:139–51.

184. Zovoilis A, Agbemenyah HY, Agis-Balboa RC, Stilling RM, Edbauer D, Rao P, et al. microRNA-34c is a novel target to treat dementias. EMBO J. 2011 Sep 23;30(20):4299–308.

185. De Antonellis P, Carotenuto M, Vandenbussche J, De Vita G, Ferrucci V, Medaglia C, et al. Early Targets of miR-34a in Neuroblastoma. Mol Cell Proteomics. 2014 Aug;13(8):2114–31.

186. Zhang L, Dong H, Si Y, Wu N, Cao H, Mei B, et al. miR-125b promotes tau phosphorylation by targeting the neural cell adhesion molecule in neuropathological progression. Neurobiol Aging. 2019 Jan 1;73:41–9.

187. Ma X, Liu L, Meng J. MicroRNA-125b promotes neurons cell apoptosis and Tau phosphorylation in Alzheimer's disease. Neurosci Lett. 2017 Nov 20;661:57–62.

188. Forster JI, Köglsberger S, Trefois C, Boyd O, Baumuratov AS, Buck L, et al. Characterization of differentiated SH-SY5Y as neuronal screening model reveals increased oxidative vulnerability. J Biomol Screen. 2016;21(5):496–509.

189. Wanet A, Tacheny A, Arnould T, Renard P. MiR-212/132 expression and

functions: Within and beyond the neuronal compartment. Nucleic Acids Res. 2012;40(11):4742–53.

190. Krützfeldt J, Rajewsky N, Braich R, Rajeev KG, Tuschl T, Manoharan M, et al. Silencing of microRNAs in vivo with "antagomirs." Nature. 2005;438(7068):685–9.

191. Ameres S, Horwich M, Hung J-H, Xu J, Ghildiyal M, Weng Z, et al. Target RNA-directed trimming and tailing of small silencing RNAs. PLoS One. 2017;32(7):736–40.

192. Meseguer S, Mudduluru G, Escamilla JM, Allgayer H, Barettino D. MicroRNAs-10a and -10b contribute to retinoic acid-induced differentiation of neuroblastoma cells and target the alternative splicing regulatory factor SFRS1 (SF2/ASF). J Biol Chem. 2011;286(6):4150–64.

193. Skalsky RL, Cullen BR. Reduced expression of brain-enriched microRNAs in glioblastomas permits targeted regulation of a cell death gene. PLoS One. 2011;6(9):20–3.

194. Magill ST, Cambronne XA, Luikart BW, Lioy DT, Leighton BH. microRNA-132 regulates dendritic growth and arborization of newborn neurons in the adult hippocampus. 2010;107(47).

195. Lin LF, Chiu SP, Wu MJ, Chen PY, Yen JH. Luteolin induces microRNA-132 expression and modulates neurite outgrowth in PC12 cells. PLoS One. 2012;7(8).

196. Edbauer D, Neilson JR, Foster KA, Wang C-F, Seeburg DP, Batterton MN, et al. Regulation of synaptic structure and function by FMRP- associated microRNAs miR-125b and miR-132. 2016;25(3):289–313.

197. Jasińska M, Miłek J, Cymerman IA, Łęski S, Kaczmarek L, Dziembowska M. miR-132 Regulates Dendritic Spine Structure by Direct Targeting of Matrix Metalloproteinase 9 mRNA. Mol Neurobiol. 2016;53(7):4701–12.

198. Pathania M, Torres-Reveron J, Yan L, Kimura T, Lin T V., Gordon V, et al. miR-132 enhances dendritic morphogenesis, spine density, synaptic integration, and survival of newborn olfactory bulb neurons. PLoS One. 2012;7(5).

199. Mellios N, Sugihara H, Castro J, Banerjee A, Le C, Kumar A, et al. miR-132, an experience-dependent microRNA, is essential for visual cortex plasticity.

2016;25(3):289–313.

200. Papadopoulou AS, Serneels L, Achsel T, Mandemakers W, Callaerts-Vegh Z, Dooley J, et al. Deficiency of the miR-29a/b-1 cluster leads to ataxic features and cerebellar alterations in mice. Neurobiol Dis. 2015;73:275–88.

201. Roshan R, Shridhar S, Sarangdhar MA, Banik A, Chawla M, Garg M, et al. Brain-specific knockdown of miR-29 results in neuronal cell death and ataxia in mice. RNA. 2014 Aug;20(8):1287–97.

202. Varendi K, Mätlik K, Andressoo JO. From microRNA target validation to therapy: Lessons learned from studies on BDNF. Cell Mol Life Sci. 2015;72(9):1779–94.

203. Witwer KW, Halushka MK. Toward the promise of microRNAs – Enhancing reproducibility and rigor in microRNA research. RNA Biol. 2016;13(11):1103–16.

204. Delay C, Grenier-Boley B, Amouyel P, Dumont J, Lambert JC. MiRNA-dependent target regulation: Functional characterization of singlenucleotide polymorphisms identified in genome-wide association studies of Alzheimer's disease. Alzheimer's Res Ther. 2016;8(1):1–11.

205. Cohen AD, Klunk WE. Early detection of Alzheimer's disease using PiB and FDG PET. Neurobiol Dis. 2014;72(Part A):117–22.

206. Morbelli S, Brugnolo A, Bossert I, Buschiazzo A, Frisoni GB, Galluzzi S, et al. Visual Versus semi-quantitative analysis of 18 F-FDG-PET in Amnestic MCI: An European Alzheimer's Disease Consortium (EADC) project. J Alzheimer's Dis. 2015;44(3):815–26.

207. Pagani M, De Carli F, Morbelli S, Öberg J, Chincarini A, Frisoni GB, et al. Volume of interest-based [18 F]fluorodeoxyglucose PET discriminates MCI converting to Alzheimer's disease from healthy controls. A European Alzheimer's Disease Consortium (EADC) study. NeuroImage Clin. 2015;7:34–42.

208. Knopman DS, Jack CR, Wiste HJ, Lundt ES, Weigand SD, Vemuri P, et al. 18F-fluorodeoxyglucose positron emission tomography, aging, and apolipoprotein E genotype in cognitively normal persons. Mol Psychiatry. 2015;20(6):1588–95.

209. Matthew N M, Kim M-S, Adil M, Patil AH, Lu Y, Mitchell CJ, et al. Towards the human cellular microRNAome Matthew. Genome Res. 2017;8138:1769–81.

210. Halushka MK, Fromm B, Peterson KJ, McCall MN. Big Strides in Cellular microRNA Expression Marc. 2018;123(24):4757–63.